

Taxonomic study on fourteen symphytognathid species from Asia (Araneae, Symphytognathidae)

Ya Li¹, Shuqiang Li², Yucheng Lin^{1,3}

1 Key Laboratory of Bio-resources and Eco-environment (Ministry of Education), College of Life Sciences, Sichuan University, Chengdu, Sichuan 610064, China **2** Institute of Zoology, Chinese Academy of Sciences, Beijing 100101, China **3** The Sichuan Key Laboratory for Conservation Biology of Endangered Wildlife, Sichuan University, Chengdu, Sichuan 610064, China

Corresponding authors: Yucheng Lin (linyucheng@scu.edu.cn), Shuqiang Li (lisq@ioz.an.cn)

Academic editor: Yuri Marusik | Received 27 April 2021 | Accepted 19 October 2021 | Published 19 November 2021

<http://zoobank.org/9F578799-E05F-4411-8E2D-378E3C17F3E3>

Citation: Li Y, Li S, Lin Y (2021) Taxonomic study on fourteen symphytognathid species from Asia (Araneae, Symphytognathidae). ZooKeys 1072: 1–47. <https://doi.org/10.3897/zookeys.1072.67935>

Abstract

Fourteen symphytognathid species belonging to three genera are examined, including the descriptions of eight new species and two new genera from China, Vietnam, Thailand and Myanmar: *Patu* Marples, 1951: *P. catba* S. Li & Lin, **sp. nov.** (♂, Vietnam), *P. dakou* S. Li & Lin, **sp. nov.** (♂♀, China), *P. damtao* S. Li & Lin, **sp. nov.** (♂, Vietnam), *P. jiangzhou* S. Li & Lin, **sp. nov.** (♀, China), *P. jidanweishi* Miller, Griswold & Yin, 2009 (♂♀, China), *P. nagarat* S. Li & Lin, **sp. nov.** (♂♀, Thailand), *P. nigeri* Lin & S. Li, 2009 (♀, China), *P. putao* S. Li & Lin, **sp. nov.** (♀, Myanmar), *P. qiqi* Miller, Griswold & Yin, 2009 (♀, China) and *P. xiaoxiao* Miller, Griswold & Yin, 2009 (♂♀, China); *Kirinua* S. Li & Lin, **gen. nov.**: *K. maguai* S. Li & Lin, **sp. nov.** (♂♀, China) and *K. yangshuo* S. Li & Lin, **sp. nov.** (♂♀, China); *Swilda* S. Li & Lin, **gen. nov.**: *S. longtou* (Miller, Griswold & Yin, 2009), **comb. nov.** (♂♀, China) is transferred from *Crassignatha* Wunderlich, 1995 and *S. spinathoraxi* (Lin & S. Li, 2009), **comb. nov.** (♂♀, China) is transferred from *Patu*. Diagnoses, descriptions and illustrations are provided for new taxa, as well as a distribution map. The males of *P. xiaoxiao* and *S. longtou* are described for the first time. Type specimens of *P. jidanweishi*, *P. nigeri*, *P. qiqi*, *P. xiaoxiao*, *S. longtou* and *S. spinathoraxi* are re-examined and photographed. All Asian *Patu* species are revised and two species, *P. kishidai* Shinkai, 2009 and *P. bispina* Lin, Pham & S. Li, 2009, are transferred to *Crassignatha* and proposed as new combinations: *Crassignatha kishidai* **comb. nov.** and *C. bispina* **comb. nov.** In addition, DNA barcodes and genetic distances of ten species treated in this paper were obtained to confirm identification.

Keywords

Dwarf orb-weavers, new species, new genus, new combination, China, Vietnam, Thailand, Myanmar

Introduction

Symphytognathidae Hickman, 1931 is a small spider family mainly distributed in tropical and subtropical regions of the Oriental and Neotropical realms. Ninety symphytognathid species in eight genera are known, of which 45 species and six genera occur in Asia (WSC 2021).

Before the current study, fourteen species from China, Colombia, Fiji, Japan, New Guinea, Samoa, Seychelles and Vietnam were assigned to *Patu* Marples, 1951. Miller et al. (2009) mentioned that *Patu* is a particularly problematic genus because of insufficient study of the copulatory organs, the scarcity of material in collections and the minute size of these animals. A complete revision of this genus is still lacking and the taxonomic placement of some doubtful species needs to be clarified.

The aim of this paper is to provide data on Asian *Patu* and related genera, including descriptions of new species and genera, based on recent collections from China, Vietnam, Thailand and Myanmar.

Materials and methods

More than 1200 adult symphytognathid specimens were examined in a 95% ethanol solution under a Leica M205 C stereomicroscope. The digital photos were montaged using Helicon Focus 3.10 (Khmelik et al. 2006) image stacking software. Male palps and epigynes were examined and photographed after dissection. The left palp was photographed and described (if missing, the right was used). Epigynes were treated with lactic acid before being embedded in Hoyer's Gum and placed on an ultra-thin slide to take photos of both sides of the vulva. All measurements are in millimetres. Leg measurements are given as follows: total length (femur, patella, tibia, metatarsus and tarsus).

Tissue samples were taken from the prosoma of 17 individuals of *Patu*, *Kirinua* S. Li & Lin, gen. nov. and *Swilda* S. Li & Lin, gen. nov., including five new and five known species (the abdomens and male palps were kept as vouchers). All of the molecular data were obtained from specimens collected at the type localities, although not from the type specimens themselves. A partial fragment (636 bp) of the mitochondrial gene cytochrome *c* oxidase subunit I (COI) was amplified and sequenced to calculate the genetic distances between morphologically-similar species to confirm identifications and for sex pairing.

The primers used were: LCO1490 (5'-GGTCAACAAATCATCATAAAGATATTGG-3') and HCO2198 (5'-TAAACTTCAGGGTGACCAAAAAA TCA-3'). Raw sequences were edited and assembled using BioEdit v.7.2.5 (Hall 1999) and the uncorrected pairwise distances between species were calculated using MEGA7.0.14 (Kumar et al. 2016). Results of the genetic distance analysis are shown in Appendix Table A1.

Morphological abbreviations used in the figures are given in Table 1. New sequences, generated for this study, are available from GenBank and the accession numbers are reported in Table 2. References to figures in the cited papers are listed in lowercase (fig. or figs) and figures in this paper are noted with an initial capital (Fig. or Figs). With the exception of the types of previously-described species kept in **HNU** and **IZCAS**, all molecular vouchers are deposited in **NHMSU** in Chengdu, China and examined morphological material is deposited in **NHMSU** and **IZCAS**.

Table 1. List of abbreviations used in the text or figures.

Male palp		Epigyne	
AP	apical process on tegulum	Atr	atrium
Co	conductor	CD	copulatory duct
Cy	cymbium	CO	copulatory opening
CA	cymbial apophysis	FD	fertilisation duct
CP1	proximal cymbial process	PI	parmula
CP2	distal cymbial process	S	spermatheca
E	embolus	Sp	scape
Fe	femur	Somatic characters	
MA	median apophysis	ALE	anterior lateral eyes
Pa	patella	PLE	posterior lateral eyes
T	tegulum	PME	posterior median eyes
Ti	tibia	PER	posterior eye row
TP	tegular process	TS	male clasping spines on tibia II
Institutions			
HNU	College of Life Sciences, Hunan Normal University, Changsha, China		
IZCAS	Institute of Zoology, Chinese Academy of Sciences, Beijing, China		
NHMSU	Natural History Museum of Sichuan University, Chengdu, China		

Table 2. GenBank accession numbers for DNA sequence data from ten symphytognathid species.

Species	Identifier	Sample	COI*	Collection localities
<i>Patu dakou</i> sp. nov.	HA135	1♂	MW970248	China, Yunnan, Longling County
	HA135	1♀	MW970247	
<i>Patu jiangzhou</i> sp. nov.	HA012	1♀	MW970234	China, Guangxi, Fengshan County
	HA119	1♂	MW970243	
<i>Patu jidanweishi</i>	HA119	1♀	MW970242	China, Yunnan, Fugong County
	HA087	1♂	MW970240	
<i>Patu nagarat</i> sp. nov.	HA087	1♀	MW970239	Thailand, Khon Kaen Pro.
	HA129	1♀	MW970246	
<i>Patu nigeri</i>	HA123	1♂	MW970245	China, Yunnan, Gongshan County
	HA123	1♀	MW970244	
<i>Kirinua maguai</i> sp. nov.	HA008	1♀	MW970250	China, Guangxi, Fengshan County
	HA018	1♂ juv.	MW970236	
<i>Kirinua yangshuo</i> sp. nov.	HA018	1♀	MW970235	China, Guangxi, Yangshuo County
	HA112	1♂	MW970249	
<i>Swilda longtou</i>	HA112	1♀	MW970241	China, Yunnan, Fugong County
	HA082	1♂	MW970238	
<i>Swilda spinathoraxi</i>	HA082	1♀	MW970237	China, Yunnan, Mengla County
	HA082	1♂	MW970237	

Taxonomy

Family Symphytognathidae Hickman, 1931

Genus *Patu* Marples, 1951

Patu Marples, 1951: 47.

Patu Forster, 1959: 318.

Patu Forster & Platnick, 1977: 15.

Type species. *Patu vitiensis* Marples, 1951 by original designation, from Fiji.

Diagnosis. *Patu* can be distinguished from *Anapistula* Gertsch, 1941 by having 6 eyes vs. four or lacking and from *Anapogonia* Simon, 1905, tentatively placed in Symphytognathidae (Platnick and Forster 1989: 76), by the chelicerae fused at the mid-line vs. unfused. *Patu* differs from *Globignatha* Balogh & Loksa, 1968 and *Symphytognatha* Hickman, 1931 by the chelicerae fused only at mid-line vs. almost fully fused, see Lin 2019: fig. 1H. It differs from *Curimagua* Forster & Platnick, 1977 by having 6 eyes in diads and the female lacking palps (Fig. 8A and C) vs. 6 eyes in triads and female palps reduced to vestiges (Forster and Platnick 1977: figs 40 and 63). *Patu* differs from *Iardinis* Simon, 1899 (*I. martensi* Brignoli, 1978 from Nepal and *I. musardi* Brignoli, 1980 from India) by having clasping spines on tibia II on the male, but lacking in the latter and from *Crassignatha* Wunderlich, 1995 and *Swilda* gen. nov. by lacking a latero-posterior abdominal scutum in the male and the rod-shaped or oval spermathecae (Figs 1C, 9F and 10G) vs. having an abdominal scutum and spherical spermathecae (Figs 19A, 21A and 22E; Li, Lin and Li 2020: figs 16C and 22D). *Patu* is similar to *Kirinua* gen. nov. by the absence of a latero-posterior abdominal scutum in the male and the carapace surface lacking granular or spinous ornaments in both sexes, but it can be distinguished by the male having sulci and pores on the clypeus, rather than a pair of pocket-shaped pits in the latter and the male palpal cymbium lacks accessory structures (e.g. primary conductor, cymbial process or apophysis); females can be distinguished by having rod-shaped or oval spermathecae rather than spherical or subspherical spermathecae in the latter.

Description. Tiny, total length 0.40–0.80. Carapace round in male, pear-shaped in female dorsally, nearly triangular laterally (Figs 6A, 2D, 8A and 8D). Six eyes in 3 diads, ocular base black, AME absent, lateral eyes adjacent, cephalic part raised (Figs 2C, 2F, 8C and 8F). Clypeus concave, with modified sulci and pores (fig. 69A–D in Miller et al. 2009). Female lacking palps. Chelicerae fused at middle, with a single tooth (fig. 69E and F in Miller et al. 2009). Labium wider than long, fused to sternum (Figs 2B, 2E, 8B and 8E). Sternum heart shaped, truncated posteriorly. Male tibia II with 1–2 clasping spines subdistally (Figs 1C, 2C, 6C and 8C). Abdomen globular dorsally, subovoid laterally, without latero-posterior abdominal scutum (Figs 1C, 4C and 8C). Spinnerets without annular plates. Colulus absent.

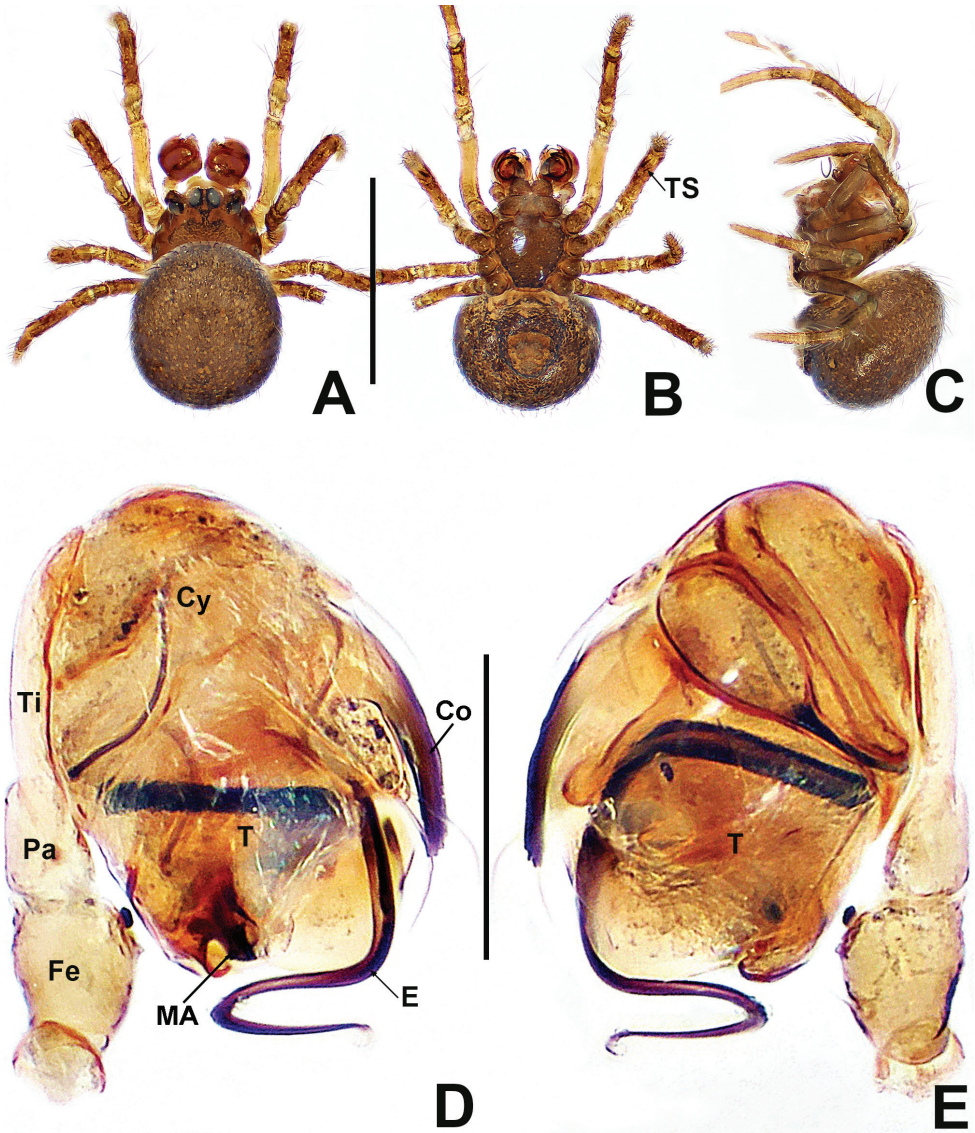


Figure 1. *Patu catba* sp. nov. **A** male habitus, dorsal **B** male habitus, ventral **C** male habitus, lateral **D** male palp, prolateral **E** male palp, retrolateral. Abbreviations: Co = conductor; Cy = cymbium; E = embolus; Fe = femur; MA = median apophysis; Pa = patella; T = tegulum; Ti = tibia; TS = male clasp spines on tibia II. Scale bars: 0.50 (**A–C**); 0.10 (**D, E**).

Male palp (Figs 4D, E, 8A and B): bulb nearly ovate, large, not less than $\sim 1/4$ size of carapace. Cymbium membranous, translucent, wrapping around bulb prolaterally, without modified teeth, processes or apophyses. Conductor usually absent (if present, long, finger-like, starting at dorsal side of bulb, close to embolic base, see Figs 1D and

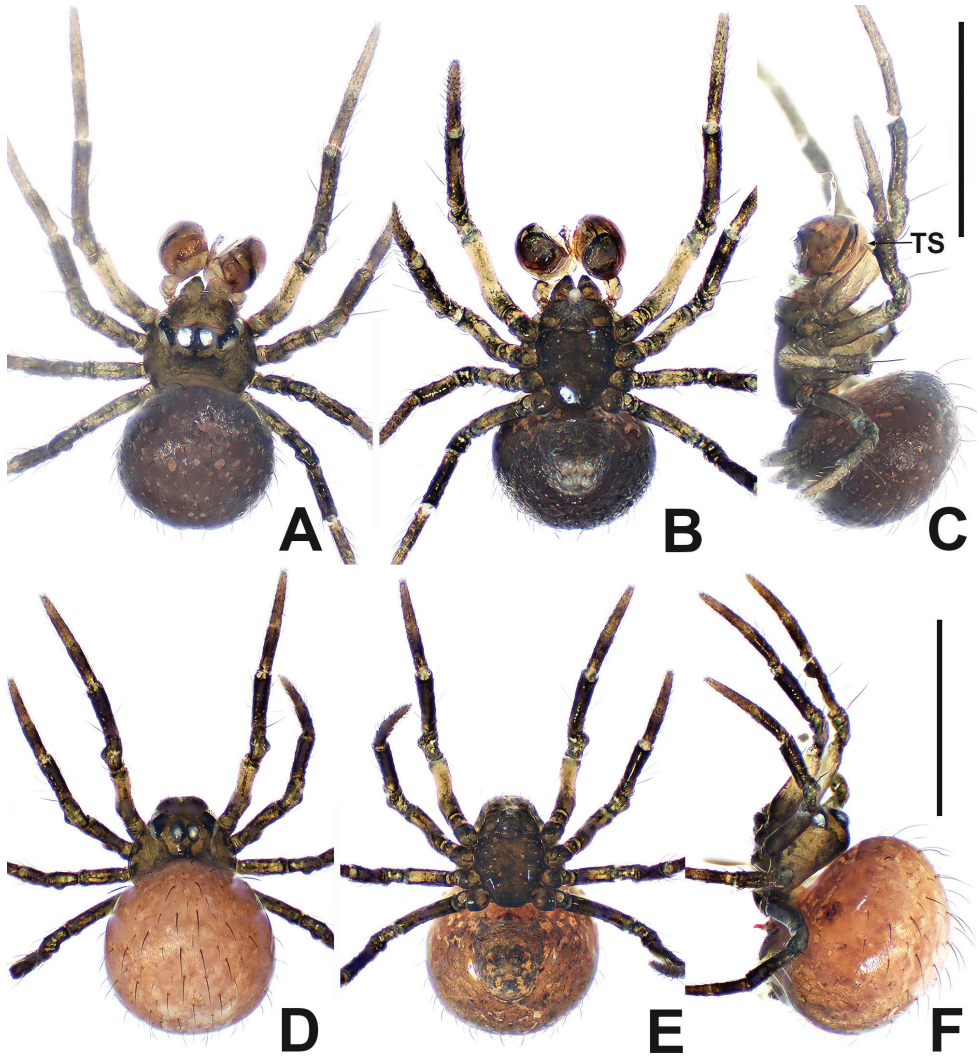


Figure 2. *Patu dakou* sp. nov. **A** male habitus, dorsal **B** male habitus, ventral **C** male habitus, lateral **D** female habitus, dorsal **E** female habitus, ventral **F** female habitus, lateral. Abbreviation: TS = male clashing spines on tibia II. Scale bars: 0.50 (**A–F**).

4D). Tegulum cup shaped, with 1 or 2 protrusions (median apophysis and tegular process) (Figs 1D, 7A and 9A). Embolus long, slender, tubular, coiling into at least 2 loops within tegulum, distal part of embolus embedded inside bulb (Figs 3A, B, 14A and B) or extends and twists at tip of bulb (Figs 1D, E, 4D, E, 7A, B, 9A and B).

Epigyne (Figs 7E, F, 9E, F, 14D and E): weakly sclerotised. Scape or parmula short, tongue-shaped or long, finger-like. Spermathecae long, ovate or kidney-shaped, separated by less than 2 lengths. Copulatory openings separated. Copulatory ducts membranous or faintly sclerotised, usually partially or completely surround spermathecae

(exceptions are *P. nigeri* Lin & S. Li, 2009 and *P. qiqi*). Fertilisation ducts short, thin, typically originate from the lateral or anterior side of spermathecae.

Composition. *Patu catba* sp. nov. (♂), *P. dakou* sp. nov. (♂♀), *P. damtao* sp. nov. (♂), *P. digua* Forster & Platnick, 1977 (♂♀), *P. eberhardi* Forster & Platnick, 1977 (♂♀), *P. jiangzhou* sp. nov. (♀), *P. jidanweishi* Miller, Griswold & Yin, 2009 (♂♀), *P. marplei* Forster, 1959 (♂), *P. nagarat* sp. nov. (♂♀), *P. nigeri* (♂♀), *P. putao* sp. nov. (♀), *P. qiqi* Miller, Griswold & Yin, 2009 (♂♀), *P. saladito* Forster & Platnick, 1977 (♀), *P. samoensis* Marples, 1951 (♂♀), *P. silho* Saaristo, 1996 (♂♀), *P. vitiensis* Marples, 1951 (♂♀), *P. woodwardi* Forster, 1959 (♂♀) and *P. xiaoxiao* Miller, Griswold & Yin, 2009 (♂♀). Li, Lin and Li (2020) have previously suggested that the other two Asian species, *P. bispina* Lin, Pham & S. Li, 2009 from Vietnam and *P. kishidai* Shinkai, 2009 from Japan, do not belong to this genus and should be transferred to *Crassignatha*. Based on the above diagnosis of *Patu*, we formally propose two new combinations: *Crassignatha bispina* comb. nov. and *C. kishidai* comb. nov.

Distribution. China (Guangxi, Hainan, and Yunnan), Colombia, Fiji, Myanmar, New Guinea, Samoa, Seychelles, Thailand, Vietnam.

Remarks. Of the male *Patu* species described here, the embolus is either embedded within the tegulum or not, the conductor is present or absent and the regular process is present or absent. The similarities of the palps are the nearly ovate bulb and the cymbium lacking any teeth, processes or apophyses. In the females, the epigyne and vulva distinctly differ in the type, shape and size of posterior process of the epigyne (scape or parmula) and in the texture, length and course of the copulatory ducts. The similarities of the vulvae are the ovate or short, club-shaped spermathecae.

Patu catba S. Li & Lin, sp. nov.

<http://zoobank.org/2CB7474E-ACD6-410C-8344-E507BDC06219>

Figures 1, 23

Type material. *Holotype* ♂ (IZCAS-Ar 41036) VIETNAM: Cat Ba National Park, Hai Phong Province, in leaf litter of natural forest (20.80133°N, 107.00353°E; 116 m alt.), 23.IX.2007, D. Pham leg.

Etymology. The specific epithet derives from the type locality; noun in apposition.

Diagnosis. This new species differs from other *Patu* species with the exception of *P. damtao* sp. nov. by having a long, sclerotised conductor dorsally on the bulb (Figs 1D and 4D). It can be distinguished from *P. damtao* sp. nov. by the blunt conductor swollen basally, the shorter embolus forming no more than one loop and the presence of a median apophysis (Fig. 1D and E) vs. a sharp conductor constricted basally, a longer embolus forming more than one loop and the absence of a median apophysis (Fig. 4D and E).

Description. Male (IZCAS-Ar 41036). Total length 0.56. Carapace 0.24 long, 0.28 wide, 0.32 high. Clypeus 0.14 high. Sternum 0.16 long, 0.16 wide. Abdomen 0.40 long, 0.36 wide, 0.40 high. Length of legs: I 0.74 (0.20, 0.10, 0.16, 0.12, 0.16);

II 0.66 (0.20, 0.10, 0.12, 0.10, 0.14); III 0.50 (0.12, 0.08, 0.08, 0.08, 0.14); IV 0.56 (0.12, 0.10, 0.12, 0.10, 0.12).

Somatic characters (Fig. 1A–C). **Colouration:** carapace brown, nut brown at margins, ocular base black, thoracic region reticulated medially. Chelicerae, endites and labium dark brownish. Sternum nut brown. Legs brownish to dark yellow, except femur I yellow. Abdomen brown and grey, with dense, light dots. **Prosoma:** carapace wider than long, nearly pyriform. Eyes with ocular tubercles, PME > ALE > PLE, ALE protruded, PER recurved. Sternum slightly swollen, smooth and glossy, sparsely punctate. **Legs:** with 1 dorso-distal seta on each patella and 1 seta on each tibia subproximally. Tibia II with 2 subdisto-ventral clasping spines. **Opisthosoma:** dorsally rounded, laterally nearly ovoid. Spinnerets brown, darker at edges.

Palp (Fig. 1D and E): large, $\sim \frac{1}{3}$ size of carapace. Femur slightly swollen, patella $\sim \frac{1}{2}$ length of tibia, tibia flat. Cymbium translucent, membranous, surrounds bulb prolaterally, with a finger-like extension, with 2 distal, long setae. Bulb subovate. Tegulum smooth. Median apophysis short, not extending beyond apex of bulb. Conductor long, finger-like, sclerotised, basally swollen, distally blunt. Embolus ca. $2\times$ length of conductor, ribbon-like, middle portion embedded in tegulum, distal portion looped at the apex of bulb.

Female. Unknown.

Distribution. Vietnam (Fig. 23).

***Patu dakou* S. Li & Lin, sp. nov.**

<http://zoobank.org/6F994EA1-BBCC-4226-9C71-1ECF912D901B>

Figures 2, 3, 23

Type material. **Holotype** ♂ (NHMSU Ar 132) and **paratypes** 2♂ 7♀ (NHMSU Ar 133–141) **CHINA:** Yunnan Province, Longling County, Zhen'an Township, Bangbie Village at stream at 6.8 km on S317 Road, shaded embankments along stream, dusting webs in understorey (24.81333°N, 98.83280°E; 1560 m alt.), 22.VIII.2018, Y. Lin et al. leg.; 1♂ (NHMSU-HA135) and 1♀ (NHMSU-HA135) used for sequencing, GenBank: MW970248 and MW970247, same data as for preceding.

Etymology. Formed from the Chinese word (dà kǒu), referring to the large copulatory opening of the epigyne (Fig. 3C and E); noun.

Diagnosis. The new species differs from other congeners with the exception of *P. nigeri* by the embolus completely encased in the tegulum, the knob-shaped parmula and the proximal position of the copulatory ducts forming a pair of horn-like structures (Fig. 3A–F). The male of *P. dakou* sp. nov. is similar to that of *P. nigeri*, but it can be distinguished by the more basal position of the embolus (Fig. 3A and B vs. fig. 4A and B in Lin and Li 2009). The female is similar to that of *P. nagarat* sp. nov. in the configuration of the vulva, but it differs by the nearly adjacent spermathecae, the knob-shaped parmula and the fertilisation ducts originating from the anterior side of the spermathecae vs. separated spermathecae, a triangular parmula and the fertilisation ducts originating laterally on the spermathecae (Fig. 3D–F vs. Fig. 9D–F).

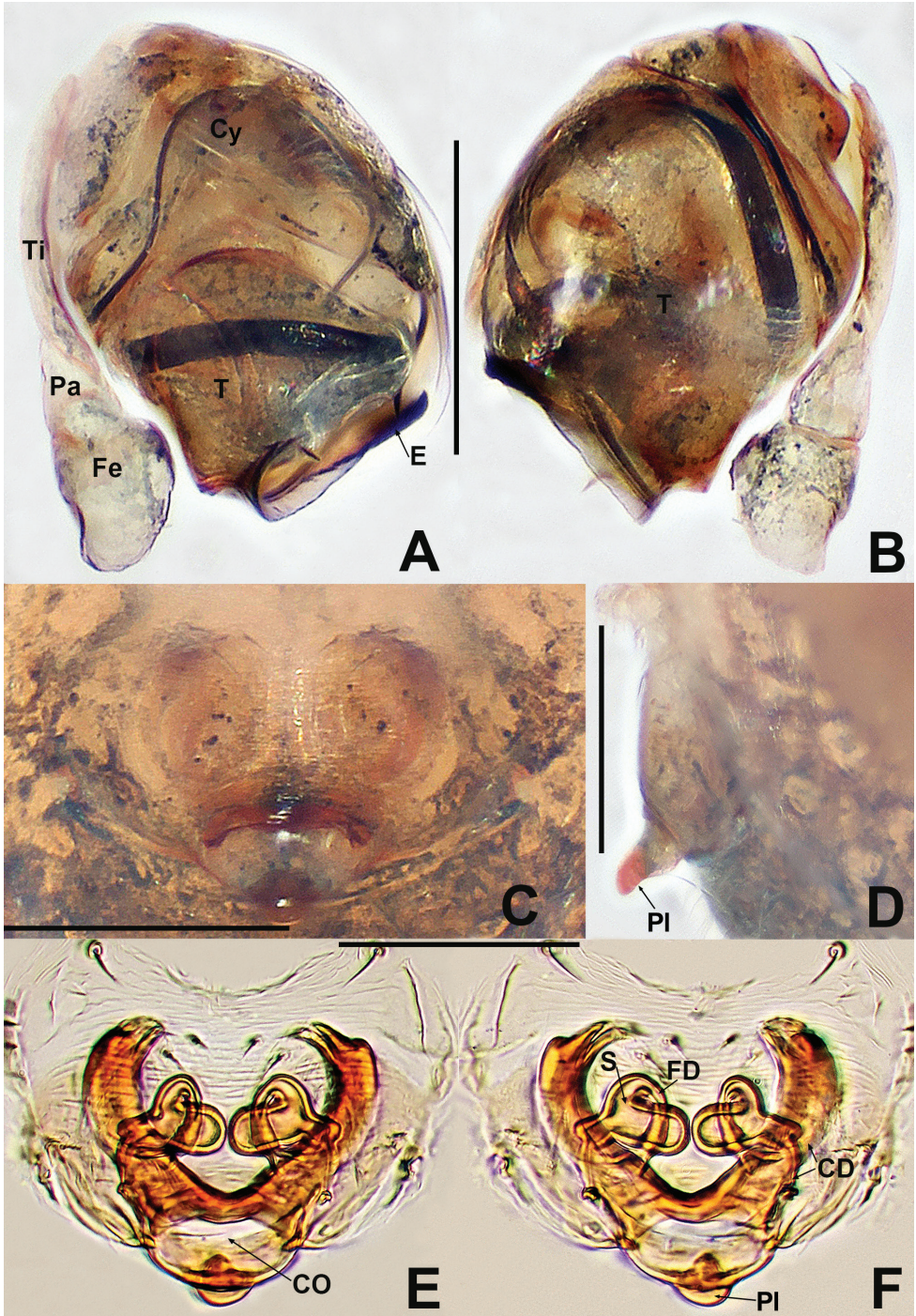


Figure 3. *Patu dakou* sp. nov. **A** male palp, prolateral **B** male palp, retrolateral **C** epigyne, ventral **D** epigyne, lateral **E** vulva, ventral **F** vulva, dorsal. Abbreviations: CD = copulatory ducts; CO = copulatory opening; Cy = cymbium; E = embolus; FD = fertilisation ducts; Fe = femur; MA = median apophysis; Pa = patella; Pl = parmula; S = spermathecae; T = tegulum; Ti = tibia. Scale bars: 0.10 (A–F).

Description. Male (NHMSU Ar 132). Total length 0.56. Carapace 0.28 long, 0.28 wide, 0.28 high. Clypeus 0.08 high. Sternum 0.20 long, 0.20 wide. Abdomen 0.36 long, 0.40 wide, 0.36 high. Length of legs: I 0.80 (0.20, 0.06, 0.24, 0.12, 0.18); II 0.64 (0.12, 0.06, 0.16, 0.14, 0.16); III 0.46 (0.12, 0.06, 0.10, 0.08, 0.10); IV 0.58 (0.16, 0.10, 0.12, 0.08, 0.12).

Somatic characters (Fig. 2A–C). **Colouration:** carapace dark grey, darker on thoracic margin and centre. Chelicerae, endites and labium black. Sternum black. Legs light brown, with black pigmentation. Abdomen charcoal grey, dorsally lighter than ventrally, with irregular light spots. **Prosoma:** carapace as long as wide, dorsally rounded, laterally conical. ALE protruded, PER straight. Chelicerae with an anterior small hump (Fig. 2B). Labium semi-lunar. Sternum flat, smooth. **Legs:** Each patella with a long disto-dorsal seta. Tibia II with 1 ventral clasping spine sub-distally. **Opisthosoma:** dorsally rounded, laterally oval, covered with long, sparse, black setae. Spinnerets apically pale grey.

Palp (Fig. 3A and B): large, ~ ½ size of carapace. Femur equal to 1.5× width of patella, patella short, ca. half of tibial length, tibia flat. Cymbial distal extension with a few long setae. Bulb nearly ovoid, anteriorly flat. Tegulum broad, smooth. Embolus originates retrolaterally, entirely encased in tegulum, coiled into ca. 3 loops. Sperm duct convoluted throughout. Embolic tip looped at apex of bulb.

Female (NHMSU Ar 133). Total length 0.64. Carapace 0.28 long, 0.28 wide, 0.24 high. Clypeus 0.10 high. Sternum 0.20 long, 0.20 wide. Abdomen 0.48 long, 0.48 wide, 0.48 high. Length of legs: I 0.68 (0.16, 0.10, 0.14, 0.12, 0.16); II 0.60 (0.12, 0.10, 0.12, 0.12, 0.14); III 0.50 (0.12, 0.10, 0.08, 0.08, 0.12); IV 0.58 (0.18, 0.10, 0.08, 0.08, 0.14).

Somatic characters (Fig. 2D–F). **Colouration:** prosoma same as in male, opisthosoma light, ventrally darker than dorsally, post-gaster region and area around spinnerets black. **Prosoma:** carapace round. Cephalic region lower than in male. PER slightly procurved. Mouthparts and sternum as in male, except longer labium. **Legs:** as in male. **Opisthosoma:** dorsally rounded, laterally ovate, covered with sparse, long, black setae. Spinnerets dark grey.

Epigyne (Fig. 3C–F): internal structures faintly visible via cuticle. Parmula knob-shaped, protruded, distally sclerotised. Copulatory opening large, oval. Copulatory duct arising from the ventral base of parmula, its proximal part forming a pair of sclerotised, broad, horn-like structures at both sides of spermathecae. Spermathecae shorter than width of copulatory opening, claviform, nearly touching. Fertilisation ducts start at the anterolateral margin of spermathecae and curve downwards to centre of vulva.

Distribution. China (Yunnan) (Fig. 23).

***Patu damtao* S. Li & Lin, sp. nov.**

<http://zoobank.org/8D9961F6-2B24-4233-8F45-77D043BFB1F7>

Figures 4, 23

Type material. Holotype ♂ (IZCAS-Ar 41037) VIETNAM: Dam Tao National Park (21.47200°N, 105.63644°E; 1023 m alt.), 31.X.2012, H. Zhao and Z. Chen leg.

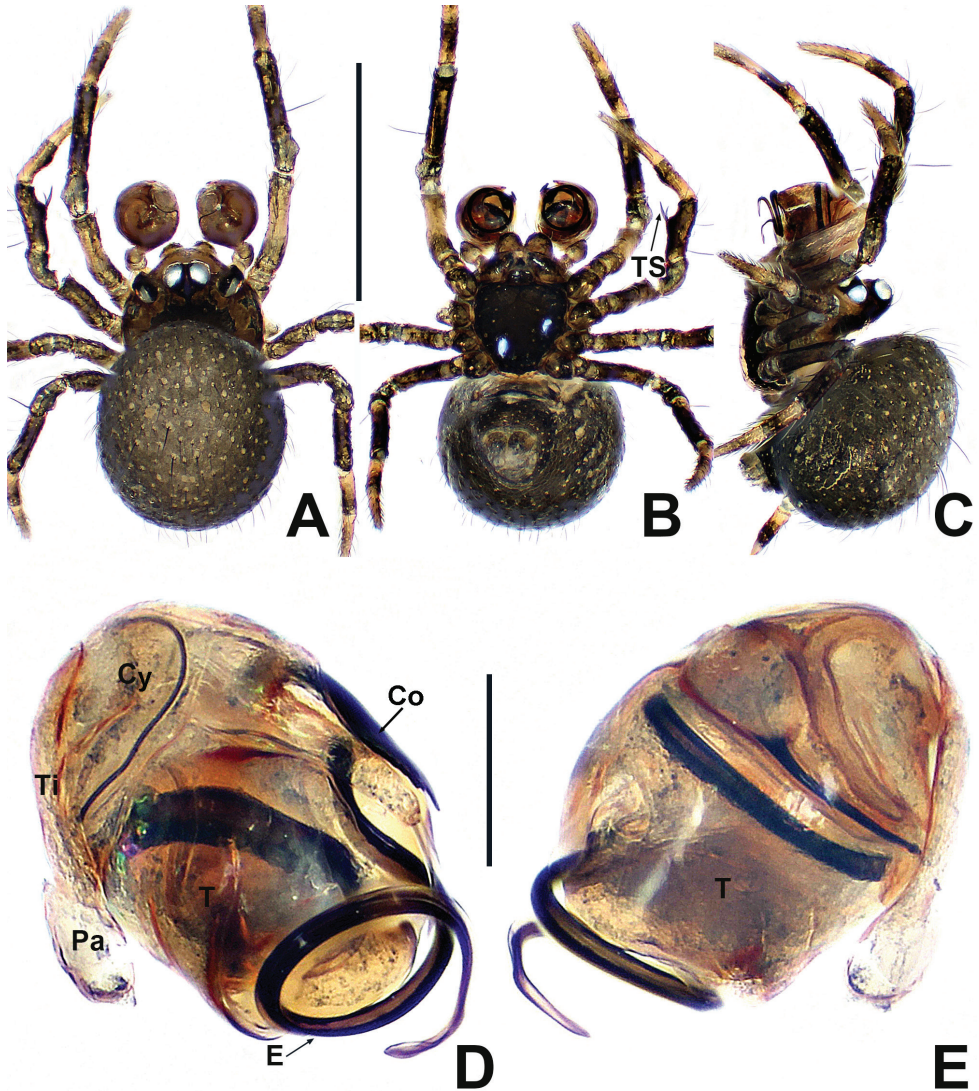


Figure 4. *Patu damtao* sp. nov. **A** male habitus, dorsal **B** male habitus, ventral **C** male habitus, lateral **D** male palp, prolateral **E** male left palp, retrolateral. Abbreviations: Co = conductor; Cy = cymbium; E = embolus; Pa = patella; T = tegulum; Ti = tibia; TS = male clasp spines on tibia II. Scale bars: 0.50 (**A–C**); 0.10 (**D, E**).

Etymology. The specific epithet derives from the name of the type locality; noun in apposition.

Diagnosis. *Patu damtao* sp. nov. can be distinguished from other congeners, with the exception of *P. catba* sp. nov., by having a conductor and lacking a regular process (Fig. 4D). It is similar to *P. catba* sp. nov. in the shape of the male palp, but it differs by lacking a median apophysis, the embolus has more coils and is 4× the length of the

conductor vs. having a median apophysis and an embolus with fewer coils that is ca. 2× the length of the conductor (Figs 4D and E vs. 1D and E).

Description. Male (IZCAS-Ar 41037). Total length 0.60. Carapace 0.24 long, 0.28 wide, 0.32 high. Clypeus 0.16 high. Sternum 0.20 long, 0.20 wide. Abdomen 0.40 long, 0.36 wide, 0.44 high. Length of legs: I 0.84 (0.24, 0.10, 0.18, 0.14, 0.18); II 0.68 (0.20, 0.10, 0.12, 0.10, 0.16); III 0.52 (0.12, 0.08, 0.10, 0.10, 0.12); IV 0.64 (0.16, 0.10, 0.14, 0.10, 0.14).

Somatic characters (Fig. 4A–C). **Colouration:** carapace dark, darker in thoracic centre, clypeus light grey. Chelicerae, endites and labium dark. Sternum black. Legs dim yellow, with black pigmentation, tibia darkest. Abdomen charcoal grey, dorsally lighter, covered with light dots. **Prosoma:** carapace wider than long, laterally triangular. Eyes with ocular mound, PME > ALE > PLE, ALE protruded, PER recurved. Chelicerae anteriorly plump. Labium semi-lunar. Sternum smooth, slightly plump. **Legs:** densely covered with bristles on tibia, metatarsi and tarsi. Patella with 1 seta disto-dorsally. Tibia with 1 subproximal seta dorsally. Tibia II with 2 adnate clasping spines. **Opisthosoma:** dorsally globular, laterally ovoid. Spinnerets darkish.

Palp (Fig. 4D and E): relatively large, ~ ½ size of carapace. Patella short, about half of tibial length. Tibia flat and lamellar. Cymbium translucent, surrounding the bulb prolaterally. Bulb elongate ovoid. Tegulum smooth, cup-shaped, apically truncated. Conductor strongly sclerotised, long, spatulate, ~ ¼ length of embolus, protruded from dorsal base of tegulum, basally narrow and distally sharp. Embolus long, ca. 4× length of conductor, ribbon shaped, protruded below the conductor, coiled into ~ 1¼ loops at the apex of tegulum.

Female. Unknown.

Distribution. Vietnam (Fig. 23).

***Patu jiangzhou* S. Li & Lin, sp. nov.**

<http://zoobank.org/7EB5BAB4-6C46-48F3-8B55-CBA0B67850F9>

Figures 5, 23

Type material. Holotype ♀ (IZCAS-Ar 41038) CHINA: Guangxi Zhuang Autonomous Region, Hechi City, Fengshan County, Jiangzhou Township, underground gallery (a limestone cave) (24.33144°N, 106.98716°E; 449 m alt.), 25.III.2015, Y. Li and Z. Chen leg.; 1♀ (NHMSU-HA012) used for sequencing, GenBank: MW970234, same data as preceding.

Etymology. The specific epithet derives from the name of the type locality; noun in apposition.

Diagnosis. This new species is similar to *P. putao* sp. nov. and *P. woodwardi* in the configuration of the vulva, but it differs by the smaller spermathecae that are separated by their width, the shorter copulatory ducts and the larger, trumpet-shaped copulatory openings (Fig. 5D and F–G) vs. the larger, adjacent spermathecae, the longer copulatory ducts and the smaller, circular copulatory openings (cf. Fig. 11D and F–G and fig. 123 in Forster 1959).

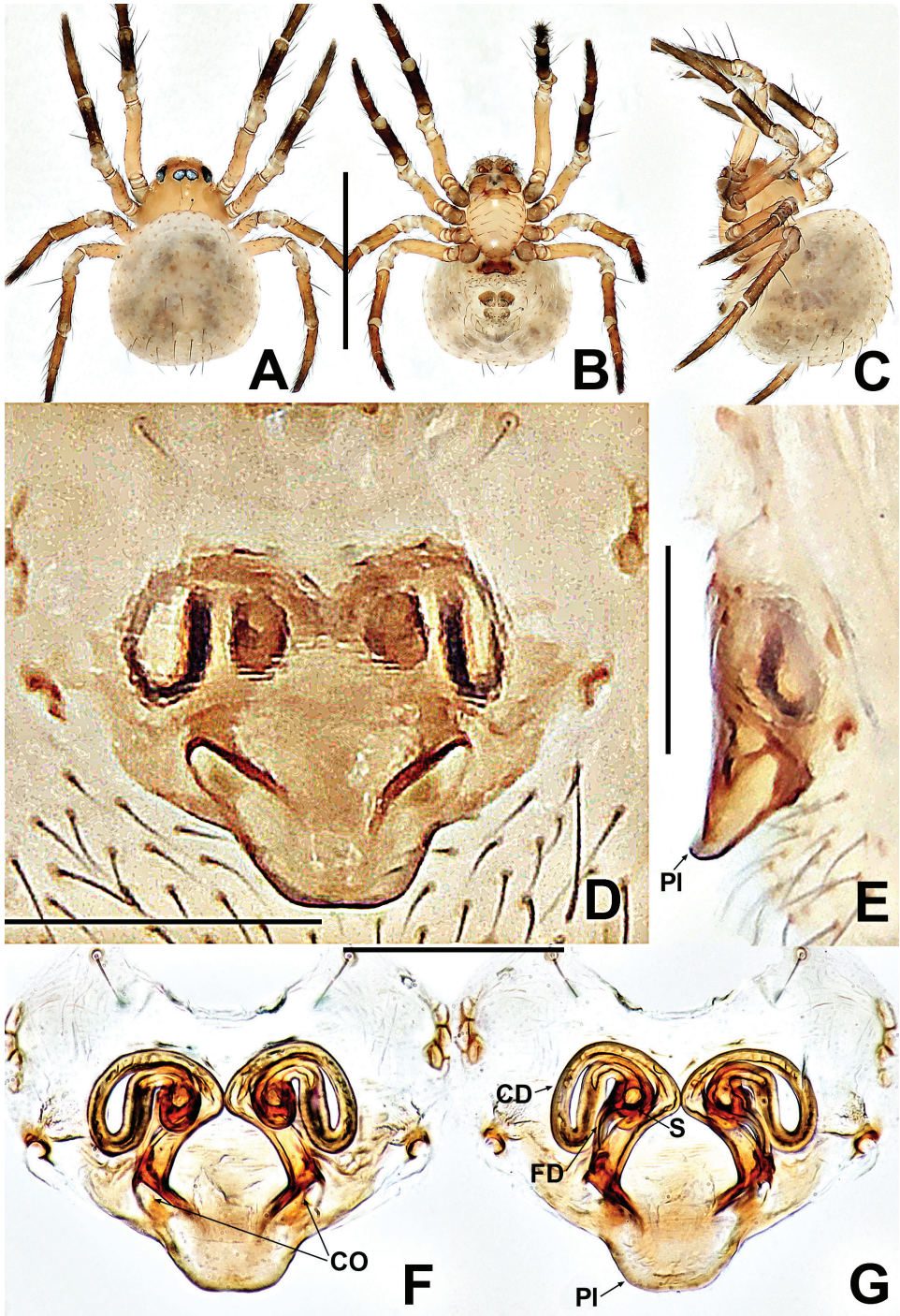


Figure 5. *Patu jiangzhou* sp. nov. **A** female habitus, dorsal **B** female habitus, ventral **C** female habitus, lateral **D** epigyne, ventral **E** epigyne, lateral **F** vulva, ventral **G** vulva, dorsal. Abbreviations: CD = copulatory ducts; CO = copulatory opening; FD = fertilisation ducts; PI = parmula; S = spermathecae. Scale bars: 0.50 (**A-C**); 0.10 (**D-G**).

Description. Female (IZCAS-Ar 41038). Total length 0.60. Carapace 0.24 long, 0.24 wide, 0.24 high. Clypeus 0.10 high. Sternum 0.16 long, 0.16 wide. Abdomen 0.44 long, 0.44 wide, 0.44 high. Length of legs: I 0.80 (0.24, 0.12, 0.16, 0.12, 0.16); II 0.74 (0.22, 0.12, 0.14, 0.10, 0.16); III 0.60 (0.14, 0.10, 0.12, 0.10, 0.14); IV 0.76 (0.22, 0.10, 0.16, 0.12, 0.16).

Somatic characters (Fig. 5A–C). **Colouration:** carapace yellow. Mouthparts light brown. Sternum pale yellow. Legs light brown, tibia, metatarsi and tarsi dark grey. Abdomen pale. Spinnerets light brown. **Prosoma:** carapace smooth, as long as wide and high, dorsally pear-shaped. Cephalic part moderately raised. ALE > PME > PLE. PER straight, lateral eyes adjacent, PME contiguous. Chelicerae stubby, with sparse, short setae anteriorly. Endites nearly quadrilateral. Labium rectangular, wider than long. Sternum faintly plump, smooth, with sparse setae. **Legs:** 1 long disto-dorsal seta on all patella; tibia I and II with 3 dorsal setae and 1 on tibia III and IV; dense, thin setae on tibia, metatarsi and tarsi. **Opisthosoma:** almost globose, cuticle modified by sparse, long setae and faintly ossified dots. Spinnerets brown, anterior spinnerets more fuscous than posterior spinnerets.

Epigyne (Fig. 5D–G): distinctly sclerotised, internal structures faintly visible via the cuticle. Parmula tongue-shaped, wider than long, slightly protruded. Copulatory openings trumpet-shaped, located at basal side of parmula bilaterally. Spermathecae small, ovoid, separated by ca. 1.5× their diameter. Copulatory ducts long, twisted four times before connecting with the anterior margin of spermathecae. Fertilisation ducts shorter and thinner than copulatory ducts, originate at posterolateral margin of spermathecae, slightly bent and extended downwards, parallel to proximal part of copulatory ducts.

Male. Unknown.

Distribution. China (Guangxi) (Fig. 23).

***Patu jidanweishi* Miller, Griswold & Yin, 2009**

Figures 6, 7, 23

Patu jidanweishi Miller, Griswold & Yin, 2009: 64, figs 65A–E, 66A, B, 67A–D, 68A–F, 69A–F, 70A–F and 71A–F (♂♀).

Type materials examined. **Holotype** ♂ (CASENT 9029293, HNU) and **paratypes** 1♀ (CASENT 9022328, HNU) **CHINA:** Yunnan Province, Lushui County, Pianma Township, Changyanhe, 9.3 km ESE Pianma, mixed broadleaf deciduous and evergreen forest, Winkler extraction of sifted leaf litter (25.99363°N, 98.66651°E; 2470 m alt.), 12.V.2005, C. Griswold, D. Kavanaugh and K. Guo leg.; 1♂ 1♀ (CASENT 9019863, HNU): Yunnan Province, Gaoligongshan, 0.4 km SSE Shibali forest station, dusting webs in understorey of good forest (27.16337°N, 98.78208°E; 2475 m alt.), 5.V.2004, C. Griswold leg.; 1♂ 1♀ (CASENT 9020650, HNU), 1♂ 1♀ (CASENT 9019876, HNU), 1♂ 2♀ 1 juv. (CASENT 9024143, HNU): Yunnan Province, Gaol-

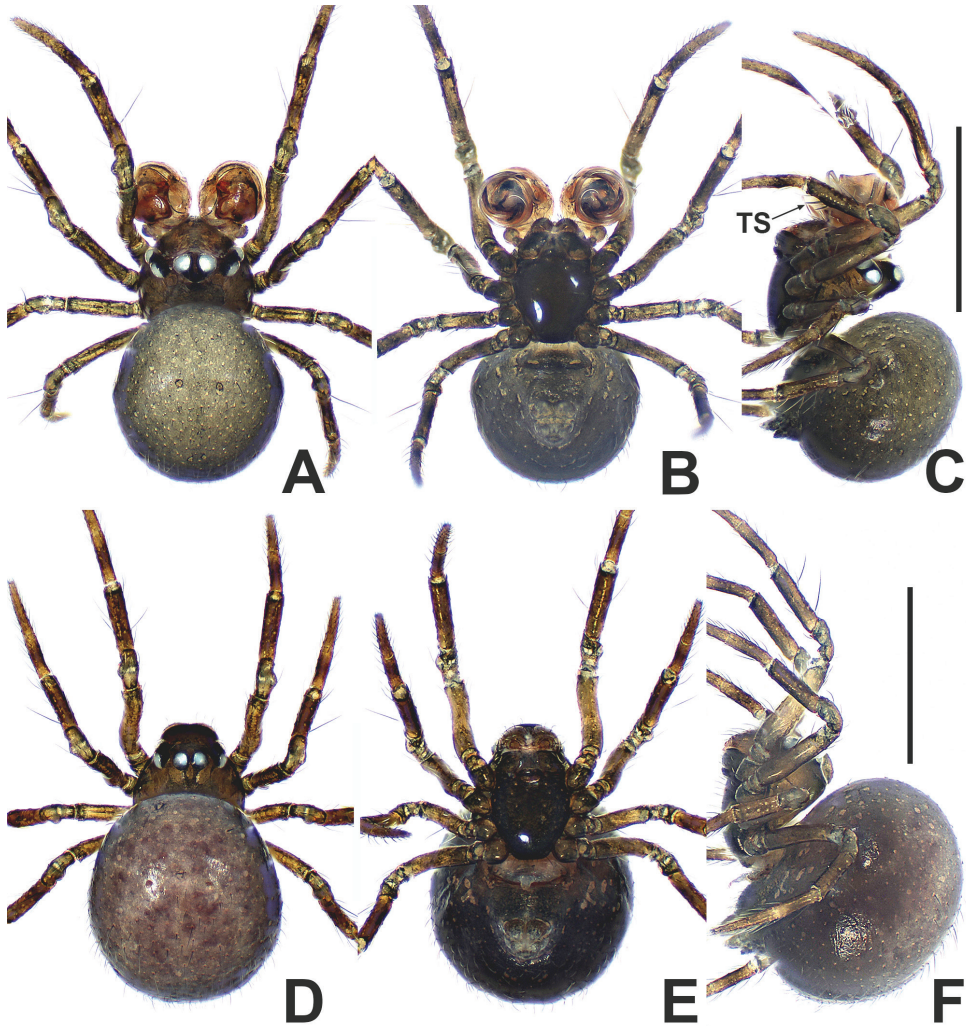


Figure 6. *Patu jidanweishi* **A** male habitus, dorsal **B** male habitus, ventral **C** male habitus, lateral **D** female habitus, dorsal **E** female habitus, ventral **F** female habitus, lateral. Abbreviation: TS = male clasp spines on tibia II. Scale bars: 0.50 (**A–F**).

igongshan, 0.5 km radius of Shibali forest station, dusting webs in forest (27.16519°N, 98.77891°E; 2525 m alt.), 1–9.V.2004, C. Griswold leg.; 2♂ 1♀ (CASENT 9020351, HNU); Yunnan Province, Gaoligongshan, Shibali forest station, good forest, pitfall traps (27.16636°N, 98.77667°E; 2563 m alt.), 3–11.V.2004, C. Griswold and D. Kavanaugh leg.; 4♂ 4♀ (CASENT 9000375, HNU), 14♀ (CASENT 9000373, HNU), 2♂ 10♀ 1 juv. (CASENT 9000371, HNU), 1♀ (CASENT 9000369, HNU), 1♀ (CASENT 9023115, HNU): Yunnan Province, Gaoligongshan, Nujiang Prefecture, Nujiang State Nature Reserve, Qiqihe, 9.9 km W of Gongshan (27.715°N, 98.565°E; 2000 m alt.), 9–14.VII.2000, H. Yan et al. leg.

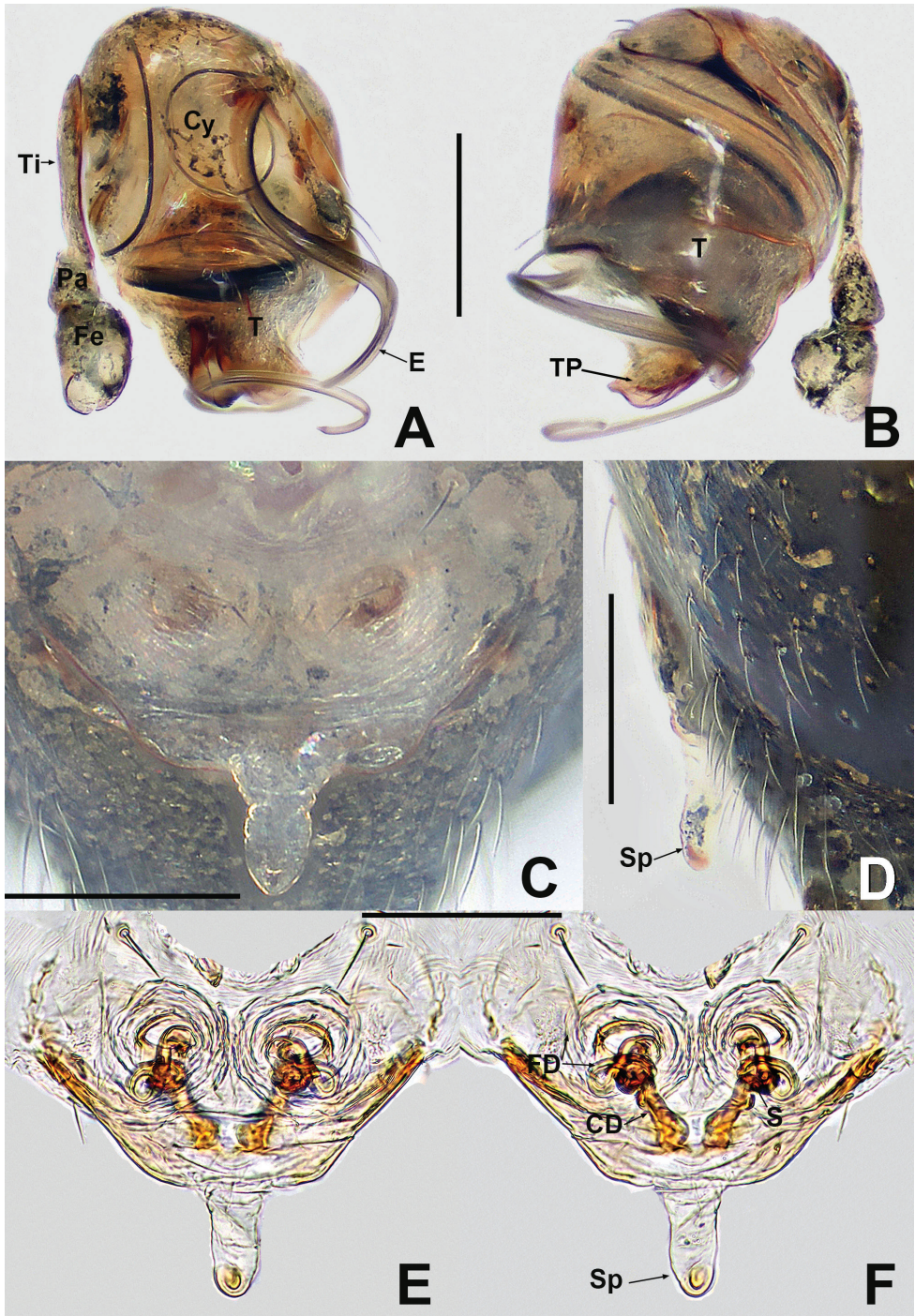


Figure 7. *Patu jidanweishi* **A** male palp, prolateral **B** male palp, retrolateral **C** epigyne, ventral **D** epigyne, lateral **E** vulva, ventral **F** vulva, dorsal. Abbreviations: CD = copulatory ducts; Cy = cymbium; E = embolus; FD = fertilisation ducts; Fe = femur; Pa = patella; S = spermathecae; Sp = scape; T = tegulum; Ti = tibia; TP = tegular process. Scale bars: 0.10 (**A–F**).

Other material examined. 5♂ 60♀ (NHMSU-HA119) **CHINA:** Yunnan Province, Lushui County, Pianma Township, Changyanhe River, 9.3 km ESE Pianma, mixed broadleaf deciduous and evergreen forest (25.99363°N, 98.66651°E; 2470 m alt.), 10.VIII.2018, Y. Lin et al. leg.; 1♂ (NHMSU-HA119) and 1♀ (NHMSU-HA119) used for sequencing, GenBank: MW970243 and MW970242, same data as for preceding; 8♂ 34♀ (NHMSU-HA120) **CHINA:** Yunnan Province, Nujiang Prefecture, Gaoligong Mt. Nature Reserve, Qiqihe (27.71500°N, 98.56500°E; 2000 m alt.), 17.VIII.2018, Y. Lin et al. leg.; 14♂ 86♀ (NHMSU-HA121) **CHINA:** Yunnan Province, Fugong County, along the road from Shiyueliang Town to Shibali Village, native forest of mountainside (27.15546°N, 98.80573°E; 2193 m alt.), 19.VIII.2018, Y. Lin et al. leg.

Diagnosis. This species differs from other congeners, except for *P. nagarat* sp. nov., by lacking a median apophysis and a conductor and having a regular process and a long scape (Fig. 7A, B and F). It is similar to *P. nagarat* in the shape of the bulb and the configuration of the vulva, but it can be distinguished by the lack of a median apophysis, a regular process that is shaped like the head of a sparrow (Fig. 7B) and by the rugose, finger-like scape and the more widely separated spermathecae (Fig. 7A–F) vs. having a median apophysis and a pyramidal regular process, a broader, triangular parmula and spermathecae are closer (Fig. 9A–F).

Description. See Figs 6A–F and 7A–F and Miller et al. (2009).

Distribution. China (Yunnan) (Fig. 23).

***Patu nagarat* S. Li & Lin, sp. nov.**

<http://zoobank.org/91389FD1-6FEA-4E6D-A256-08765F7EA895>

Figures 8, 9, 23

Type material. *Holotype* ♂ (IZCAS-Ar 41039) and *paratypes* 5♀ (IZCAS-Ar 41040–41044) **THAILAND:** Khon Kaen Province, Chum Phae District, Nanoog Toom Subdistrict, Nagarat Cave (16.81402°N, 101.95663°E; 531 m alt.), 30.IX.2016, H. Zhao et al. leg.; 1♂ 3♀ (NHMSU-HA087), same data as holotype; 1♂ (NHMSU-HA087) and 1♀ (NHMSU-HA087) used for sequencing, GenBank: MW970240 and MW970239, same data as for preceding.

Etymology. The specific epithet derives from the type locality; noun in apposition.

Diagnosis. The male of *P. nagarat* sp. nov. can be distinguished from that of other congeners by having a bifurcate, sclerotised median apophysis and a pyramidal regular process and lacking a conductor (Fig. 9A and B) vs. lacking a median apophysis (or if present, it is not furcate) and/or having a conductor (Figs 1D, 4D, 7A and 14A). The female is similar to that of *P. jidanweishi* in the configuration of the vulva, but it differs by having a triangular parmula and the spermathecae are closer together, rather than a finger-like scape and more widely separated spermathecae (cf. Figs 9C–F and 7C–F).

Description. Male (IZCAS-Ar 41039). Total length 0.60. Carapace 0.24 long, 0.28 wide, 0.32 high. Clypeus 0.14 high. Sternum 0.20 long, 0.20 wide. Abdomen 0.44 long, 0.44 wide, 0.48 high. Length of legs: I 1.06 (0.32, 0.12, 0.22, 0.16, 0.24);

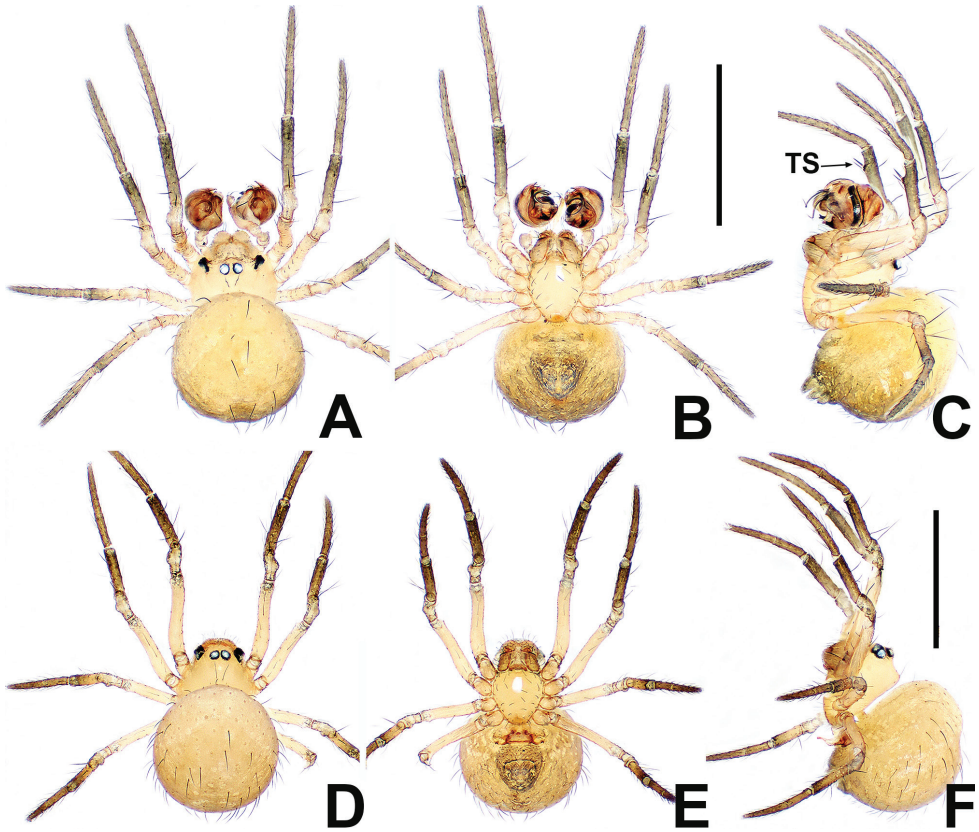


Figure 8. *Patu nagarat* sp. nov. **A** male habitus, dorsal **B** male habitus, ventral **C** male habitus, lateral **D** female habitus, dorsal **E** female habitus, ventral **F** female habitus, lateral. Abbreviation: TS = male claspingspines on tibia II. Scale bars: 0.50 (**A–F**).

II 0.92 (0.26, 0.12, 0.18, 0.14, 0.22); III 0.70 (0.22, 0.10, 0.12, 0.12, 0.14); IV 0.80 (0.26, 0.10, 0.16, 0.12, 0.16).

Somatic characters (Fig. 8A–C). **Colouration:** body pale yellow, opisthosoma darker than prosoma, slightly grey on abdominal ventre and posterior. Leg colour a gradient, pale from femora and patella, darkening distally to dark greyish. **Prosoma:** carapace wider than long, dorsally oval. Eyes subequal in size. ALE protruded, PER straight, PME separated by $\sim \frac{1}{3}$ their diameter. Cephalic part with 2 setae apically, vertical anteriorly, sloped posteriorly. Chelicerae anterior surface flat. Labium semi-circular. Sternum slightly plump, smooth, with a few setae. **Legs:** patella with 1 long disto-dorsal seta, tibia with 1 proximal and 1 mesal long dorsal seta. Tibia II with 2 ventral claspingspines subdistally, 1 thick and 1 thin (Fig. 8C). **Opisthosoma:** globular cuticle with sparse, long, black setae. Spinnerets grey.

Palp (Fig. 9A and B): relatively large, $\sim \frac{1}{2}$ of carapace size. Femur swollen, nearly as wide as long. Patella short, narrower than femur. Tibia flat and lamellar, length equal to $\sim 2 \times$ patella. Cymbium wrapping around bulb prolaterally and ventrally, its distal extension forming triangular lamina, with 2 long setae distally. Tegulum broad,

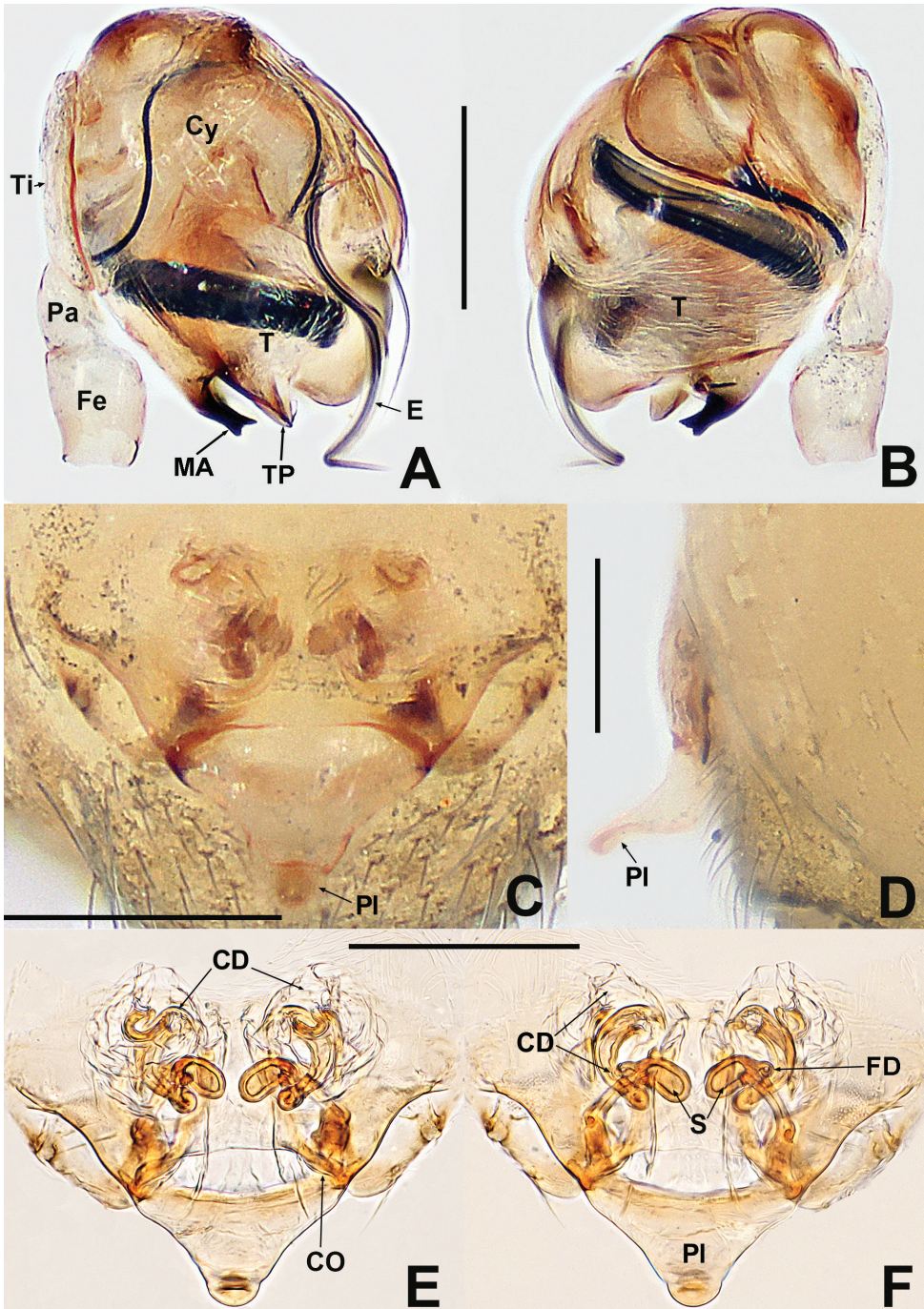


Figure 9. *Patu nagarat* sp. nov. **A** male palp, prolateral **B** male palp, retrolateral **C** epigyne, ventral **D** epigyne, lateral **E** vulva, ventral **F** vulva, dorsal. Abbreviations: CD = copulatory ducts; CO = copulatory opening; Cy = cymbium; E = embolus; FD = fertilisation ducts; Fe = femur; MA = median apophysis; Pa = patella; PI = parmula; S = spermathecae; T = tegulum; Ti = tibia; TP = tegular process. Scale bars: 0.10 (**A-F**).

rugose, with pyramidal process. Median apophysis strongly sclerotised, bifurcate distally. Sperm duct thin, faintly visible. Embolus long, slender, with a circuitous course in basal haematodocha and tegulum. Embolus filiform, protrudes from under cymbial extension, snaking to apex of tegulum.

Female (IZCAS-Ar 41040). Total length 0.64. Carapace 0.32 long, 0.28 wide, 0.28 high. Clypeus 0.10 high. Sternum 0.20 long, 0.20 wide. Abdomen 0.44 long, 0.44 wide, 0.44 high. Length of legs: I 0.90 (0.28, 0.12, 0.18, 0.14, 0.18); II 0.86 (0.26, 0.12, 0.16, 0.12, 0.20); III 0.66 (0.18, 0.10, 0.10, 0.10, 0.18); IV 0.82 (0.28, 0.12, 0.14, 0.10, 0.18).

Somatic characters (Fig. 8D–F). **Colouration:** same as in male. **Prosoma:** carapace ovate dorsally. Ocular area slightly more anterior than in male. Cephalic part slightly lower than in male. **Legs:** colour of tibia, metatarsi and tarsi darker than in male. **Opisthosoma:** same as in male.

Epigyne (Fig. 9C–F): weakly sclerotised, with a few setae medially, internal structures of vulva faintly visible via the cuticle. Parmula large, triangular, protruded ventrally. Copulatory openings located on the bilateral corners of parmula base. Spermathecae oval, distally tilted slightly downwards. Copulatory ducts mostly membranous and rugose. Proximal portion of copulatory ducts weakly sclerotised, originating at ventrolateral corners of parmula base, distal portion connected to the posterolateral margin of spermathecae. Fertilisation ducts short, starting at the anterolateral margin of spermathecae.

Distribution. Thailand (Fig. 23).

Patu nigeri Lin & S. Li, 2009

Figures 10, 23

Patu nigeri Lin & Li, 2009: 50, figs 3A, B, 4A, B, 5A–F, 6A and B (♂♀).

Type material. **Holotype** ♂ (IZCAS) and **paratypes** 2♂ 6♀ (IZCAS) **CHINA:** Yunnan Province, Mengla County, Menglun Town, Xishuangbanna Tropical Botanical Garden (21.91667°N, 101.26667°E; 556 m alt.), 19–26.III.2007, G. Zheng leg.

Other material examined. 1♀ (NHMSU-HA058) **CHINA:** Yunnan Province, Mengla County, Menglun Town, Xishuangbanna Tropical Botanic Garden, Rubber-Tea plantation (21.92585°N, 101.28205°E; 561 m alt.), 10–20.VI.2007, G. Zheng leg.; 1♀ (NHMSU-HA129) **CHINA:** Yunnan Province, Gongshan County, Dulongjiang Township, Langwanduo Village, mid-mountain forest (27.70345°N, 98.35133°E; 1473 m alt.), 15.VIII.2018, Y. Lin et al. leg.; 1♀ (NHMSU-HA129) used for sequencing, GenBank: MW970246, same data as preceding.

Diagnosis. The male of *P. nigeri* differs from that of other congeners, except *P. dakou* sp. nov., *P. silho*, and *P. xiaoxiao*, by lacking an exposed embolus (fig. 4A and B in Lin and Li 2009), a median apophysis and a tegular process. The male differs from *P. dakou* sp. nov. by the smaller tegulum (~ ¾ size of that of *P. dakou* sp. nov.) (Fig. 3A vs. fig. 4A in Lin and Li 2009), from *P. silho* by the elongate oval palpal bulb (short oval in *P. silho*)

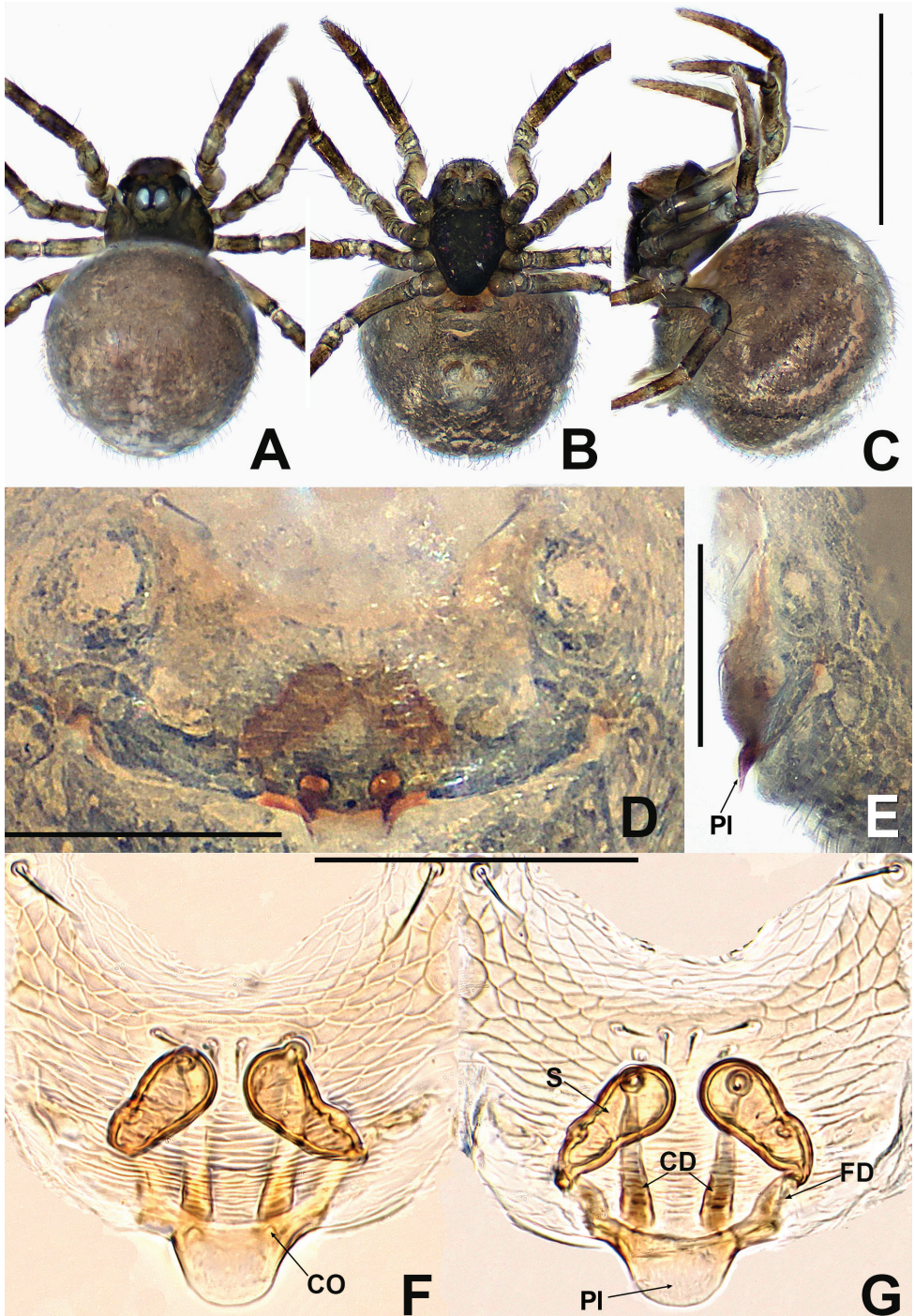


Figure 10. *Patu nigeri* **A** female habitus, dorsal **B** female habitus, ventral **C** female habitus, lateral **D** epigyne, ventral **E** epigyne, lateral **F** vulva, ventral **G** vulva, dorsal. Abbreviations: CD = copulatory ducts; CO = copulatory opening; FD = fertilisation ducts; PI = parma; S = spermathecae. Scale bars: 0.50 (A-C); 0.10 (D-G).

(fig. 4A and B in Lin and Li 2009 vs. fig. 5A and B in Saaristo, 1996) and differs from *P. xiaoxiao* by the absence of a tegular process (finger-like tegular process in *P. xiaoxiao*) (fig. 4A and B in Lin and Li 2009 vs. Fig. 14A and B). The female of *P. nigeri* is similar to that of *P. putao* sp. nov. by the shape of the epigyne (Figs 10D, E, 11D and E) and to *P. qiqi* in the configuration of the vulva (Figs 10G and 12G), but it can be easily distinguished from *P. putao* sp. nov. by the short and straight copulatory ducts, rather than long and twisted as in *P. putao* sp. nov. (cf. Figs 10F–G and 11F–G) and from *P. qiqi* by the tongue-shaped parmula that does not obscure the copulatory openings, rather than an indistinct scape that hides the copulatory openings (cf. Figs 10G and 12G).

Description. See Fig. 10A–G and Lin and Li (2009).

Distribution. China (Yunnan) (Fig. 23).

***Patu putao* S. Li & Lin, sp. nov.**

<http://zoobank.org/3FE3C44A-F22B-4189-A2CC-3D5E4B48B47D>

Figures 11, 23

Type material. *Holotype* ♀ (IZCAS-Ar 41045) **MYANMAR:** Kachin State, Putao, Hponkanrazi Wildlife Sanctuary, near Camp 3, (27.61352°N, 96.98333°E; 2691 m alt.), 11.V.2017, J. Wu and Z. Chen leg.

Etymology. The specific epithet derives from the type locality; noun in apposition.

Diagnosis. This new species is similar to *P. jiangzhou* sp. nov. and *P. nigeri* in the shape of the epigyne, the tongue-shaped parmula and the exposed copulatory openings, but it differs from *P. jiangzhou* sp. nov. by the rounded copulatory openings, the longer copulatory ducts and the larger, reniform spermathecae, rather than trumpet-shaped copulatory openings, shorter copulatory ducts and smaller, oval spermathecae (cf. Figs 11D and F–G vs. 5D and F–G) and from *P. nigeri* by the longer, twisted copulatory ducts that wrap around the spermathecae, rather than the shorter, straight copulatory ducts that do not wrap around the spermathecae (cf. Figs 11G and 10G).

Description. Female (IZCAS-Ar 41045). Total length 0.68. Carapace 0.28 long, 0.28 wide, 0.28 high. Clypeus 0.10 high. Sternum 0.20 long, 0.20 wide. Abdomen 0.52 long, 0.56 wide, 0.56 high. Length of legs: I 0.76 (0.24, 0.08, 0.16, 0.12, 0.16); II 0.68 (0.20, 0.10, 0.12, 0.12, 0.14); III 0.60 (0.18, 0.08, 0.10, 0.12, 0.12); IV 0.74 (0.22, 0.10, 0.16, 0.12, 0.14).

Somatic characters (Fig. 11A–C). **Colouration:** carapace centrally yellow, marginally pale brown. Chelicerae brown, endites and labium dark brownish. Sternum centrally yellow, brown at margins. Femora and patella brown-yellow, other segments dark brown. Abdomen light yellow, dark pigmentation around spinnerets and posterior. **Prosoma:** carapace as long as wide, dorsally pear shaped. ALE > PME > PLE. PME contiguous, PER straight. Chelicerae anterior surface flat, densely covered with short setae. Endites rectangular. Labium subtriangular. Sternum plump, surface smooth, with sparse setae. **Legs:** all patellae with 1 dorsal seta, tibia I and II with 2 dorsal setae, 1 on tibia III and IV. Metatarsi and tarsi densely covered with fine setae. **Opisthosoma:** subrounded dorsally, postgaster area with short setae. Spinnerets dark.

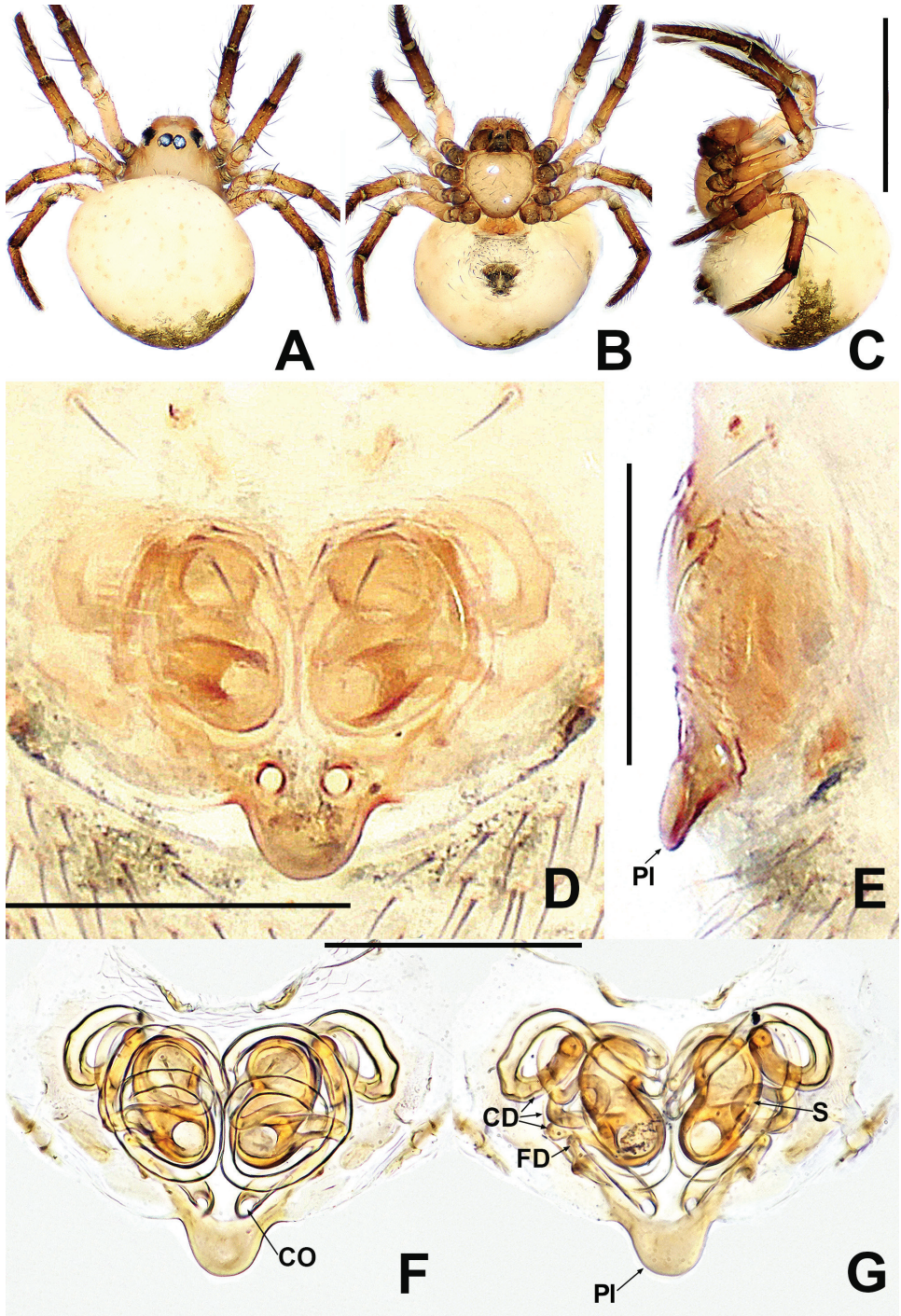


Figure 11. *Patu putao* sp. nov. **A** female habitus, dorsal **B** female habitus, ventral **C** female habitus, lateral **D** epigyne, ventral **E** epigyne, lateral **F** vulva, ventral **G** vulva, dorsal. Abbreviations: CD = copulatory ducts; CO = copulatory opening; FD = fertilisation ducts; PI = parmula; S = spermathecae. Scale bars: 0.50 (**A-C**); 0.10 (**D-G**).

Epigyne (Fig. 11D–G): faintly sclerotised, internal structures faintly visible via the cuticle. Parmula tongue-shaped, protruded, bilateral basal corners concave. Copulatory openings round. Spermathecae kidney shaped, separated by ca. $\frac{1}{2}$ – $\frac{1}{3}$ their width. Copulatory ducts long, with a complex course, twisting around the spermathecae nearly 4 times. Fertilisation ducts short, starting at posterolateral margins of spermathecae.

Male. Unknown.

Distribution. Myanmar (Fig. 23).

***Patu qiqi* Miller, Griswold & Yin, 2009**

Figures 12, 23

Patu qiqi Miller, Griswold & Yin, 2009: 66, figs 65F–H, 67E, F, 73A and B (♂♀).

Type material. **Holotype** ♀ (CASENT 9029328, HNU) and **paratypes** 5♀, 2 juv. (CASENT 9029327, HNU) **CHINA:** Yunnan Province, Gaoligongshan, Nujiang Prefecture, Nujiang State Nature Reserve, Qiqihe, 9.9 air km W of Gongshan (27.715°N, 98.565°E; 2000 m alt.), 9–14.VII.2000, H. Yan et al. leg.

Other material examined. 2♀ (NHMSU-HA122) **CHINA:** Yunnan Province, Gongshan County, at 54 km of from Gongshan County to Dulongjiang Town, in primary forest, leaf litter (27.87840°N, 98.42274°E; 2525 m alt.), 13.VIII.2018, Y. Lin et al. leg.

Diagnosis. The male differs from other *Patu* species, with the exception of *P. nigeri*, *P. silbo* and *P. xiaoxiao*, by the palp with an unexposed embolus (fig. 73A and B in Miller et al. 2009). It differs by having a hooked median apophysis vs. lacking in *P. nigeri* and *P. silbo* (cf. fig. 73A in Miller et al. 2009 and fig. 4A and B in Lin and Li 2009 and fig. 5A and B in Saaristo 1996) and it differs from *P. xiaoxiao* by lacking a tegular process (cf. fig. 73A in Miller et al. 2009 and Fig. 14A). The female is most similar to that of *P. nigeri* in the shape of the epigyne and the configuration of the vulva, but it can be easily distinguished by the indistinct scape and the hidden copulatory openings vs. a tongue-shaped parmula and exposed copulatory openings (cf. Figs 12F–G vs. 10F–G).

Description. See Fig. 12A–G and Miller et al. (2009).

Distribution. China (Yunnan) (Fig. 23).

***Patu xiaoxiao* Miller, Griswold & Yin, 2009**

Figures 13, 14, 23

Patu xiaoxiao Miller, Griswold & Yin, 2009: 67, fig. 67G and H (♀).

Type material. **Holotype** ♀ (CASENT 9022329, HNU) and **paratypes** 1♀ (CASENT 9029325, HNU) **CHINA:** Yunnan Province, Lushui County, Pianma Township, Changyanhe River, 9.3 km of ESE Pianma, mixed broadleaf deciduous and evergreen forest, Winkler extraction of sifted leaf litter (25.99363°N, 98.66651°E; 2470 m alt.), 12.V.2005, C. Griswold leg.

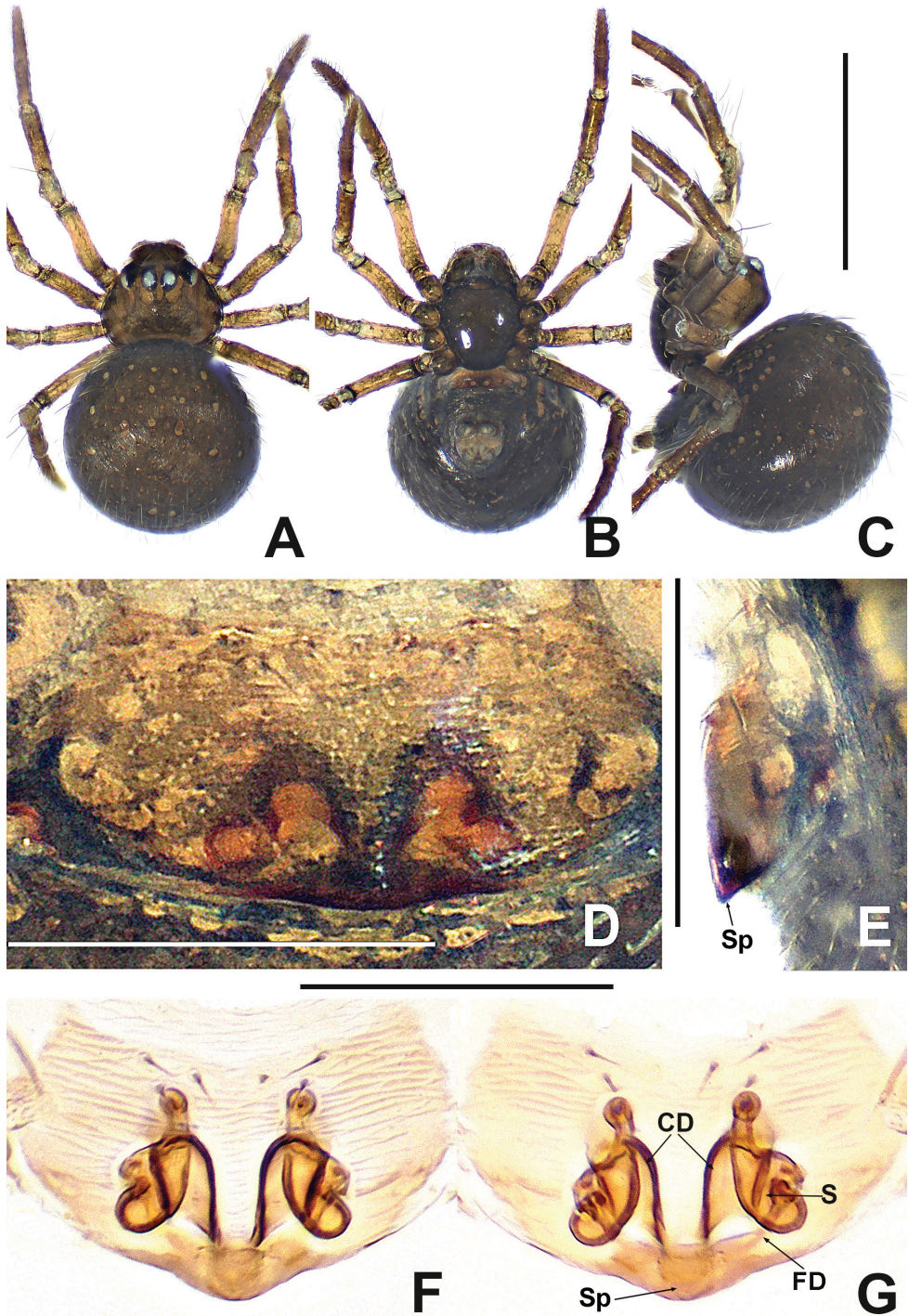


Figure 12. *Patu qiqi* **A** female habitus, dorsal **B** female habitus, ventral **C** female habitus, lateral **D** epigyne, ventral **E** epigyne, lateral **F** vulva, ventral **G** vulva, dorsal. Abbreviations: CD = copulatory ducts; FD = fertilisation ducts; S = spermathecae; Sp = scape. Scale bars: 0.50 (**A-C**); 0.10 (**D-G**).

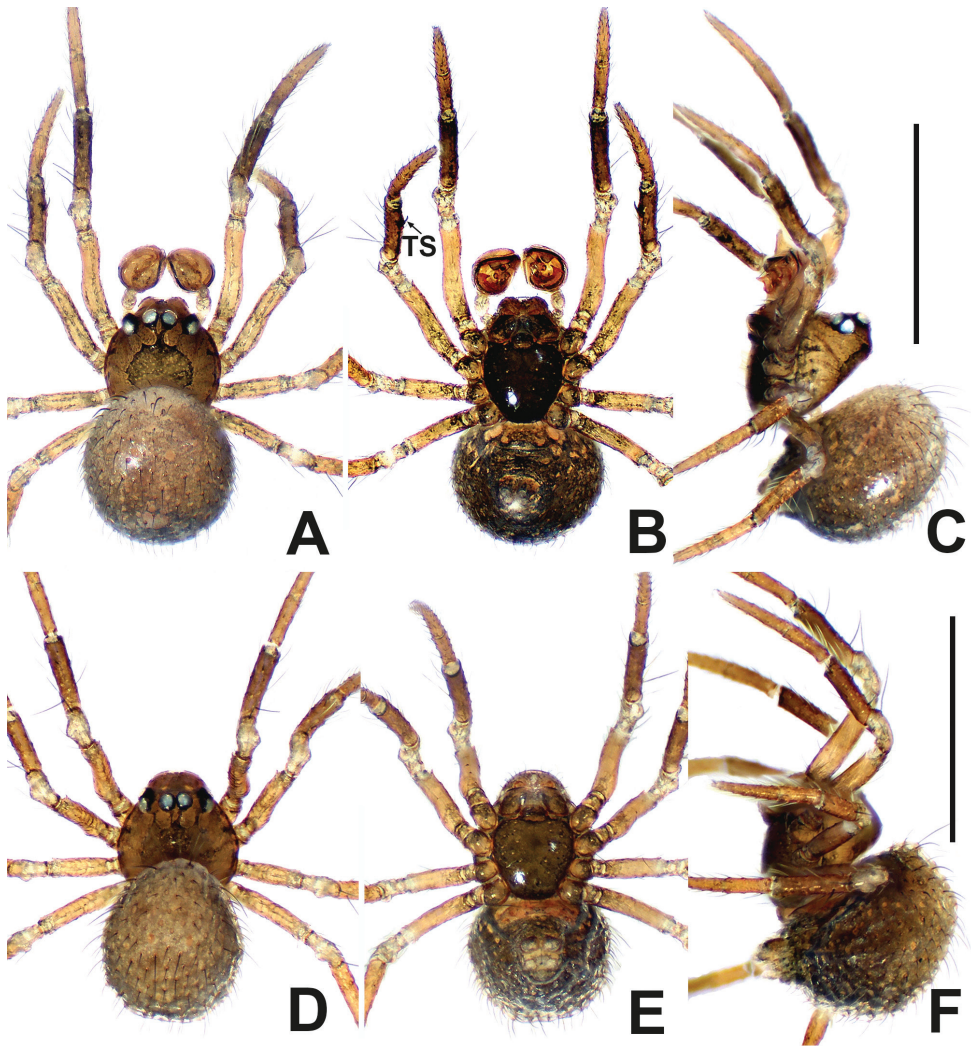


Figure 13. *Patu xiaoxiao* **A** male habitus, dorsal **B** male habitus, ventral **C** male habitus, lateral **D** female habitus, dorsal **E** female habitus, ventral **F** female habitus, lateral. Abbreviation: TS = male clasp spines on tibia II. Scale bars: 0.50 (**A–F**).

Other material examined. 1♂ 1♀ (NHMSU-HA123) **CHINA:** Yunnan Province, Lushui County, Pianma Township, Changyanhe River, 9.3 km of ESE Pianma, mixed broadleaf deciduous and evergreen forest, in leaf litter (25.99363°N, 98.66651°E; 2470 m alt.), 10.VIII.2018, Y. Lin et al. leg.; 1♂ (NHMSU-HA123) and 1♀ (NHMSU-HA123) used for sequencing, GenBank: MW970245 and MW970244, same data as preceding; 2♀ (NHMSU-HA124), Fugong County, Shiyueliang Town, along the road from Shiyueliang to Shibali Village, primary forest (27.15546°N, 98.80573°E; 2193 m alt.), 19.VIII.2018, Y. Lin et al. leg.

Diagnosis. The male of *P. xiaoxiao* can be distinguished from other congeners, with the exception of *P. woodwardi*, by the stout bulb lacking a conductor or me-

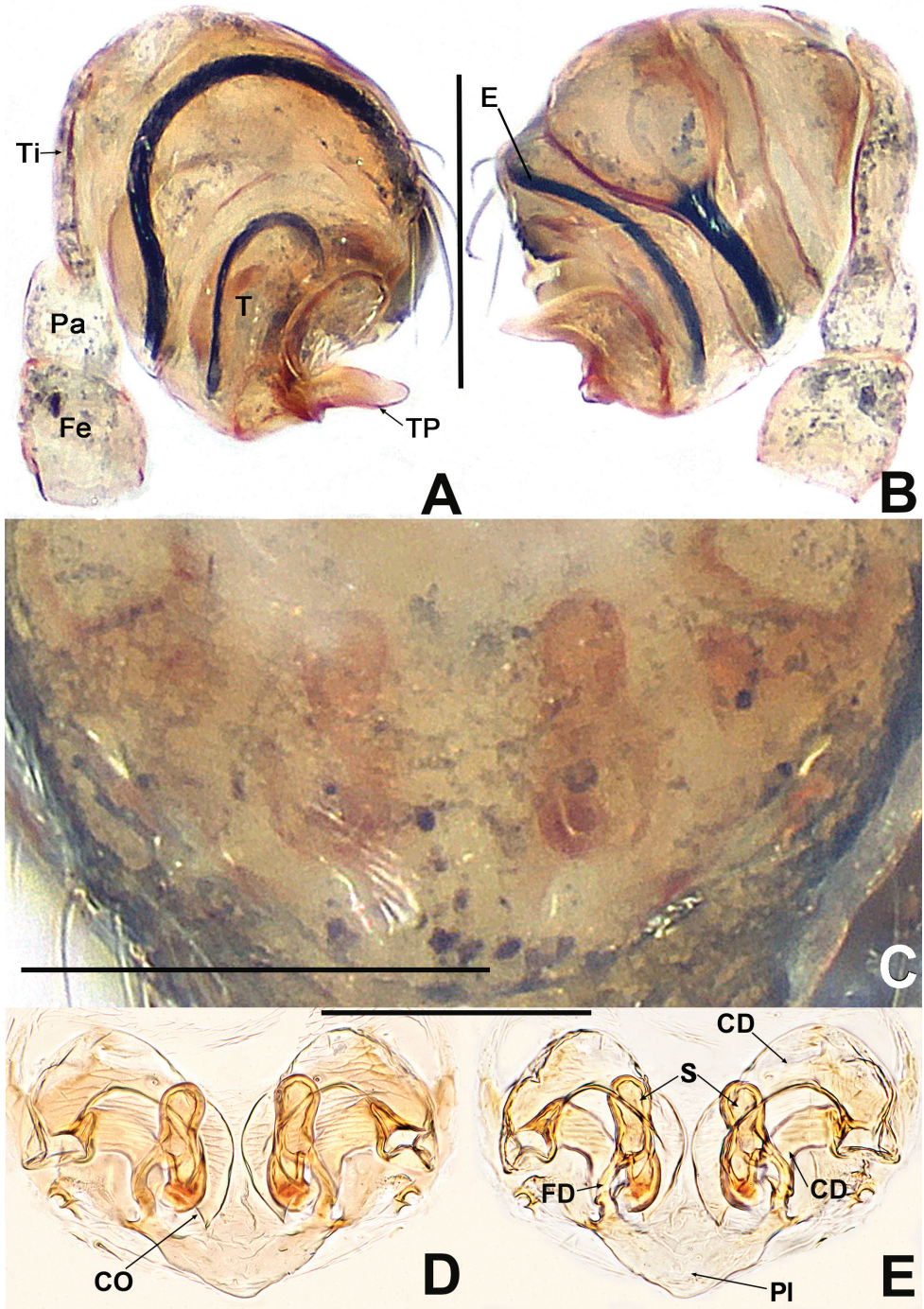


Figure 14. *Patu xiaoxiao* **A** male palp, prolateral **B** male palp, retrolateral **C** epigyne, ventral **D** vulva, ventral **E** vulva, dorsal. Abbreviations: CD = copulatory ducts; Co = conductor; CO = copulatory opening; E = embolus; FD = fertilisation ducts; Fe = femur; MA = median apophysis; Pa = patella; PI = parmula; S = spermathecae; T = tegulum; Ti = tibia; TP = tegular process. Scale bars: 0.10 (**A-E**).

dian apophysis and having a finger-like tegular process (Fig. 14A and B). It differs from *P. woodwardi* by having the entire embolus completely embedded in the bulb (cf. Fig. 14A and B and fig. 120 in Forster 1959). Females of *P. xiaoxiao* differs from those of other congeners by having a wide, triangular parmula, dumb-bell-shaped spermathecae separated by $\sim 1.5\times$ their width and arranged longitudinally in parallel, the copulatory ducts coiling into a loop and connecting to the postero-lateral corner of the spermathecae, the fertilisation ducts begin latero-medially on the spermathecae (Fig. 14C–E).

New morphological data. Male (NHMSU-HA123). Total length 0.56. Carapace 0.28 long, 0.28 wide, 0.28 high. Clypeus 0.12 high. Sternum 0.20 long, 0.20 wide. Abdomen 0.36 long, 0.36 wide, 0.44 high. Length of legs: I 0.80 (0.20, 0.10, 0.20, 0.12, 0.18); II 0.72 (0.20, 0.10, 0.14, 0.12, 0.16); III 0.58 (0.14, 0.08, 0.14, 0.10, 0.12); IV 0.66 (0.18, 0.10, 0.14, 0.12, 0.12).

Somatic characters (Fig. 13A–C). **Colouration:** carapace light brown, thoracic centre and margin with darker patches. Mouthparts nut brown, endites and labium black. Sternum black, with a few light, small dots. Leg colour light yellow gradually grading to very dark brown, tibia darkest brown. Abdomen dorsally light grey, laterally dark greyish, ventrally and posteriorly charcoal black. **Prosoma:** carapace as long as wide, nearly round. Cephalic part vertical anteriorly and sloped posteriorly. Eyes, subequal in size. PER slightly recurved, ALE protruded. Chelicerae anterior surface flat. Labium semi-circular, wider than long. Sternum smooth, slightly plump. **Legs:** each patella with 1 disto-dorsal seta, 1 proximal and 1 disto-dorsal seta on each tibia. Tibia II with 2 ventral clasping spines. **Opisthosoma:** dorsally globose, laterally ovoid, clothed with black, long setae, cuticle rough with dots of varying shades and sizes. Spinnerets dark brown.

Palp (Fig. 14A and B): size $\sim\frac{1}{4}$ of carapace. Femur swollen, wider than patella, patella as long as $\sim\frac{1}{2}$ length of tibia. Tibia flat and lamellar. Tegulum smooth, with finger-like apical process. Embolus long, starting at retrolatero-medial part of tegulum, coiled into 2 loops inside bulb. Tip of embolus hidden within tegulum, not extended from top of bulb.

Female. Total length 0.56. Carapace 0.28 long, 0.28 wide, 0.24 high. Clypeus 0.08 high. Sternum 0.20 long, 0.20 wide. Abdomen 0.36 long, 0.32 wide, 0.40 high. Length of legs: I 0.70 (0.20, 0.06, 0.16, 0.14, 0.14); II 0.62 (0.14, 0.08, 0.14, 0.12, 0.14); III 0.52 (0.12, 0.06, 0.12, 0.08, 0.14); IV 0.60 (0.12, 0.08, 0.16, 0.10, 0.14).

Somatic characters (Fig. 13D–F). **Colouration:** as in male, except lighter mouthparts and sternum. **Prosoma:** carapace longer than wide, pear-shaped. Eye arrangement as in male. PER straight. Cephalic part lower than in male. **Legs:** spination as in male, except for lack of clasping spines on tibia II. **Opisthosoma:** subovoid in dorsal view, cuticle. Spinnerets dark grey.

Epigyne (Fig. 14C–E): faintly sclerotised, internal structures nearly invisible via the cuticle. Parmula triangular, length equal to ca. $\frac{1}{2}$ width, slightly protruded. Spermathecae nearly dumb-bell-shaped, longitudinally parallel, separated by $\sim 1.5\times$ their width. Copulatory openings large. Copulatory ducts translucent, their width equal to ca. $2.5\times$ width of fertilisation ducts and folded at middle, distal part connected

with postero-lateral part of spermathecae. Fertilisation duct shorter than a spermatheca length, narrow, originates from the lateral central position of spermathecae.

Distribution. China (Yunnan) (Fig. 23).

Remarks. *Patu xiaoxiao* was described, based on three females. Based on supplementary materials from the type locality collected in 2018, the male is described for the first time here.

Genus *Kirinua* S. Li & Lin, gen. nov.

<http://zoobank.org/5FD94CCF-CB91-485B-A2BF-6FABEDF07B53>

Type species. *Kirinua maguai* sp. nov., from Guangxi, China.

Etymology. The generic name is derived from Kirin, one of the most powerful creatures ever known in East Asia. The gender is masculine.

Diagnosis. *Kirinua* gen. nov. can be distinguished from *Globignatha* and *Symphytognatha* by the chelicerae, which are fused only near the base (Figs 15I and 17I) vs. entirely fused (Balogh and Loksa 1968: fig. 10; Lin 2019: fig. 1H) and from *Anapistula* by having 6 eyes vs. 4 (except *A. boneti* Forster, 1958 with 6 eyes). It can be distinguished from *Anapogonia*, *Curimagua* and *Iardinis* by 6 eyes in three diads vs. 6 eyes in two triads and from *Crassignatha* and *Swilda* gen. nov. by lacking an abdominal scutum in males and a mostly smooth carapace in both sexes (Figs 15A–H and 17A–H) vs. abdominal scutum usually present in the male and carapace generally covered with tubercles or tiny thorn-like protrusions (Figs 19A, D, 21A and D; Li et al. 2020: fig. 1A–F; Rivera-Quiroz et al. 2021: figs 10b and 11b). *Kirinua* gen. nov. is similar to *Patu* in having 1–2 disto-ventral clasping spines on male tibia II, lacking an abdominal scutum latero-posteriorly in the male and the generally smooth carapace in both sexes (Figs 15A–H and 17A–H), but it can be distinguished by the male palp having cymbial structures (e.g. primary apophysis, process) and the female having nearly spherical spermathecae (Figs 16A, G, 18A and F) vs. male palp lacking cymbial structures and female with rod-shaped or oval spermathecae (Figs 3A, B, F, 9A, B and F).

Description. Tiny, total length 0.60–0.80. Carapace rounded or pear-shaped dorsally, nearly triangular laterally (Figs 15A, 15D, 17A and 17D). Six eyes in 3 diads, cephalic part raised (Figs 15A, 15D, 17A and 17D). Clypeus concave, with pair of inverted, weakly sclerotised grooves in male (Figs 15G, H, 17G and H). Female lacking palps. Chelicerae fused at middle, with 2 adnate teeth (Figs 15I and 17I). Labium wider than long, fused to sternum, anterior margin with shallow notch in the middle (Figs 15B, E, 17B and E). Sternum heart-shaped, slightly plump, truncated posteriorly. Male tibia II with 2 subdistal ventral clasping spines (Figs 15C and 17C). Abdomen round in dorsal view, subovoid in lateral view, without posterior lobes or tubercles (Figs 15C, F, 17C and F). Anterior spinnerets larger than posteriors, median spinnerets hardly visible. Colulus absent.

Male palp (Figs 16A–C, 18A and B): relatively large, ~ ½ size of carapace. Cymbium distinctly sclerotised, with 2 processes and a primary cymbial apophysis. Median

apophysis present, finger-like, nearly as long as cymbial apophysis. Tegulum with a triangular apical process. Embolus short, stout, strongly sclerotised, tip furcate or blunt.

Epigyne (Figs 16D–G and 18C–F): distinctly sclerotised. Scape present, inconspicuous, inflexible. Spermathecae globose, separated by at least 2 diameters. Copulatory ducts long, proximally fused, expanded into a broad atrium, distally curved or coiled between spermathecae. Fertilisation ducts short, thin. Inlet of copulatory duct and outlet of fertilisation duct nearly located at same position on spermatheca.

Composition. *Kirinua maguai* sp. nov. and *K. yangshuo* sp. nov.

Distribution. China (Guangxi) (Fig. 23).

Relationships. *Kirinua* gen. nov. is characterised by their tiny size, chelicerae fused at mid-line, AMEs and book lungs absent, female lacking palps and tarsi much longer than metatarsi. This new genus is similar to *Patu* by having 2 clasping spines on male tibia II, lacking an abdominal scutum latero-posteriorly in the male and the carapace of both sexes lacks modified pits or sculpturing (Figs 15A–H and 17A–H). The new genus differs from *Patu* by the highly modified structures of the cymbium (e.g. primary apophysis, process) and the epigyne has nearly spherical spermathecae and a broad atrium (Figs 16A, G, 18A and F).

***Kirinua maguai* S. Li & Lin, sp. nov.**

<http://zoobank.org/F32044F2-1449-4A5F-BC7F-5EC66AB5596A>

Figures 15, 16, 23

Type material. **Holotype** ♂ (IZCAS-Ar 41046) and **paratype** 1♀ (IZCAS-Ar 41047) **CHINA:** Guangxi Zhuang Autonomous Region, Hechi City, Fengshan County, Pingle Township, Maguai Cave (24.43194°N, 106.96737°E, 618 m alt.), 23.III.2015, Y. Li and Z. Chen leg.; 1♀ (NHMSU-HA008) used for sequencing, GenBank: MW970250, same data as for preceding.

Other material examined. 1♀ (NHMSU-HA005) **CHINA:** Guangxi Zhuang Autonomous Region, Hechi City, Fengshan County, Pingle Township, Sanmen Cave (24.43163°N, 106.97124°E, 659 m alt.), 23.III.2015, Y. Li and Z. Chen leg.; 1♀ (NHMSU-HA011) same Province and County, Fengcheng Township, nameless cave (24.31023°N, 107.00213°E, 402 m alt.), 24.III.2015, Y. Li and Z. Chen leg.; 1♂ prosoma (NHMSU-HA016) same region, Hechi City, Donglan County, Bala Township, nameless cave (24.44368°N, 107.34726°E, 385 m alt.), 18.III.2015, Y. Li and Z. Chen leg.

Etymology. The specific epithet derives from the name of the type locality; noun in apposition.

Diagnosis. Males of the new species can be distinguished from those of *K. yangshuo* sp. nov. by the shorter, distally blunt embolus vs. a distally sharp, longer embolus (ca. 2× length of the former) and by a blunt cymbial apophysis vs. a truncated cymbial apophysis (Figs 16A and 18A). The female differs from that of *K. yangshuo* sp. nov. by the small atrium without a knob-shaped lateral hump vs. a large atrium with a knob-shaped lateral hump and by the shorter, copulatory duct coiled less than 2 times vs. the longer copulatory duct coiled more than 5 times (Figs 16F–G and 18E–F).

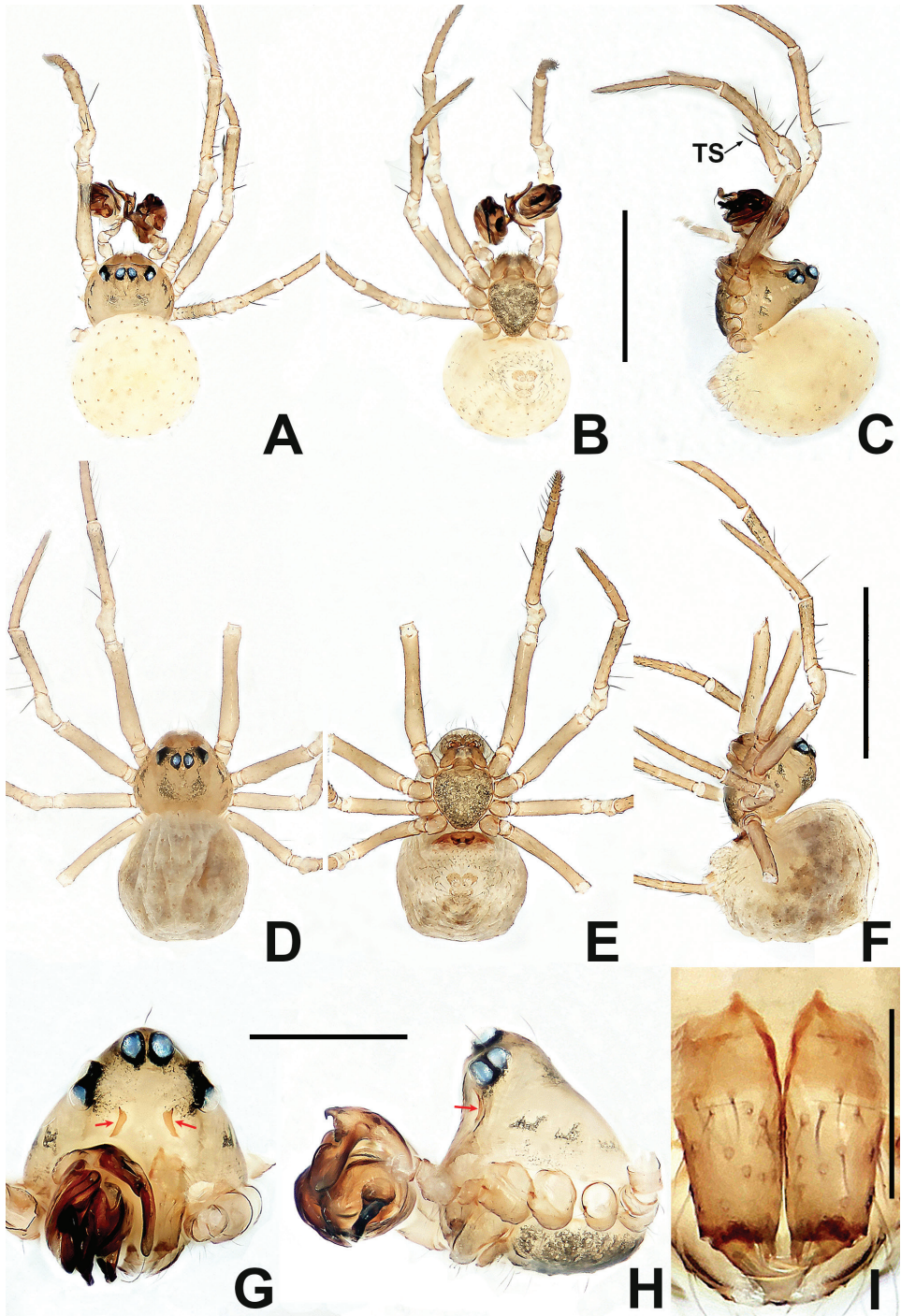


Figure 15. *Kirinua maguai* sp. nov. **A** male habitus, dorsal **B** male habitus, ventral **C** male habitus, lateral **D** female habitus, dorsal **E** female habitus, ventral **F** female habitus, lateral **G** male prosoma, anterior **H** male prosoma, lateral **I** male chelicerae, anterior. Abbreviation: TS = male clasp spines on tibia II. Scale bars: 0.50 (**A-F**); 0.20 (**G, H**); 0.10 (**I**).

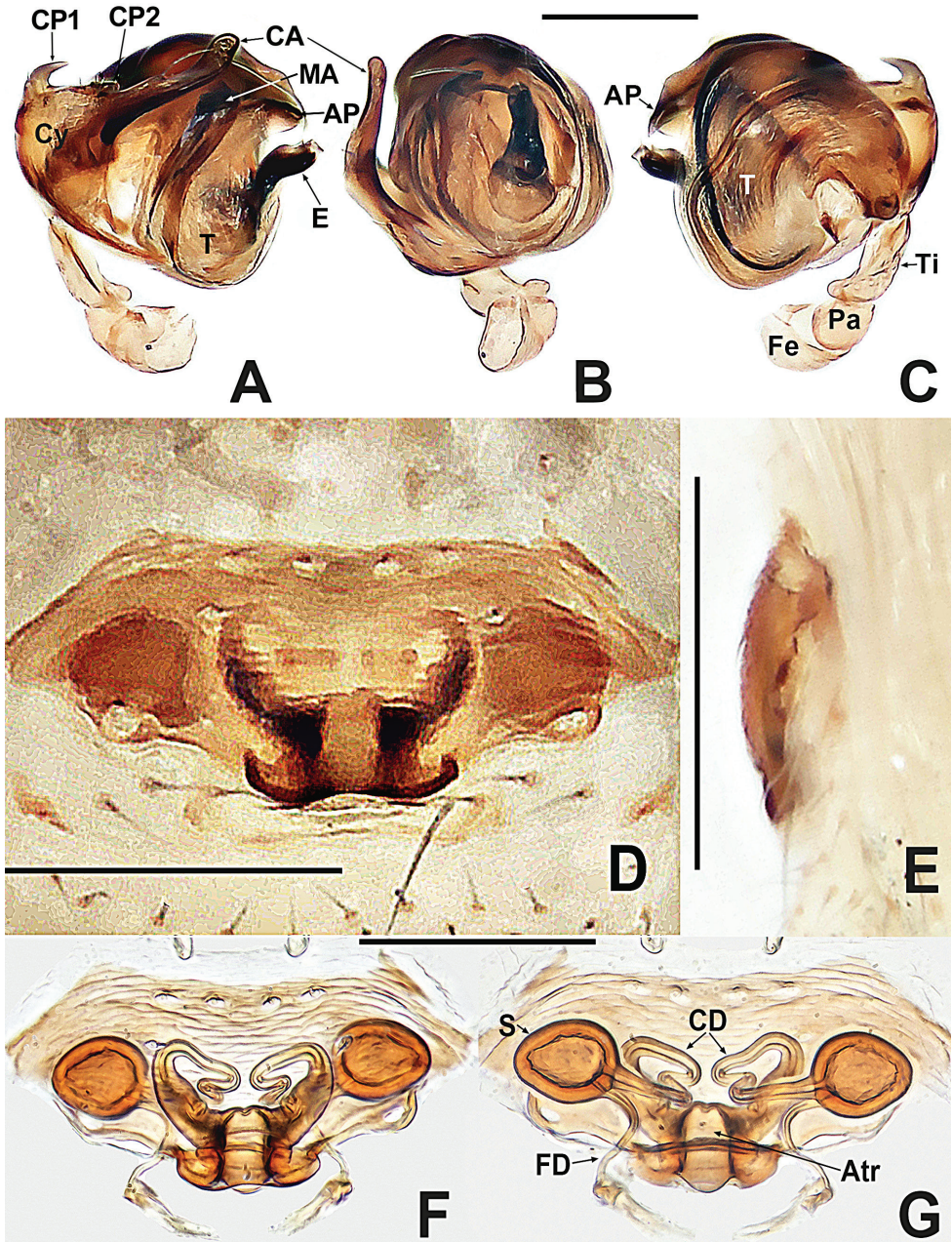


Figure 16. *Kirinua maguai* sp. nov. **A** male palp, prolateral **B** male palp, ventral **C** male palp, retrolateral **D** epigyne, ventral **E** epigyne, lateral **F** vulva, lateral **G** vulva, ventral, dorsal. Abbreviations: Atr = atrium; AP = apical process; CA = cymbial apophysis; CD = copulatory ducts; Co = conductor; CO = copulatory opening; Cy = cymbium; CP1 = proximal cymbial process; CP2 = distal cymbial process; E = embolus; FD = fertilisation ducts; Fe = femur; MA = median apophysis; Pa = patella; S = spermathecae; T = tegulum; Ti = tibia. Scale bars: 0.10 (**A–G**).

Description. Male (IZCAS-Ar 41046). Total length 0.64. Carapace 0.32 long, 0.28 wide, 0.32 high. Clypeus 0.10 high. Sternum 0.20 long, 0.16 wide. Abdomen 0.44 long, 0.44 wide, 0.52 high. Length of legs: I 1.08 (0.30, 0.12, 0.24, 0.18, 0.24); II 0.98 (0.30, 0.12, 0.20, 0.14, 0.22); III 0.74 (0.20, 0.10, 0.14, 0.16, 0.14); IV 0.94 (0.32, 0.10, 0.20, 0.12, 0.20).

Somatic characters (Fig. 15A–C and G–I). **Colouration:** carapace pale yellow, with irregular darker patches at thoracic area and margins. Mouthparts pale brown. Sternum light grey. Legs pale yellow. Abdomen pale. **Prosoma:** carapace longer than wide, as long as high. ALE largest, PME smallest, PER slightly recurved. Clypeus slightly concave. Clypeal notches separated by width of PME (Fig. 15G). Chelicerae covered with sparse, long setae anteriorly. Endites longer than wide. Labium wider than long, with shallow notch on anterior margin. Sternum slightly plump. **Legs:** each patella with 1 disto-dorsal seta, tibia with 2 dorsal setae, 1 subproximal and 1 subdistal, metatarsus I with 1 subproximal dorsal seta. **Opisthosoma:** round in dorsal view and ovoid in lateral view, with sparse, long setae, posteriorly extended beyond spinnerets. Spinnerets light yellow.

Palp (Fig. 16A–C): strongly sclerotised. Femur and patella swollen, tibia longer than femur or patella, with a small retrolateral basal tubercle. Cymbium large, with 1 hook-like process, 1 nodular process with few short setae and 1 long, finger-like distal cymbial apophysis. Bulb flattened. Median apophysis strip-shaped, located below cymbial apophysis. Rugose tegulum with triangular apical process. Embolus stiff, shorter than median apophysis, slightly bent at middle, blunt distally.

Female (IZCAS-Ar 41047). Total length 0.64. Carapace 0.32 long, 0.32 wide, 0.28 high. Clypeus 0.10 high. Sternum 0.20 long, 0.20 wide. Abdomen 0.44 long, 0.40 wide, 0.48 high. Length of legs: I 1.10 (0.34, 0.14, 0.22, 0.18, 0.22); II 0.96 (0.28, 0.12, 0.20, 0.16, 0.20); III 0.78 (0.24, 0.10, 0.12, 0.14, 0.18); IV 0.92 (0.26, 0.12, 0.20, 0.14, 0.20).

Somatic characters (Fig. 15D–F). **Colouration:** same as in male. **Prosoma:** carapace nearly pear-shaped in dorsal view. Cephalic part elevated, lower than in male. PER slightly procurved. **Legs:** spination of each leg as in male. **Opisthosoma:** as in male, except for wrinkled abdominal cuticle that may be caused by ethanol dehydration.

Epigyne (Fig. 16D–G) internal structures faintly visible via the translucent epigynal cuticle. Scape barely visible. Vulva relatively complex. Spermathecae subglobose, close to posterior margin, separated by about 2 diameters. Fertilisation duct thinner than copulatory duct, located dorso-posteriorly on copulatory duct, originates from posteromedial margin of spermatheca, curved outwards at sides of atrium, then extended downwards (Fig. 16G).

Distribution. China (Guangxi) (Fig. 23).

***Kirinua yangshuo* S. Li & Lin, sp. nov.**

<http://zoobank.org/A5AFCA25-600D-4825-ACA6-91733DFC91B8>

Figures 17, 18, 23

Type material. *Holotype* ♂ (IZCAS-Ar 41048) and *paratypes* 2♀ (IZCAS-Ar 41049, 41050) CHINA: Guangxi Zhuang Autonomous Region, Guilin City, Yangshuo County, Xinping Township, Bingshiyan Cave (24.94477°N, 110.60615°E), 11.I.2013, J. Du

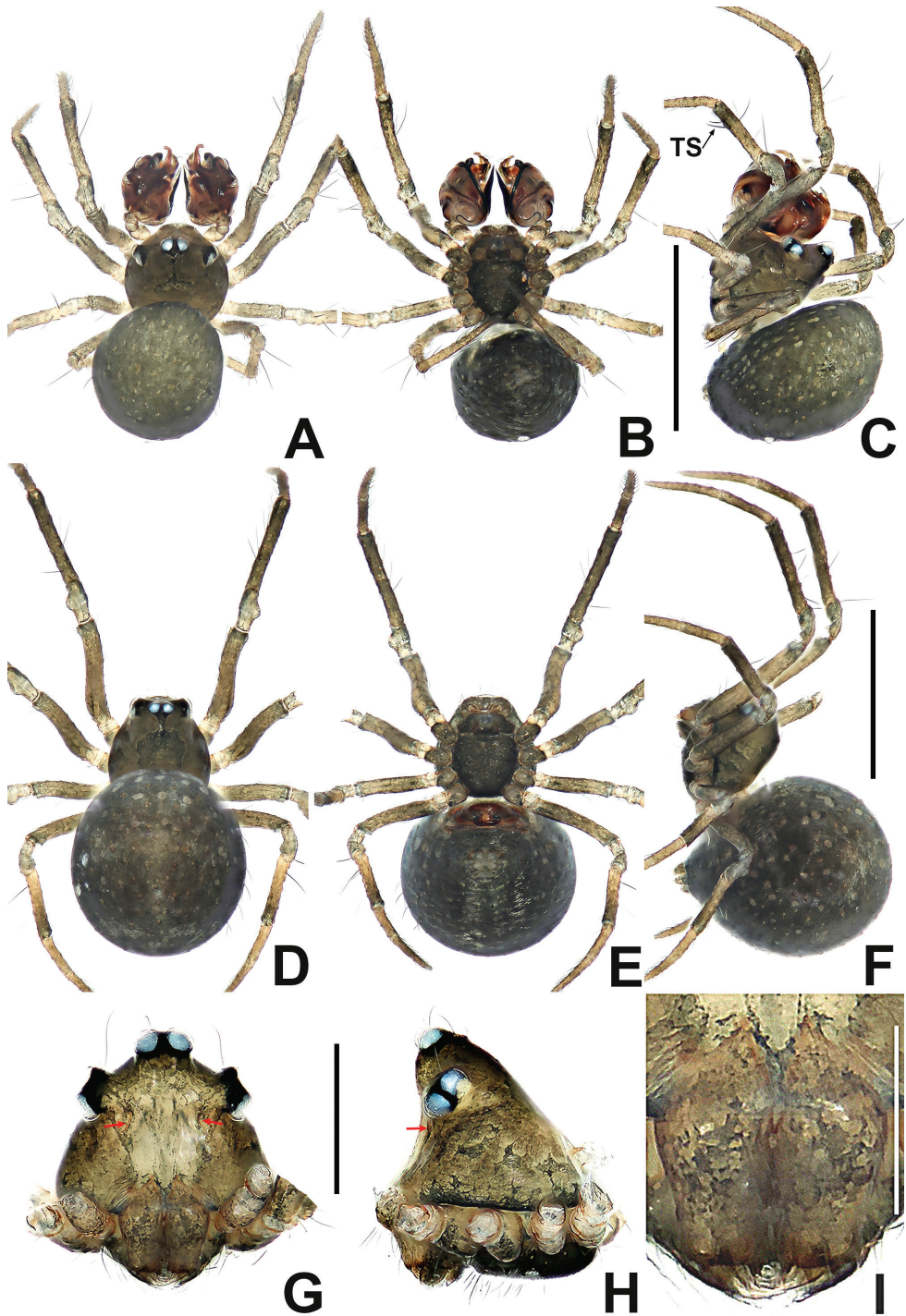


Figure 17. *Kirinua yangshuo* sp. nov. **A** male habitus, dorsal **B** male habitus, ventral **C** male habitus, lateral **D** female habitus, dorsal **E** female habitus, ventral **F** female habitus, lateral **G** male prosoma, anterior **H** male prosoma, lateral **I** male chelicerae, anterior. Abbreviation: TS = male clasp spines on tibia II. Scale bars: 0.50 (**A–F**); 0.20 (**G, H**); 0.10 (**I**).

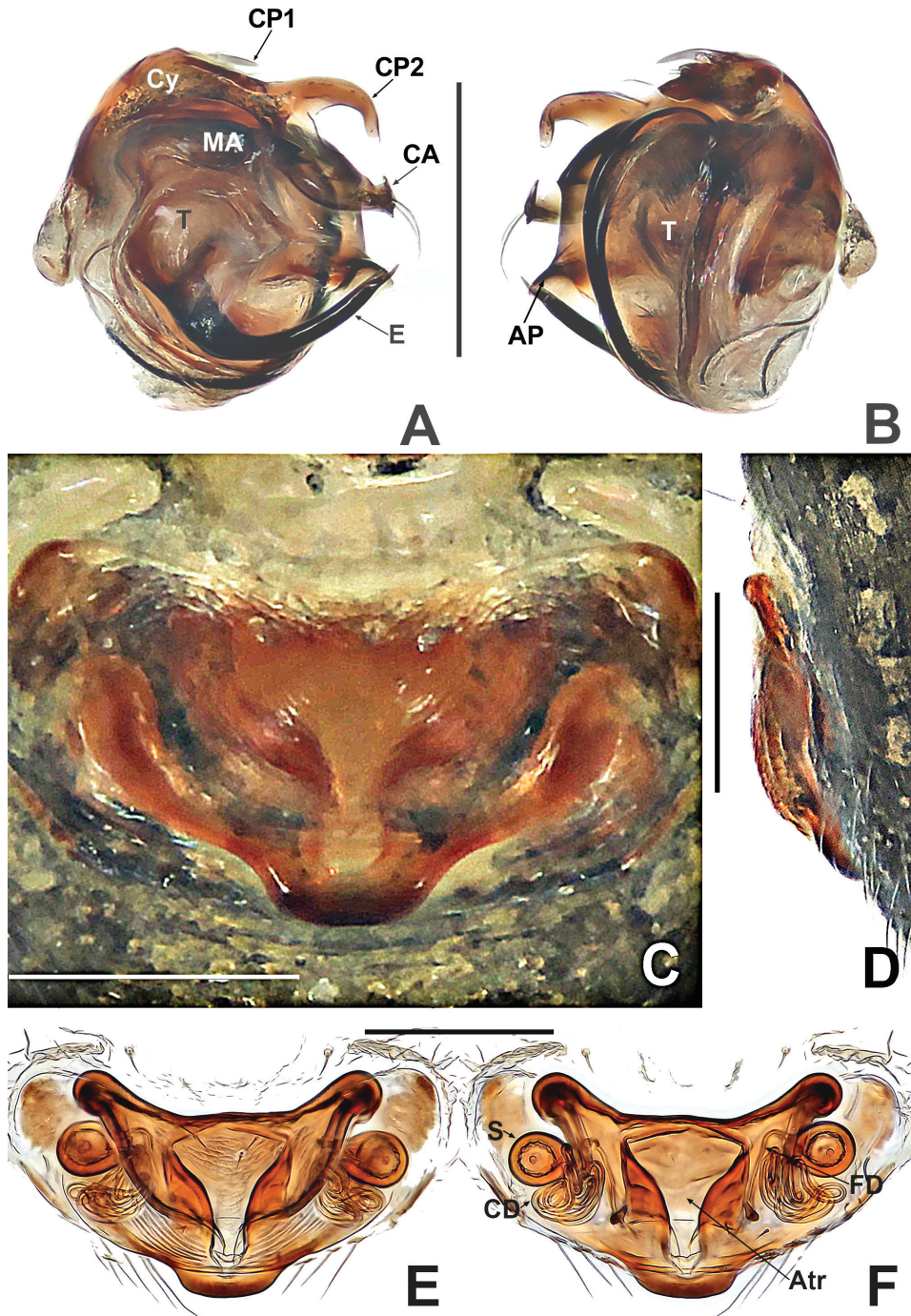


Figure 18. *Kirinua yangshuo* sp. nov. **A** male palp, prolateral **B** male palp, retrolateral **C** epigyne, ventral **D** epigyne, lateral **E** vulva, ventral **F** vulva, dorsal. Abbreviations: Atr = atrium; AP = apical process; CA = cymbial apophysis; CD = copulatory ducts; Co = conductor; CO = copulatory opening; Cy = cymbium; CP1 = proximal cymbial process; CP2 = distal cymbial process; E = embolus; FD = fertilisation ducts; MA = median apophysis; S = spermathecae; T = tegulum. Scale bars: 0.10 (**A-F**).

and X. Wang leg.; 1♂ juvenile (NHMSU-HA018) and 1♀ (NHMSU-HA018) used for sequencing, GenBank: MW970236 and MW970235, same data as for preceding.

Etymology. The specific epithet derives from the name of the type locality; noun in apposition.

Diagnosis. See diagnosis for *K. maguai* sp. nov.

Description. Male (IZCAS-Ar 41048). Total length 0.60. Carapace 0.28 long, 0.24 wide, 0.36 high. Clypeus 0.20 high. Sternum 0.16 long, 0.16 wide. Abdomen 0.28 long, 0.28 wide, 0.48 high. Length of legs: I 1.04 (0.30, 0.12, 0.24, 0.14, 0.24); II 0.86 (0.24, 0.12, 0.20, 0.10, 0.20); III 0.66 (0.16, 0.10, 0.12, 0.10, 0.18); IV 0.82 (0.26, 0.10, 0.16, 0.14, 0.16).

Somatic characters (Fig. 17A–C and G–I). **Colouration:** body dark, nearly black. Legs light brown, with black pigmentation. **Prosoma:** carapace longer and higher than wide. Cephalic apex at PME position. ALE > PLE = PME, PME separated by ca. half a radius, PER recurved. Clypeus concave, paired notches separated by more than width of PME (Fig. 17G and H). Labium short, with shallow notch. **Legs:** each patella with 1 long dorsal seta, each tibia with 2 long dorsal setae. **Opisthosoma:** shape as in *K. maiguai* sp. nov., spinnerets dark.

Palp (Fig. 18A and B): strongly sclerotised. Proximal cymbial process (CP1) small, sharp, needle-like, distal cymbial process (CP2) large, hooked. Cymbial apophysis (CP) truncated, with 2 distal long setae. Distal bifurcation of median apophysis located directly below the hooked CP2 (Fig. 18A). Tegulum translucent, weakly rugose, with a triangular apical process. Embolus longer than median apophysis, robust, horn-like, strongly sclerotised, gradually tapering, bent at nearly proximal 1/3, forked at terminus.

Female (IZCAS-Ar 41049). Total length 0.80. Carapace 0.32 long, 0.28 wide, 0.32 high. Clypeus 0.10 high. Sternum 0.20 long, 0.20 wide. Abdomen 0.52 long, 0.52 wide, 0.60 high. Length of legs: I 1.20 (0.40, 0.10, 0.30, 0.18, 0.22); II 0.90 (0.22, 0.12, 0.22, 0.14, 0.20); III 0.74 (0.20, 0.10, 0.14, 0.10, 0.20); IV 0.86 (0.26, 0.10, 0.18, 0.12, 0.20).

Somatic characters (Fig. 17D–F). **Colouration:** same as in male. **Prosoma:** carapace longer than wide, as long as high. Cephalic part lower than in male, flat dorsally. PER slightly recurved. **Legs:** spination of each leg as in male. **Opisthosoma:** laterally oviform. Spinnerets Located ventrally.

Epigyne (Fig. 18C–F): plate wider than long, strongly sclerotised. Scape wider than long, slightly protruded. Spermathecae globose, separated by more than 3.5 diameters. Copulatory ducts long, their proximal parts enlarged, forming a broad, inverted, subtriangular atrium, with knob-shaped lateral humps; middle part coiled more than 5 times; distal part connected longitudinally to spermatheca. Fertilisation duct slightly bent, runs along lateral wall of atrium, originating above coiled part of copulatory duct.

Distribution. China (Guangxi) (Fig. 23).

Genus *Swilda* S. Li & Lin, gen. nov.

<http://zoobank.org/CC843E39-93C5-44A5-9C50-5E7ABBF17B21>

Type species. *Crassinatha longtou* Miller, Griswold & Yin, 2009, from Gaoligong Mountain, south-western China.

Etymology. The generic name *Swilda* is derived from the Swild Studio (in Chinese: Xi Nan Shan Di Gong Zuo Shi). It is named after the organisation in honour of its dedication to promoting public advocacy for wildlife conservation and nature education in southwest China. The gender is masculine.

Diagnosis. *Swilda* gen. nov. is easily distinguished from other symphytognathids, except *Crassignatha*, by having an anteromedially-split dorsal scutum in the male and a highly ornamented spinous and pitted carapace in both sexes (Figs 19A, D, 21A and D). It resembles *Crassignatha* in carapace texture and the spherical spermathecae. The male differs from those of *Crassignatha* by having a conductor and lacking a cymbial tooth (Figs 20A and 22A) vs. lacking a conductor, but having a cymbial tooth (figs 2A, 8A and 10A in Li et al. 2020); the female differs in lacking a scape and by the separated copulatory openings (Figs 20F and 22E) vs. having a protruded scape and the adnate copulatory openings located at the apex of the scape in *Crassignatha* (figs 2G, 4G and 8G in Li et al. 2020).

Description. Minute, body length 0.50–1.00. Carapace rounded or pyriform, strongly sclerotised, surface spinous and pitted (Figs 19A, 19D, 21A and 21D). Cephalic part raised, higher in male than in female. Six eyes, white, in 3 diads. Clypeus high, more than 2× diameter of ALE, concave. Chelicerae fused at middle, with 1 bifid tooth. Labium tongue-shaped, fused to coarse, pitted sternum. Sternum heart-shaped, slightly plump, truncated posteriorly (Figs 19B, 19E, 21B and 21E). Male tibia II with one clasping spine (Figs 19B and 21B). Abdomen globose in both sexes, male usually with a weakly sclerotised abdominal scutum split at mid-line (Figs 19A and 21A), sclerotised annular plate encircles spinnerets (Figs 19B, 19E, 21B and 21E). Colulus absent.

Pedicle orifice wide, wider than epigyne, with 2 pairs of lateral setae, posterior margin rebordered. Epigastric scutum distinctly sclerotised ventrally (not encircling pedicle).

Male palp (Figs 20A, B, 22A and B): femur swollen, wider than patella, tibia lamellar. Bulb oblate; cymbium well developed, covers bulb on prolatero-ventral side, with 2 processes (CP1, CP2). Median apophysis present. Conductor longer than median apophysis, protruded out of bulb. Embolus long, tubular, sclerotised, originates at prolateral margin of tegulum, curved and extended beneath distal part of cymbium.

Epigyne (Figs 20C–F and 22C–E): sclerotised, posterior margin slightly protruded. Parmula inconspicuous. Copulatory openings separated, located at posterior margin. Spermathecae globose, separated by less than 2 diameters. Copulatory ducts slender, twisted, encircling spermathecae, connected to anteromedial surface of spermathecae. Fertilisation ducts originate at posterolateral surface of spermathecae.

Composition. *Swilda longtou* (Miller et al, 2009) comb. nov. and *S. spinathoraxi* (Lin & Li, 2009) comb. nov.

Relationships. *Swilda* gen. nov. is characterised by its tiny size, fused chelicerae at mid-line, AMEs and book lungs absent, female lacking palps and tarsi much longer than metatarsi. Here, the male of *C. longtou* is described for the first time and specimens of *P. spinathoraxi* are re-examined. We found the morphological features of these two species to be very similar to those of *Crassignatha* (see Li et al. 2020: 65), sharing the following combination of characters: a clasping spine on tibia II and an abdominal

scutum latero-posteriorly in the male and a decorated carapace and sclerotised epigastric scutum in both sexes (Figs 19A–F and 21A–F). The differences between these two species and *Crassinatha* are: a pitted and spinous carapace, a sclerotised annular plate that encircles the spinnerets (cf. Figs 19A–F and 21A–F vs. figs 1A–F and 7A–F in Li et al. 2020), only 1 male clasping spine (cf. Figs 19B and 21B vs. figs 1B and 12C in Li et al. 2020: only 1 spine in a few species), male palps lack a cymbial tooth, but have a conductor (cf. Figs 20A and 22A vs. figs 2A and 8A in Li et al. 2020) and the epigyne lacks a protruded scape (cf. Figs 20E–F and 22E–E vs. figs 2E and 6E in Li et al. 2020).

The genetic distance we estimated, based on COI, also indicated differences between these two species and members of other genera (see Appendix Table A1). Phylogenetic analysis of molecular data indicates that *P. spinathoraxi* and *C. longtou* are clearly congeneric. Additionally, the combined genetic evidence from five genes supports the monophyly of *Swilda* gen. nov. and the sister group relationship of the two genera (unpubl. data). Therefore, *Swilda* gen. nov. is proposed as a new genus in which to place *S. longtou* (Miller et al, 2009) comb. nov., transferred from *Crassinatha* and *S. spinathoraxi* comb. nov., transferred from *Patu*. We designate *Swilda longtou* as the type species for this new genus.

Distribution. China (Yunnan) (Fig. 23).

***Swilda longtou*, (Miller et al., 2009), comb. nov.**

Figures 19, 20, 23

Crassinatha longtou Miller, Griswold & Yin, 2009: 76, figs 89E, F, 90A–C, 91A–F and 92A–D (♀).

Type material. *Holotype* ♀ (CASENT 9029292, HNU) and *paratypes* 3♀, 1 juv. (CASENT 9020733, HNU), 2♀ (CASENT 9020732, HNU) **CHINA:** Yunnan Province, 10 km of W Nuijiang on Shibali Rd., N fork, Yamu He, Gaoligongshan, moist earthen embankments (27.13795°N, 98.82240°E; 1850 m alt.), 25.IV.2004, C. Griswold leg.; 1♀ (CASENT 9020740, HNU): Yunnan Province, Fugong County, 4.5 km N of Aludi Village, 22.1 km N of Fugong, in stream gorge (26.10829°N, 98.87162°E; 1250 m alt.), 23.IV.2004, C. Griswold leg.

Other material examined. 5♂, 10♀ (NHMSU-HA112) **CHINA:** Yunnan Province, 10 km of W of Nuijiang on Shibali Rd., N fork, Yamu He, Gaoligongshan, moist earthen embankments (27.13795°N, 98.82240°E; 1850 m alt.), 19.VIII.2018, Y. Lin et al. leg.; 1♂ (NHMSU-HA112) and 1♀ (NHMSU-HA112) used for sequencing, GenBank: MW970249 & MW970241, same data as for preceding. 5♂, 11♀ (NHMSU-HA111): Yunnan Province, Fugong County, Shilajia Village, Yamu He (27.13440°N, 98.82625°E; 1792 m alt.), 19.VIII.2018, Y. Lin et al. leg.

Diagnosis. The male of *S. longtou* can be distinguished from that of *S. spinathoraxi* by the larger proximal cymbial process (CP1), the human-ear-shaped median apophysis and the wider and longer conductor (Fig. 20A) vs. needle-like proximal

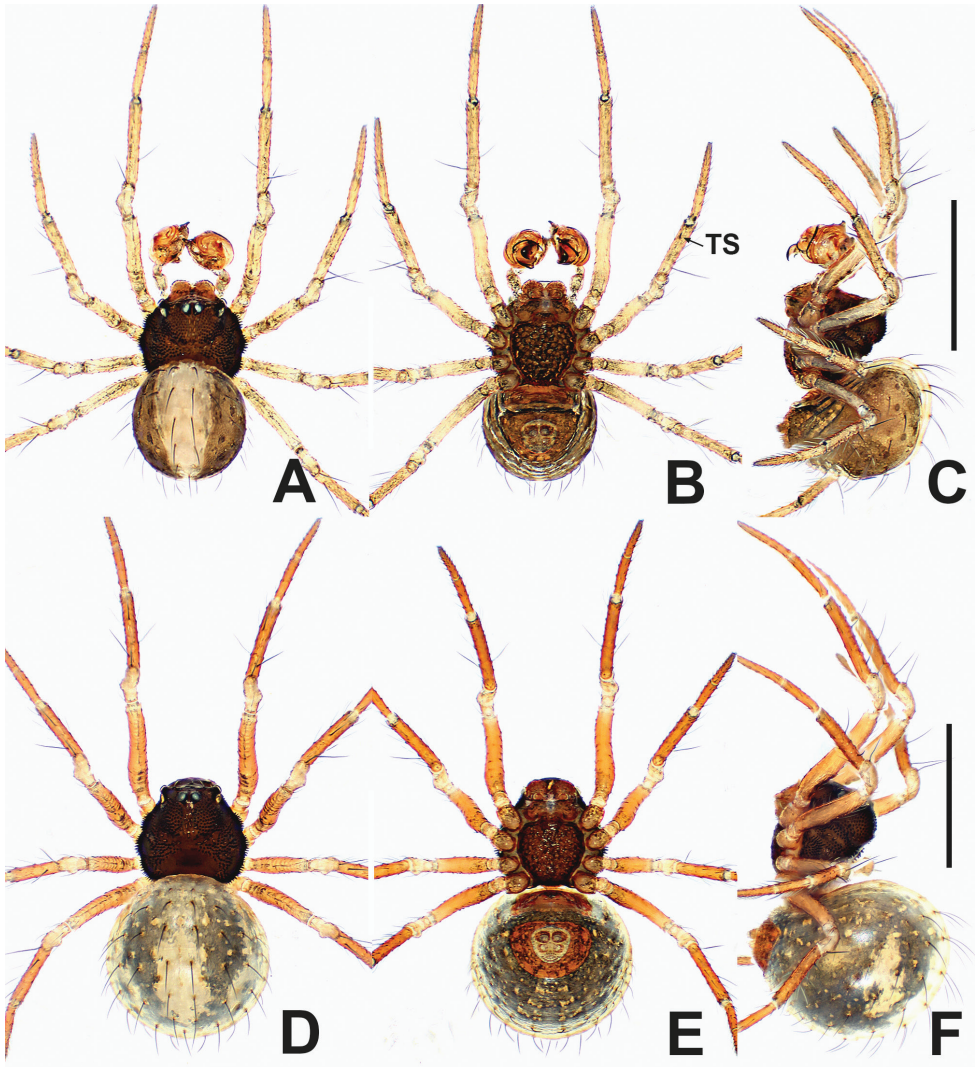


Figure 19. *Swilda longtou* **A** male habitus, dorsal **B** male habitus, ventral **C** male habitus, lateral **D** female habitus, dorsal **E** female habitus, ventral **F** female habitus, lateral. Abbreviation: TS = male clasping spines on tibia II. Scale bars: 0.50 (**A–F**).

cymbial process (CP1), mastoid median apophysis and narrower and shorter conductor (Fig. 21A). The female differs by the separated copulatory openings, spermathecae separated by less than one diameter in *S. longtou* vs. adjacent copulatory openings, spermathecae separated by more than one diameter in *S. spinathoraxi* (cf. Figs 20E and F and 22D and E).

Male (NHMSU-HA112). Total length 0.68. Carapace 0.32 long, 0.36 wide, 0.36 high. Clypeus 0.16 high. Sternum 0.24 long, 0.24 wide. Abdomen 0.44 long, 0.44 wide, 0.48 high. Length of legs: I 1.24 (0.38, 0.14, 0.30, 0.20, 0.22); II 1.00 (0.30,

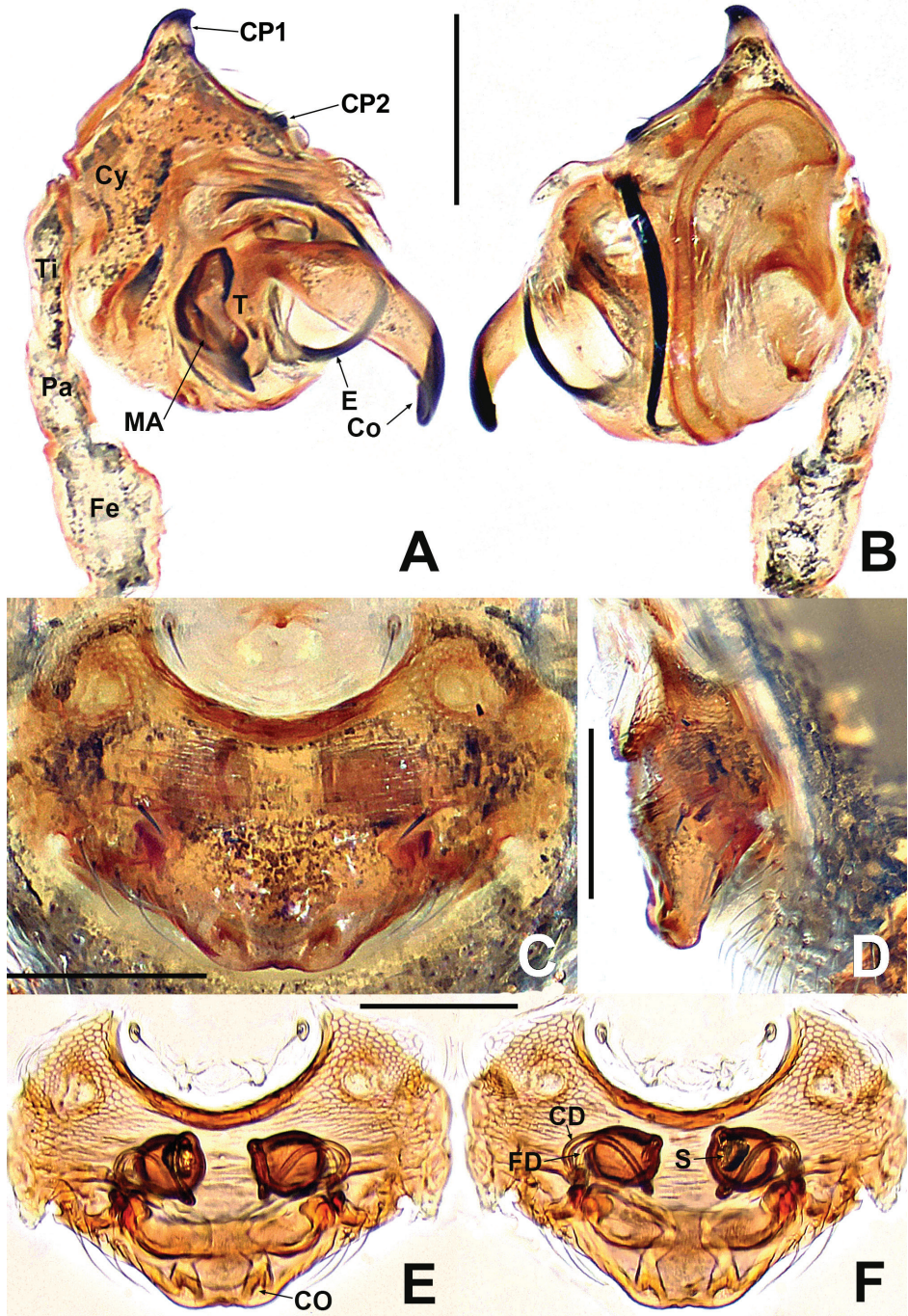


Figure 20. *Swilda longtou* **A** male palp, prolateral **B** male palp, retrolateral **C** epigyne, ventral **D** epigyne, lateral **E** vulva, ventral **F** vulva, dorsal. Abbreviations: CA = cymbial apophysis; CD = copulatory ducts; Co = conductor; CO = copulatory opening; Cy = cymbium; CP1 = proximal cymbial process; CP2 = distal cymbial process; E = embolus; FD = fertilisation ducts; Fe = femur; MA = median apophysis; Pa = patella; S = spermathecae; T = tegulum; Ti = tibia. Scale bars: 0.10 (**A–F**).

0.12, 0.22, 0.16, 0.20); III 0.80 (0.20, 0.10, 0.18, 0.14, 0.18); IV 0.96 (0.26, 0.12, 0.24, 0.18, 0.16).

Somatic characters (Fig. 19A–C). **Colouration:** carapace and sternum dark brown. Chelicerae, endites and labium brown. Abdomen pale dorsally, fuscous laterally and ventrally. **Prosoma:** PME separated by $\sim \frac{3}{4}$ their diameter. ALE protruded, PER slightly recurved. Cervical groove distinct, thoracic fovea shallow. Sternum slightly plump, surface coarse with pits, truncated posteriorly. **Legs:** light brown, distal tibia darker, femora I and II slightly swollen basally. Patella with 1 long dorso-distal seta. Tibia I and II with 2 long dorsal setae, 1 on tibia III and IV. Tibia II with 1 large subdisto-ventral spine. **Opisthosoma:** spherical in dorsal view, with sparse, long setae, with a posterolateral scutum. Spinnerets brown, surrounded by a circular plate.

Palp (Fig. 20A and B): bulb oblate, $\sim \frac{1}{3}$ size of carapace. Cymbium broad retro-laterally, with 2 sclerotised processes, large proximally (CP1) and small distally (CP2). Tegulum smooth. Median apophysis human-ear-shaped. Conductor large, longer than wide, basally constricted, distally curved. Sperm duct originates at prolateral base of bulb, embedded in the bulb. Embolus long, tubular, strongly sclerotised, mesally curved and distally extended below apex of cymbium.

Female (NHMSU-HA112). Total length 0.92. Carapace 0.36 long, 0.36 wide, 0.32 high. Clypeus 0.16 high. Sternum 0.24 long, 0.24 wide. Abdomen 0.56 long, 0.56 wide, 0.64 high. Length of legs: I 1.10 (0.28, 0.14, 0.30, 0.18, 0.20); II 0.96 (0.22, 0.14, 0.22, 0.16, 0.22); III 0.88 (0.22, 0.12, 0.20, 0.12, 0.22); IV 0.94 (0.28, 0.10, 0.22, 0.14, 0.20).

Somatic characters (Fig. 19D–F). Habitus features and modifications as in male, but without postero-lateral scutum.

Epigyne (Fig. 20C–F): sclerotised, with 2 macrosetae and some setae (Fig. 20C). Internal structures faintly visible via translucent cuticle. Globular spermathecae separated by slightly less than one diameter. Fertilisation ducts short, originating anterolaterally on spermathecae. Copulatory ducts long, arising postero-laterally on spermathecae, coiling $1\frac{1}{4}$ times around spermathecae from copulatory openings.

Distribution. China (Yunnan) (Fig. 23).

***Swilda spinathoraxi*, (Lin & Li, 2009), comb. nov.**

Figures 21–23

Patu spinathoraxi Lin & Li, 2009: 60, figs 14A, B, 15A, B, 16A–E, 17A and B (♂♀).

Type material. *Holotype* ♀ (IZCAS) and *paratypes* 15♂ 19♀ (IZCAS) CHINA: Yunnan Province, Mengla County, Menglun Town, Rubber Plantation near Menglun Nature Reserve (21.90000°N, 101.26667°E; 569 m alt.), 1–15.V.2007, G. Zheng leg.; 2♂ 2♀ (IZCAS): Yunnan Province, Mengla County, Menglun Town, Menglun Nature Reserve, rubber-tea plantation (21.91667°N, 101.26667°E; 572 m alt.), 5–12.I.2007, G. Zheng leg.; 2♀ (IZCAS) same locality, secondary seasonal tropical rainforest (21.90000°N, 101.28333°E; 612 m alt.), 10.VIII.2007, G. Zheng leg.

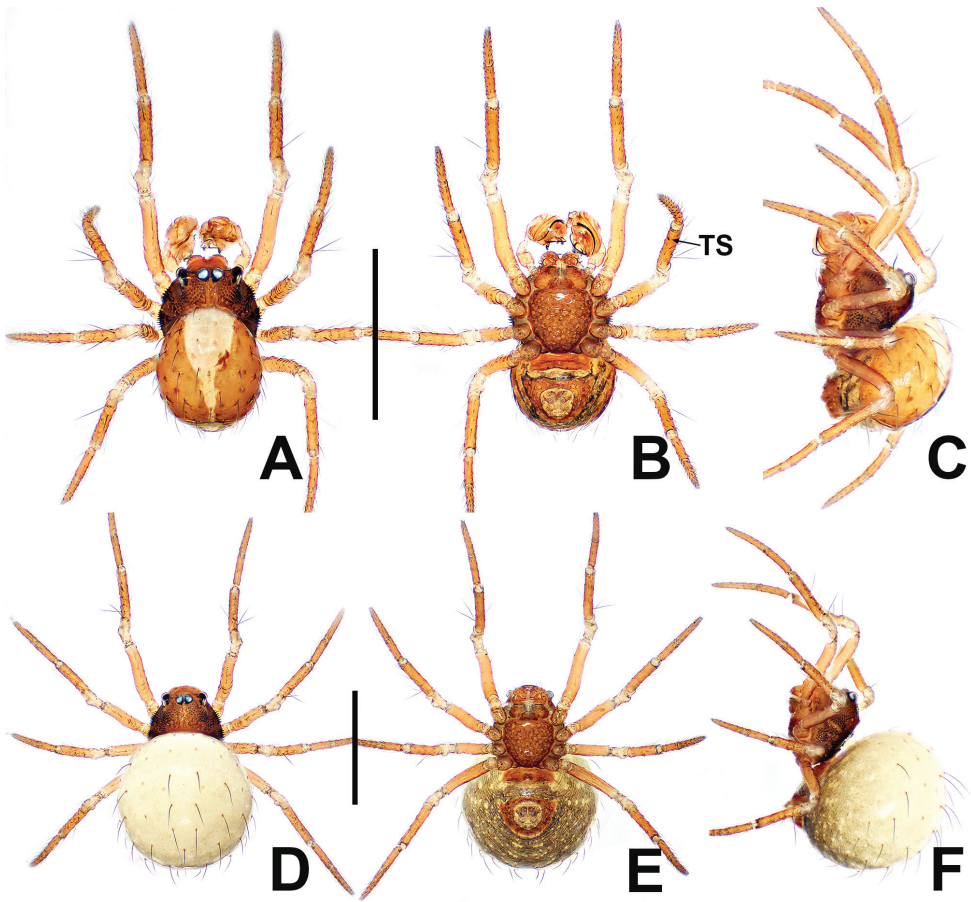


Figure 21. *Swilda spinathoraxi* **A** male habitus, dorsal **B** male habitus, ventral **C** male habitus, lateral **D** female habitus, dorsal **E** female habitus, ventral **F** female habitus, lateral. Abbreviation: TS = male clasp spines on tibia II. Scale bars: 0.50 (**A–F**).

Other material examined. 1♂ 1♀ (NHMSU-HA082) CHINA: Yunnan Province, Mengla County, Menglun Town, Xishuangbanna Tropical Botanic Garden, in forest of *Paramichelia baillonii* (21.91207°N, 101.26836°E; 527 m alt.), 2.X.2017, Y. Lin and Y. Li leg.; 1♂ (NHMSU-HA082) and 1♀ (NHMSU-HA082) used for sequencing, GenBank: MW970238 and MW970237, same data as for preceding; 1♂ (NHMSU-HA060): Yunnan Province, Mengla County, Menglun Town, Xishuangbanna Tropical Botanic Garden, Rubber-Tea plantation (21.91077°N, 101.27095°E, 572 m alt.), 8–12.VIII.2006, G. Zheng leg.; 1♀ (NHMSU-HA076): Yunnan Province, Xishuangbanna Natural Reserve, monsoon forest off greenstone road, in the bamboo forest (21.90707°N, 101.28183°E, 607 m alt.), 24.V.2013, Z. Zhao and Z. Chen leg.

Diagnosis. see diagnosis for *S. longtou*.

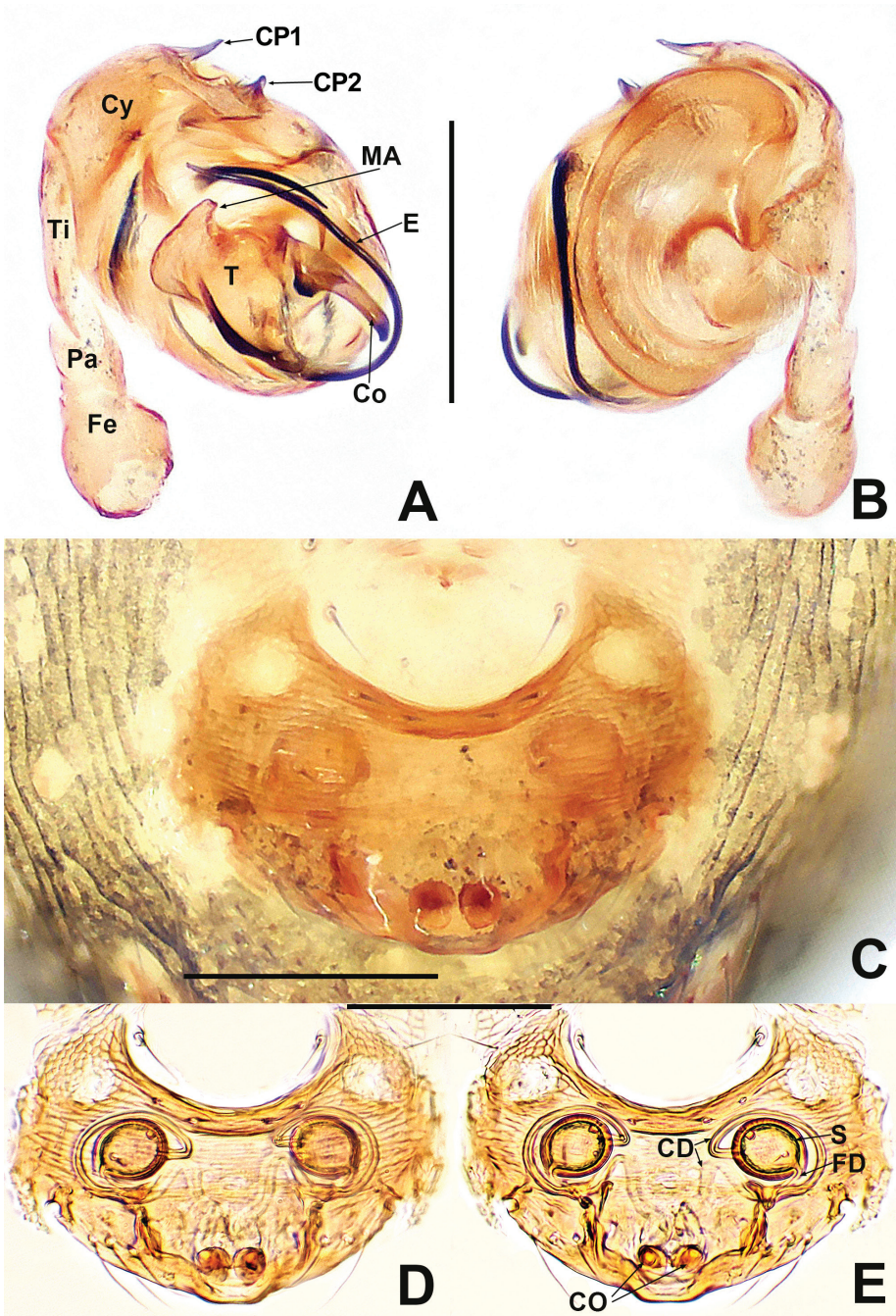


Figure 22. *Swilda spinathoraxi* **A** male palp, prolateral **B** male palp, retrolateral **C** epigyne, ventral **D** vulva, ventral **E** vulva, dorsal. Abbreviations: CA = cymbial apophysis; CD = copulatory ducts; Co = conductor; CO = copulatory opening; Cy = cymbium; CP1 = proximal cymbial process; CP2 = distal cymbial process; E = embolus; FD = fertilisation ducts; Fe = femur; MA = median apophysis; Pa = patella; S = spermathecae; T = tegulum; Ti = tibia. Scale bars: 0.10 (**A-E**).

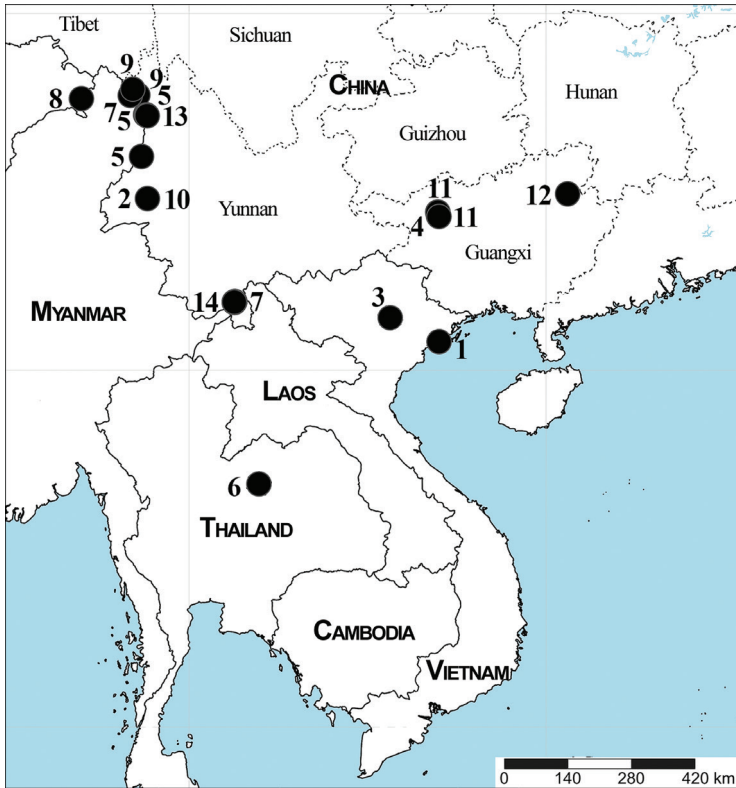


Figure 23. Distribution records of fourteen species of genera *Patu*, *Kirinua* gen. nov. and *Swilda* gen. nov. in Asia 1 *P. catba* sp. nov. 2 *P. dakou* sp. nov. 3 *P. damtao* sp. nov. 4 *P. jiangzhou* sp. nov. 5 *P. jidanweishi* 6 *P. nagarat* sp. nov. 7 *P. nigeri* 8 *P. putao* sp. nov. 9 *P. qiqi* 10 *P. xiaoxiao* 11 *K. maguai* sp. nov. 12 *K. yangshuo* sp. nov. 13 *S. longtou* 14 *S. spinathoraxi*.

Description. Male (NHMSU-HA082). Total length 0.52. Carapace 0.28 long, 0.32 wide, 0.32 high. Clypeus 0.14 high. Sternum 0.20 long, 0.20 wide. Abdomen 0.40 long, 0.32 wide, 0.36 high. Length of legs: I 1.00 (0.28, 0.12, 0.24, 0.16, 0.20); II 0.78 (0.18, 0.12, 0.18, 0.12, 0.18); III 0.58 (0.12, 0.08, 0.12, 0.10, 0.16); IV 0.80 (0.20, 0.12, 0.18, 0.12, 0.18).

Somatic characters (Fig. 21A–C). **Colouration:** carapace brown, sternum light brown ventrally. Legs light brown. Abdomen pale at middle, light brown laterally and ventrally. **Prosoma:** PME separated by $\sim 1/3$ their diameter. ALE protruded, PER slightly recurved. Clypeus concave, smooth. Sternum surface rugose, pitted, slightly plump. **Legs:** with long disto-dorsal spine on patella; 2 long dorsal spines on tibiae I and II, 1 on tibia III and IV. **Opisthosoma:** round dorsally, ovoid laterally, extended posteriorly beyond spinnerets, abdominal surface with sparse, long setae, with a postero-lateral scutum. Spinnerets light brown, surrounded by an annular plate.

Palp (Fig. 22A and B): bulb oblate, femur plump. Cymbium broad, with needle-like apical process and nodular distal one. Tegulum nearly rectangular. Median apophysis small, tubercle-like. Conductor long, wide basally, narrow mesally and distally.

Embolus long, jutting out from prolateral margin of tegulum, curved upwards, extended beneath distal part of cymbium.

Female (NHMSU-HA076). Total length 0.80. Carapace 0.32 long, 0.32 wide, 0.28 high. Clypeus 0.12 high. Sternum 0.20 long, 0.20 wide. Abdomen 0.56 long, 0.56 wide, 0.60 high. Length of legs: I 0.84 (0.24, 0.12, 0.20, 0.12, 0.16); II 0.72 (0.18, 0.10, 0.16, 0.12, 0.16); III 0.60 (0.16, 0.10, 0.12, 0.10, 0.12); IV 0.78 (0.20, 0.10, 0.20, 0.12, 0.16).

Somatic characters (Fig. 21D–F). **Colouration:** prosoma and legs as in male. Abdomen pale dorsally and light grey ventrally. Carapace modified as in male. Cephalic part lower than in male. **Legs:** the spination same as in male, except tibia II lacking clasping spine. **Opisthosoma:** globose, with sparse, long setae, without posterolateral scutum. Other modifications same as in male.

Epigyne (Fig. 22C–E): sclerotised, cuticle weakly rugose. Epigynal posteromargin slightly protruded. Spermathecae separated by ca. 1.5 diameters. Copulatory openings adjacent. Copulatory ducts long, encircle spermathecae, forming $\sim \frac{3}{4}$ loop from posterior to anterolateral connecting with the inner middle margins of spermathecae. Fertilisation ducts short, starting at postero-lateral margin of spermathecae, extending to lateral of posterior epigynal margin.

Distribution. China (Yunnan) (Fig. 23).

Discussion

The taxonomy of genus *Patu* is revised in the current study and the taxonomic positions of some puzzling Asian *Patu* species are resolved. However, the species here are only the “tip of the iceberg” of Asian *Patu* species (Yao et al. 2021, Li et al. 2021) and further studies are necessary to revise the worldwide *Patu* spiders.

Acknowledgements

The manuscript benefited greatly from comments by Yuri Marusik (Magadan, Russia) and an anonymous reviewer. English was checked by Sarah Crews (San Francisco, USA). Yingchun Li (Biodiversity Institute of Gongshan Administration Bureau, Gongshan, China) helped in fieldwork. Xianjin Peng and Xiang Xu (Hunan Normal University, Changsha, China) facilitated the loan of type material of Chinese symphytognathids from the Gaoligong Mountains. This study was supported by the National Natural Science Foundation of China to Yucheng Lin (NSFC-31772410, 31750002, 31972870).

References

Forster RR (1959) The spiders of the family Symphytognathidae. Transactions and Proceedings of the Royal Society of New Zealand 86: 269–329.

- Forster RR, Platnick NI (1977) A review of the spider family Symphytognathidae (Arachnida, Araneae). *American Museum Novitates* 2619: 1–29.
- Hall TA (1999) BioEdit: a user-friendly biological sequence alignment editor and analysis program for Windows 95/98/NT. *Nucleic Acids Symposium Series* 41: 95–98.
- Hickman VV (1931) A new family of spiders. *Proceedings of the Zoological Society of London* (B) 1931: 1321–1328. <https://doi.org/10.1111/j.1096-3642.1931.tb01063.x>
- Khmelik VV, Kozub D, Glazunov A (2006) Helicon Focus 3.10.3. Available from <http://www.heliconsoft.com/heliconfocus.html> [accessed on 10 September 2018]
- Kumar S, Stecher G, Tamura K (2016) MEGA7: Molecular Evolutionary Genetics Analysis Version 7.0 for Bigger Datasets. *Molecular Biology & Evolution* 33(7): 1870–1874. <https://doi.org/10.1093/molbev/msw054>
- Li J, Yan X, Lin Y, Li S, Chen H (2021) Challenging Wallacean and Linnean shortfalls: *Ectosticta* spiders (Araneae, Hypochilidae) from China. *Zoological Research* 42(6): 791–794. <https://doi.org/10.24272/j.issn.2095-8137.2021.212>
- Li S (2020) Spider taxonomy for an advanced China. *Zoological Systematics* 45(2): 73–77. <https://doi.org/10.11865/zs.202011>
- Li Y, Lin Y, Li S (2020) A review of *Crassignatha* (Araneae, Symphytognathidae). *ZooKeys* 988: 63–128. <https://doi.org/10.3897/zookeys.988.56188>
- Lin Y (2019) First report of the spider genus *Symphytognatha* from Asia (Araneae, Symphytognathidae). *Zootaxa* 4638(2): 291–295. <https://doi.org/10.11646/zootaxa.4638.2.8>
- Lin Y, Li S (2009) First described *Patu* spiders (Araneae, Symphytognathidae) from Asia. *Zootaxa* 2154: 47–68. <https://doi.org/10.11646/zootaxa.2154.1.3>
- Lin Y, Pham DS, Li S (2009) Six new spiders from caves of northern Vietnam (Araneae: Tetrablemmidae: Ochyroceratidae: Telemidae: Symphytognathidae). *Raffles Bulletin of Zoology* 57: 323–342.
- Lin Y, Tao Y, Li S (2013) Two new species of the genus *Anapistula* (Araneae, Symphytognathidae) from Southern China. *Acta Zootaxonomica Sinica* 38(1): 53–58.
- Marples BJ (1951) Pacific symphytognathid spiders. *Pacific Science* 5: 47–51.
- Marples BJ (1955) Spiders from western Samoa. *Journal of the Linnean Society of London, Zoology (Zool.)* 42: 453–504. <https://doi.org/10.1111/j.1096-3642.1955.tb02217.x>
- Miller JA, Griswold CE, Yin CM (2009) The symphytognathoid spiders of the Gaoligongshan, Yunnan, China (Araneae, Araneoidea): Systematics and diversity of micro-orbweavers. *ZooKeys* 11: 9–195. <https://doi.org/10.3897/zookeys.11.160>
- Rivera-Quiroz FA, Petchard B, Miller JA (2021) First records and three new species of the family Symphytognathidae (Arachnida, Araneae) from Thailand, and the circumscription of the genus *Crassignatha* Wunderlich, 1995. *ZooKeys* 1012: 21–53. <https://doi.org/10.3897/zookeys.1012.57047>
- Saaristo MI (1996) Symphytognathidae (Arachnida, Araneae), a new spider family for the granitic islands of Seychelles. *Phelsuma* 4: 53–56.
- WSC (2021) World Spider Catalog. Version 22.5. Natural History Museum Bern. [accessed August 15, 2021]. <https://doi.org/10.24436/2>
- Yao Z, Wang X, Li S (2021) Tip of the iceberg: species diversity of *Pholcus* spiders (Araneae, Pholcidae) in Changbai Mountains, Northeast China. *Zoological Research* 42(3): 267–271. <https://doi.org/10.24272/j.issn.2095-8137.2020.214>

Nine new species of the spider family Araneidae (Arachnida, Araneae) from Xishuangbanna, Yunnan, China

Xiaoqi Mi¹, Shuqiang Li²

1 College of Agriculture and Forestry Engineering and Planning, Guizhou Provincial Key Laboratory of Biodiversity Conservation and Utilization in the Fanjing Mountain Region, Tongren University, Tongren 554300, Guizhou, China **2**Institute of Zoology, Chinese Academy of Sciences, Beijing 100101, China

Corresponding author: Shuqiang Li (lisq@ioz.ac.cn)

Academic editor: Zhiyuan Yao | Received 22 August 2021 | Accepted 25 October 2021 | Published 19 November 2021

<http://zoobank.org/DE29D6A5-E9BA-4FB4-92C2-6985AE680753>

Citation: Mi X, Li S (2021) Nine new species of the spider family Araneidae (Arachnida, Araneae) from Xishuangbanna, Yunnan, China. ZooKeys 1072: 49–81. <https://doi.org/10.3897/zookeys.1072.73345>

Abstract

Nine new species of the orb-weaver spider family Araneidae Clerck, 1757 from Menglun Town, Xishuangbanna, Yunnan, China are described: *Acusilas tongi* sp. nov. (♂♀), *Chorizopes yui* sp. nov. (♂♀), *Chorizopesoides guoi* sp. nov. (♂♀), *Deione cheni* sp. nov. (♀), *D. yangi* sp. nov. (♂♀), *Hypsosinga pulla* sp. nov. (♂♀), *Mangora baii* sp. nov. (♂♀), *M. cephalo* sp. nov. (♂♀) and *Milonia gemella* sp. nov. (♂♀). The genus *Milonia* Thorell, 1890 is recorded from China for the first time. The previous description of *Chorizopesoides wulingensis* (Yin, Wang & Xie, 1994) from Libo County, Guizhou by Mi and Wang (2018) refers to *Chorizopesoides annasestakovae* sp. nov. (♂♀). Diagnostic photos of the habitus and copulatory organs of the new species are provided.

Keywords

Morphology, new record, orb-weaver spider, taxonomy

Introduction

The spider family Araneidae Clerck, 1757 is the third largest family in Araneae, with a total of 3067 species in 177 genera worldwide (WSC 2021). In China, 402 species in 50 genera have been recorded (Li 2020, Yao and Li 2021, Li et al. 2021).

Xishuangbanna Tropical Botanical Garden (XTBG) in Menglun Town lies in Mengla County, Yunnan Province, southwest China. A total of 782 spider species have

been recorded from this area through an “All Species Inventory” (Li 2020). The number of Araneidae species of this region continually increases due to ongoing research, e.g. – a taxonomic revision of the orb-weaver genus *Eriovixia* Archer, 1951 from this area indicated 13 species, 7 new to science by Mi and Li (2021). This paper is the second paper of our work on Araneidae from the region. Nine new species of the genera *Acusilas* Simon, 1895, *Chorizopes* O. Pickard-Cambridge, 1871, *Chorizopesoides* Mi & Wang, 2018, *Deione* Thorell, 1898, *Hypsosinga* Ausserer, 1871, *Mangora* O. Pickard-Cambridge, 1889 and *Milonia* Thorell, 1890 are described.

Materials and methods

All specimens were collected by beating shrubs, fogging, or hand collecting and are preserved in 75% ethanol. Type specimens of new species are deposited in the Institute of Zoology, Chinese Academy of Sciences (IZCAS) in Beijing. The type specimens of *Chorizopesoides annasestakovae* sp. nov. and comparative material of *Deione lingulata* Han, Zhu & Levi, 2009 are deposited in Tongren University (TRU). The specimens were examined with an Olympus SZ51 stereomicroscope. The epigyna were cleared in trypsin enzyme solution for examination and imaging. The left male palps were dissected in ethanol for examination, description, and imaging. Photos of the habitus and copulatory organs were taken with a Kuy Nice CCD mounted on an Olympus BX53 compound microscope. Compound focus images were generated using Helicon Focus v. 6.7.1.

All measurements are given in millimeters. Leg measurements are given as: total length (femur, patella + tibia, metatarsus, tarsus). References to figures in the cited papers are listed in lowercase (fig. or figs); figures in this paper are noted with an initial capital (Fig. or Figs). Abbreviations used in the text and figures are as follows: ALE anterior lateral eye; AME anterior median eye; BE broken embolus; C conductor; CD copulatory duct; CO copulatory opening; E embolus; ET embolic thorn; FD fertilization duct; MA median apophysis; MOA median ocular area; MP median plate; PLE posterior lateral eye; PME posterior median eye; SA subterminal apophysis; Sc scape; Sp spermatheca; TA terminal apophysis; TE tegular extension.

Taxonomy

Family Araneidae Clerck, 1757

Genus *Acusilas* Simon, 1895

Acusilas Simon, 1895: 785; Schmidt and Scharff 2008: 7.

Type species. *Acusilas coccineus* Simon, 1895 from Indonesia

Comments. Nine *Acusilas* species from Asia and one species from Africa are known.

***Acusilas tongi* sp. nov.**

<http://zoobank.org/9ED4228E-0711-4E28-A95F-8C4FC129B2EC>

Figs 1, 2, 20A

Type material. **Holotype.** ♂ (IZCAS-Ar42503), CHINA: Yunnan, Xishuangbanna, Mengla County, Menglun Township, Menglun Nature Reserve, primary tropical seasonal rainforest (21°57.43'N, 101°12.28'E, ca 792 m), 19–25. XI.2006, G. Zheng leg. **Paratypes:** 1♂ (IZCAS-Ar42504), rubber plantation (approx. 20 years old) (21°54.47'N, 101°15.98'E, ca 570 m), 5–12. XI.2006, G. Zheng leg.; 1♀ (IZCAS-Ar42505), rubber plantation (approx. 20 years old) (21°54.65'N, 101°16.26'E, ca 570 m), 5–12. XII.2006, G. Zheng leg.; 1♀ (IZCAS-Ar42506), secondary tropical seasonal moist forest (21°54.61'N, 101°17.01'E, ca 630 m), 28. VII.2007, G. Zheng leg.; 1♂ (IZCAS-Ar42507), low evergreen forest along G213 roadside (21°53.79'N, 101°17.15'E, ca 590 m), 27. XI.2009, G. Tang leg.; 1♀ (IZCAS-Ar42508), Xishuangbanna Tropical Botanical Garden, grapefruit plantation (21°54.07'N, 101°16.36'E, ca 540 m), 22. VII.2018, X. Mi leg.; 1♂ (IZCAS-Ar42509), Xishuangbanna Tropical Botanical Garden, Yulinjiegou scenic spot (21°55.13'N, 101°16.08'E, ca 550 m), 29. VII.2018, X. Mi leg.; 1♀ (IZCAS-Ar42510), Teak plantation (21°54.03'N, 101°16.39'E, ca 550 m), 10. VIII.2018, Z. Bai et al. leg.; 1♂ (IZCAS-Ar42511), site 5 around the dump (21°54.37'N, 101°16.07'E, ca 620 m), 6. V.2019, Y. Tong leg.

Etymology. The species is named after Dr. Yanfeng Tong (Shenyang Normal University), one of the collectors of the type specimens; noun (name) in genitive case.

Diagnosis. The new species resembles *A. malaccensis* in habitus but can be distinguished by the: 1) interrupted stripes on the female abdomen vs. uninterrupted (Murphy and Murphy, 1983: fig. 16); 2) spermatheca ovoid vs. globular (Murphy and Murphy, 1983: fig. 12).

Description. **Male** (holotype, Figs 1A, B, 2D, E, 20A). Total length 2.15. Carapace 1.15 long, 0.90 wide. Abdomen 1.05 long, 1.15 wide. Clypeus 0.08 high. Eye sizes and interdistances: AME 0.13, ALE 0.05, PME 0.10, PLE 0.08, AME-AME 0.08, AME-ALE 0.03, PME-PME 0.10, PME-PLE 0.08, MOA length 0.28, anterior width 0.28, posterior width 0.28. Leg measurements: I 2.75 (0.90, 0.95, 0.50, 0.40), II 2.55 (0.80, 0.85, 0.50, 0.40), III 1.65 (0.55, 0.55, 0.30, 0.25), IV 2.25 (0.75, 0.75, 0.40, 0.35). Carapace pear-shaped, yellowish brown, cervical groove obvious, posterior eyes surrounded with black. Chelicerae yellowish brown, four promarginal teeth, lacking retromarginal teeth. Endites, labium yellow. Sternum yellow, with sparse, dark setae. Legs yellowish brown without annulations. Abdomen blunt anteriorly, pointed posteriorly, about 1.1 times wider than long, dorsum grayish yellow with irregular dark patches; venter grayish yellow with darker spots forming inconspicuous stripes. Spinnerets yellow.

Palp (Figs 1A–C, 20A): median apophysis prominent, about 4/5 length of cymbium; embolus about two times length of cymbium, runs anti-clockwise, curved about 180° from its origin, with two thorns at base (embolic thorn, stipes extended), distal end pointed toward tip of median apophysis.

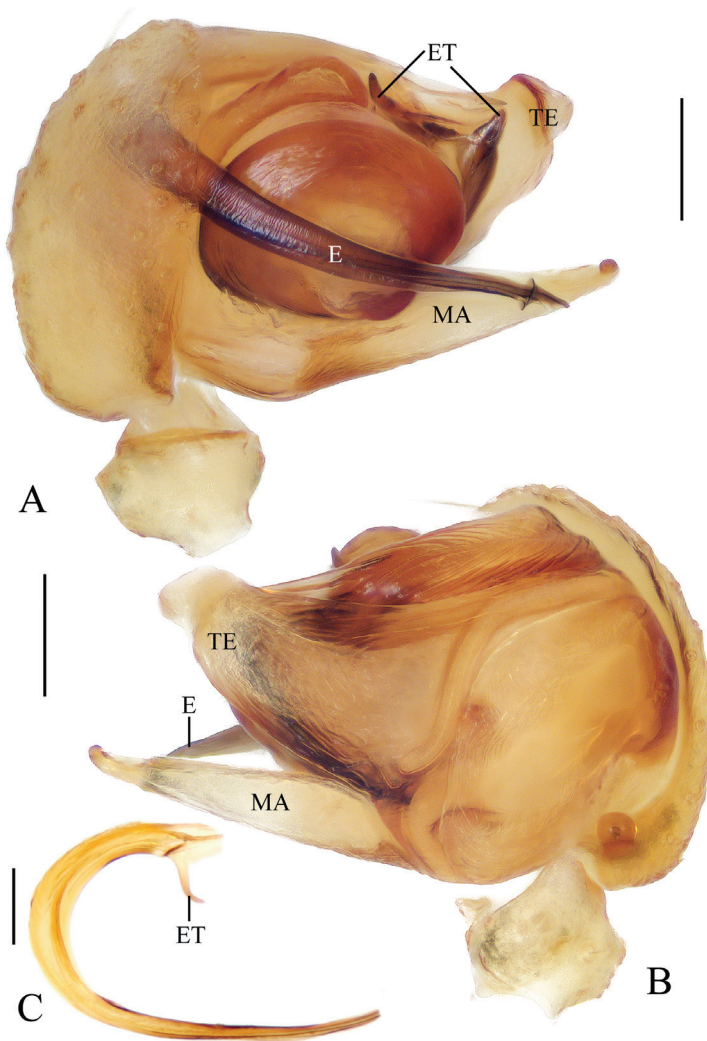


Figure 1. *Acusilas tongi* sp. nov., male palp **A, B** holotype **C** broken embolus **A** prolateral view **B** retrolateral view **C** broken embolus in female paratype's epigyne. Scale bars: 0.1mm

Female (paratype IZCAS-Ar42505, Fig. 2A–C, F–H). Total length 8.20. Carapace 4.20 long, 3.20 wide. Abdomen 5.10 long, 4.40 wide. Clypeus 0.15 high. Eye sizes and interdistances: AME 0.18, ALE 0.13, PME 0.18, PLE 0.15, AME-AME 0.22, AME-ALE 0.10, PME-PME 0.25, PME-PLE 0.18, MOA length 0.55, anterior width 0.55, posterior width 0.55. Leg measurements: I 12.00 (3.60, 4.50, 2.70, 1.20), II 11.30 (3.50, 4.00, 2.60, 1.20), III 7.30 (2.50, 2.60, 1.30, 0.90), IV 11.10 (3.50, 4.00, 2.50, 1.10). Carapace pear-shaped, yellow, cervical groove obvious, posterior eyes surrounded with black. Chelicerae yellow, four promarginal teeth, three retromarginal teeth. Endites and labium yellow. Sternum yellow, with sparse, dark setae. Legs: femur, patella, and basal 1/4 of tibia yellow, remaining 3/4 of tibia, metatarsus, and tarsus

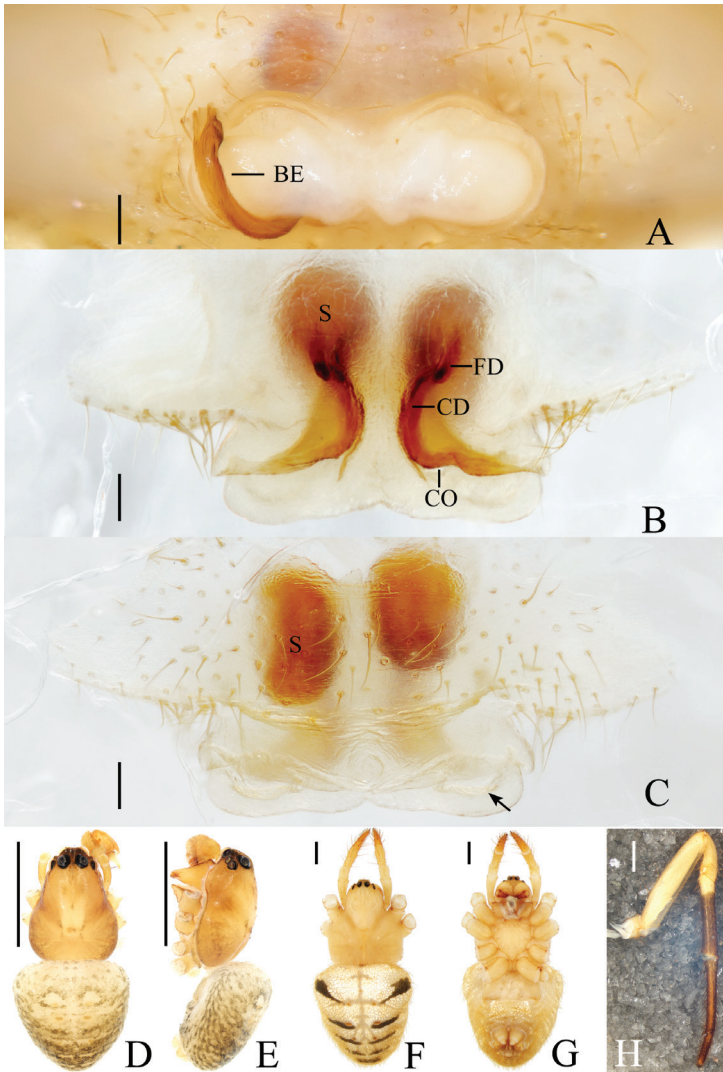


Figure 2. *Acusilas tongi* sp. nov. **A–C, F–H** female paratype IZCAS-Ar42505 **D, E** holotype **A** epigyne, ventral view **B** *ibid.*, posterior view **C** *ibid.*, anterior view **D** habitus, dorsal view **E** *ibid.*, lateral view **F** *ibid.*, dorsal view **G** *ibid.*, ventral view **H** left leg I, prolateral view. Scale bars: 0.1mm (**A–C**); 1mm (**D–H**)

dark brown. Abdomen triangular in dorsal view, slightly longer than wide, yellow with nine transverse black stripes; venter yellow with dozens of white spots medially.

Epigyne (Fig. 2A–C): wider than long, with narrow rim anteriorly and laterally, concave anteriorly; posterior lip hooked (see arrow in Fig. 2C); copulatory openings narrow, located posteriorly; copulatory ducts shorter than spermatheca; spermathecae oval.

Variation. Total length: ♂♂ 1.75–2.25; ♀♀ 8.2–10.80.

Distribution. China (Yunnan).

Genus *Chorizopes* O. Pickard-Cambridge, 1871

Chorizoopes O. Pickard-Cambridge, 1871: 738; Tikader 1982: 157; Kallal and Hormiga 2019: 473

Type species. *Chorizoopes frontalis* O. Pickard-Cambridge, 1871 from Sri Lanka

Comments. A total of 29 species of *Chorizopes* are known from China, India, Pakistan, Sri Lanka, Myanmar, Korea, Japan, and Madagascar. Illustrations indicate that the following species may belong to other genera: *C. calciopae* (Simon, 1895), *C. kastoni* Gajbe & Gajbe, 2004, *C. khandaricus* Gajbe, 2005, *C. khedaensis* Reddy & Patel, 1993, *C. pateli* Reddy & Patel, 1993, *C. quadrituberculata* Roy, Sen, Saha & Raychaudhuri, 2014, *C. rajanpurensis* Mukhtar & Tahir, 2013, *C. tikaderi* Sadana & Kaur, 1974.

Chorizopes yui sp. nov.

<http://zoobank.org/18204F0A-7C55-4B53-BFC7-3074E9C74E6B>

Figs 3, 4

Type material. *Holotype*. ♂ (IZCAS-Ar42512), CHINA: Yunnan, Xishuangbanna, Mengla County, Menglun Township, Menglun Nature Reserve, high plantations near G213 roadside (21°54.12'N, 101°16.93'E, ca 590 m), 24.XI.2009, G. Tang leg. *Paratypes*: 1♂ (IZCAS-Ar42513), *Anogeissus acuminata* plantation (approx. 20 years old) (21°53.99'N, 101°16.81'E, ca 610 m), 19.VIII.2007, G. Zheng leg.; 2♀ (IZCAS-Ar42514–42515), garbage dump, secondary tropical forest (21°54.38'N, 101°16.82'E, ca 620 m), 23.XI.2009, G. Tang leg.; 1♂ (IZCAS-Ar42516), Lüshilin Forest Park, limestone tropical seasonal rainforest (21°54.56'N, 101°16.86'E, ca 610 m), 29.XI.2009, G. Tang leg.; 1♀ (IZCAS-Ar42517), secondary tropical forest, bamboo plantation along G213 roadside (21°53.82'N, 101°16.99'E, ca 610 m), 3.VIII.2018, Z. Bai leg.; 1♂ (IZCAS-Ar42518), Xishuangbanna Tropical Botanical Garden, site 1 around the dump (21°53.28'N, 101°16.75'E, ca 630 m), 25.IV.2019, Z. Bai leg.; 1♀ (IZCAS-Ar42519), Xishuangbanna Tropical Botanical Garden, Baihuayuan (21°55.60'N, 101°14.87'E, ca 540 m), 3.V.2019 night, C. Wang leg.

Etymology. The species is named after Dr. Hao Yu, one of the collectors of the type specimens; noun (name) in genitive case.

Diagnosis. The new species can be distinguished from congeneric species by the: 1) yellowish white abdomen with a dark rhomboid patch; 2) triangular copulatory openings; 3) translucent, thread-like terminal apophysis; 4) fan-shaped median apophysis in prolateral view.

Description. Male (holotype, Figs 3A, B, D, 4D, E). Total length 3.60. Carapace 1.60 long, 1.00 wide. Abdomen 2.00 long, 1.20 wide. Clypeus 0.10 high. Eye sizes and interdistances: AME 0.13, ALE 0.08, PME 0.10, PLE 0.09, AME-AME 0.13, AME-ALE 0.45, PME-PME 0.18, PME-PLE 0.35, MOA length 0.33, anterior width 0.35, posterior width 0.35. Leg measurements: I 3.65 (1.05, 1.30, 0.80, 0.50), II

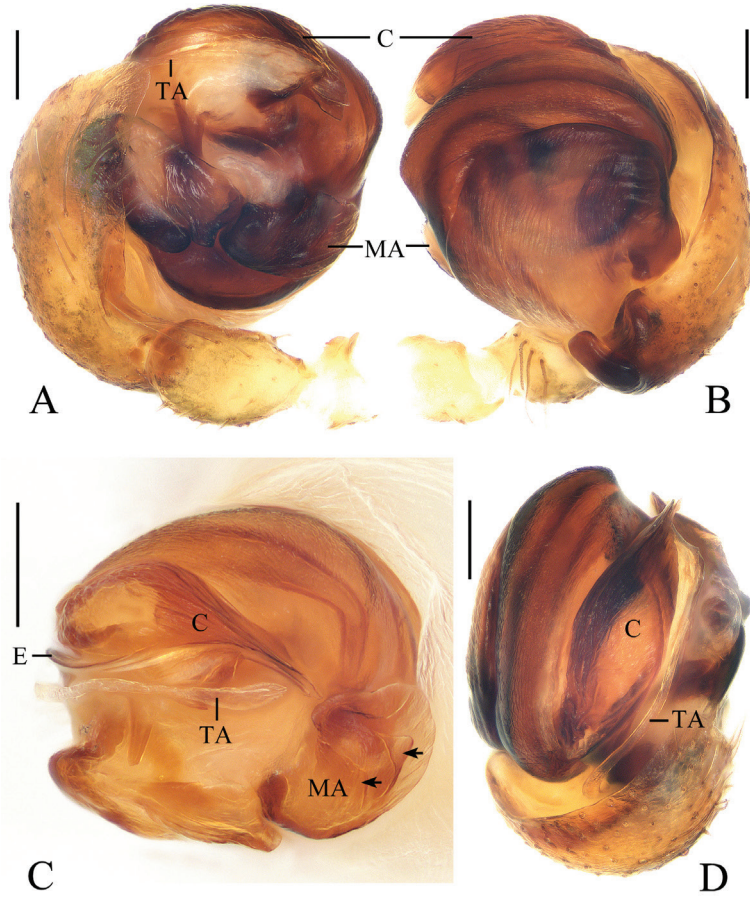


Figure 3. *Chorizopes yui* sp. nov., male palp **A, B, D** holotype **C** male paratype IZCAS-Ar42513. **A** prolateral view **B** retrolateral view **C** expanded in lactic acid **D** apical view. Scale bars: 0.1mm

3.75 (1.05, 1.45, 0.75, 0.50), III 2.25 (0.60, 0.75, 0.45, 0.45), IV 4.15 (1.15, 1.50, 0.90, 0.60). Carapace oval, brown, elevated, cervical groove inconspicuous. Chelicerae brown, seven promarginal teeth. Endites yellow, labium triangular, brown. Sternum triangular, yellowish brown, with pale setae. Legs yellow with brown annulations. Abdomen cylindrical, with pair of lateral tubercles and two vertically arranged tubercles posteriorly, grayish yellow with dark rhomboid patch; venter grayish yellow with large, white patch medially. Spinnerets yellowish brown.

Palp (Fig. 3): paracybium flattened; median apophysis fan-shaped in prolateral view, with two lamellar spurs (see arrows in Fig. 3C); embolus length about equal to bulb diameter, curved, slightly flattened; conductor about 4/5 length of bulb diameter in prolateral view; terminal apophysis translucent, slender, curved, length almost equal to that of embolus.

Female (paratype IZCAS-Ar42514, Fig. 4A–C, F, G). Total length 6.50. Carapace 2.10 long, 1.40 wide. Abdomen 4.70 long, 2.60 wide. Clypeus 0.13 high. Eye sizes

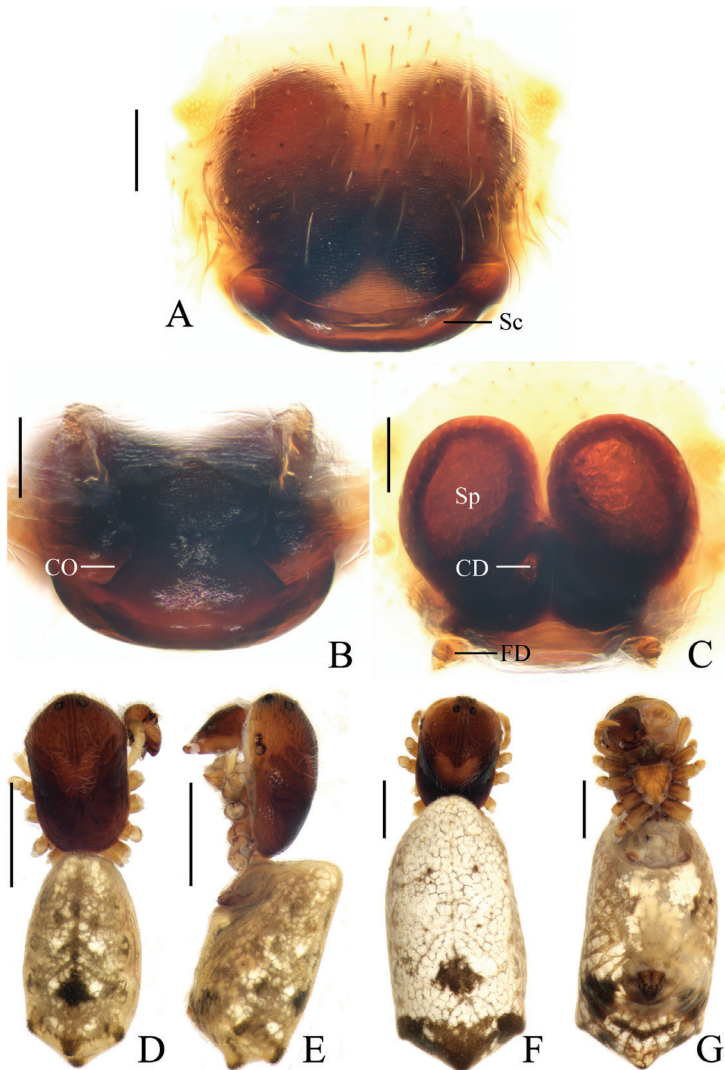


Figure 4. *Chorizopes yui* sp. nov. **A–C, F, G** female paratype IZCAS-Ar42514 **D, E** holotype **A** epigyne, ventral view **B** *ibid.*, posterior view **C** vulva, dorsal view **D** habitus, dorsal view **E** *ibid.*, lateral view **F** *ibid.*, dorsal view **G** *ibid.*, ventral view. Scale bars: 0.1mm (**A–C**); 1mm (**D–G**)

and interdistances: AME 0.13, ALE 0.08, PME 0.09, PLE 0.10, AME-AME 0.20, AME-ALE 0.53, PME-PME 0.25, PME-PLE 0.73, MOA length 0.40, anterior width 0.43, posterior width 0.43. Leg measurements: I 4.70 (1.35, 1.70, 1.05, 0.60), II 4.60 (1.35, 1.65, 1.00, 0.60), III 3.15 (0.85, 1.10, 0.60, 0.60), IV 5.70 (1.60, 2.15, 1.25, 0.70). Habitus like in male, coloration of abdomen slightly paler.

Epigyne (Fig. 4A–C): about 1.1 times wider than long; scape about four times wider than long, strongly rebordered; copulatory openings triangular, located posteriorly; copulatory ducts short, twisted; spermathecae ovoid, touching each other.

Variation. Total length: ♂♂ 2.90–3.60; ♀♀ 6.00–6.50.

Distribution. China (Yunnan).

Genus *Chorizopesoides* Mi & Wang, 2018

Chorizopesoides: Mi and Wang 2018: 82

Type species *Chorizopes wulingensis* Yin, Wang and Xie, 1994 from Hunan, China

Comments. The only two species that have been described in this genus were both recorded from China (WSC 2021).

Chorizopesoides guoi sp. nov.

<http://zoobank.org/18783528-2199-4DDB-9168-3FED612331CA>

Figs 5, 6, 20B

Type material. Holotype. ♂ (IZCAS-Ar42520), CHINA: Yunnan, Xishuangbanna, Mengla County, Menglun Town, Menglun Nature Reserve, primary tropical seasonal rainforest (21°55.04'N, 101°16.50'E, ca 560 m), 22.VII.2007, G. Zheng leg.

Paratypes: 2♂3♀ (IZCAS-Ar42521–42525), same data as holotype; 1♀ (IZCAS-Ar42526), primary tropical seasonal rainforest (21°57.43'N, 101°12.28'E, ca 792 m), 1–15.VI.2007, G. Zheng leg.; 1♂1♀ (IZCAS-Ar42527–42528), secondary tropical seasonal moist forest (21°54.72'N, 101°16.94'E, ca 650 m), 27.VII.2007, G. Zheng leg.; 3♂2♀ (IZCAS-Ar42529–42533), secondary tropical seasonal moist forest (21°54.61'N, 101°17.01'E, ca 630 m), 28.VII.2007, G. Zheng leg.

Other material examined. 1♀ (IZCAS-Ar42534), Xishuangbanna Tropical Botanical Garden, eastern part (21°54.07'N, 101°16.36'E, ca 540 m), 16.VII.2018, X. Mi leg.; 1♀ (IZCAS-Ar42535), Xishuangbanna Tropical Botanical Garden, vine garden (21°55.76'N, 101°15.73'E, ca 490 m), 17.VII.2018, night, X. Mi leg.; 1♀ (IZCAS-Ar42536), G213 roadside near 68 km (21°53.82'N, 101°16.79'E, ca 620 m), 27.VII.2018, X. Mi leg.

Comparative material. *Chorizopesoides wulingensis*, **Holotype** ♀, CHINA: Hunan, Sangzhi County, Nanmuping, 17.XIII.1984, J.F. Wang leg. (Fig. 7)

Etymology. The species is named after Professor Guo Zheng, one of the collectors of the type specimens; noun (name) in genitive case.

Diagnosis. The new species resembles *C. wulingensis* and *C. annasestakovae* sp. nov. in appearance, but females can be distinguished from both by the: 1) copulatory ducts spirally coiled vs. circular (Fig. 7C; Mi and Wang, 2018: fig. 3E); 2) pale abdomen with distinct black stripes vs. dark brown abdomen with indistinct stripes; 3) pale cephalon behind eyes vs. dark cephalon with two small, pale spots (Fig. 7D) or without spots (Mi and Wang, 2018: fig. 1C). From *C. wulingensis* by the: 1) scape shorter than half a spermatheca diameter vs. longer than half a spermatheca diameter (Fig. 7); 2) median plate narrower than a spermatheca diameter vs. wider than a sper-

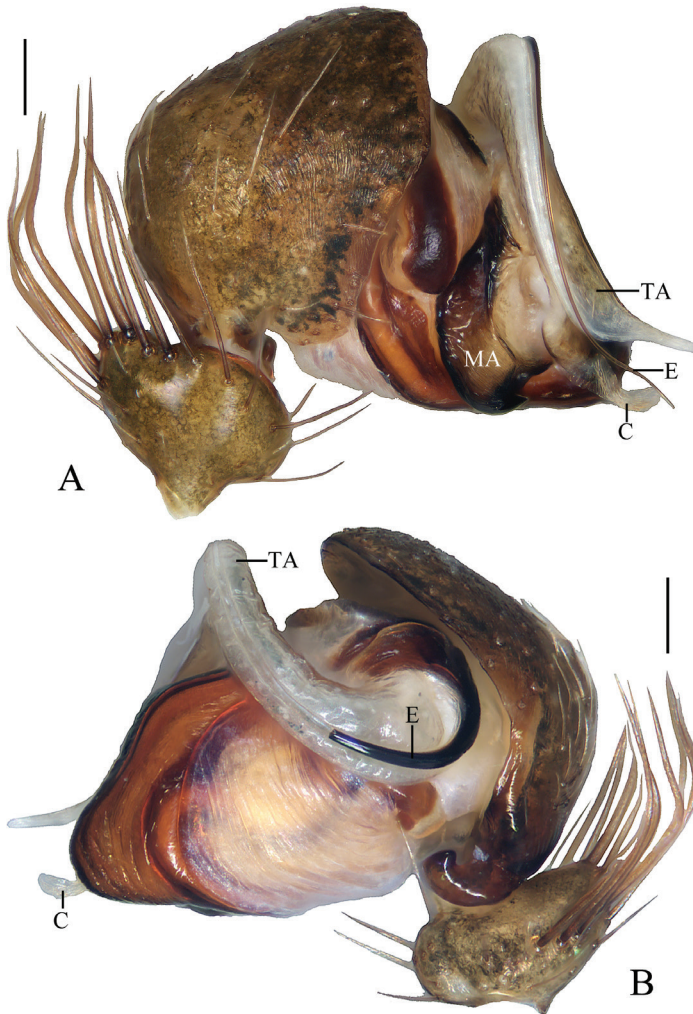


Figure 5. *Chorizopesoides guoi* sp. nov., holotype, male palp **A** prolateral view **B** retrolateral view (embolus broken). Scale bars: 0.1mm

matheca diameter (Fig. 7); it can be distinguished from *C. annastakovae* sp. nov. by the: 1) scape not concave vs. concave (Mi and Wang, 2018: fig. 3D–E); 2) shape of the epigyne wider than long vs. as long as wide; 3) palpal tibia wider than long with a cluster of macrosetae vs. as long as tibia width without conspicuous macrosetae (Mi and Wang, 2018: fig. 3A, C); 4) tegulum triangularly elongated (retrolateral view) vs. not so elongated and rounder (Mi and Wang, 2018: fig. 3C); 5) median apophysis slender, two times longer than wide vs. shorter and higher (Mi and Wang, 2018: fig. 3A); 6) tip of the embolus extending beyond the edge of the tegulum (apical view) vs. shorter embolus, not reaching the edge of the tegulum (Mi and Wang, 2018: fig. 3B).

Description. Male (holotype, Figs 5A, B, 6D, E, 20B). Total length 2.90. Carapace 1.60 long, 0.95 wide. Abdomen 1.65 long, 1.40 wide. Clypeus 0.18 high. Eye

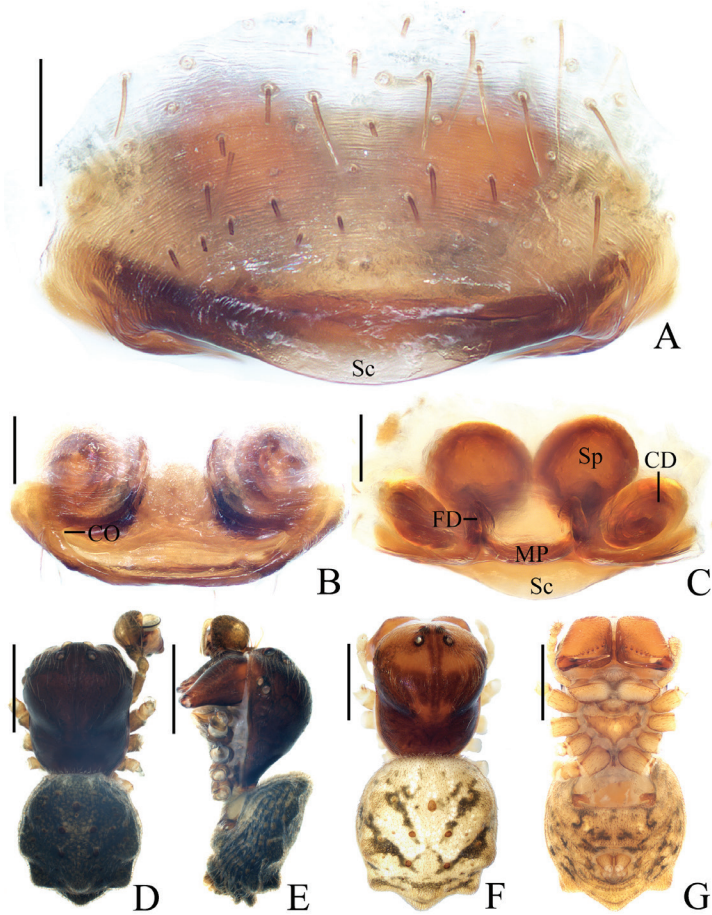


Figure 6. *Chorizopesoides guoi* sp. nov. **A–C, E, F** female paratype IZCAS-Ar42521 **D, E** holotype **A** epigyne, ventral view **B** ibid., posterior view **C** vulva, dorsal view **D** habitus, dorsal view **E** ibid., lateral view **F** habitus, dorsal view **G** ibid., ventral view. Scale bars: 0.1mm (**A–C**); 1mm (**D–G**)

sizes and interdistances: AME 0.13, ALE 0.08, PME 0.10, PLE 0.08, AME-AME 0.13, AME-ALE 0.40, PME-PME 0.25, PME-PLE 0.43, MOA length 0.30, anterior width 0.33, posterior width 0.43. Leg measurements: I 3.41 (0.95, 1.13, 0.80, 0.53), II 3.46 (0.90, 1.15, 0.88, 0.53), III 2.40 (0.70, 0.80, 0.50, 0.40), IV 3.29 (0.95, 1.13, 0.73, 0.48). Carapace rectangular, dark brown, with sparse, pale setae, cervical groove obvious. Chelicerae dark brown, five promarginal teeth. Endites wider than long, dark brown basally, paler distally, labium wider than long, triangular, dark brown. Sternum triangular, dark brown, paler medially. Legs yellow with brown annulations. Abdomen about 1.2 times longer than wide, with three pairs of lateral tubercles and three vertical caudal tubercles, dorsum grayish black with lots of brown sigilla; venter grayish black. Spinnerets yellowish brown.

Palp (Figs 5, 20B): tibia with a cluster of macrosetae (approx. 12) distal-dorsally, macrosetae about 1.5 times length of tibia; median apophysis about 1/2 length of bulb

diameter in apical view, distal end pointed; embolus extremely long, slender, more than two times length of bulb diameter; terminal apophysis membranous, equal in length to embolus; conductor membranous, shorter than median apophysis in prolateral view.

Female (paratype IZCAS-Ar42521, Fig. 6A–C, E, F). Total length 3.55. Carapace 1.75 long, 1.40 wide. Abdomen 2.00 long, 1.75 wide. Clypeus 0.15 high. Eye sizes and interdistances: AME 0.13, ALE 0.08, PME 0.10, PLE 0.08, AME-AME 0.15, AME-ALE 0.45, PME-PME 0.25, PME-PLE 0.48, MOA length 0.30, anterior width 0.30, posterior width 0.40. Leg measurements: I 3.31 (0.90, 1.10, 0.78, 0.53), II 3.19 (0.88, 1.08, 0.75, 0.48), III 2.46 (0.70, 0.83, 0.48, 0.45), IV 3.45 (1.00, 1.25, 0.75, 0.45). Habitus as in male, coloration much paler.

Epigyne (Fig. 6A–C): about two times wider than long, scape shorter than half a spermatheca diameter; copulatory openings concave, located at lateral side of posterior surface; copulatory ducts long, coiled 720°; spermathecae globular, touching each other.

Variation. Total length: ♂♂ 2.55–3.05; ♀♀ 3.25–4.85.

Distribution. China (Yunnan).

***Chorizopesoides annasestakovae* sp. nov.**

<http://zoobank.org/DDE89FA3-8775-4EC0-ABDC-05C59F23E69F>

Chorizopesoides wulingensis Mi & Wang, 2018: 82, figs 1A–D, 2A–C, 3A–E (misidentified).

Type material. Holotype. ♂ (TRU), CHINA: Guizhou, Qiannan, Libo County, Dotang Township, Yaosuo Village, Bizuo (25°16.84'N, 108°4.47'E, ca 601 m), 7–8. VIII.2013, X. Mi & M. Liao leg. (MXQ20130807). **Paratype** 1♀ (TRU), same data as holotype.

Etymology. The specific name comes from Dr. Anna Šestáková, who confirmed the new species; noun (name) in genitive case.

Diagnosis. See *Chorizopesoides guoi* sp. nov.

Description. See Mi and Wang (2018).

Distribution. China (Guizhou).

Comments. Compared to the holotype of *C. wulingensis*, the previous description of *C. wulingensis* from Libo County, Guizhou by Mi and Wang (2018) refers to *C. annasestakovae* sp. nov.

Genus *Deione* Thorell, 1898

Deione Thorell, 1898: 365; *Deione* Han et al. 2009: 56; Mi et al. 2010: 35.

Type species *Deione thoracica* Thorell, 1898 from Myanmar

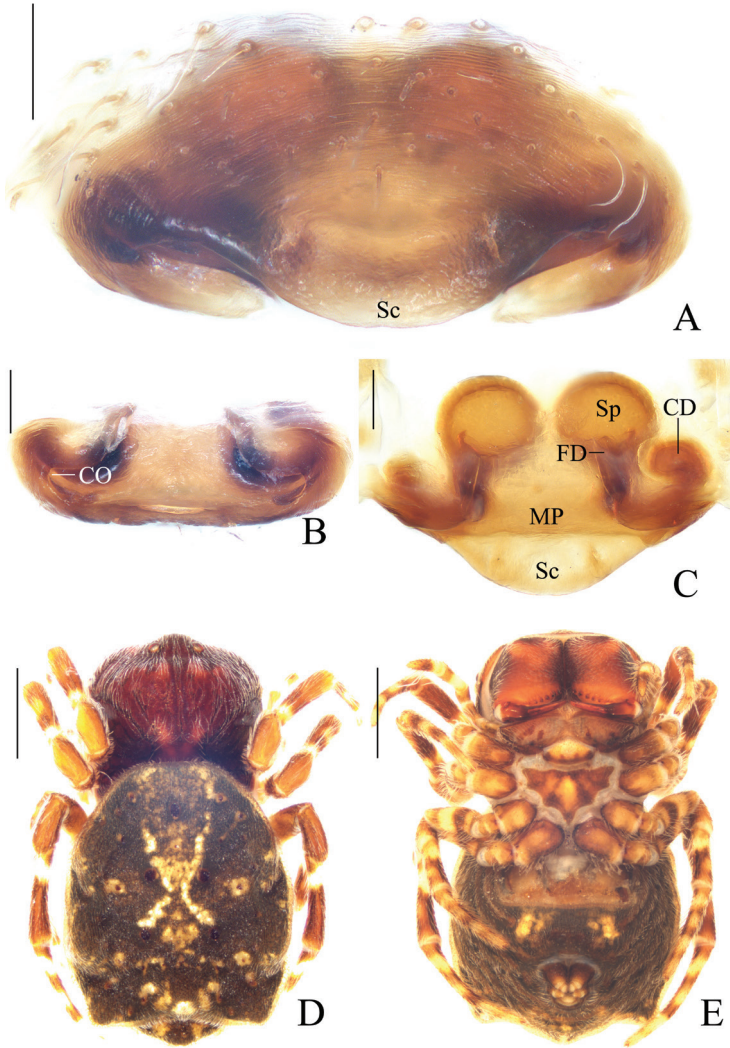


Figure 7. *Chorizopesoides wulingensis*, holotype **A** epigyne, ventral view **B** ibid., posterior view **C** vulva, dorsal view **D** habitus, dorsal view **E** ibid., ventral view. Scale bars: 0.1mm (**A–C**); 1mm (**D, E**)

***Deione cheni* sp. nov.**

<http://zoobank.org/13408A71-9FA3-4B2F-BAA6-1919E989F767>

Fig 8

Type material. Holotype. ♀ (IZCAS-Ar42537), CHINA: Yunnan, Xishuangbanna, Mengla County, Menglun Town, Menglun Nature Reserve, secondary tropical seasonal moist forest (21°54.72'N, 101°16.94'E, ca 650 m), 16–31.V.2007, G. Zheng

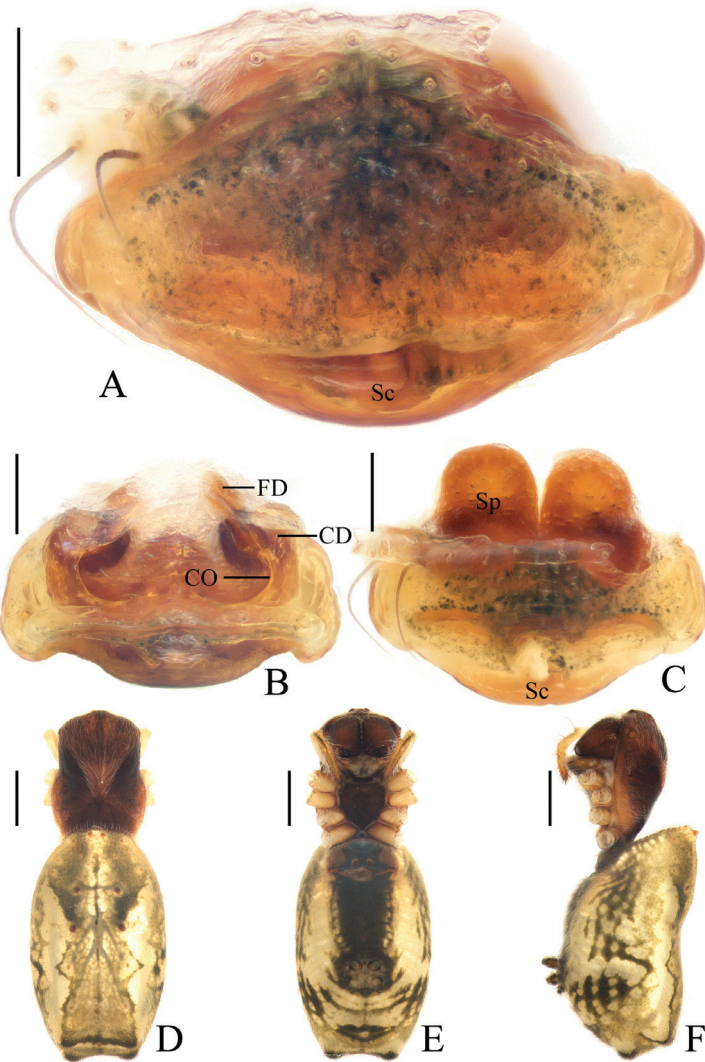


Figure 8. *Deione cheni* sp. nov., holotype **A** epigyne, ventral view **B** ibid., posterior view **C** ibid., anterior view **D** habitus, dorsal view **E** ibid., ventral view **F** ibid., lateral view. Scale bars: 0.1mm (**A–C**); 1mm (**D–F**)

leg. **Paratypes:** 1♀ (IZCAS-Ar42538), Xishuangbanna Tropical Botanical Garden, site 3 around the dump (21°54.34'N, 101°16.79'E, ca 620 m), 2.V.2019, Y. Tong leg.; 2♀ (IZCAS-Ar42539–42540), Xishuangbanna Tropical Botanical Garden, low bamboo plantation (21°53.89'N, 101°16.72'E, ca 570 m), 12.V.2019, Z. Bai leg.

Etymology. The species is named after Mr. Zhigang Chen, one of the collectors of the type specimens; noun (name) in genitive case.

Diagnosis. The new species resembles congeneric species in habitus, but it can be distinguished by the: 1) rhomboid epigyne in ventral view; 2) short, ventrally directed scape.

Description. Female (holotype, Fig. 8). Total length 6.30. Carapace 2.50 long, 1.70 wide. Abdomen 4.20 long, 2.50 wide. Clypeus 0.13 high. Eye sizes and interdistances: AME 0.15, ALE 0.10, PME 0.15, PLE 0.10, AME-AME 0.15, AME-ALE 0.53, PME-PME 0.20, PME-PLE 0.58, MOA length 0.43, anterior width 0.35, posterior width 0.45. Leg measurements: I 5.00 (1.50, 1.75, 1.15, 0.60), II 4.95 (1.50, 1.75, 1.15, 0.55), III 3.45 (1.05, 1.25, 0.65, 0.50), IV 4.90 (1.45, 1.80, 1.10, 0.55). Carapace rectangular, dark brown, with dense, pale setae. Chelicerae dark brown, 5 promarginal teeth, 3 retromarginal teeth. Endites dark brown basally, yellow distally, labium triangular, dark brown. Sternum heart-shaped, dark brown. Legs yellow with brown annulations. Abdomen oval, about 1.7 times longer than wide, with two pairs of long setae anteriorly, two pairs of vertically arranged lateral tubercles posteriorly, dorsum yellow with big grayish brown patch, patch with two pairs of constrictions laterally; venter yellow with big grayish black patch medially. Spinnerets grayish yellow, at posterior 1/3 of the abdomen.

Epigyne (Fig. 8A–C): rhomboid, about 1.8 times wider than long, with very short, ventrally directed scape; copulatory openings arcuate; copulatory ducts shorter than a spermatheca length; spermathecae elliptical, touching each other.

Variation. Total length: ♀♀ 4.90–6.30.

Distribution. China (Yunnan).

***Deione yangi* sp. nov.**

<http://zoobank.org/9FDA3B40-D368-413A-907F-2049B62DD19B>

Figs 9, 10, 20C

Type material. Holotype. ♀ (IZCAS-Ar42541), CHINA: Yunnan, Xishuangbanna, Mengla County, Menglun Town, Menglun Nature Reserve, primary tropical seasonal rainforest (21°57.67'N, 101°11.89'E, ca 790 m), 19–26.IV.2007, G. Zheng leg.

Paratypes: 1♀ (IZCAS-Ar42542), primary tropical seasonal rainforest (21°57.59'N, 101°12.21'E, ca 822 m, ca 730 m), 8.VIII.2007, G. Zheng leg.; 1♂ (IZCAS-Ar42543), Xishuangbanna Tropical Botanical Garden, Edible Botanical Garden (21°54.95'N, 101°16.18'E, ca 610 m), 28.VII.2018, X. Mi leg.

Comparative material. *Deione lingulata*, 5♂3♀, CHINA: Hainan, Wuzhishan City, Shuiman Township, Wuzhishan National Natural Reserve (18°54.17'N, 109°41.14'E, ca 870 m), 10.VIII.2020, X. Mi leg. (Figs 11, 20D)

Etymology. The species is named after Mr. Yuanfa Yang (Tongren, Guizhou), one of the collectors of the type specimens; noun (name) in genitive case.

Diagnosis. The new species resembles *D. lingulata* in habitus and copulatory organs but differs in the: 1) thin terminal apophysis, distally the width about equal to the nearest part of embolus vs. terminal apophysis thick, distally about four times wider than the nearest part of the embolus (Han et al. 2009: figs. 12, 13; Fig. 11); 2) median apophysis elliptical in prolateral view vs. triangular (Han et al. 2009: fig. 12;

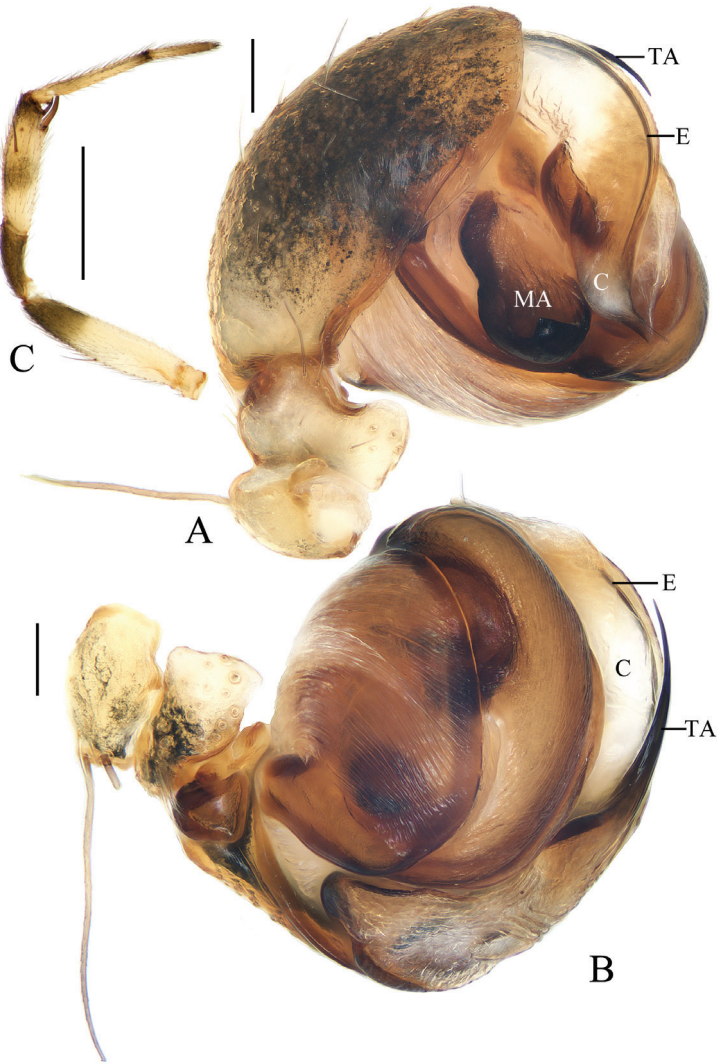


Figure 9. *Deione yangi* sp. nov., male paratype IZCAS-Ar42543, palp **A** prolateral view **B** retrolateral view **C** left leg II, prolateral view. Scale bars: 0.1mm (**A, B**); 1mm (**C**)

Fig. 11A); 3) scape triangular vs. almost rectangular (Han et al. 2009: figs. 8, 9); and 4) spermathecae touching vs. less than their diameter apart (Han et al. 2009).

Description. Female (holotype, Fig. 10A–C, F, G). Total length 6.20. Carapace 2.70 long, 2.00 wide. Abdomen 3.90 long, 2.40 wide. Clypeus 0.10 high. Eye sizes and interdistances: AME 0.18, ALE 0.13, PME 0.15, PLE 0.13, AME-AME 0.15, AME-ALE 0.50, PME-PME 0.20, PME-PLE 0.53, MOA length 0.48, anterior width 0.45, posterior width 0.45. Leg measurements: I 7.70 (2.20, 2.70, 1.90, 0.90), II 6.90 (2.00, 2.40, 1.70, 0.80), III 4.60 (1.50, 1.60, 0.90, 0.60), IV 6.50 (1.90, 2.30, 1.60, 0.70). Carapace almost rectangular, brown, with pale setae, cervical groove obvious. Chelicerae brown, five promarginal teeth, four retromarginal teeth in left chelicera, and

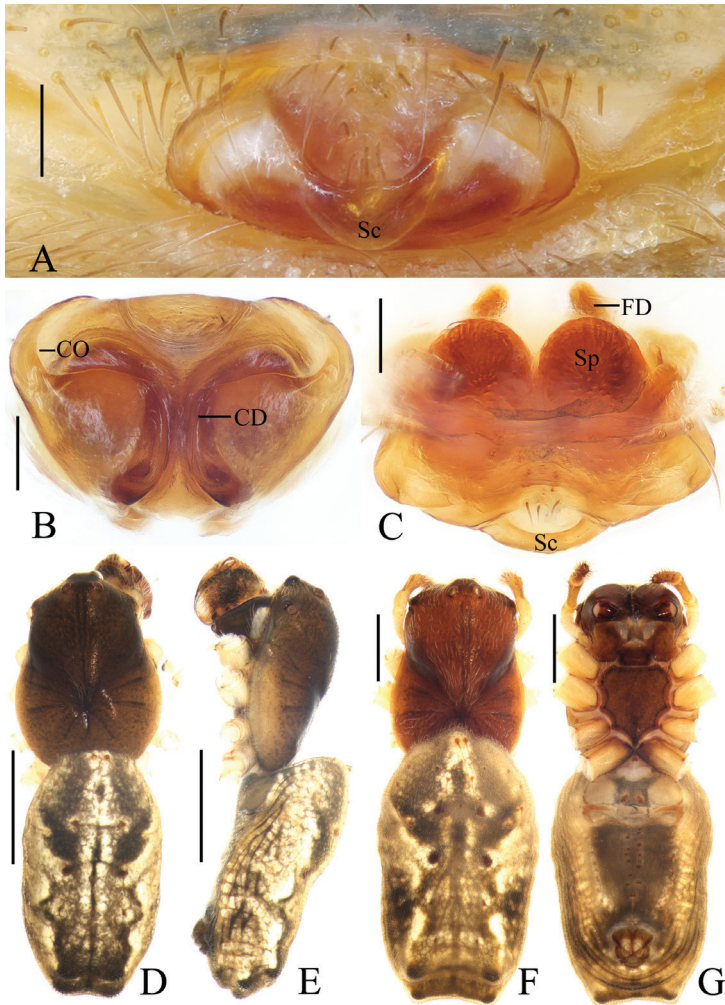


Figure 10. *Deione yangi* sp. nov. **A–C, F, G** holotype **D, E** male paratype IZCAS-Ar42543 **A** epigyne, ventral view **B** *ibid.*, posterior view **C** vulva, anterior view **D** habitus, dorsal view **E** *ibid.*, lateral view **F** *ibid.*, dorsal view **G** *ibid.*, ventral view. Scale bars: 0.1mm (**A–C**); 1mm (**D–G**)

five in right. Endites almost rectangular, brown, paler distally, labium triangular, dark brown, paler distally. Sternum heart-shaped, brown. Legs yellow with brown annulations. Abdomen oval, about 1.6 times longer than wide, with two pairs of long setae anteriorly, two pairs of vertically arranged lateral tubercles posteriorly, dorsum grayish brown with yellow patches anteriorly and laterally; venter yellow, big gray patch medially. Spinnerets grayish yellow, at posterior 1/4 of the abdomen.

Epigyne (Fig. 10A–C): about 1.8 times wider than long; scape triangular; copulatory openings arcuate, situated laterally in posterior view; copulatory ducts longer than spermatheca, arcuate in posterior view; spermathecae globular, touching each other.

Male (paratype IZCAS-Ar42543, Figs 9, 10D, E, 20C). Total length 3.75. Carapace 1.70 long, 1.35 wide. Abdomen 2.15 long, 1.30 wide. Clypeus 0.10 high. Eye

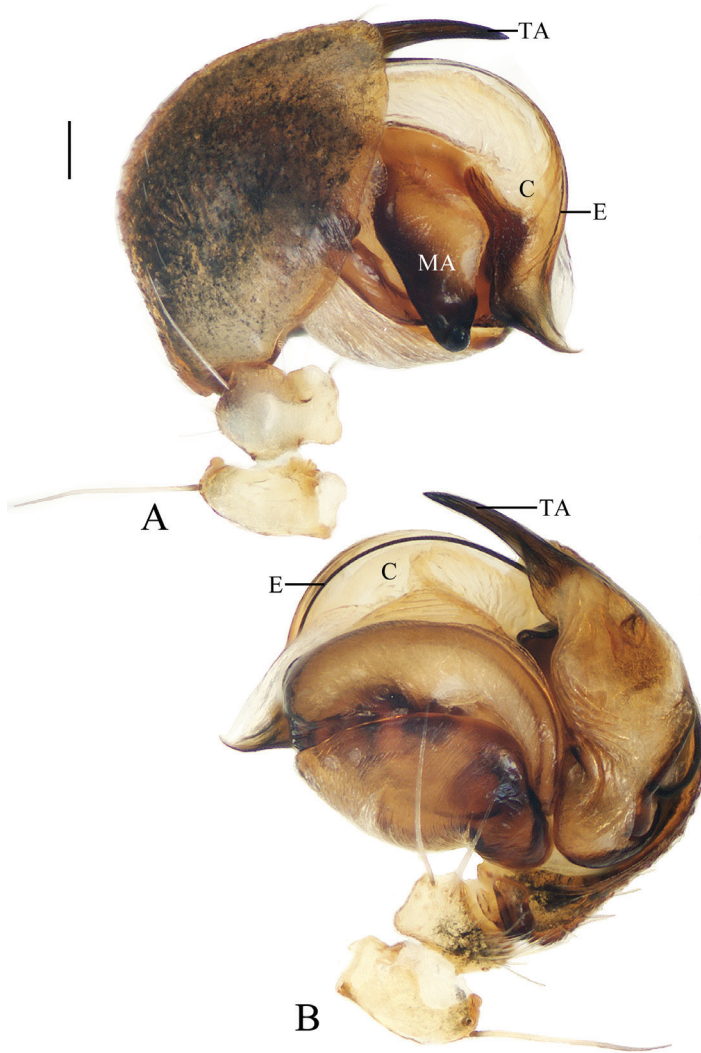


Figure 11. *Deione lingulata*, male palp **A** prolateral view **B** retrolateral view. Scale bars: 0.1mm

sizes and interdistances: AME 0.15, ALE 0.10, PME 0.13, PLE 0.10, AME-AME 0.10, AME-ALE 0.23, PME-PME 0.15, PME-PLE 0.28, MOA length 0.38, anterior width 0.35, posterior width 0.38. Leg measurements: I 4.25 (1.25, 1.60, 0.95, 0.45), II 4.35 (1.45, 1.50, 0.95, 0.45), III 2.75 (0.90, 0.95, 0.55, 0.35), IV 3.85 (1.15, 1.45, 0.85, 0.40). Habitus similar to that of female, but tibia II expanded, with 3 macrosetae and chelicerae with 3 retromarginal teeth.

Palp (Figs 9A, B, 20C): median apophysis elliptical in prolateral view, pointed distally; embolus slender, longer than bulb diameter; conductor as wide as bulb, membranous; terminal apophysis spinose, slightly curved.

Variation. Total length: ♀♀ 6.20–6.50.

Distribution. China (Yunnan).

Genus *Hyposinga* Ausserer, 1871

Hyposinga Ausserer, 1871: 823; Yin et al. 1997: 306; Yin et al. 2012: 689.

Type species. *Singa sanguinea* C.L. Koch, 1844 from Germany

***Hyposinga pulla* sp. nov.**

<http://zoobank.org/6155FE2D-7491-4983-8BFA-A763F57926F4>

Figs 12, 13, 21A

Type material. *Holotype* ♂ (IZCAS-Ar42544), CHINA: Yunnan, Xishuangbanna, Mengla County, Menglun Town, Menglun Nature Reserve, G213 roadside, Mannanxing (21°53.49'N, 101°17.11'E, ca 560 m), 9.VIII.2018, C. Wang leg. *Paratypes*: 1♀ (IZCAS-Ar42545), same data as holotype; 2♂ (IZCAS-Ar42546–42547), along G213 roadside (21°53.55'N, 101°16.39'E, ca 540 m), 3.VIII.2018, C. Wang leg.

Etymology. The specific name comes from the Latin word “pulla”, meaning “dark, blackish”, referring to the dark markings at the eye region; adjective.

Diagnosis. The new species resembles *H. pygmaea* (Sundevall, 1831) in habitus but can be distinguished by the: 1) enlarged copulatory ducts vs. not enlarged (Yin et al. 1997: fig. 215d); 2) spermathecae touching vs. separated from each other (Yin et al. 1997: fig. 215d); 3) embolus length less than half a bulb diameter vs. longer than a bulb diameter (Yin et al. 1997: fig. 215e).

Description. **Male** (holotype, Figs 12, 13C, D, 21A). Total length 2.40. Carapace 1.10 long, 0.95 wide. Abdomen 1.45 long, 0.90 wide. Clypeus 0.18 high. Eye sizes and interdistances: AME 0.06, ALE 0.04, PME 0.05, PLE 0.04, AME-AME 0.05, AME-ALE 0.03, PME-PME 0.05, PME-PLE 0.05, MOA length 0.15, anterior width 0.15, posterior width 0.15. Leg measurements: I 4.00 (1.30, 1.35, 0.90, 0.45), II 3.60 (1.15, 1.20, 0.85, 0.40), III 2.45 (0.80, 0.75, 0.55, 0.35), IV 3.75 (1.25, 1.20, 0.90, 0.40). Carapace pear shaped, yellow with black patch in eye region, cervical groove inconspicuous, fovea transverse. Chelicerae yellow, three promarginal teeth, two retro-marginal teeth. Endites yellow, labium triangular, yellow. Sternum yellow, with sparse, dark setae. Legs grayish brown, without annulations. Abdomen elliptical, about 1.6 times longer than wide, covered with pale setae, dorsum black-brown; venter grayish brown with big black patch medially. Spinnerets brownish black.

Palp (Figs 12, 21A): with two patellar bristles; median apophysis hooked; embolus shorter than half bulb diameter, covered by terminal and subterminal apophyses in prolateral view; conductor thick; terminal apophysis membranous, bifurcated distally; subterminal apophysis membranous, width almost same as width of terminal apophysis; tegulum extended near conductor.

Female (paratype IZCAS-Ar42545, Fig. 13A, B, E, F). Total length 2.75. Carapace 1.00 long, 0.90 wide. Abdomen 2.00 long, 1.45 wide. Clypeus 0.13 high. Eye sizes and interdistances: AME 0.06, ALE 0.04, PME 0.05, PLE 0.04, AME-AME 0.05, AME-ALE 0.05, PME-PME 0.05, PME-PLE 0.05, MOA length 0.15, anterior

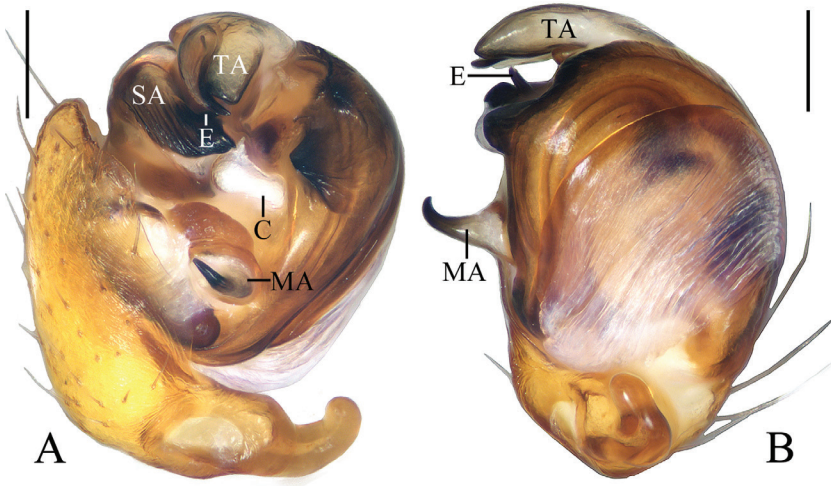


Figure 12. *Hyposinga pulla* sp. nov., holotype, male palp **A** prolateral view **B** ventral view. Scale bars: 0.1mm

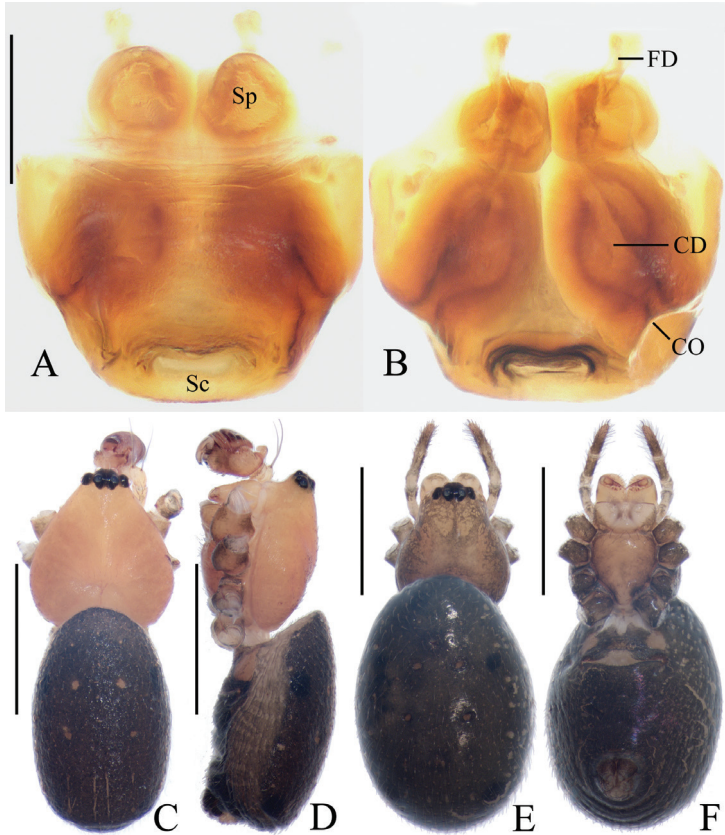


Figure 13. *Hyposinga pulla* sp. nov. **A, B, E, F** female paratype IZCAS-Ar42545 **C, D** holotype **A** epigyne, anterior view **B** ibid., posterior view **C** habitus, dorsal view **D** ibid., lateral view **E** ibid., dorsal view **F** ibid., ventral view. Scale bars: 0.1mm (A, B); 1mm (C–F)

width 0.15, posterior width 0.18. Leg measurements: I 3.10 (0.95, 1.05, 0.70, 0.40), II 2.85 (0.90, 0.95, 0.65, 0.35), III 2.00 (0.65, 0.60, 0.45, 0.30), IV 3.00 (1.00, 0.95, 0.70, 0.35). Habitus similar to that of male; carapace a little darker.

Epigyne (Fig. 13A, B): pentagonal in anterior view, about 1.4 times wider than long; copulatory openings laterally situated; copulatory ducts large, wider than spermatheca diameter at its widest part; spermathecae globular, touching each other.

Variation. Total length: ♂♂ 2.40–2.55.

Distribution. China (Yunnan).

Genus *Mangora* O. Pickard-Cambridge, 1889

Mangora O. Pickard-Cambridge, 1889: 14; Yin et al. 1997: 329; Yin et al. 2012: 711.

Type species *Mangora picta* O. Pickard-Cambridge, 1889 from Guatemala

Comments. Unlike the typical *Mangora* species, the two new species in this region both lack trichobothria on the tibia of leg III, but they have some common characters with *Mangora*, such as the cephalic region of the carapace is about half the maximum width of the thoracic region, the palp with one patellar bristle, and the abdomen oval; thus, we place the two species in *Mangora*, and phylogenetic analysis will focus on the placement of the two new species.

Mangora bairi sp. nov.

<http://zoobank.org/9A48184E-E930-4177-B798-24A4B8A7C89D>

Figs 14, 15, 21B

Type material. Holotype. ♂ (IZCAS-Ar42548) CHINA: Yunnan, Xishuangbanna, Mengla County, Menglun Town, Menglun Nature Reserve, secondary forest near mountain top (21°57.92'N, 101°12.05'E, ca 820 m), 2.VI.2013, Z. Zhao & Z. Chen leg.

Paratypes: 1♀ (IZCAS-Ar42549), secondary tropical seasonal rainforest (21°55.43'N, 101°16.44'E, ca 600 m), 19–25.XI.2006, G. Zheng leg.; 1♀ (IZCAS-Ar42550), secondary tropical seasonal moist forest (21°54.72'N, 101°16.94'E, ca 650 m), 19–25.XI.2006, G. Zheng leg.; 1♀ (IZCAS-Ar42551), secondary tropical seasonal rainforest (21°55.43'N, 101°16.44'E, ca 600 m), 5–12.XII.2006, G. Zheng leg.; 1♀ (IZCAS-Ar42552), secondary tropical seasonal rainforest (21°55.43'N, 101°16.44'E, ca 600 m), 19–26.V.2007, G. Zheng leg.; 1♂ (IZCAS-Ar42638), G213 roadside, secondary forest (21°54.46'N, 101°16.76'E, ca 640 m), 20.XI.2009, G. Tang leg.; 1♂ (IZCAS-Ar42562), secondary forest near mountain top (21°57.96'N, 101°12.19'E, ca 787 m), 31.V.2013, Z. Zhao & Z. Chen leg.; 1♂ (IZCAS-Ar42639), secondary tropical forest, around garbage dump (21°54.17'N, 101°16.87'E, ca 609 m), 31.VII.2018, Z. Bai leg.

Etymology. The species is named after Mr. Zilong Bai, one of the collectors of the type specimens; noun (name) in genitive case.

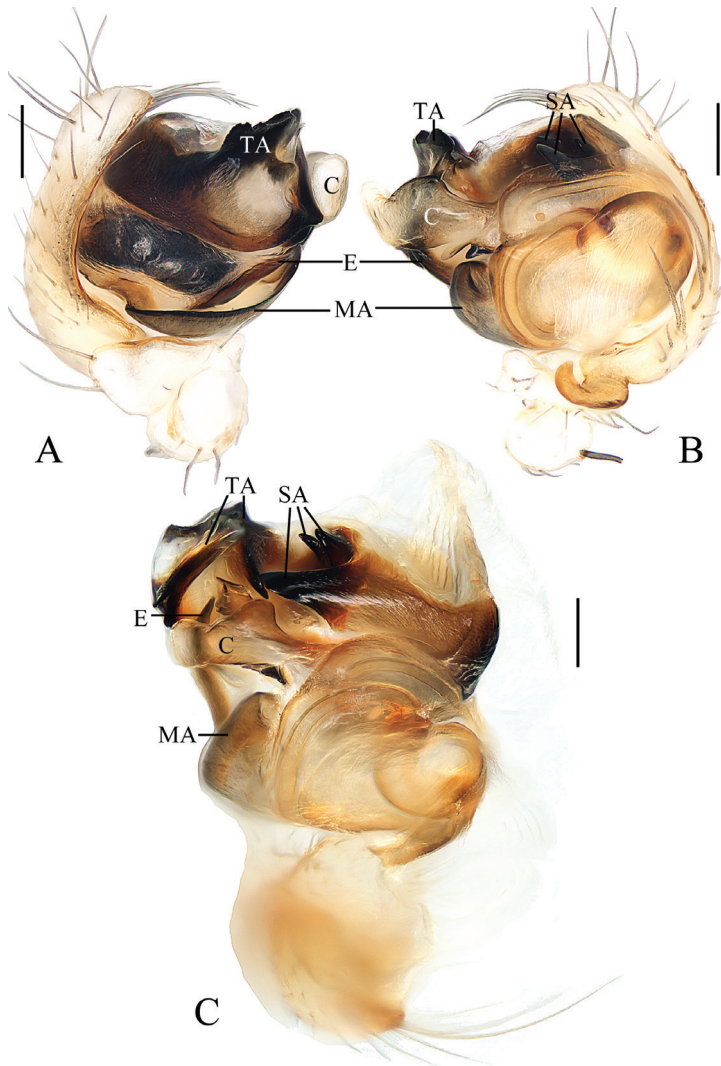


Figure 14. *Mangora baii* sp. nov., male palp **A, B** holotype **C** male paratype IZCAS-Ar42638 **A** prolateral view **B** ventral view **C** expanded in lactic acid. Scale bars: 0.1mm

Diagnosis. The new species differs from congeners by the following combination of characters: 1) the abdomen has two transverse patches and one longitudinal patch; 2) the scape is distally widened; 3) the conductor is long, membranous, and basally trifurcated.

Description. Male (holotype, Figs 14A, B, 15C, D, 21B). Total length 2.60. Carapace 1.40 long, 1.10 wide. Abdomen 1.55 long, 1.00 wide. Clypeus 0.08 high. Eye sizes and interdistances: AME 0.10, ALE 0.05, PME 0.08, PLE 0.05, AME-AME 0.08, AME-ALE 0.03, PME-PME 0.03, PME-PLP 0.10, MOA length 0.30, anterior width 0.30, posterior width 0.20. Leg measurements: I 5.00 (1.35, 1.75, 1.30, 0.60), II 4.40 (1.30, 1.40, 1.15, 0.55), III 2.95 (0.90, 0.95, 0.70, 0.40), IV 4.20 (1.30, 1.35,

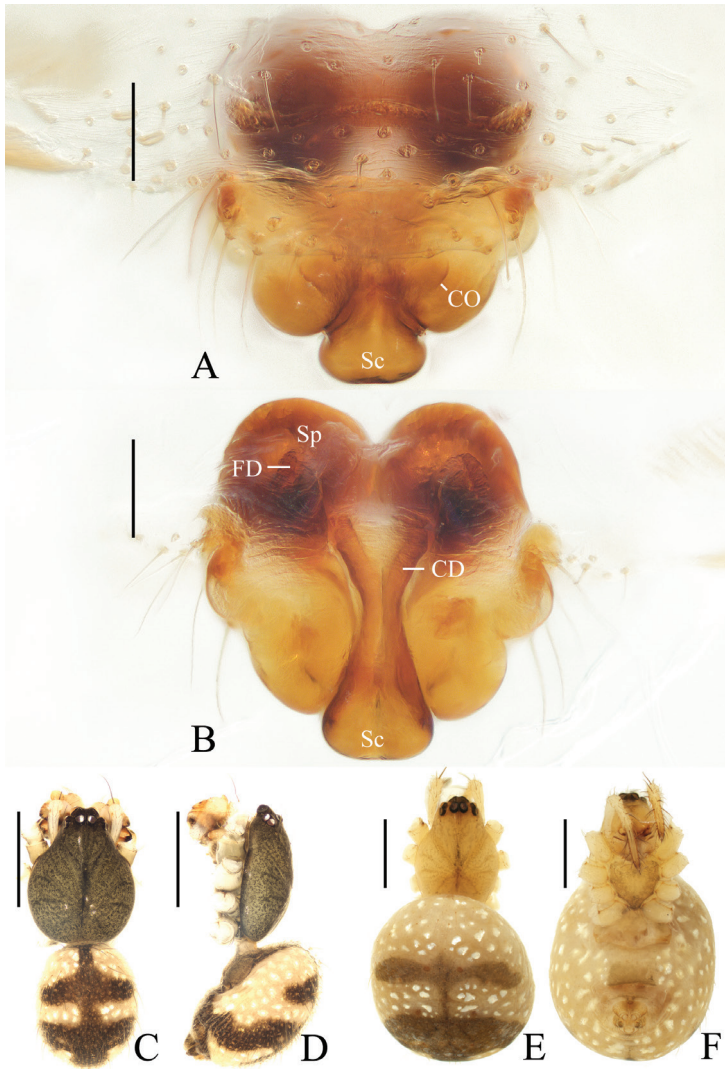


Figure 15. *Mangora baii* sp. nov. **A, B, E, F** female paratype IZCAS-Ar42551 **C, D** holotype **A** epigyne, ventral view **B** ibid., posterior view **C** habitus, dorsal view **D** ibid., lateral view **E** ibid., dorsal view **F** ibid., ventral view. Scale bars: 0.1mm (**A, B**); 1mm (**C-F**)

1.05, 0.50). Carapace pear shaped, grayish yellow with black eye region, cervical groove slightly obvious, fovea longitudinalis. Chelicerae yellow, four promarginal and three retromarginal teeth. Endites grayish yellow, with a protuberance on anterior lateral margin, labium grayish brown, paler distally. Sternum heart-shaped, grayish yellow. Legs yellow without annulations, femur II with furrow basally, tibia II with 13 macrosetae. Abdomen oval, about 1.55 times longer than wide, with long, grayish brown setae, dorsum grayish yellow with two transverse and one longitudinal grayish brown patch; venter grayish yellow, big grayish brown patch medially. Spinnerets grayish yellow.

Palp (Figs 14, 21B): with one patellar bristle; cymbium tip with cluster of long macrosetae, median apophysis about a bulb diameter width, lamellar; embolus tapered and slightly curved; conductor length about equal to bulb diameter, membranous, basally trifurcated; terminal apophysis extremely large, almost triangular in apical view; subterminal apophysis with 3 protuberances.

Female (paratype IZCAS-Ar42551, Fig. 15A, B, E, F). Total length 3.85. Carapace 1.75 long, 1.20 wide. Abdomen 2.65 long, 2.30 wide. Clypeus 0.05 high. Eye sizes and interdistances: AME 0.13, ALE 0.10, PME 0.13, PLE 0.10, AME-AME 0.08, AME-ALE 0.05, PME-PME 0.03, PME-PLE 0.10, MOA length 0.35, anterior width 0.30, posterior width 0.25. Leg measurements: I 6.10 (1.75, 2.10, 1.55, 0.70), II 5.15 (1.50, 1.75, 1.25, 0.65), III 3.50 (1.10, 1.15, 0.75, 0.50), IV 5.15 (1.55, 1.75, 1.25, 0.60). Habitus similar to that of male but endites without protuberances.

Epigyne (Fig. 15A, B): wider than long, with distally widened scape; copulatory openings narrow, situated at anterior base of lateral lobes; copulatory ducts slightly curved; spermathecae globular, touching each other.

Variation. Total length: ♂♂ 2.45–2.60; ♀♀ 3.10–3.85.

Distribution. China (Yunnan).

***Mangora cephal* sp. nov.**

<http://zoobank.org/580FDD3B-F09F-48B5-BB94-A59A9A8B6483>

Figs 16, 17, 21C

Type material. Holotype. ♂ (IZCAS-Ar42553), CHINA: Yunnan, Xishuangbanna, Mengla County, Menglun Town, Menglun Nature Reserve, secondary tropical montane evergreen broad-leaf forest (21°57.53'N, 101°12.30'E, ca 860 m), 19–25.XI.2006, G. Zheng leg. **Paratypes:** 1♀ (IZCAS-Ar42554), rubber plantation (approx. 20 years old) (21°54.65'N, 101°16.26'E, ca 570 m), 16–24.IX.2006, G. Zheng leg.; 1♂ (IZCAS-Ar42555), rubber plantation (approx. 20 years old) (21°54.67'N, 101°16.26'E, ca 570 m), 5–12.X.2006, G. Zheng leg.; 1♀ (IZCAS-Ar42556), rubber plantation (approx. 20 years old) (21°54.46'N, 101°15.98'E, ca 570 m), 5–12.X.2006, G. Zheng leg.; 1♀ (IZCAS-Ar42557), rubber plantation (approx. 20 years old) (21°54.68'N, 101°16.32'E, ca 590 m), 5–12.X.2006, G. Zheng leg.; 1♀ (IZCAS-Ar42558), rubber plantation (approx. 20 years old) (21°54.46'N, 101°15.98'E, ca 570 m), 19–25.X.2006, G. Zheng leg.; 1♀ (IZCAS-Ar42559), rubber plantation (approx. 20 years old) (21°54.67'N, 101°16.26'E, ca 570 m), 19–26.V.2007, G. Zheng leg.; 1♂ (IZCAS-Ar42560), rubber plantation (approx. 20 years old) (21°54.463'N, 101°15.978'E, 569 m), 5–12.XII.2006, G. Zheng leg.; 1♂ (IZCAS-Ar42561), *Paramichelia baillonii* plantation (approx. 20 years old) (21°54.77'N, 101°16.04'E, ca 560 m), 19–25.XII.2006, G. Zheng leg.

Etymology. The specific name is derived from the Greek word “cephalos”, meaning “head”, referring to the brown cephalic region of the females; noun in apposition.

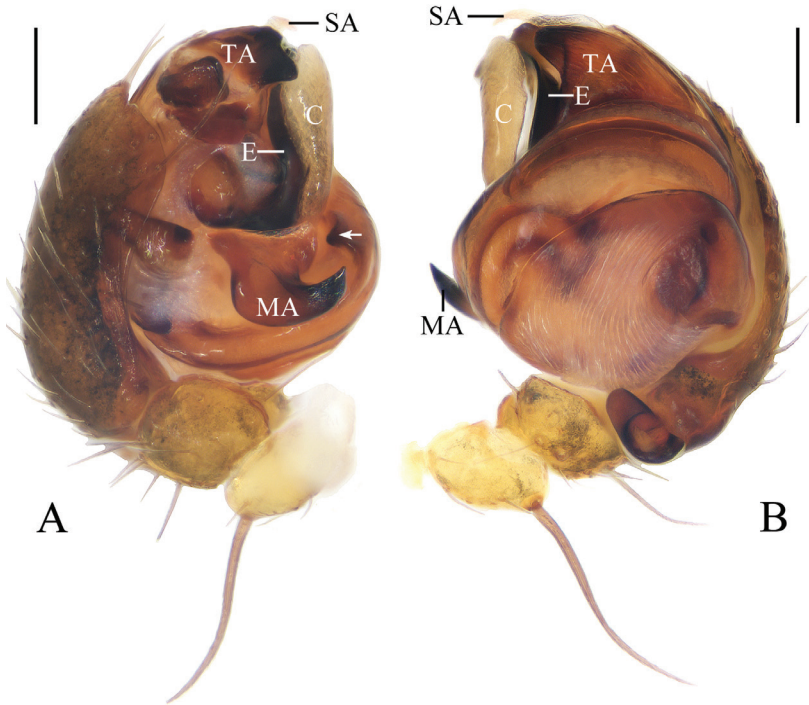


Figure 16. *Mangora cephalo* sp. nov., holotype, male palp **A** prolateral view **B** retrolateral view. Scale bars: 0.1mm

Diagnosis. The new species differs from congeneric species by the following combination of characters: 1) a somewhat rectangular scape; 2) a slender, translucent subterminal apophysis; 3) a tegular protuberance near the base of the median apophysis; and 4) an abdomen with an arcuate brown patch anteriorly and four transverse brown patches medially and posteriorly.

Description. Male (holotype, Figs 16, 17D, E, 21C). Total length 2.40. Carapace 1.20 long, 0.90 wide. Abdomen 1.20 long, 1.00 wide. Clypeus 0.10 high. Eye sizes and interdistances: AME 0.10, ALE 0.05, PME 0.08, PLE 0.05, AME-AME 0.08, AME-ALE 0.05, PME-PME 0.03, PME-PLE 0.08, MOA length 0.23, anterior width 0.25, posterior width 0.20. Leg measurements: I 3.90 (1.20, 1.25, 1.00, 0.45), II 3.30 (1.00, 1.00, 0.90, 0.40), III 2.20 (0.70, 0.70, 0.50, 0.30), IV 3.40 (1.05, 1.05, 0.90, 0.40). Carapace pear shaped, dark brown, cervical groove inconspicuous, fovea longitudinal. Chelicerae dark brown, four promarginal teeth, two retromarginal teeth. Endites and labium dark brown, paler distally. Sternum dark brown with indistinct, darker radial patches. Legs yellow without annulations, femur II with a furrow basally, tibia II with seven macrosetae. Abdomen elliptical, about 1.2 times longer than wide, dorsum yellow with arcuate brown patch anteriorly, four transverse brown patches medially and posteriorly; venter grayish yellow laterally, brown medially. Spinnerets grayish yellow.

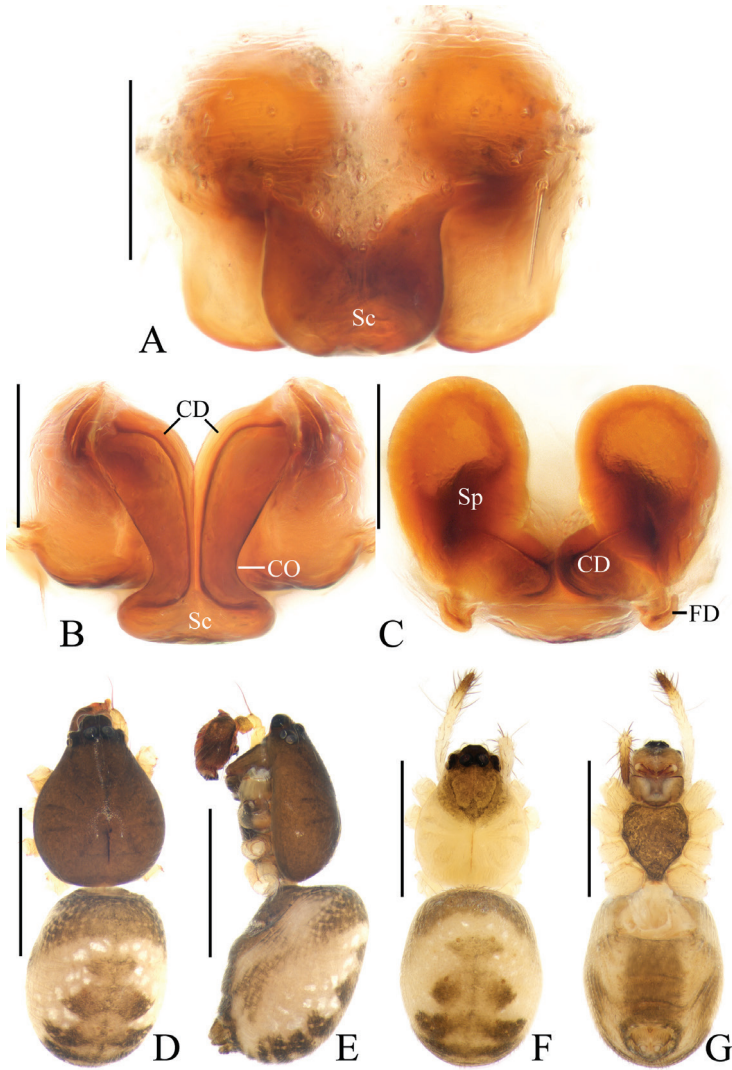


Figure 17. *Mangora cephalala* sp. nov. **A–C, F, G** female paratype IZCAS-Ar42559, **D, E** holotype **A** epigyne, ventral view **B** ibid., posterior view **C** vulva, dorsal view **D** habitus, dorsal view **E** ibid., lateral view **F** ibid., dorsal view **G** ibid., ventral view. Scale bars: 0.1mm (**A–C**); 1mm (**D–G**)

Palp (Figs 16, 21C): with one patellar bristle; tegulum with a protuberance near base of median apophysis (see arrow in Fig. 16A); median apophysis hooked; embolus thick, slightly curved; conductor membranous, as long as embolus in prolateral view; terminal apophysis prominent, pointed distally; subterminal apophysis slender, translucent.

Female (paratype IZCAS-Ar42559, Figs 17A–C, F, G). Total length 2.45. Carapace 1.10 long, 0.85 wide. Abdomen 1.60 long, 1.10 wide. Clypeus 0.03 high. Eye sizes and interdistances: AME 0.10, ALE 0.05, PME 0.08, PLE 0.05, AME-AME 0.08, AME-ALE 0.05, PME-PME 0.05, PME-PLE 0.08, MOA length 0.23, anterior

width 0.23, posterior width 0.20. Leg measurements: I 4.10 (1.25, 1.30, 1.05, 0.50), II 3.65 (1.15, 1.20, 0.90, 0.40), III 2.30 (0.75, 0.70, 0.50, 0.35), IV 3.50 (1.05, 1.10, 0.90, 0.45). Habitus similar to that of male but thoracic region yellow.

Epigyne (Fig. 17A–C) about 1.1 times wider than long; with rectangular scape; copulatory openings wide, covered by lateral part of scape in ventral view; copulatory ducts long, slightly curved, covered by posterior plate in posterior view; spermathecae ovoid, separated from each other.

Variation. Total length: ♂♂ 2.10–2.40; ♀♀ 2.10–2.60.

Distribution. China (Yunnan).

Genus *Milonia* Thorell, 1890

Milonia Thorell, 1890: 180.

Type species *Milonia brevipes* Thorell, 1890 from Sumatra

Comments. This is a poorly understood genus; all seven species were described more than 100 years ago. Among them, two are known from juveniles, five are known from a single-sex, and no high-quality illustrations of the genitalia were provided in the published literature. We place the new species in this genus based on the following characters: large chelicerae, cylindrical abdomen in female, relatively stout legs, spinnerets of the female situated at the middle part of the ventral abdomen.

Milonia gemella sp. nov.

<http://zoobank.org/E7B60026-AE2F-4931-9A75-F1FA4E6E23EA>

Figs 18, 19, 21D

Type material. *Holotype.* ♂ (IZCAS-Ar42562), CHINA: Yunnan, Xishuangbanna, Mengla County, Menglun Town, Menglun Nature Reserve, G213 roadside, secondary forest (21°54.46'N, 101°16.76'E, ca 640 m), 20.XI.2009, G. Tang leg. *Paratypes:* 1 ♀ (IZCAS-Ar42563), primary tropical seasonal rainforest (21°57.53'N, 101°12.38'E, ca 899 m), 4–11.V.2007, G. Zheng leg.; 1 ♀ (IZCAS-Ar42564), secondary tropical forest, around garbage dump (21°54.17'N, 101°16.87'E, ca 609 m), 31.VII.2018, Z. Bai leg.; 1 ♀ (IZCAS-Ar42565), Xishuangbanna Tropical Botanical Garden, site 1 around the dump (21°54.28'N, 101°16.75'E, ca 630 m), 25.IV.2019, Z. Bai leg.

Etymology. The specific name is from the Latin word “gemella”, meaning “twin born”, referring to the two white spots on the abdomen ventrally; adjective.

Diagnosis. The new species can be distinguished from congeneric species by the following combination of characters: 1) dorsal abdomen with two pairs of small grayish brown spots medially and a large dark brown spot posteriorly; 2) triangular scape; and 3) prominent and bifurcated terminal apophysis.

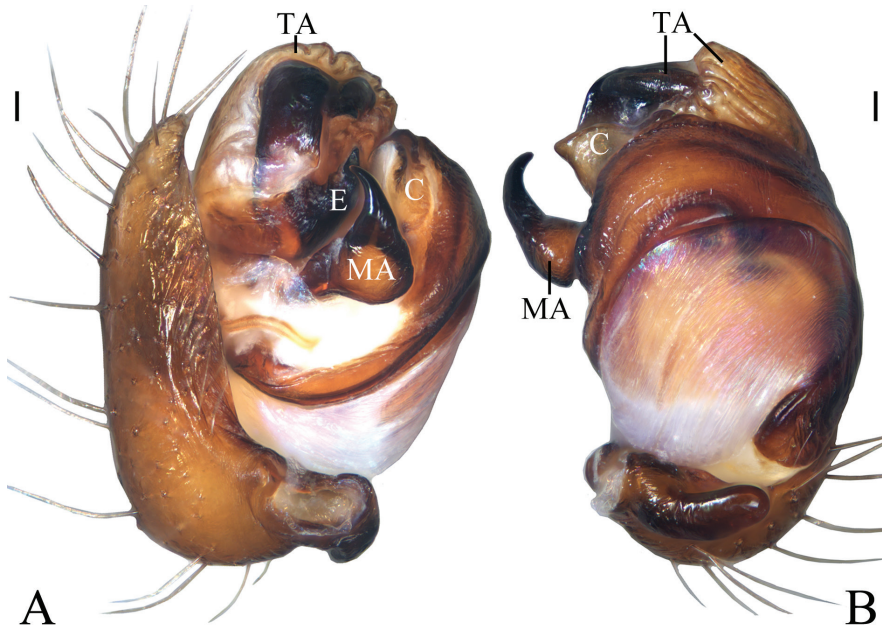


Figure 18. *Milonia gemella* sp. nov., holotype, male palp **A** prolateral view **B** ventral view. Scale bars: 0.1mm

Description. Male (holotype, Figs 18, 19D, E, 21D). Total length 6.30. Carapace 2.90 long, 1.80 wide. Abdomen 3.40 long, 2.10 wide. Clypeus 0.13 high. Eye sizes and interdistances: AME 0.15, ALE 0.10, PME 0.13, PLE 0.10, AME-AME 0.23, AME-ALE 0.28, PME-PME 0.05, PME-PLE 0.38, MOA length 0.38, anterior width 0.40, posterior width 0.28. Leg measurements: I 7.30 (2.10, 2.75, 1.55, 0.90), II 6.75 (1.90, 2.40, 1.60, 0.85), III 4.00 (1.25, 1.40, 0.75, 0.60), IV 5.30 (1.65, 2.00, 1.05, 0.60). Carapace elliptical, brown, with pale setae, cervical groove obvious. Chelicerae brown, four promarginal teeth, three retromarginal teeth. Endites brown, paler distally, labium triangular, brown, paler distally. Sternum pentagonal, dark brown with pale setae. Legs brown, without annulations. Abdomen elliptical, about 1.6 times longer than wide, covered with dark setae, dorsum yellow with two pairs of grayish brown spots medially, big black spot posteriorly; venter yellowish brown with pair of white spots. Spinnerets yellowish brown, at posterior 1/3 of the abdomen.

Palp (Figs 18, 21D): with two patellar bristles; median apophysis stout at base, with a slender, curved spur; embolus broad at base, abruptly tapered to a fine tip; conductor broad at base, tapering to a narrow tip; terminal apophysis extremely large, strongly sclerotized, bifurcated distally, one long, narrow branch, one shorter, wider branch (see arrows in Fig. 21D).

Female (paratype IZCAS-Ar42564, Fig. 19A–C, F, G). Total length 9.40. Carapace 3.60 long, 2.40 wide. Abdomen 6.10 long, 3.10 wide. Clypeus 0.23 high. Eye siz-

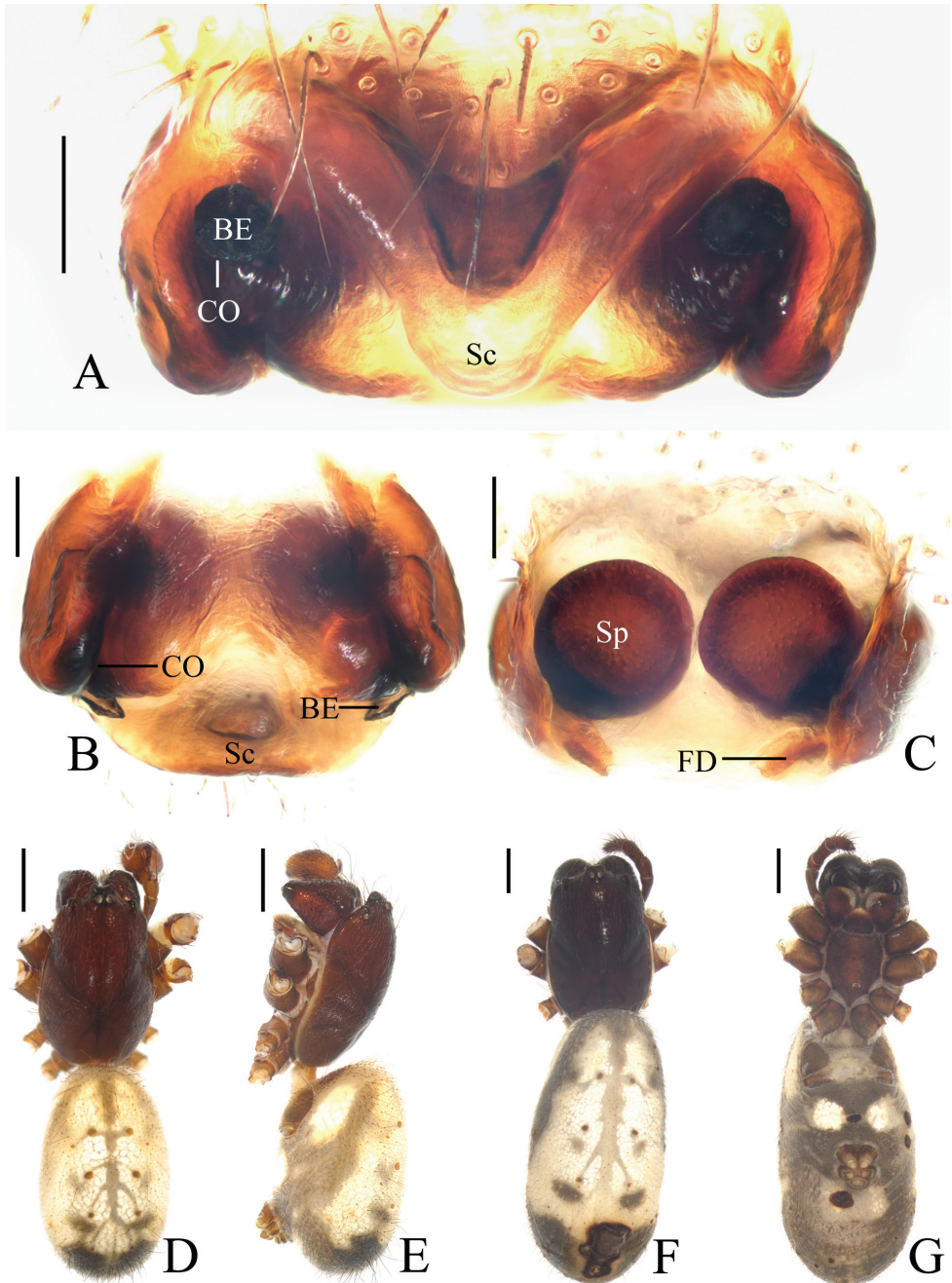


Figure 19. *Milonia gemella* sp. nov. **A-C, F, G** female paratype IZCAS-Ar42564 **D, E** holotype **A** epigyne, ventral view **B** ibid., posterior view **C** vulva, dorsal view **D** habitus, dorsal view **E** ibid., lateral view **F** ibid., dorsal view **G** ibid., ventral view. Scale bars: 0.1 mm (**A-C**); 1mm (**D-G**)

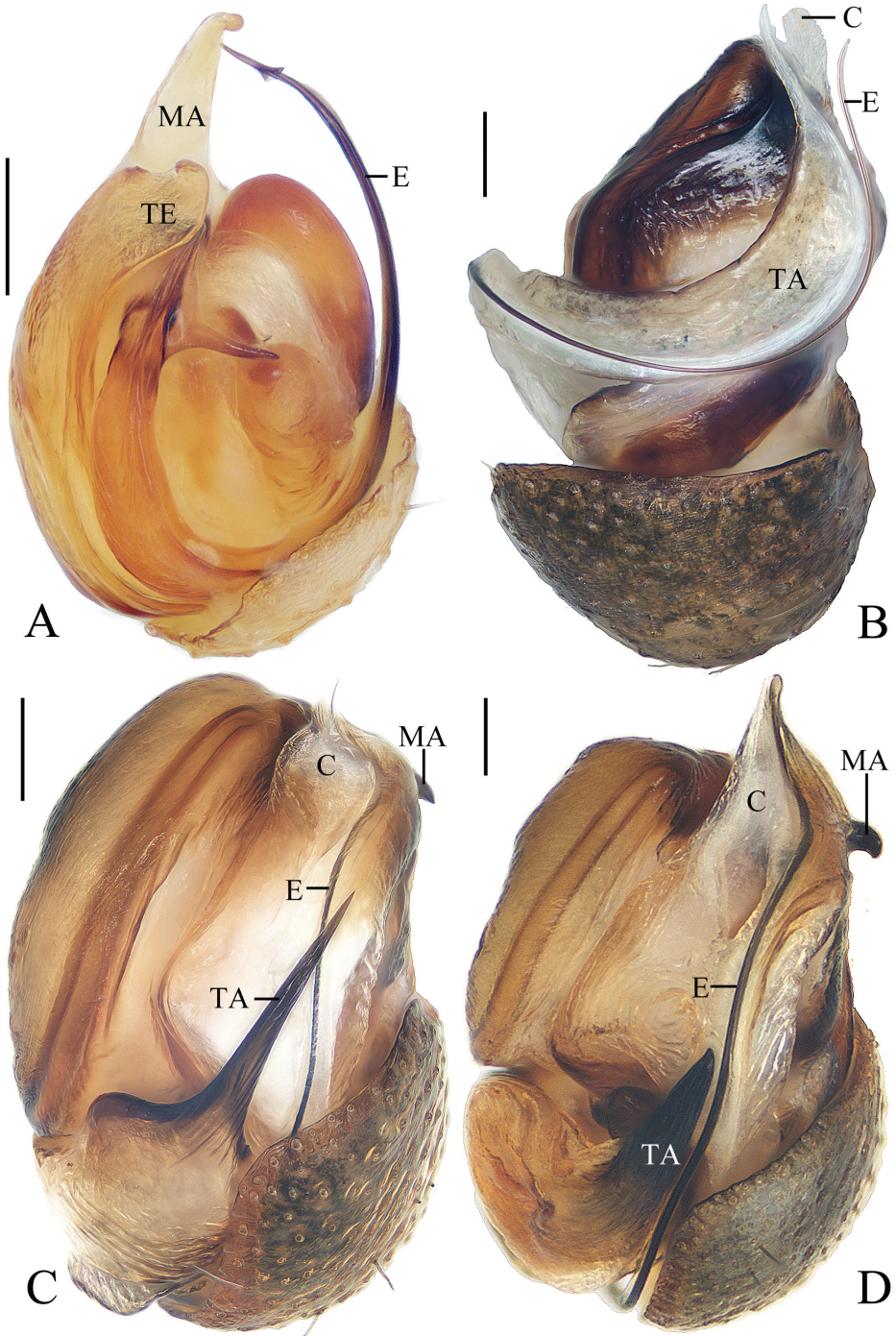


Figure 20. Male palps, apical view **A** *Acusilas tongi* sp. nov. **B** *Chorizopesoides guoi* sp. nov. **C** *Deione yangi* sp. nov. **D** *Deione lingulata*. Scale bars: 0.1

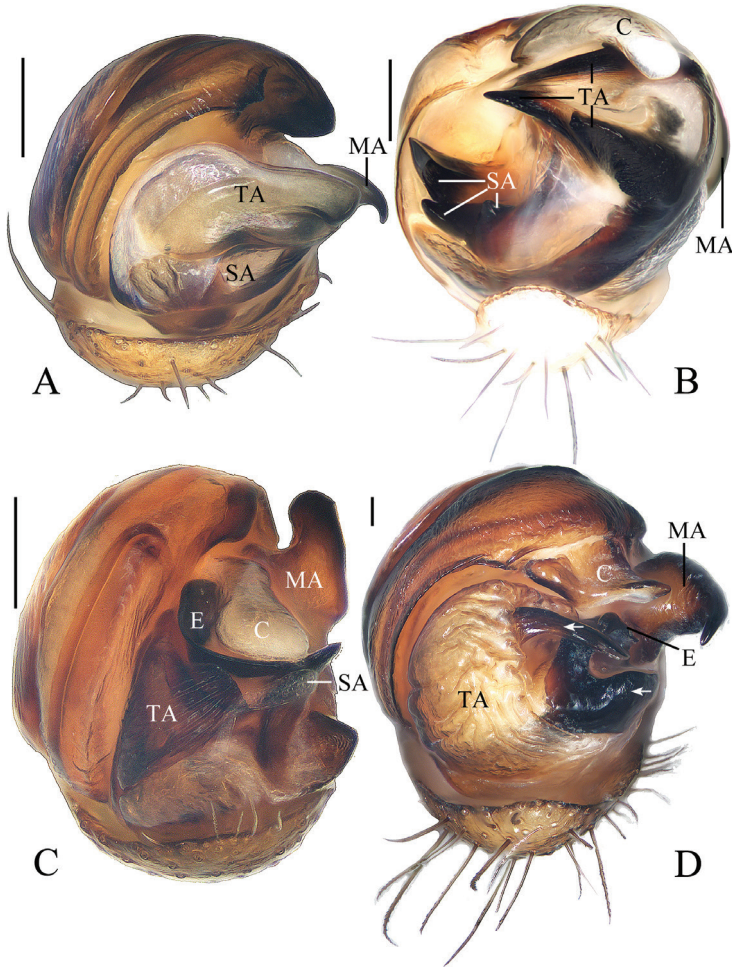


Figure 21. Male palps, apical view **A** *Hyposinga pulla* sp. nov. **B** *Mangora baii* sp. nov. **C** *Mangora cephalata* sp. nov. **D** *Milonia gemella* sp. nov. Scale bars: 0.1mm

es and interdistances: AME 0.18, ALE 0.10, PME 0.13, PLE 0.10, AME-AME 0.15, AME-ALE 0.45, PME-PME 0.05, PME-PLE 0.63, MOA length 0.45, anterior width 0.45, posterior width 0.28. Leg measurements: I 8.45 (2.40, 3.05, 2.05, 0.95), II 7.55 (2.10, 2.85, 1.75, 0.85), III 4.20 (1.00, 1.75, 0.85, 0.60), IV 6.40 (1.95, 2.50, 1.25, 0.70). Habitus similar to that of male but abdomen about two times longer than wide.

Epigyne (Fig. 19A–C) about two times wider than long; short, triangular scape, flanked by round copulatory openings; copulatory ducts shorter than a spermatheca diameter; spermathecae globular, touching each other.

Variation. Total length: ♀♀ 9.20–9.40.

Distribution. China (Yunnan).

Acknowledgments

The manuscript benefited greatly from comments by Zhiyuan Yao, Akio Tanikawa, Yuri Marusik, Anna Šestáková. Sarah Crews checked the English. Theo Blick checked etymologies of the new taxa. Guo Tang, Guo Zheng, Yanfeng Tong, Hao Yu, Cheng Wang, Jiahui Gan, Zhigang Chen, Zilong Bai, Yuanfa Yang, and Hong Liu helped with fieldwork. This research was supported by the National Natural Science Foundation of China (NSFC-31660609), the Science and Technology Project Foundation of Guizhou Province ([2020]1Z014), and the Key Laboratory Project of Guizhou Province ([2020]2003).

References

- Ausserer A (1871) Neue Radspinnen. Verhandlungen der Kaiserlich-Königlichen Zoologisch-Botanischen Gesellschaft in Wien 21: 815–832.
- Han GX, Zhu MS, Levi HW (2009) On two rare south-east Asian araneid genera: *Deione* and *Talhythbia* (Araneae: Araneidae). Zootaxa 2297: 55–63. <https://doi.org/10.11646/zootaxa.2297.1.5>
- Kallal RJ & Hormiga G (2019) Evolution of the male palp morphology of the orb-weaver hunting spider *Chorizopes* (Araneae: Araneidae) revisited on a new phylogeny of Araneidae, and description of a third species from Madagascar. Invertebrate Systematics 33(3): 473–487. <https://doi.org/10.1071/IS18061>
- Li S (2020) Spider taxonomy for an advanced China. Zoological Systematics 45(2): 73–77. <https://doi.org/10.11865/zs.202011>
- Li J, Yan X, Lin Y, Li S, Chen H (2021) Challenging Wallacean and Linnean shortfalls: *Ectosticta* spiders (Araneae, Hypochilidae) from China. Zoological Research 42(6): 791–794. <https://doi.org/10.24272/j.issn.2095-8137.2021.212>
- Mi X, Li S (2021) On nine species of the spider genus *Eriovixia* (Araneae, Araneidae) from Xishuangbanna, China. ZooKeys 1034: 199–236. <https://doi.org/10.3897/zookeys.1034.60411>
- Mi X, Peng X & Yin C (2010) Two new species of the rare orbweaving spider genus *Deione* (Araneae: Araneidae) from China. Zootaxa 2491: 34–40. <https://doi.org/10.11646/zootaxa.2491.1.2>
- Mi X, Wang C (2018) *Chorizopesoides*, a new genus of orb-weaver spider from China (Araneae: Araneidae). Oriental Insects 52(1): 79–87. <https://doi.org/10.1080/00305316.2017.1347843>
- Murphy J, Murphy F (1983) The orb weaver genus *Acusilas* (Araneae, Araneidae). Bulletin of the British Arachnological Society 6: 115–123.
- Pickard-Cambridge O (1871) On some new genera and species of Araneida. Proceedings of the Zoological Society of London 38(3, 1870): 728–747. [pl. 44]
- Pickard-Cambridge O (1889) Arachnida. Araneida. In: Biologia Centrali-Americana, Zoology. London 1, 1–56.

- Schmidt JB, Scharff N (2008) A taxonomic revision of the orb-weaving spider genus *Acusilas* Simon, 1895 (Araneae, Araneidae). *Insect Systematics & Evolution* 39(1): 1–38. <https://doi.org/10.1163/187631208788784147>
- Simon E (1895) *Histoire naturelle des araignées*. Deuxième édition, tome premier. Roret, Paris, 761–1084.
- Thorell T (1873) Remarks on synonyms of European spiders. Part IV. C. J. Lundström, Uppsala, 375–645.
- Tikader BK (1982) Part 1. Family Araneidae (= Argiopidae). Typical orb-weavers. In: *The fauna of India. Spiders: Araneae*. Vol. II. Zoological Survey of India, Calcutta, 293 pp.
- Thorell T (1890) Studi sui ragni Malesi e Papuani. IV, 1. *Annali del Museo Civico di Storia Naturale di Genova* 28: 5–421.
- Thorell T (1898) Viaggio di Leonardo Fea in Birmania e regioni vicine. LXXX. Secondo saggio sui Ragni birmani. II. Retitelariae et Orbitelariae. *Annali del Museo Civico di Storia Naturale di Genova* 39: 271–378.
- WSC (2021) World Spider Catalog, version 22.5. Natural History Museum Bern. <https://doi.org/10.24436/2> [accessed on 2021-8-20]
- Yao Z, Wang X, Li S (2021) Tip of the iceberg: species diversity of *Pholcus* spiders (Araneae, Pholcidae) in Changbai Mountains, Northeast China. *Zoological Research* 42(3): 267–271. <https://doi.org/10.24272/j.issn.2095-8137.2020.214>
- Yin CM, Wang JF, Zhu MS, Xie LP, Peng XJ, Bao YH (1997) *Fauna Sinica: Arachnida: Araneae: Araneidae*. Science Press, Beijing, 460 pp.
- Yin CM, Peng XJ, Yan HM, Bao YH, Xu X, Tang G, Zhou QS, Liu P (2012) *Fauna Hunan: Araneae in Hunan, China*. Hunan Science and Technology Press, Changsha, 1590 pp.

A new species of the genus *Tylototriton* (Urodela, Salamandridae) from western Thailand

Porrawee Pomchote¹, Parada Peerachidacho¹, Axel Hernandez^{2,3}, Pitak Sapewisit⁴,
Wichase Khonsue¹, Panupong Thammachoti¹, Kanto Nishikawa^{5,6}

1 Department of Biology, Faculty of Science, Chulalongkorn University, Bangkok 10330, Thailand **2** Department of Environmental Sciences, Faculty of Sciences and Technics, University Pasquale Paoli of Corsica, Corte 20250, France **3** Laboratory for Amphibian Systematic and Evolutionary Research, College of Biology and Environment, Nanjing Forestry University, Nanjing 210000, China **4** Department of Biology, Faculty of Science, Chiang Mai University, Chiang Mai 50200, Thailand **5** Graduate School of Global Environmental Studies, Kyoto University, Kyoto 606–8501, Japan **6** Graduate School of Human and Environmental Studies, Kyoto University, Kyoto 606–8501, Japan

Corresponding author: Porrawee Pomchote (porrawee.p@chula.ac.th)

Academic editor: Luis Ceriaco | Received 15 September 2021 | Accepted 1 November 2021 | Published 19 November 2021

<http://zoobank.org/E68B9AFC-3D00-43BB-8C13-9BF3A8FEB559>

Citation: Pomchote P, Peerachidacho P, Hernandez A, Sapewisit P, Khonsue W, Thammachoti P, Nishikawa K (2021) A new species of the genus *Tylototriton* (Urodela, Salamandridae) from western Thailand. ZooKeys 1072: 83–105. <https://doi.org/10.3897/zookeys.1072.75320>

Abstract

We describe a new species of the newt genus *Tylototriton* from Umphang Wildlife Sanctuary, Tak Province, western Thailand based on molecular and morphological evidence and named here as *Tylototriton umphangensis* **sp. nov.** The new species is assigned to the subgenus *Tylototriton* and differs from other species in having dark-brown to blackish-brown body and limbs, truncate snout, prominent antero-medial ends of the expansion of the dentary bones, laterally protruding quadrate regions, indistinct and small rib nodules, a well-segmented vertebral ridge, and rough dorsolateral bony ridges, which are steeper anterior, and curved medially at the posterior ends. The molecular data show that *Tylototriton umphangensis* **sp. nov.** differs from *T. uyenoii* sensu stricto by a 5% genetic sequence divergence of the mitochondrial NADH dehydrogenase subunit 2 region gene. The new species and *T. uyenoii* are both endemic to Thailand, distributed along the Northwest Thai (Dawna) Uplands of Indochina. To clarify the species boundary between *Tylototriton umphangensis* **sp. nov.** and *T. uyenoii*, additional field research is needed in adjacent areas. *Tylototriton umphangensis* **sp. nov.** is restricted to evergreen hill forests in Umphang Wildlife Sanctuary. We suggest that the new species should be classified as Endangered (EN) in the IUCN Red List.

Keywords

conservation, crocodile newt, cryptic species, South-east Asia, taxonomy

Introduction

The salamandrid genus *Tylototriton* Anderson, 1871, commonly known as crocodile newts, includes 32 nominal species ranging across eastern Himalaya, eastern Nepal, northern India, Bhutan, Myanmar, central to southern China (including Hainan island), and southwards through Laos to Thailand and Vietnam (Hernandez 2016; Bernardes et al. 2020; Pomchote et al. 2020a, 2020b; Poyarkov et al. 2021a). Outside of breeding season, all known species are terrestrial and micro-endemic, regarded mostly as niche specialists that are generally found at middle to high elevations in subtropical, moist, forested environments. These provide a relatively narrow thermal range (15–24.0 °C) with a high annual rainfall, especially during the monsoon season, which ensures favorable breeding conditions and survival of *Tylototriton* species (Hernandez et al. 2018).

The genus is subdivided into three subgenera, *Tylototriton*, *Yaotriton*, and *Liangshantriton* (e.g., Dubois and Raffaëlli 2009; Fei et al. 2012; Nishikawa et al. 2013a, 2013b; Phimmachak et al. 2015; Wang et al. 2018; Poyarkov et al. 2021a) and includes several, as yet, unnamed taxa, which contain cryptic species that are morphologically difficult to distinguish (Hernandez 2016; Poyarkov et al. 2021a). Recent studies have provided a better understanding of the ecology, biology, taxonomy, phylogenetic relationships, and conservation of these endangered species that have been highly harvested in recent years throughout South-east Asia (Phimmachak et al. 2015; Hernandez et al. 2018; Wang et al. 2018; Bernardes et al. 2020; Pomchote et al. 2020a, 2020b; Poyarkov et al. 2021a). Several recent phylogenetic studies have also revealed the presence of undescribed cryptic lineages, which actually might represent independent species, in South-east Asia, especially in the Indochina region (Wang et al. 2018; Zaw et al. 2019; Bernardes et al. 2020; Pomchote et al. 2020a, 2020b; Poyarkov et al. 2021a).

To our knowledge, Thailand contains five *Tylototriton* species (Nishikawa et al. 2013a; Le et al. 2015; Pomchote et al. 2020a, 2020b). They are distributed allopatrically in high mountainous areas at altitudes above 1,000 m mean sea level throughout the northern (*T. verrucosus*, *T. uyenoii*, *T. anguliceps*, and *T. phukhaensis*), northeastern (*T. panhai*), and western (*T. uyenoii*) regions (Hernandez and Pomchote 2020a, 2020b, 2020c; Pomchote et al. 2020a, 2020b). Recent field surveys recorded several new *Tylototriton* populations distributed in the western region of Thailand, where the southernmost record in Asia of the genus was recorded (Hernandez and Pomchote 2020c). These populations were previously identified as *T. uyenoii* according to their morphological appearance and distribution, and they range from the Daen Lao and Thanon Thong Chai Ranges, southwards to the Dawna Range (Hernandez 2016, 2017; Hernandez et al. 2019).

However, according to Hernandez (2016), these newly found *T. uyenoii* populations show different phenotypes and an allopatric distribution in scattered and sepa-

rated mountainous areas, resulting in the recent description of *T. phukhaensis* by Pomchote et al. (2020b). Moreover, the limited number of specimens examined in previous studies (Hernandez 2016, 2017; Hernandez et al. 2019; Hernandez and Pomchote 2020c), lack any detailed morphological examination and molecular analysis leading to the question of the taxonomic status of these populations.

As polymorphic species provide an opportunity to examine the role of isolation in populations that may contribute to the process of divergence, we assessed the western populations of *Tylotriton* species in the Umphang Wildlife Sanctuary (UPWS), Tak Province, which is located through the Dawna Range in western Thailand. This divergent population was discovered several years ago (Hernandez 2016; Hernandez et al. 2019). The molecular and morphological evidence indicate that the crocodile newt specimens from UPWS belong to a lineage distinct from the known *Tylotriton* species. As a consequence, we describe the UPWS newts as a new species, *Tylotriton umphangensis* **sp. nov.**, and discuss its taxonomic relationships, distribution, and implications for conservation.

Materials and methods

Sampling

The field survey was performed on 19 June 2021 at UPWS, Tak Province, western Thailand (Fig. 1) using the visual encounter survey method (Heyer et al. 1994). Four specimens were found in a small pond that drains into a stream. The pond was surrounded by hill evergreen forest and located on the mountain at an elevation of approximately 1,150 m a.m.s.l. (above mean sea level). Specimens of *Tylotriton* were caught by hand and kept in plastic boxes for examination. The biological and physical parameters of their habitats were recorded.

All four newts were checked for sex and maturity using the cloacal characters (Pomchote et al. 2008) and were subsequently sexed as breeding males. All specimens were used for molecular and morphological analyses.

Live specimens were anesthetized by immersion in a solution of tricaine methane sulfonate (MS-222; 5 g/L) for about 5 min (Pomchote et al. 2020a), euthanized by a solution of chloretone (Heyer et al. 1994), and then measured for morphometrics and body weight (BW), as detailed below. The tissue samples (liver) of each individual were taken, and then stored in 95% (v/v) ethanol for molecular study prior to preservation. The voucher specimens were subsequently preserved in 70% (v/v) ethanol and deposited at the Chulalongkorn University Museum of Natural History (CUMZ).

Molecular analyses

Total DNA was extracted from the liver using a PureDireX™ genomic isolation kit (Bio-Helix, Taiwan). The mitochondrial NADH dehydrogenase 2 gene (ND2) was

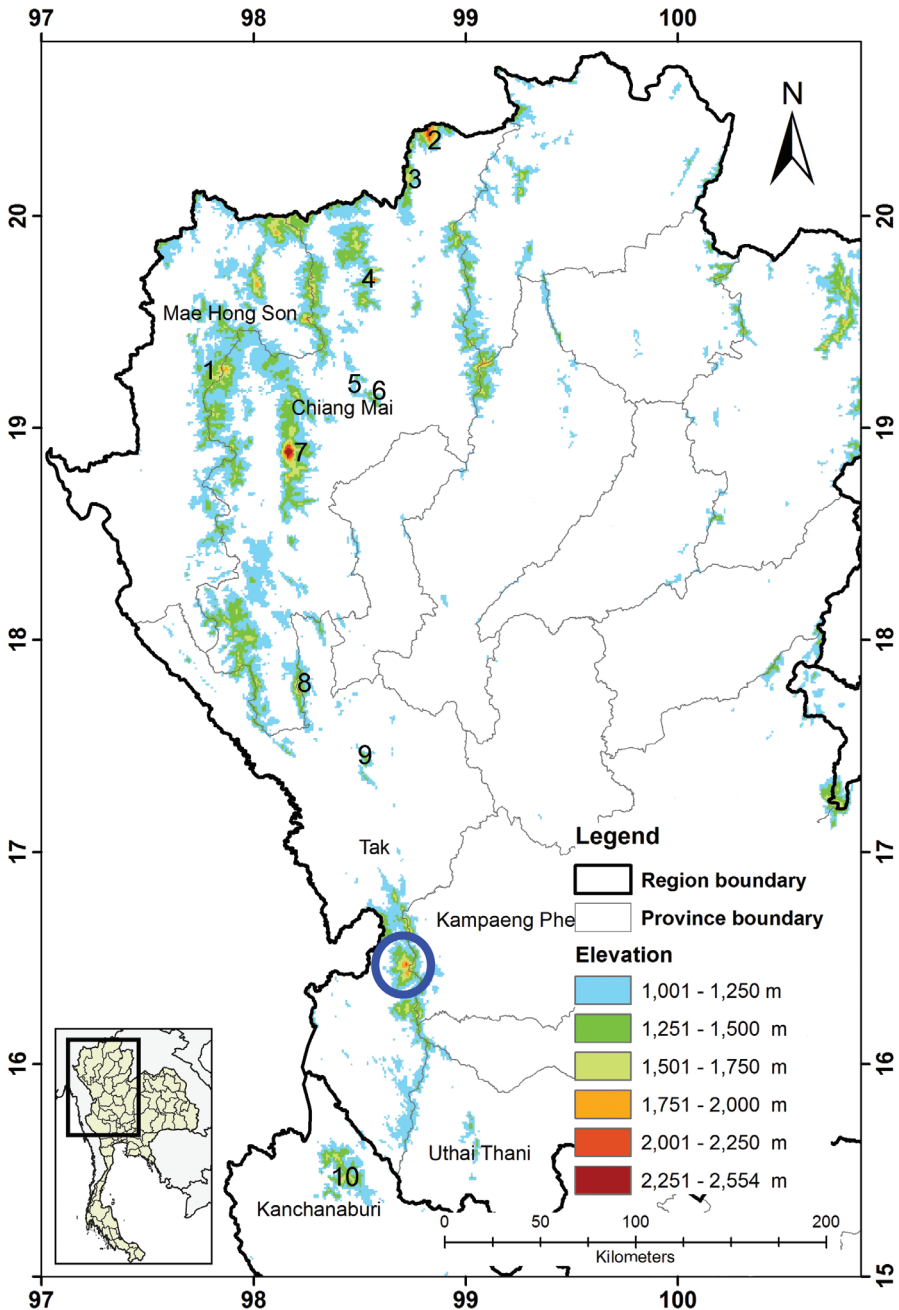


Figure 1. Localities for the *Tylototriton umphangensis* sp. nov., (circle = type locality) at Umphang Wildlife Sanctuary, Tak Province and the distribution of its closely related species, *T. uyenoi* (number) in Thailand: **1** Nantok Mae Surin NP, Mae Hong Son Province **2** Doi Mak Lang **3** Doi Ang Khang **4** Chiang Dao WS **5** Doi Suthep-Pui **6** Doi Chang Kien **7** Doi Inthanon **8** Doi Mon Jong, Chiang Mai Province **9** Doi Soi Malai, Tak Province and **10** Khao Laem NP, Kanchanaburi Province. NP = National Park and WS = Wildlife Sanctuary. The map is modified by N. Taewcharoen.

amplified using the polymerase chain reaction (PCR) with the SL-1 (5'-ATAGAG-GTTCAAACCCTCTC-3') and the SL-2 (5'-TTAAAGTGTCTGGGTTGCATTCA G-3') primers (Wang et al. 2018). Each PCR reaction consisted of 15 μ L of OnePCR™ Ultra (GeneDirex, Taiwan), which is a premixed solution, 1.5 μ L of each primer (10 μ M), 9 μ L of UltraPure™ DNase/RNase-Free distilled water (Invitrogen, USA), and 3 μ L of DNA template. The thermal cycling was performed at 94 °C for 4 min, followed by 35 cycles of 94 °C for 30 s, 55 °C for 1 min, and 72 °C for 90 s (Wang et al. 2018). The PCR products were checked by agarose gel electrophoresis to confirm their size and estimate the concentration. The desired PCR products were purified and commercially sequenced by Bioneer Inc. in South Korea.

We combined the four new sequences of the UPWS samples obtained in this study with those of the other related species available from GenBank (Table 1). The optimum substitution models were selected using Kakusan 4 (Tanabe 2011). We then constructed phylogenetic trees by Bayesian inference (BI) and maximum likelihood (ML) analyses using MrBayes v. 3.1.2 (Huelsenbeck and Ronquist 2001) and RAxML v. 8 (Stamatakis 2014), respectively. The criterion used for model selection was AIC, with the codon-equal-rate model with the general time reversible model (GTR) + Gamma (G) being selected for ML and the codon-proportional model with the Hasegawa-Kishino-Yano-1985 (HKY85) model + G for each codon position for the BI. The BI analysis was performed as two independent runs of four Markov chains for 10 million generations, sampling one tree every 100 generations and calculating a consensus topology for 70,000 trees after discarding the first 30,001 trees (burn-in = 3,000,000). For the BI, we considered posterior probabilities (bpp) of 95% or greater as significant support (Leaché and Reeder 2002). The robustness of the ML tree was tested using bootstrap analysis (Felsenstein 1985) with 2,000 replicates, and we accepted tree topologies with bootstrap values (bs) of $\geq 70\%$ to be significantly supported (Huelsenbeck and Hillis 1993). Pairwise comparisons of uncorrected sequence divergences (p-distance by 1,013 base pairs; bp) were calculated using MEGA v. 7 (Kumar et al. 2016).

Morphological examination

The morphometric characters of the UPWS newts were compared with those of *T. uyenoii* because their appearances and color pattern are rather similar; moreover, previous studies identified the UPWS newts as *T. uyenoii* (Hernandez et al. 2019). Note that the other four *Tylototriton* species from Thailand (*T. verrucosus*, *T. anguliceps*, *T. phukhaensis*, and *T. panhai*) were not included in this morphometric study for two reasons. Firstly, the external morphology of *T. verrucosus*, *T. anguliceps*, and *T. phukhaensis* was clearly different from that of *T. uyenoii* (see Pomchote et al. 2020a, 2020b), although morphological comparisons using the published literature were made (see comparisons below). Secondly, *T. panhai* has different color pattern from that of the other Thai *Tylototriton* species; moreover, *T. panhai* is a member of another lineage, the subgenus *Yaotriton* (Nishikawa et al. 2013a).

Table 1. Specimens of *Tylototriton* and other related species used for the molecular analyses. CAS = California Academy of Sciences; CIB = Chengdu Institute of Biology; CUMZ (A) = Natural History Museum of Chulalongkorn University Section Amphibians; KIZ = Kunming Institute of Zoology; KUHE = Graduate School of Human and Environmental Studies, Kyoto University; MVZ = Museum of Vertebrate Zoology, University of California, Berkeley; NMNS = National Museum of Natural Science, Taiwan; VNMN = Vietnam National Museum of Nature; ZMMU = Zoological Museum of Moscow State University. *Topotype.

Sample no.	Species	Voucher no.	Locality	GenBank no.	Source
1	<i>Tylototriton umphangensis</i> sp. nov.	CUMZ-A-8243	Umphang Wildlife Sanctuary, Tak, Thailand	OK092618	This study
2	<i>Tylototriton umphangensis</i> sp. nov.	CUMZ-A-8244	Umphang Wildlife Sanctuary, Tak, Thailand	OK092619	This study
3	<i>Tylototriton umphangensis</i> sp. nov.	CUMZ-A-8245	Umphang Wildlife Sanctuary, Tak, Thailand	OK092620	This study
4	<i>Tylototriton umphangensis</i> sp. nov.	CUMZ-A-8246	Umphang Wildlife Sanctuary, Tak, Thailand	OK092621	This study
5	<i>Tylototriton uyenoii</i> *	KUHE 19147	Doi Suthep, Chiang Mai, Thailand	AB830733	Nishikawa et al. (2013a)
6	<i>Tylototriton phukhaensis</i> *	CUMZ-A-7719	Doi Phu Kha National Park, Nan, Thailand	MN912575	Pomchote et al. (2020b)
7	<i>Tylototriton anguliceps</i> *	VNMN A.2014.3	Muong Nhe, Dien Bien, Vietnam	LC017832	Le et al. (2015)
8	<i>Tylototriton verrucosus</i> *	KIZ 201306055	Husa, Yunnan, China	AB922818	Nishikawa et al. (2014)
9	<i>Tylototriton parhai</i> *	No voucher	Phu Luang Wildlife Sanctuary, Loei, Thailand	AB830736	Nishikawa et al. (2013a)
10	<i>Tylototriton shanjing</i> *	NMNS 3682	Jingdong, Yunnan, China	AB830721	Nishikawa et al. (2013a)
11	<i>Tylototriton pulcherrimus</i>	KUHE 46406	Yunnan, China	AB830738	Nishikawa et al. (2013a)
12	<i>Tylototriton podichthys</i>	KUHE 34399	Xam Neua, Houa Phan, Laos	AB830727	Nishikawa et al. (2013a)
13	<i>Tylototriton panwaensis</i> *	CAS 245418	Panwa, Myitkyina, Myanmar	KT304279	Grismer et al. (2018)
14	<i>Tylototriton yangi</i>	KUHE 42282	Yunnan, China	AB769546	Nishikawa et al. (2013b)
15	<i>Tylototriton shanorum</i> *	CAS 230940	Taunggyi, Shan, Myanmar	AB922823	Nishikawa et al. (2014)
16	<i>Tylototriton himalayanus</i>	MVZ no number	Nepal	DQ517854	Weisrock et al. (2006)
17	<i>Tylototriton kachinorum</i> *	ZMMU A5953	Indawgyi, Kachin, Myanmar	MK097273	Zaw et al. (2019)
18	<i>Tylototriton kweichowensis</i>	MVZ 230371	Daguan, Yunnan, China	DQ517851	Weisrock et al. (2006)
19	<i>Tylototriton talangensis</i>	KUHE 43361	Unknown, China	AB769543	Nishikawa et al. (2013b)
20	<i>Echinotriton andersoni</i> *	KUHE no number	Nago, Okinawa, Japan	AB769545	Nishikawa et al. (2013b)

We compared the reported morphometrics of a total of 12 specimens, the four *Tylototriton* sp. from UPWS (four males: CUMZ-A-8243 to -8246) of this study, and eight specimens of *T. uyenoii* obtained previously from the same localities of the holotype and paratypes of *T. uyenoii* (Nishikawa et al. 2013a). The specimens of *T. uyenoii* were loaned from the Natural History Museum, National Science Museum, Thailand (THNHM): topotypic specimens THNHM 10319–10320, 20170 (three males) from Doi (= Mountain in Thai language) Suthep-Doi Pui National Park (NP), Chiang Mai Province; and THNHM 13866, 13868, 13870–13871 (four males), and THNHM 13869 (one female) from Doi Inthanon NP, Chiang Mai Province, which is the same locality as the paratypes.

The following 27 measurements were taken for morphometric comparisons, where the character definitions are given in Nishikawa et al. (2011): **SVL** (snout–vent length); **HL** (head length); **HW** (head width); **MXHW** (maximum head width); **SL**

(snout length); **LJL** (lower jaw length); **ENL** (eyelid-nostril length); **IND** (internarial distance); **IOD** (interorbital distance); **UEW** (upper eyelid width); **UEL** (upper eyelid length); **OL** (orbit length); **AGD** (axilla-groin distance); **TRL** (trunk length); **TAL** (tail length); **VL** (vent length); **BTAW** (basal tail width); **MTAW** (medial tail width); **BTAH** (basal tail height); **MXTAH** (maximum tail height); **MTAH** (medial tail height); **FLL** (forelimb length); **HLL** (hindlimb length); **2FL** (second finger length); **3FL** (third finger length); **3TL** (third toe length); and **5TL** (fifth toe length). All measurements were taken using a digital sliding caliper to the nearest 0.01 mm, subsequently rounded to 0.1 mm. Each measurement was taken three times and the average was used for further analyses. Their body weights (**BW**) were recorded using a digital weighing scale to the nearest 0.1 gm.

For morphological comparisons, the data for the other related species were taken from the related literatures (Fang and Chang 1932; Liu 1950; Nussbaum et al. 1995; Böhme et al. 2005; Hou et al. 2012; Nishikawa et al. 2013a, 2014; Khatiwada et al. 2015; Le et al. 2015; Phimmachak et al. 2015; Grismer et al. 2018, 2019; Zaw et al. 2019; Pomchote et al. 2020a, 2020b).

Statistical analysis

We compared the SVL, BW, and the other 25 ratio values to SVL (presented as % SVL) between *Tylototriton* sp. from UPWS and the other *T. uyenoii* specimens. Differences in morphological characters between the *Tylototriton* sp. from UPWS and *T. uyenoii* were analyzed by the Mann-Whitney *U* test. The relationships of all morphometric characters were examined using principal component analysis (PCA). Note that the vent length of the one *T. uyenoii* female (THNHM 13869) was excluded from the morphological comparison because this parameter is much longer in males than in females [RVL 7.4 vs 1.7 and 1.9; 9.3 vs 4.0 in *T. uyenoii*, data from Nishikawa et al. (2014) and the present study, respectively]. All statistical analyses were performed using the SPSS v. 22 for Windows. Statistical significance was accepted at the $p < 0.05$ level.

Results

Molecular analyses

We obtained 452–1,039 bp sequences of the partial ND2 region for 20 specimens, including the outgroup (Table 1). The sequences of the four specimens from UPWS (this study) were the same, and of the 1,039 nucleotide sites, 340 were variable and 158 were parsimony informative within the ingroup (sequence statistics available upon request from the senior author). The mean likelihood score of the BI analyses for all trees sampled at stationary was -4033.667 . The likelihood value of the ML tree was -3955.266 .

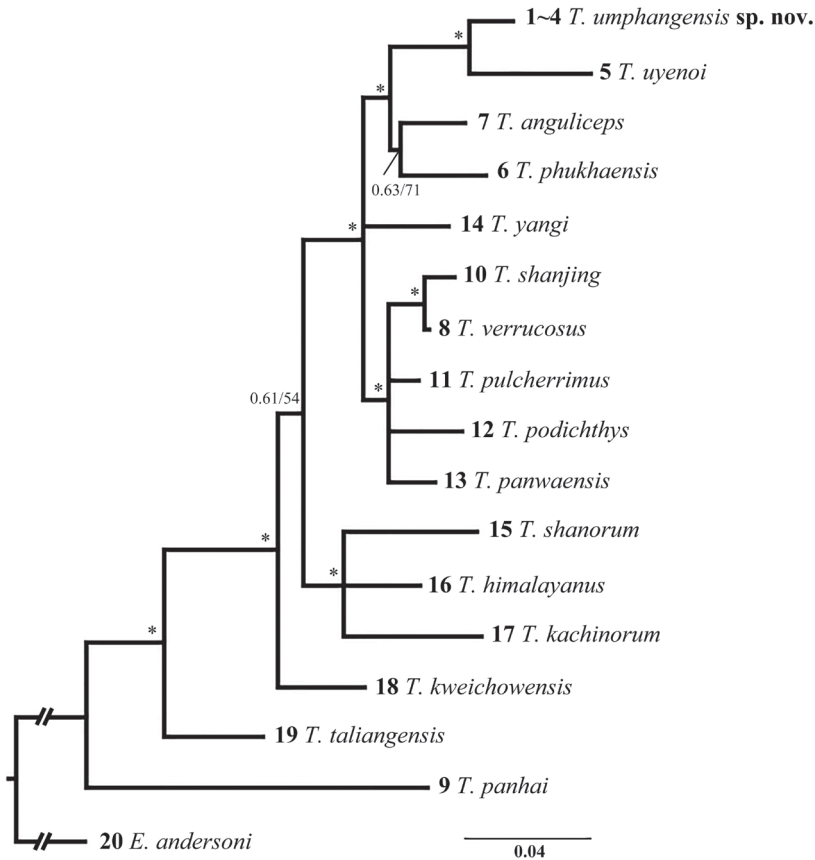


Figure 2. Bayesian inference tree based on the partial ND2 gene for the samples examined. Numbers above branches represent the bpp/bs, and asterisks indicate nodes with $\text{bpp} \geq 0.95$ and $\text{bs} \geq 70\%$. Numbers at branches tips are the sample numbers, as shown in Table 1. Scale bar = 0.04 substitutions/site.

Phylogenetic analyses employing the BI and ML criteria yielded nearly identical topologies and so we present only the BI tree in Figure 2. Monophyly of the subgenus *Tylotriton* (all samples except Samples 9 and 20) was fully supported in the BI and ML trees ($\text{bpp} = 98\%$ and $\text{bs} = 96\%$). Within the subgenus, *T. taliangensis* was first separated from the remaining lineages. The latter group was further divided into two clades: one including *T. shanorum*, *T. himalayanus*, and *T. kachinorum*; the other included the remaining lineages. The newts from UPWS (same sequence) were nested in the latter clade and was first clustered with *T. uyenoii* with significant support.

The p -distances between each pair of a total 17 haplotypes recognized above ranged from 1.4% (between *T. verrucosus* and *T. shanjing*) to 18.8% (between *Echinotriton* and *T. uyenoii* and between *Echinotriton* and *T. kachinorum*) (Table 2). The distance between the newts from UPWS and its sister species *T. uyenoii* was 5.0%, which was larger than the 24 heterospecific combinations in this study.

Table 2. Genetic uncorrected *p*-distance (%) of the ND2 region between samples examined in this study.

Species	Sample no.																		
	1	5	6	7	8	9	10	11	12	13	14	15	16	17	18	19			
1 <i>Tylosotriton umphangensis</i> sp. nov.																			
5 <i>Tylosotriton uyenoii</i>	0.050																		
6 <i>Tylosotriton phukhaensis</i>	0.061	0.091																	
7 <i>Tylosotriton anguliceps</i>	0.052	0.082	0.045																
8 <i>Tylosotriton verrucosus</i>	0.039	0.073	0.057	0.057															
9 <i>Tylosotriton panhai</i>	0.136	0.145	0.138	0.134	0.127														
10 <i>Tylosotriton shanjing</i>	0.043	0.073	0.061	0.057	0.014	0.132													
11 <i>Tylosotriton pulcherrimus</i>	0.048	0.073	0.054	0.045	0.025	0.116	0.029												
12 <i>Tylosotriton podichthys</i>	0.063	0.098	0.068	0.057	0.041	0.127	0.054	0.039											
13 <i>Tylosotriton panuaensis</i>	0.043	0.082	0.059	0.045	0.020	0.122	0.034	0.018	0.029										
14 <i>Tylosotriton yangi</i>	0.043	0.075	0.059	0.039	0.034	0.132	0.043	0.027	0.045	0.027									
15 <i>Tylosotriton shanorum</i>	0.075	0.095	0.079	0.070	0.059	0.122	0.063	0.059	0.079	0.063	0.070								
16 <i>Tylosotriton himalayanus</i>	0.068	0.084	0.063	0.057	0.054	0.118	0.054	0.057	0.063	0.057	0.063	0.052							
17 <i>Tylosotriton kachinorum</i>	0.091	0.118	0.088	0.079	0.073	0.134	0.082	0.079	0.082	0.066	0.082	0.079	0.054						
18 <i>Tylosotriton kweichowensis</i>	0.070	0.091	0.068	0.054	0.052	0.118	0.057	0.054	0.066	0.054	0.057	0.063	0.052	0.066					
19 <i>Tylosotriton taliangensis</i>	0.077	0.088	0.073	0.075	0.057	0.107	0.057	0.057	0.070	0.061	0.073	0.068	0.057	0.075	0.043				
20 <i>Echinotriton andersoni</i>	0.186	0.188	0.179	0.184	0.172	0.175	0.175	0.166	0.177	0.166	0.184	0.179	0.175	0.188	0.168	0.156			

Morphological examination

A total of 12 specimens were used for morphometric comparisons (Table 3). With respect to the SVL, the UPWS population was significantly larger than *T. uyenoii* ($p = 0.027$), but with significantly smaller RHL ($p = 0.042$), RENL ($p = 0.007$), RUEW ($p = 0.017$), RUEL ($p = 0.007$), and ROL ($p = 0.007$) % SVL measurements, and a significantly larger R2FL ($p = 0.007$) measurement than those for *T. uyenoii*.

In life, the dorsal ground color was dark brown to black (Nishikawa et al. 2013a; Pomchote et al. 2020a), while in preservative, the background coloration of *T. uyenoii* was light brown to cream (Nishikawa et al. 2013a) or light brown to brown (this study), although the UPWS samples tended to be the blackish both in life and in preservative. In *T. uyenoii*, the dorsal and ventral head, parotoids, vertebral ridge, rib nodules, limbs, vent, and tail were orange to reddish-brown in life (Nishikawa et al. 2013a; Pomchote et al. 2020a) and light brown to orange-brown (Nishikawa et al. 2013a) or cream to orange-brown (this study) in preservative, although the UPWS samples had darker markings than *T. uyenoii*, both in life and in preservative (Figs 3–5).

The UPWS samples and *T. uyenoii* also showed a few similar morphological characteristics. For example, the sagittal ridge on head and the parotoids were distinct and projected posteriorly. However, morphological differences between the UPWS population and *T. uyenoii* were also present (Fig. 4).

The snout of the UPWS population was truncate, while that of *T. uyenoii* was almost rounded to blunt, except for two specimens (THNHM 10319 and 10320) that were relatively truncate. In lateral view, the degree that the snout projects beyond the lower jaw was more distinct in *T. uyenoii* than in the UPWS population that hardly projected beyond the lower jaw.

The dorsolateral bony ridges of the UPWS population were rough, steeper anteriorly, and curved medially at the posterior ends, while those of *T. uyenoii* were rough, especially from above the eye to above the anterior end of the parotoid, less steep anteriorly, and weakly or rather curved medially at the posterior ends.

In lateral view, the parotoids of the UPWS population were oriented rather parallel to the body axis and the posterior part curved upwards, while those of *T. uyenoii* were oriented obliquely downwards or rather parallel relative to the body axis.

In dorsal view, the quadrate regions of the UPWS population protruded laterally, while those of *T. uyenoii* were weakly curving.

In the urodeles, the dentaries are elongated, paired bones that curve medially. The left and right dentaries touch each other antero-medially on the lower jaw. At the antero-medial ends, some expansions are developed posteriorly in the dorsal view, while in the anterior view this expansion slightly develops in the ventral direction (e.g., Villa et al. 2014; Parra Olea et al. 2020; Ponssa and Abdala 2020). This expansion is prominently present in the UPWS population (Fig. A4), both in life and in preservative, whereas it was absent in *T. uyenoii* (Figs B4–C4).

The vertebral ridge of the UPWS population and *T. uyenoii* was segmented from the anterior end to the tail base but was less segmented in *T. uyenoii* than in the UPWS

Table 3. Morphometric comparisons of the examined specimens of *Tylostotriton* [mean \pm SD of SVL (in mm), mean \pm SD of BW (g), and median of ratios of characters (R: % SVL), with range in parentheses]. Character abbreviations refer to the text.

	<i>T. umphangensis</i> sp. nov.		<i>T. uyanoi</i>		<i>T. umphangensis</i> sp. nov.		<i>T. uyanoi</i>	
	4 males	1 female	7 males	1 female	4 males	7 males	1 female	
SVL	72.0 \pm 4.4* (65.6–75.3)	60.9	62.7 \pm 4.8 (55.5–67.4)	60.9	76.8 (75.4–77.4)	75.2 (71.9–77.5)	76.2	
BW	12.1 \pm 1.4 (10.2–13.3)				104.7 (91.9–107.3)	106.3 (67.4–117.0)	85.2	
RHL	23.0* (22.0–25.2)	24.9	25.2 (24.1–26.1)	24.9	8.0 (7.3–9.4)	9.1 (7.8–11.5)	4.0	
RHW	21.4 (19.4–22.7)	26.5	22.3 (19.9–25.4)	26.5	14.5 (12.6–15.1)	13.1 (12.2–15.0)	13.1	
RMXHW	25.6 (25.0–26.9)	28.1	25.5 (24.6–28.6)	28.1	2.3 (2.2–2.4)	2.7 (1.6–3.3)	2.1	
RSL	8.8 (8.2–9.8)	9.0	8.7 (7.8–9.4)	9.0	15.0 (11.9–15.3)	11.8 (10.0–13.8)	15.5	
RLJL	22.8 (22.1–23.5)	23.2	22.9 (20.7–23.3)	23.2	11.1 (8.8–12.1)	12.0 (10.3–13.8)	16.9	
RENL	5.8* (5.6–6.2)	6.9	7.1 (6.2–7.4)	6.9	10.6 (7.9–12.0)	10.0 (8.0–13.6)	16.2	
RIND	6.2 (5.8–6.5)	7.6	6.4 (6.0–7.8)	7.6	37.0 (34.2–40.5)	39.4 (35.6–42.6)	33.1	
RIOD	13.2 (12.9–13.7)	14.2	13.2 (12.4–14.3)	14.2	38.4 (35.2–41.9)	43.6 (37.9–50.9)	40.1	
RUEW	2.5* (2.3–2.9)	2.9	3.2 (2.6–3.5)	2.9	7.1* (6.7–8.1)	5.9 (5.1–6.5)	4.7	
RUEL	6.0* (5.5–6.4)	7.5	7.2 (6.5–7.8)	7.5	7.6 (5.6–8.9)	6.6 (5.5–8.2)	6.3	
ROL	3.0* (2.7–3.3)	4.2	4.6 (4.0–5.0)	4.2	9.3 (8.9–11.0)	9.0 (8.3–12.5)	9.1	
RAGD	53.7 (51.9–54.4)	50.8	52.2 (46.7–57.2)	50.8	4.9 (4.8–5.7)	4.4 (3.5–6.5)	4.1	

* $p < 0.05$ compared to *T. uyanoi* (Mann-Whitney *U* test)

samples, especially the two paratypes CUMZ-A-8245 and 8246, which were prominently segmented.

The rib nodules of *T. uyenoii* were isolated, rounded, distinct but small, and forming knob-like warts, with the number of rib nodules ranging from 12–15, but almost all the specimens had 14 warts on each side of body. In contrast, the rib nodules of the UPWS newts were indistinct and small in shape, ranging from 14–15 warts.

The overall morphological differences were examined using PCA for the UPWS population and *T. uyenoii*. The first two principal components (PCs) explained 49.0% of the total variation. The two-dimensional plots of PC1 vs PC2 showed that the UPWS population was clustered together and separated from *T. uyenoii* (Fig. 6).

Based on the molecular and morphological evidence, the *Tylototriton* sp. from UPWS, Tak Province, western Thailand is confirmed as an undescribed species. Therefore, we describe it as a new species, *Tylototriton umphangensis* sp. nov.

Systematics

Tylototriton umphangensis sp. nov.

<http://zoobank.org/D280A352-65C9-4F84-91BF-53F19B954E87>

Thai name: Ka Tang Nam Umphang

English name: Umphang crocodile newt

Figures 3–5

T. uyenoii: (referring to the population from Umphang, Tak Province): Hernandez et al. 2019, page 18.

Holotype. CUMZ-A-8243, adult male, collected from Umphang Wildlife Sanctuary, Tak Province, western Thailand, approximate coordinate 16°12'N, 98°58'E; ca 1,150 m a.m.s.l., collected on 19 June 2021 by Porrawee Pomchote and Pitak Sapewisut.

Paratypes. CUMZ-A-8244, CUMZ-A-8245, and CUMZ-A-8246; three adult males, same data as the holotype.

Etymology. The specific epithet *umphangensis* refers to Umphang Wildlife Sanctuary, the type locality of the new species.

Diagnosis. The new species is placed in the genus *Tylototriton* by having a combination of dorsal granules present, dorsolateral bony ridges on head present, knob-like warts (rib nodules) on dorsolateral body present, and quadrate spine absent. *Tylototriton umphangensis* sp. nov. differs from its congeners by having the following morphological characters: medium-sized, adult SVL 65.6–75.3 mm in males; skin rough with fine granules; snout truncate; quadrate regions laterally protruding; antero-medial ends of dentaries distinctly expanded; dorsolateral bony ridges on head prominent, steep, rough, narrow, and posterior ends curved medially; parotoids distinct, oriented rather parallel to the body axis and posterior part curved upwards in the lateral view; vertebral ridge



Figure 3. Male *Tylostrotiton umphangensis* sp. nov.

distinct and segmented; rib nodules 14–15, small, and indistinct; limbs long and thin; tips of forelimbs and hindlimbs overlapping when adpressed along the body; tail thin.

Description of holotype. Body rather slim and long (RTRL 76.6%); skin rough; fine granules dense on dorsum, dense on sides of body and tail, and arranged in transverse striations on mid-ventrum; head longer than wide (HW/HL 0.97), hexagonal in shape, depressed, and slightly oblique in profile; snout truncate, hardly projecting beyond lower jaw; nostrils close to snout tip, not visible from dorsal view; quadrate regions protruding laterally from dorsal view; antero-medial ends of dentaries distinctly expanded; dorsolateral bony ridges on head narrow, rough, and posterior ends curved proximally; sagittal ridge on head short and weak; labial fold absent; tongue oval, attached to anterior floor of mouth, free laterally and posteriorly; vomerine tooth series in an inverted V-shape, converging anteriorly and reaching choanae; parotoids distinct, projecting posteriorly, posterior ends slightly curved medially, oriented rather parallel to body axis and curved upwards in lateral view; gular fold present; costal folds absent; vertebral ridge prominent, narrow, and slightly segmented from neck to groin, separated from sagittal ridge on head; two low and flat bony ridges on the dorsal head surface forming a “V” shape, connected with the anterior end of vertebral ridge; rib nodules small, indistinct, forming knob-like warts, 15 on each side of body from axilla to base

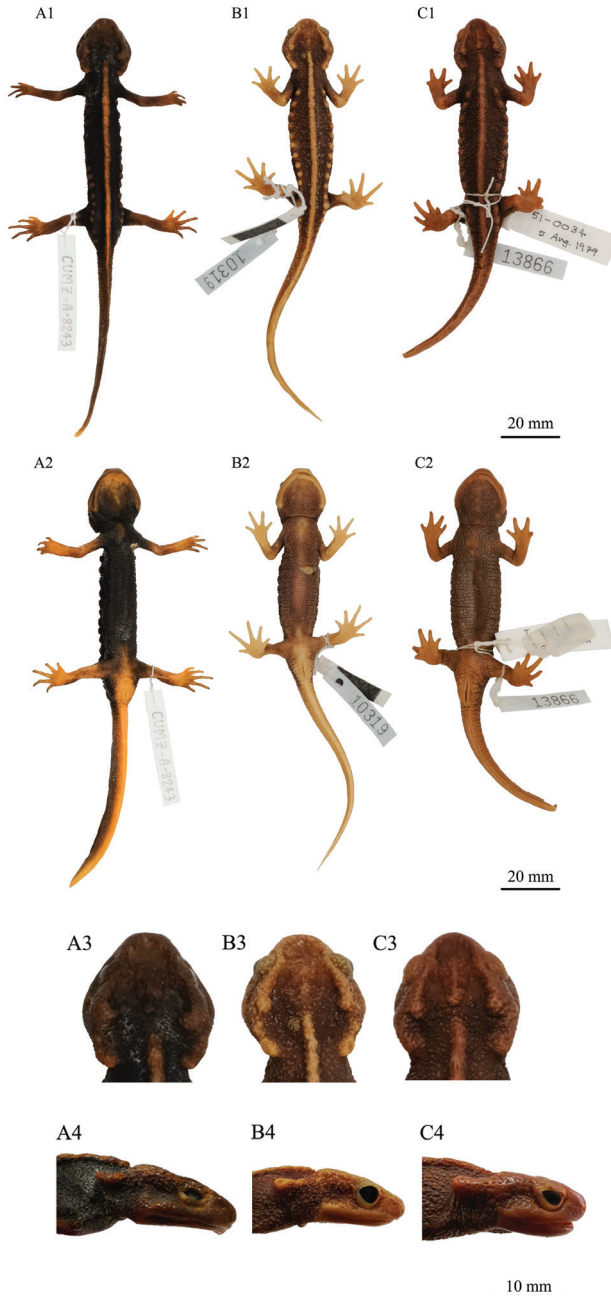


Figure 4. The male holotype of *Tylotriton umphangensis* sp. nov. and other specimens of *T. uyanoi* in preservative. **A** Holotype specimen of *Tylotriton umphangensis* sp. nov. (CUMZ-A-8243) **B** Topotypic specimen of *T. uyanoi* (THNHM 10319) from Doi Suthep-Doi Pui NP, Chiang Mai Province **C** specimen of *T. uyanoi* (THNHM 13866) from Doi Inthanon NP, Chiang Mai Province **A1–C1** dorsal view of the body. **A2–C2** ventral view of the body. **A3–C3** dorsal view of the head **A4–C4** lateral view of the head. Scale bars: 20 mm (**A1–C1, A2–C2**); 10 mm (**A3–C3, A4–C4**).

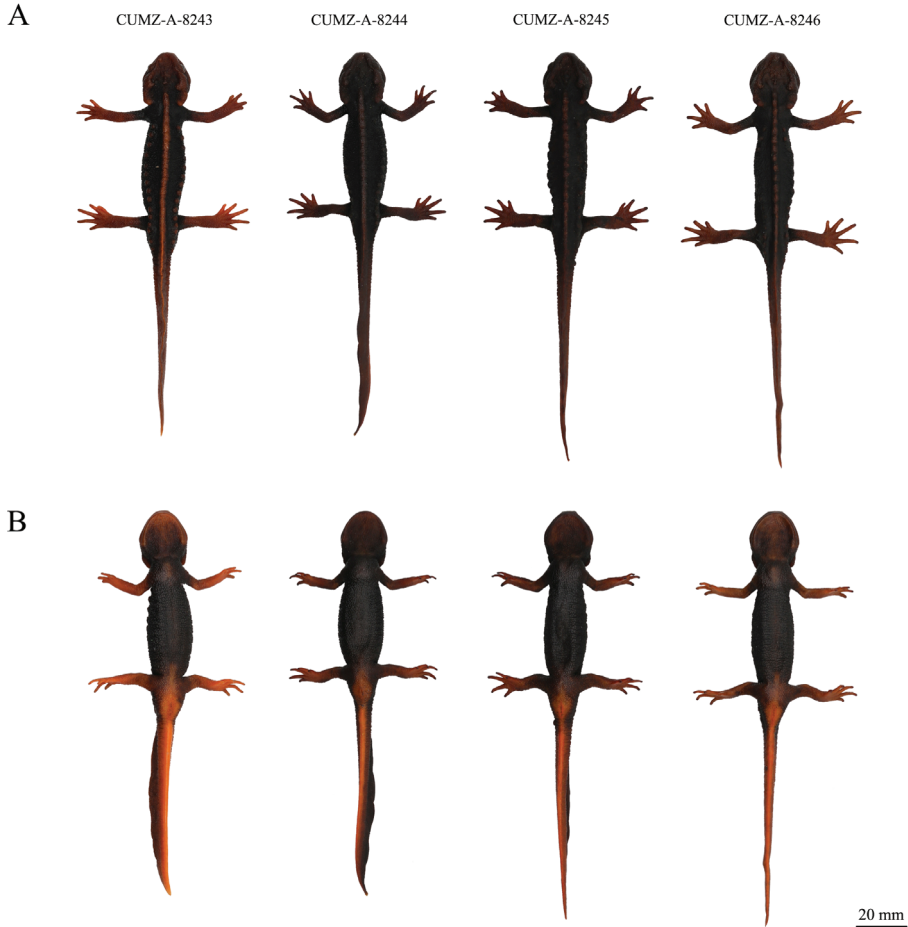


Figure 5. Holotype (CUMZ-A-8243) and paratypes (CUMZ-A-8244, CUMZ-A-8245, and CUMZ-A-8246) of *Tylototriton umphangensis* sp. nov. before preservation. **A** dorsal view **B** ventral view. Scale bar: 20 mm.

of tail; rib nodules slightly increasing in size from most anterior to fourth nodule, then decreasing posteriorly; forelimbs (34.2% SVL) shorter than hindlimbs (40.0% SVL); tips of forelimb and hindlimb overlapping when adpressed along body; fingers and toes well developed, free of webbing; fingers four, comparative finger lengths $2 > 3 > 1 > 4$; toes five, comparative toe lengths $4 > 3 > 2 > 5 > 1$; tail laterally compressed, dorsal fin more distinct posteriorly, ventral edge smooth, tip pointed; tail short (91.9% SVL); cloaca slightly swollen; vent slit longitudinal.

Color of holotype. In life, dorsal ground coloration is dark-brown to blackish-brown, while the ventral color is slightly lighter than dorsum. Dorsal, ventral, and lateral of head, parotoids, vertebral ridge, rib nodules, limbs, vent region, and whole tail are orange-brown. Tip of tail is slightly lighter than dorsal and lateral sides of tail. Ven-

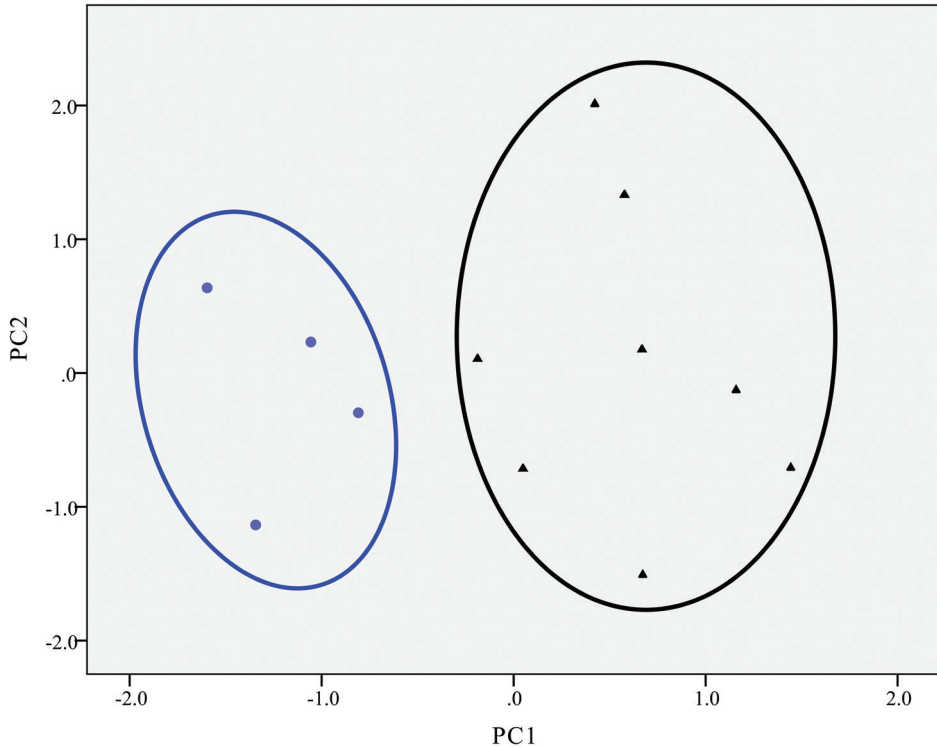


Figure 6. The PCA plots of PC1 vs PC2 for morphometric parameters between the UPWS population (*Tylototriton umphangensis* sp. nov. described herein) (circle) and specimens of *T. uyenoii* (triangle).

tral side of head, part of pectoral and pubic region, limbs, and tail prominently lighter than dorsum. The lightest is the ventral edge of the tail. The lighter region between the ventral edge of the tail and the area of the vent is connected. Color of digit tips is dark brown. After a week in preservation, the color pattern is rather similar to that in life.

Measurement of holotype (in mm). SVL 72.7; HL 16.4; HW 15.9; MXHW 18.1; SL 6.3; LJL 16.7; ENL 4.2; IND 4.3; IOD 9.6; UEW 1.6; UEL 4.7; OL 2.1; AGD 39.3; TRL 55.7; TAL 66.8; VL 6.3; BTAW 10.6; MTAW 1.7; BTAH 11.2; MXTAH 8.8; MTAH 8.7; FLL 24.9; HLL 29.1; 2FL 5.3; 3FL 4.1; 3TL 6.5; and 5TL 3.5.

Variation. Some differences in morphology were observed among the four specimens. The dorsolateral bony ridges on the head of one paratype (CUMZ-A-8245) are rougher than the holotype and the other paratypes. The sagittal ridge on the head of one paratype (CUMZ-A-8244) is smaller and weaker than the holotype and the other paratypes. Two paratypes (CUMZ-A-8245 and CUMZ-A-8246) have a more distinctly segmented vertebral ridge than the holotype and the other paratype. The holotype has much more distinct rib nodules than the three paratypes. Sizes of rib nodules varied from rounded anteriorly to irregularly shaped posteriorly among the paratypes. One paratype (CUMZ-A-8246) has an undulated surface of the dorsal fin, while the other type specimens have an even-surfaced dorsal fin. Type specimens are



Figure 7. Habitat at the type locality of *Tylotriton umphangensis* sp. nov. at Umphang Wildlife Sanctuary, Tak Province, western Thailand.

generally similar in color pattern, but the coloration of the dorsal, ventral, and lateral head, parotoids, vertebral ridge, rib nodules, limbs, and whole tail is much lighter in the holotype than the three paratypes. The color of the digit tips of the holotype is dark brown, but those of the paratypes are black. Morphological variations between the specimens are shown in Figure 5.

Comparisons. *Tylotriton umphangensis* sp. nov. differs from the other species of subgenus *Tylotriton* as follows: from *T. taliangensis* by having orange-brown markings on the head, trunk, limbs, and tail (vs uniformly black body except for distal fingers, toes, and posterior parotoids in *T. taliangensis*); from *T. kweichowensis* and *T. pseudoverrucosus* by having separated rib nodules (vs connected orange markings forming continuous dorsolateral lines in *T. kweichowensis* and *T. pseudoverrucosus*); from *T. shanorum* and *T. anguliceps* by having a sagittal ridge and rather steep dorsolateral bony ridges on the head (vs no sagittal ridge and rather flat dorsolateral bony ridges on head in *T. shanorum*, and prominent sagittal ridge and the posterior ends of dorsolateral bony ridges distinctly curved medially in *T. anguliceps*); from *T. ngarsuensis* by having truncate snout in dorsal view (vs rounded in *T. ngarsuensis*); from *T. himalayanus* by lacking grooves on either side at the basal tail (vs present in *T. himalayanus*); from

T. yangi by having uniformly orange-brown parotoids (vs black coloration except for posterior end of parotoids with orange coloration in *T. yangi*); from *T. kachinorum*, *T. pulcherrimus*, and *T. shanjing* by having light orange-brown on part of pubic region (vs light yellowish-grey ventral surfaces in *T. kachinorum*, and yellowish-orange to bright yellow ventral trunk in *T. pulcherrimus* and *T. shanjing*); from *T. verrucosus* by having rough dorsolateral bony ridges (vs smooth in *T. verrucosus*); from *T. podichthys* and *T. phukhaensis* by having short and weak sagittal ridge on the head (vs indistinct sagittal ridge on head in *T. podichthys*, and narrow, long, and prominent sagittal ridge on head in *T. phukhaensis*); from *T. panwaensis* by having narrow vertebral ridge (vs wide in *T. panwaensis*).

Distribution. Umphang Wildlife Sanctuary, Tak Province, western Thailand (Fig. 1). The Umphang Wildlife Sanctuary is located along the Dawna Range, which is a mountain range in eastern Myanmar and northwestern Thailand. Thus, this species is expected to also occur in Myanmar and elsewhere in western Thailand.

Natural history. All specimens were found during the afternoon at around 14:30 h hidden under leaf litter and between stems of arrowroot plants (family Marantaceae) in a small ephemeral pond (Fig. 7) during the rainy season, which is the breeding season of *Tylototriton* species. The pond had clear water and the bottom was covered with dense leaf litter. The surrounding area was composed of hill evergreen forest. The pond size was approximately 520 cm long, 270 cm wide, and 17 cm in maximum depth. The water temperature was 23.1 °C. The water quality parameters were: pH 6.4; dissolved oxygen 4.13 mg/L; conductivity 23 µS/cm; total dissolved solid 15 mg/L; and turbidity 7.6 NTU. No fish were observed.

Discussion

Molecular and morphological evidence indicate that the newts found at UPWS, Tak Province, western Thailand are a distinct, new species described here. With our description of this new species, the number of *Tylototriton* species is now 33, with six of them present in Thailand: *T. verrucosus*, *T. uyenoii*, *T. panhai*, *T. anguliceps*, *T. phukhaensis*, and *T. umphangensis* sp. nov. Three of these six species are endemic to Thailand (*T. uyenoii*, *T. phukhaensis*, and *T. umphangensis* sp. nov.). Thus, Thailand has the third highest number of species of *Tylototriton* and the second highest in Indochina; the highest number of species is in China (17) followed by Vietnam (7) (Frost 2021).

Tylototriton umphangensis sp. nov. has been confused with *T. uyenoii* because of these species have morphological similarities and a similar distribution (Hernandez et al. 2019). In the present study, we compared *T. umphangensis* sp. nov. with *T. uyenoii*, the latter having been described and named based on a holotype and eight paratypes (total of nine adult males) collected from Phuping Rajanives Palace, Doi Suthep and the Royal Garden Siribhume, Doi Inthanon, Chiang Mai Province, respectively (Nishikawa et al. 2013a). According to Nishikawa et al. (2013a), *T. uyenoii* specimens are basically similar in morphology and color pattern, but show variations in the degree of segmented ver-

tebral ridge, size of rib nodules, texture of dorsolateral bony ridges, and color markings. These morphological variations are also present in the specimens of *T. umphangensis* sp. nov. that we examined in our study. However, *T. umphangensis* sp. nov. can be distinguished from the most closely related species (*T. uyenoii*) and other congeners.

Geographic isolation may limit gene flow and promote genetic differentiation among populations which can result in the formation of new species (Eckert et al. 2008; Qian et al. 2017). Tak Province is located in the Northwest Thai (Dawna) Uplands of Indochina (Poyarkov et al. 2021b), which consists of several high-mountain areas in the three major mountain ranges: (i) Thanon Thong Chai and (ii) Daen Lao Ranges in northernmost Tak Province, and (iii) Dawna Range in most areas of Tak Province. The Thanon Thong Chai Range has *T. uyenoii* in Namtok Mae Surin NP, Mae Hong Son Province (Pomchote et al. 2020a). The Daen Lao Range has *T. uyenoii* populations in Doi Ang Khang, Doi Chang Kien, Chiang Dao Wildlife Sanctuary (WS), Doi Inthanon, Doi Mak Lang or Doi Lang, and Doi Suthep-Pui in Chiang Mai Province (Pomchote et al. 2008; Nishikawa et al. 2013a; Michaels 2014; Hernandez 2016; Hernandez et al. 2019); Doi Soi Malai, Tak Province (Hernandez 2017); and Doi Mon Jong, Chiang Mai Province (Hernandez et al. 2019). The Dawna Range supports *T. uyenoii* in Khao Laem NP in Kanchanaburi Province (Hernandez and Pomchote 2020c) and Umphang, Tak Province (Hernandez et al. 2019; this study) (Fig. 1).

Hernandez et al. (2018) stated that *Tylototriton* species are niche specialists because they reside at high elevations with moist, and cool conditions, a narrow thermal range, and high rainfall during the breeding season. This is consistent with previous studies that Thai *Tylototriton* species are distributed in high mountainous areas at an altitude of more than 1,000 m a.m.s.l. (Pomchote et al. 2008, 2020a, 2020b). Following to previous studies (Pomchote et al. 2008, 2020a, 2020b), we defined lowland and highland areas according to the distribution of six *Tylototriton* species in Thailand: lowlands are areas below 1,000 m a.m.s.l. and uplands are areas above 1,000 m a.m.s.l. Thus, the lowland areas, located between each highland area, of the Northwest Thai Uplands may serve as a barrier restricting the gene flow between *Tylototriton* populations. Consequently, further morphological and molecular analyses, as well as field surveys in Tak Province and its nearby areas located along Thanon Thong Chai, Daen Lao, and Dawna Ranges, need to be done to clarify the species boundary between *T. umphangensis* sp. nov. and *T. uyenoii*.

According to previous data (Watchara Sanguansombat and Chattraphas Pongcharoen, personal communication) and the check list of fauna diversity of UPWS (Department of National Parks, Wildlife and Plant Conservation), *T. verrucosus* (now named *T. umphangensis* sp. nov.) were first found near an artificial pond adjacent to a deserted hut near a road that was about 6 km from the Mae Klong Khi Forest Ranger Station. Our field survey was conducted there on 18 June 2021 at night, but we did not find any newts. Not only did this pond have fish (released by someone?), but this area is also under construction. Moreover, there are cattle that belong to local people roaming freely in UPWS that may cause damage to the forest, including breeding sites of the newts, as previously reported in other NPs, such as in Phu Suan Sai NP, Loei Prov-

ince that harbors *T. panhai* (Hernandez and Pomchote 2020a); and in Doi Phu Kha NP, Nan Province that harbors *T. phukhaensis* (Pomchote et al. 2020b). Thus, effects from anthropogenic activities, including cattle, should be evaluated in detail. *Tylotriton umphangensis* sp. nov. is currently only known from the hill evergreen forests of UPWS. We suggest that the new species should be classified as Endangered (EN) in the IUCN Red List and that it needs further conservation management.

Acknowledgements

We thank Amnat Fongchai, Bunruam Khunin, and Mae Klong Khi park rangers for kind support in the fieldwork; Chitchol Phalaraksh for facilitating the field support; Chatmongkon Suwannapoom, Thansuda Dowwiangkan, Jean Raffaëlli, Daniel Escoriza, Parinya Pawangkhanant, Keerati Kanya, Pichani Saengtharatip, and Manut Ruadraew for useful discussion on *Tylotriton* in the western part of Thailand; Nuttakorn Taewcharoen for minor editing of the manuscript; Sally Kanamori and Yasuho Onishi for molecular analyses; and Sunchai Makchai (THNHM) for allowing us to examine specimens. We also thank the Department of National Parks, Wildlife and Plant Conservation for research permission. The experimental protocol was approved by the Animal Care and Use Committee of Faculty of Science, Chulalongkorn University (protocol review no. 2123012). This research was supported by the Kyoto University Foundation in 2008, the Ministry of Education, Science and Culture, Japan (no. 18H03602), and JSPS Core-to-Core program B [to Kanto Nishikawa (coordinator: Masaharu Motokawa)].

References

- Anderson J (1871) Description of a new genus of newts from western Yunan. Proceedings of the Zoological Society of London 1871: 423–425.
- Bernardes M, Le MD, Nguyen TQ, Pham CT, Pham AV, Nguyen TT, Rödder D, Bonkowski M, Ziegler T (2020) Integrative taxonomy reveals three new taxa within the *Tylotriton asperrimus* complex (Caudata, Salamandridae) from Vietnam. ZooKeys 935: 121–164. <https://doi.org/10.3897/zookeys.935.37138>
- Böhme W, Schöttler T, Nguyen QT, Köhler J (2005) A new species of salamander, genus *Tylotriton* (Urodela: Salamandridae), from northern Vietnam. Salamandra 41(4): 215–220.
- Dubois A, Raffaëlli J (2009) A new ergotaxonomy of the family Salamandridae Goldfuss, 1820 (Amphibia, Urodela). Alytes 26(1–4): 1–85.
- Eckert C, Samis K, Lougheed S (2008) Genetic variation across species' geographical ranges: the central–marginal hypothesis and beyond. Molecular Ecology 17(5): 1170–1188. <https://doi.org/10.1111/j.1365-294X.2007.03659.x>
- Fang PW, Chang MLY (1932) Notes on *Tylotriton kweichowensis* sp. nov. and *asperrimus* Unterstein with synopsis to species. Sinensia, Nanking 2: 111–122.

- Fei L, Ye CY, Jiang JP (2012) Colored Atlas of Chinese Amphibians and Their Distributions. Sichuan Publishing House of Science and Technology, Chengdu, 620 pp. [in Chinese]
- Felsenstein J (1985) Confidence limits on phylogenies: an approach using the bootstrap. *Evolution* 39(4): 783–791. <https://doi.org/10.2307/2408678>
- Frost DR (2021) Amphibian Species of the World: an Online Reference. <https://amphibian-softheworld.amnh.org/index.php>
- Grismer LL, Wood Jr PL, Quah ESH, Thura MK, Espinoza RE, Grismer MS, Murdoch ML, Lin A (2018) A new species of crocodile newt *Tylototriton* (Caudata: Salamandridae) from Shan State, Myanmar (Burma). *Zootaxa* 4500(4): 553–573. <https://doi.org/10.11646/zootaxa.4500.4.5>
- Grismer LL, Wood Jr PL, Quah ESH, Thura MK, Espinoza RE, Murdoch ML (2019) A new species of crocodile newt *Tylototriton* (Caudata: Salamandridae) from northern Myanmar (Burma). *Journal of Natural History* 53(7–8): 475–495. <https://doi.org/10.1080/00222933.2019.1587534>
- Hernandez A (2016) Crocodile Newts, the Primitive Salamandridae of Asia (Genera *Echinotriton* and *Tylototriton*). Edition Chimaira, Frankfurt, 415 pp.
- Hernandez A (2017) New localities for *Tylototriton panhai* and *Tylototriton uyenoii* Nishikawa, Khonsue, Pomchote, and Matsui 2013 in northern Thailand. *Bulletin de la Société Herpétologique de France* 162: 110–112.
- Hernandez A, Pomchote P (2020a) Habitat, distribution and life history of the polytypic Panha's Crocodile Newt, *Tylototriton panhai* in northeastern Thailand. *Alytes* 37(3–4): 25–46.
- Hernandez A, Pomchote P (2020b) New locality of the angular-headed crocodile newt *Tylototriton anguliceps* Le et al., 2015, with remarks on the distribution of the genus in Thailand. *Herpetology Notes* 13: 993–996.
- Hernandez A, Pomchote P (2020c) New southernmost record for the genus *Tylototriton* in Asia: *Tylototriton uyenoii* Nishikawa, Khonsue, Pomchote and Matsui 2013 discovered in Khao Laem National Park, Kanchanaburi province, western Thailand. *Bulletin de la Société Herpétologique de France* 175: 64–67.
- Hernandez A, Escoriza D, Hou M (2018) Patterns of niche diversification in south-east Asian crocodile newts. *Zoologischer Anzeiger* 276: 86–93. <https://doi.org/10.1016/j.jcz.2018.06.001>
- Hernandez A, Escoriza D, Pomchote P, Hou M (2019) New localities for *Tylototriton uyenoii*, *T. panhai* and *T. anguliceps* in Thailand with remarks on the southernmost distribution of the genus. *The Herpetological Bulletin* 147: 15–18. <https://doi.org/10.33256/hb147.1518>
- Heyer WR, Donnelly MA, McDiarmid RW, Hayek LC, Foster MS (1994) Measuring and Monitoring Biological Diversity: Standard Method for Amphibians. Smithsonian Institution Press, Washington, DC, 320 pp.
- Hou M, Li P, Lü SQ (2012) Morphological research development of genus *Tylototriton* and primary confirmation of the status of four cryptic populations. *Journal of Huangshan University* 14(3): 61–65. [in Chinese]
- Huelsenbeck JP, Hillis M (1993) Success of phylogenetic methods in the four taxon case. *Systematic Biology* 42(3): 247–264. <https://doi.org/10.1093/sysbio/42.3.247>

- Huelsenbeck JP, Ronquist F (2001) MRBAYES: Bayesian inference of phylogenetic trees. *Bioinformatics* 17(8): 754–755. <https://doi.org/10.1093/bioinformatics/17.8.754>
- Khatiwada JR, Wang B, Ghimire S, Vasudevan K, Paudel S, Jiang J (2015) A new species of the genus *Tylostotriton* (Amphibia: Urodela: Salamandridae) from Eastern Himalaya. *Asian Herpetological Research* 6(4): 245–256. <https://doi.org/10.16373/j.cnki.ahr.140097>
- Kumar S, Stecher G, Tamura, K (2016) MEGA7: Molecular Evolutionary Genetics Analysis version 7.0 for bigger datasets. *Molecular Biology and Evolution* 33(7): 1870–1874. <https://doi.org/10.1093/molbev/msw054>
- Le DT, Nguyen TT, Nishikawa K, Nguyen SLH, Pham AV, Matsui M, Bernardes M, Nguyen TQ (2015) A new species of *Tylostotriton* Anderson, 1871 (Amphibia: Salamandridae) from northern Indochina. *Current Herpetology* 34(1): 38–50. <https://doi.org/10.5358/hsj.34.38>
- Leaché AD, Reeder TW (2002) Molecular systematics of the eastern fence lizard (*Sceloporus undulatus*): a comparison of parsimony, likelihood, and Bayesian approaches. *Systematic Biology* 51(1): 44–68. <https://doi.org/10.1080/106351502753475871>
- Liu CC (1950) Amphibians of Western China. Chicago Natural History Museum Press, Chicago, 397 pp.
- Michaels CJ (2014) Field observations, morphometrics and a new locality for *Tylostotriton uyanoi* in Chiang Mai Province, Thailand. *The Herpetological Bulletin* 130: 26–27.
- Nishikawa K, Jiang JP, Matsui M (2011) Two new species of *Pachytriton* from Anhui and Guangxi, China (Amphibia: Urodela: Salamandridae). *Current Herpetology* 30(1): 15–31. <https://doi.org/10.3105/018.030.0102>
- Nishikawa K, Khonsue W, Pomchote P, Matsui M (2013a) Two new species of *Tylostotriton* from Thailand (Amphibia: Urodela: Salamandridae). *Zootaxa* 3737(3): 261–279. <https://doi.org/10.11646/zootaxa.3737.3.5>
- Nishikawa K, Matsui M, Nguyen TT (2013b) A new species of *Tylostotriton* from northern Vietnam (Amphibia: Urodela: Salamandridae). *Current Herpetology* 32(1): 34–49. <https://doi.org/10.5358/hsj.32.34>
- Nishikawa K, Matsui M, Rao DQ (2014) A new species of *Tylostotriton* (Amphibia: Urodela: Salamandridae) from central Myanmar. *The Natural History Bulletin of the Siam Society* 60(1): 9–22.
- Nussbaum RA, Brodie Jr ED, Yang D (1995) A taxonomic review of *Tylostotriton verrucosus* Anderson (Amphibia: Caudata: Salamandridae). *Herpetologica* 51(3): 257–268.
- Parra Olea G, Garcia-Castillo MG, Rovito SM, Maisano JA, Hanken J, Wake DB (2020) Descriptions of five new species of the salamander genus *Chiropterotriton* (Caudata: Plethodontidae) from eastern Mexico and the status of three currently recognized taxa. *PeerJ* 8: e8800. <https://doi.org/10.7717/peerj.8800>
- Phimmachak S, Aowphol A, Stuart BL (2015) Morphological and molecular variation in *Tylostotriton* (Caudata: Salamandridae) in Laos, with description of a new species. *Zootaxa* 4006(2): 285–310. <https://doi.org/10.11646/zootaxa.4006.2.3>
- Pomchote P, Pariyanonth P, Khonsue W (2008) Two distinctive color patterns of the Himalayan newt *Tylostotriton verrucosus* (Urodela: Salamandridae) found in Thailand and its implication on geographic segregation. *The Natural History Journal of Chulalongkorn University* 8(1): 35–43.

- Pomchote P, Khonsue W, Sapewisut P, Eto K, Nishikawa K (2020a) Discovering a population of *Tylototriton verrucosus* (Caudata: Salamandridae) from Thailand: implications for conservation. *Tropical Natural History* 20(1): 1–15.
- Pomchote P, Khonsue W, Thammachoti P, Hernandez A, Peerachidacho P, Suwannapoom C, Onishi Y, Nishikawa K (2020b) A new species of *Tylototriton* (Urodela: Salamandridae) from Nan Province, Northern Thailand. *Tropical Natural History* 20(2): 144–161.
- Ponssa ML, Abdala V (2020) Sesamoids in Caudata and Gymnophiona (Lissamphibia): absences and evidence. *PeerJ* 8: e10595. <https://doi.org/10.7717/peerj.10595>
- Poyarkov NA, Nguyen TV, Arkhipov DV (2021a) A new species of the genus *Tylototriton* (Amphibia, Caudata, Salamandridae) from Central Vietnam. *Taprobanica* 10(1): 4–22. <https://doi.org/10.47605/tapro.v10i1.244>
- Poyarkov NA, Nguyen TV, Popov ES, Geissler P, Pawangkhanant P, Neang T, Suwannapoom C, Orlov NL (2021b) Recent progress in taxonomic studies, biogeographic analysis and revised checklist of amphibians in Indochina. *Russian Journal of Herpetology* 28(3A): 1–110. <https://doi.org/10.30906/1026-2296-2021-28-3A-1-110>
- Qian L, Sun X, Li J, Guo W, Pan T, Kang X, Jiang J, Wu J, Zhang B (2017) A new species of the genus *Tylototriton* (Amphibia: Urodela: Salamandridae) from the southern Dabie Mountains in Anhui Province. *Asian Herpetological Research* 8(3): 151–164. <https://doi.org/10.16373/j.cnki.ahr.170013>
- Stamatakis A (2014) RAxML version 8: a tool for phylogenetic analysis and post-analysis of large phylogenies. *Bioinformatics* 30(9): 1312–1313. <https://doi.org/10.1093/bioinformatics/btu033>
- Tanabe AS (2011) Kakusan4 and Aminosan: two programs for comparing non-partitioned, proportional, and separate models for combined molecular phylogenetic analyses of multilocus sequence data. *Molecular Ecology Resources* 11(5): 914–921. <https://dx.doi.org/10.1111/j.1755-0998.2011.03021.x>
- Villa A, Andreone F, Boistel R, Delfino M (2014) Skull and lower osteology of the Lanza's salamander, *Salamandra lanzai* (Amphibia, Caudata). In: Capula M, Corti C (Eds) *Scripta Herpetologica. Studies on Amphibians and Reptiles in Honour of Benedetto Lanza*. Edizioni Belvedere, Latina, 171–200.
- Wang B, Nishikawa K, Matsui M, Nguyen TQ, Xie F, Li C, Khatiwada JR, Zhang B, Gong D, Mo Y, Wei G, Chen X, Shen Y, Yang D, Xiong R, Jiang J (2018) Phylogenetic surveys on the newt genus *Tylototriton sensu lato* (Salamandridae, Caudata) reveal cryptic diversity and novel diversification promoted by historical climatic shifts. *PeerJ* 6: e4384. <https://doi.org/10.7717/peerj.4384>
- Weisrock DW, Papenfuss TJ, Macey JR, Litvinchuk SN, Polymeni R, Ugurtas IH, Zhao E, Jowkar H, Larson A (2006) A molecular assessment of phylogenetic relationships and lineage accumulation rates within family Salamandridae (Amphibia, Caudata). *Molecular Phylogenetics and Evolution* 41(2): 368–383. <https://doi.org/10.1016/j.ympev.2006.05.008>
- Zaw T, Lay P, Pawangkhanant P, Gorin VA, Poyarkov Jr NA (2019) A new species of crocodile newt, genus *Tylototriton* (Amphibia, Caudata, Salamandridae) from the mountains of Kachin State, northern Myanmar. *Zoological Research* 40(3): 151–174. <https://doi.org/10.24272/j.issn.2095-8137.2019.043>

Transcriptional identification of genes light-interacting in the extraretinal photoreceptors of the crayfish *Procambarus clarkii*

Gabina Calderón-Rosete¹, Juan Antonio González-Barrios², Celia Piña-Leyva^{2,3}, Hayde Nallely Moreno-Sandoval², Manuel Lara-Lozano^{2,3}, Leonardo Rodríguez-Sosa¹

1 Departamento de Fisiología, Facultad de Medicina, Universidad Nacional Autónoma de México, Ciudad Universitaria, C. P. 04510, México **2** Laboratorio de Medicina Genómica, Hospital Regional “Primero de Octubre” ISSSTE, 07300, México **3** Departamento de Fisiología, Biofísica y Neurociencias, Centro de Investigación y Estudios Avanzados, 07360, México

Corresponding author: Leonardo Rodríguez-Sosa (Irsosa@unam.mx)

Academic editor: L. E. Bezerra | Received 16 August 2021 | Accepted 21 October 2021 | Published 19 November 2021

<http://zoobank.org/B6780A28-CBF5-4C14-9776-F23269C39C7F>

Citation: Calderón-Rosete G, González-Barrios JA, Piña-Leyva C, Moreno-Sandoval HN, Lara-Lozano M, Rodríguez-Sosa L (2021) Transcriptional identification of genes light-interacting in the extraretinal photoreceptors of the crayfish *Procambarus clarkii*. ZooKeys 1072: 107–127. <https://doi.org/10.3897/zookeys.1072.73075>

Abstract

Crayfish serve as a model for studying the effect of environmental lighting on locomotor activity and neuroendocrine functions. The effects of light on this organism are mediated differentially by retinal and extraretinal photoreceptors located in the cerebroid ganglion and the pleonal nerve cord. However, some molecular aspects of the phototransduction cascade in the pleonal extraretinal photoreceptors remain unknown. In this study, transcriptome data from the pleonal nerve cord of the crayfish *Procambarus clarkii* (Girard, 1852) were analyzed to identify transcripts that potentially interact with phototransduction processes. The Illumina MiSeq System and the pipeline Phylogenetically Informed Annotation (PIA) were employed, which places uncharacterized genes into pre-calculated phylogenies of gene families. Here, for the first time 62 transcripts identified from the pleonal nerve cord that are related to light-interacting pathways are reported; they can be classified into the following 11 sets: 1) retinoid pathway in vertebrates and invertebrates, 2) photoreceptor specification, 3) rhabdomeric phototransduction, 4) opsins 5) ciliary phototransduction, 6) melanin synthesis, 7) pterin synthesis, 8) ommochrome synthesis, 9) heme synthesis, 10) diurnal clock, and 11) crystallins. Moreover, this analysis comparing the sequences located on the pleonal nerve cord to eyestalk sequences reported in other studies reveals 94–100% similarity between

the 55 common proteins identified. These results show that both retinal and pleonal non-visual photoreceptors in the crayfish equally expressed the transcripts involved in light detection. Moreover, they suggest that the genes related to ocular and extraocular light perception in the crayfish *P. clarkii* use biosynthesis pathways and phototransduction cascades commons.

Keywords

Caudal photoreceptor, opsins, photoresponse, phototransduction, pleonal nerve cord

Introduction

The freshwater crayfish is a model for studying locomotor behavioral and neurohormonal responses to light, which are mediated by retinal and extraretinal photoreceptors. The crayfish's pleonal nerve cord (PNC), which consists of six ganglia, also responds to photostimulation previous studies have reported motor neuron activation (Edwards 1984; Simon and Edwards 1990). As early studies postulated, light-induced reflex activity results from integrating luminous sensory information from an interplay between the transmissions of retinal and caudal photoreceptors (CPRs) (Rodríguez-Sosa et al. 2008).

In the invertebrate phototransduction mechanism, light initiates a signaling cascade that induces a depolarization of the cell membrane. One CPR is present in each half of the sixth pleonal ganglion (6th PG), with their axons coursing rostrally from the 6th PG to the brain. CPRs respond to a light stimulus with a high-frequency burst. In addition, these neurons respond trans-synaptically to mechanical stimuli. The CPR has been well-studied through electrophysiological recordings, along with analyses of the locomotor activity induced when sensing light (Welsh 1934; Wilkens and Larimer 1972; Edwards 1984; Fernández de Miguel and Aréchiga 1992). Serotonin and dopamine regulate the firing rate from these CPRs, and serotonin modulates the circadian rhythm for both spontaneous and light-induced CPR activities (Rodríguez-Sosa et al. 2006, 2007, 2011).

The CPRs are “simple” photoreceptors due to their lack of specialized structures such as the microvilli or cilia that characterize the retinal photoreceptor (Gotow and Nishi 2008). These structural differences between ocular and extraocular receptors suggest differences in the molecular cascades involved in photoreception. However, a recent study shows that two opsins are found in both the retina and the PNC of the crayfish *P. clarkii* (Kingston and Cronin 2015). This study also finds that the transcripts of both opsins are expressed in each ganglion of the PNC and in the retina with identical sequences, suggesting that CPRs use these two proteins in the phototransduction pathway, as observed in the retina by Hariyama et al. (1994).

The opsins identified include one that is sensitive to short-wavelength light (λ_{\max} = 440 nm, SWS, blue) and another sensitive to long-wavelength light (λ_{\max} = 530 nm, LWS, green). Other studies show that these simple photoreceptors have a spectral sensitivity peak at 500 nm, suggesting that they contain a rhodopsin-like photopigment (Bruno and Kennedy 1962; Larimer et al. 1966; Cronin and Goldsmith 1982;). In

addition, the left and right crayfish caudal photoreceptors show asymmetry in the spontaneous action potentials discharged in darkness and in their responses to white light and blue or green monochromatic light pulses (Sánchez-Hernández et al. 2018; Pacheco-Ortiz et al. 2018).

Furthermore, a study seeking to identify the molecular mechanism of CPR transduction finds that the injection of inositol 1,4,5-trisphosphate (IP3), calcium, and guanosine nucleotide (GTP) mimics the light response (Kruszewska and Larimer 1993). However, for crustaceans, little genomic information is available, and few sequences have been annotated in databases regarding the components involved in phototransduction cascades in extraretinal photoreceptors (Hariyama et al. 1993; Kingston and Cronin 2015; Porter et al. 2017).

In this study, we obtain and analyze the pleonal nerve cord transcriptome to identify potential light-interacting genes from the extraretinal photoreceptors of the freshwater crayfish *P. clarkii*. We also compare the encoded protein to the sequences of the eyestalk transcriptome reported in a study by Manfrin et al. (2015). All sequencing data reported here have been deposited in the GenBank database.

Materials and methods

We used four adult crayfish (*P. clarkii*) two males and two females in their intermolt stage. The animals were acquired from a local provider in the autumn and kept in the laboratory in aerated water containers for two weeks before the experiments, with a program of 12:12 h light-dark cycles; they were fed with carrots and dried fish. The care and handling of the animals during the experimental procedures was carried out according to the policies established by the Ethics Commission. This study was approved by Research of the Faculty of Medicine, UNAM (code FM/DI/128/2019).

The pleonal nerve cords were dissected and immediately placed in the Eppendorf tube with precooled TRIzol. The tissue was preserved at -80°C prior to extraction, the tissue was homogenized manually with a precooled mortar and pestle. Total RNA was extracted from the pleonal nerve cord using TRIzol reagent following the manufacturer's protocol (Catalog number 15596018, Invitrogen Co., Carlsbad, CA, USA). TRIzol solubilizes the biological material after the addition of chloroform (Catalog number P3803, Sigma-Aldrich, St. Louis, MO, USA), producing three phases: the upper aqueous phase containing RNA, the interphase with DNA, and the organic phase containing proteins. The aqueous phase was transferred to a new tube; the RNA was precipitated with isopropanol (Catalog number I9516, Sigma-Aldrich, St. Louis, MO, USA) and collected via centrifugation; the pellet was then washed with 75% ethanol (Catalog number E7023, Sigma Aldrich Co., St. Louis, MO, USA). The ethanol was then removed, and the pellet was resuspended in RNase-free H_2O and stored at -80°C . We used $5\mu\text{g}$ of total RNA to obtain the cDNA libraries, according to the manufacturer's protocol for the Illumina TruSeq RNA Library Preparation Kit v2 (Catalog number RS-122-2001, Illumina, San Diego, CA, USA). We performed Illumina

paired-end protocol 150 bp sequencing. The library obtained was sequenced using the MiSeq Reagent kit v3 system (Catalog number MS-102-3001) according to the manufacturer's protocol, to obtain the PNC transcriptome.

The raw data from the Illumina system were uploaded to the Galaxy Web Portal to execute a *de novo* assembly process, using Trinity software (Grabherr et al. 2011; Haas et al. 2013; Afgan et al. 2016). The reads had quality scores higher than 30, so we did not conduct any procedure to eliminate low-quality sequences. The adapter sequences were trimmed, and we performed the *de novo* transcriptome assembly using Trinity software, obtaining sequences in FASTA files in the Galaxy platform. Their translation was executed automatically via the OSIRIS pipeline (Oakley et al. 2014).

The resulting sequences were processed via the “Get ORFs” program. Any sequences shorter than 100 amino acids were ignored, to produce the protein sequences to be analyzed (Rice et al. 2000; Blankenberg et al. 2007). Next, we used the “Phylogenetically informed annotation” (PIA) pipeline to analyze the transcriptomic sequences from the PNC to search genes involved in light detection (Speiser et al. 2014), this pipeline is available on the Galaxy bioinformatics platform <https://galaxyproject.org/use/pia/>.

The PIA pipeline uses tools to generate maximum-likelihood phylogenetic trees for 109 genes from a Light Interaction Toolkit (LIT), a gene collection regarding light-interacting structures and their functions and development in metazoans, including those in phototransduction, eye development, pigment synthesis, circadian cycles, and other light-interacting pathways; these genes are distributed across 13 functional gene sets. This bioinformatics program places uncharacterized genes into a gene family based in pre-calculated phylogeny in a secure and accessible web server. We used the e-value $1e^{-20}$ for a BLAST search of the cutoff.

The analysis with PIA generates two results files based on the functional set of genes that are selected for analyzing the amino acid sequences. One file contains the number and sequence with all the hit proteins retrieved by the initial BLAST search, while the other file contains all selected genes placed onto their corresponding gene trees. All PIA pipeline filtered transcripts were manually analyzed to determine which sequences correspond to the possible genes implicated within the photoreception process. This procedure facilitates the elimination of duplicates and fragments and the identification of overlapping sequence sections to integrate longer sequences. For protein sequence identification, we used the Prosite database to verify the preserved domain profiles; we correlated them with functions, using the Pfam or UniProt databases (<https://pfam.xfam.org/search>; <https://www.uniprot.org>). The amino acid sequences listed in the Suppl. material 1 identified as ‘mmc3’ in the Manfrin's study (2015), were used to assess the similarity of sequences identified in the PNC and in the eyestalk, using alignments with the Clustal Omega program (<https://www.ebi.ac.uk/Tools/msa/clustalo/>).

This procedure facilitates the verification of sequence identities obtained via the PIA analysis; these sequence data have been submitted to the GenBank databases under the accession number indicated in the fourth column of Tables 1–7.

Results

The Illumina system displayed 40,867,860 raw data reads; with the Novo assembler Trinity software available on the Galaxy website, we obtained 53,967 assembled nucleotides sequences in FASTA files. The PIA phylogenetic analysis was carried out using 36,558 deduced amino acid sequences with open reading frames and a minimum length of 100 amino acids. The sequence translations were done automatically in the OSIRIS platform available on the Galaxy site. The PIA analysis generated 109 maximum-likelihood trees distributed across thirteen functional gene sets, using the meta-zoan Light Interaction Toolkit; with the software, we obtained results for all sets from the PNC transcriptome.

We combined the genes identified in the functional gene sets “Retinoid pathway vertebrate” and “Retinoid pathway invertebrate” into Set 1. Set 2 includes the functional gene set “Photoreceptor specification and retinal determination network”; thus, we present a total of 11 gene sets in 7 Tables. This filter identified 256 sequences with potential homology with some functional gene sets from the PIA pipeline. After the analysis for each sequence, we eliminated duplicate sequences; we obtained longer consensus sequences when the ends of shorter sequences overlapped correctly. Finally, we integrated a total of 62 different transcripts from the pre-calculated phylogenetic trees. The BLAST analyses for each of the amino acid sequences identified in *P. clarkii* show a high conservation grade ($\geq 90\%$) with some other crustacean species, especially the Pacific white shrimp *Penaeus vannamei*.

In addition, we compared the sequences that we identified in the transcriptome of the PNC to the sequences from the transcriptome of the eyestalk. As mentioned previously, the sequences used for this comparison were obtained directly from Table mmc3, included as Suppl. material 1 by Manfrin et al. (2015). In our study, all comparisons with the eyestalk refer to this study. To ensure positive results, we performed a search in Table mmc3 with the Excel search tool, using both the name of the identified protein and the sequence itself.

The Tables show the names of the sequences we identified in the PNC, the number of amino acids (as deduced from the nucleotides), and the accession number in GenBank, as well as a comparison with previously reported sequences in the eyestalk. The last column shows the identity percentage between both sequences. We identified 62 genes from the PNC 55 of these were also expressed in the eyestalk transcriptome, while 38 were 100% identical to their corresponding transcripts in the PNC; 19 sequences had 94–99% similarity, while two transcripts presented a similarity of 24–41% with the transcript of the same name from the eyestalk. Only five PNC identified genes were not found in the eyestalk transcriptome.

The first functional gene set in Table 1 contains eight elements that participate in the synthesis and metabolism of visual chromophores from dietary carotenoid precursors. This group includes the genes identified in two functional sets by PIA (namely,

Table 1. Transcripts identified from PNC through PIA pipeline compared with crayfish eyestalk transcriptome data.

Gene	Pleonal nerve cord (Current study)			Eyestalk (Manfrin et al. 2015)		
	Top BLAST hit-Protein	aa	Access number	Contig ID (Procl_ES)	aa	Homology percentage
Set 1. Components of the retinoid pathway in vertebrates and invertebrates						
<i>Ralbp</i>	Retinal-binding protein	159	MN110026	5420_1	431	100
<i>Rdh11</i>	Retinol dehydrogenase 11	346	MT601680	12053_0	350	100
<i>Rdh13</i>	Retinol dehydrogenase 13	149	MT601681	WCS	–	–
<i>Dhrs4</i>	Dehydrogenase/reductase SDR family member 4-like	289	MT601679	888_7	282	100
<i>Sdr16c5</i>	Epidermal retinol dehydrogenase 2-like isoform X2	122	MT601682	5911_0	309	98
<i>Crabp1</i>	Cellular retinoic acid-binding protein 1-like	115	MT601683	WCS	–	–
<i>ninaB</i>	Carotenoid oxygenase (RPE65)	108	MT601684	4243_0	523	41
<i>ninaD</i>	Class B scavenger receptor	111	MT942649	2476_0	515	100

PNC= Pleonal nerve cord; aa= amino acids; WCS= without comparable sequence in the eyestalk as in all tables.

Table 2. Transcripts identified from the PNC through PIA pipeline compared with the crayfish eyestalk data.

Gene	Pleonal nerve cord (Current study)			Eyestalk (Manfrin et al. 2015)		
	Top BLAST hit-Protein	aa	Access number	Contig ID (Procl_ES)	aa	Homology percentage
Set 2. Elements of photoreceptor specification and retinal determination network.						
<i>Egfr</i>	Tyrosine-protein kinase Fer	873	KY974273	3891_0	914	100
<i>Ppb</i>	Putative retinal homeobox protein Rx2-like	414	MN110016	1058	422	100
<i>Glass</i>	Krüppel homolog 1-like	608	MN110021	652_0	608	100
<i>En</i>	Homeobox protein engrailed-1-like isoform X1	184	MN110023	WCS	–	–
<i>notch</i>	Neurogenic locus Notch protein	1210	MN110012	9959	2464	100
<i>Hh</i>	Protein hedgehog-like	190	MN110017	WCS	–	–
<i>dlx2b</i>	Homeobox protein DLX2b-like	299	MT942642	33351_0	162	94
<i>Dlx6</i>	Homeobox protein DLX-6-like	305	MT942643	18254_0	337	100
<i>Zag-1</i>	Zinc finger E-box-binding homeobox protein zag-1-like	204	MT942647	12586_0	831	99
<i>Zfhx3</i>	Zinc finger homeobox protein 3-like	768	MT942648	6525_0	2596	99

the retinoid pathways of vertebrates and invertebrates). Almost all identified sequences perform an enzymatic function, except for the sequence with a match for the type-B scavenger receptor, which has been reported to mediate the cellular capture of carotenoids in *Drosophila* (Kiefer et al. 2002; Von Lintig et al. 2005). In this set, out of the eight sequences identified in the abdominal nerve cord, only 6 were also identified in the eyestalk. The two sequences not identified in the eyestalk were retinol dehydrogenase 13 and cellular retinoic acid-binding protein 1.

The eyestalk transcriptome contains two sequences denominated as retinol dehydrogenase 13 (Procl_ES_4929_1 and Procl_ES_29212_0), although they showed similarities of 46% and 44%, respectively, with the sequence that we identified in the PNC.

The sequence identified as Cellular retinoic acid binding protein 1 (CRABP) contains the domain that corresponds to the Lipocalin/cytosolic fatty-acid-binding protein family. Lipocalins are transporters for small hydrophobic molecules, such as lipids, steroid hormones, bilins, and retinoids. Cytosolic CRABPs may regulate the access of retinoic acid to the nuclear retinoic acid receptors (www.uniprot.org/uniprot/P40220).

Notably, in this set, we found a low identity grade (41%) between PNC and eyestalk sequences for the protein encoded by the *ninaB* gene, the carotenoid oxygenase. Carotenoid oxygenases are a family of enzymes involved in carotenoid cleavage to produce retinol, commonly known as vitamin A. There are five sequences reported in the eyestalk transcriptome (Procl_ES_659_0; 4243_0; 11203_0; 30934_0; 1244_0). All of them, including the PNC sequences, contain the RPE65 superfamily conserved domain. However, they have very low similarity among themselves (see <https://doi.org/10.5061/dryad.pg4f4qrqp>).

Set 2 in Table 2 includes the PIA identified genes for two functional sets: Photoreceptor specification and Retinal determination network. Ten genes are identified: all are putatively implicated in developmental processes such as axon morphogenesis (*Glass*), eye formation via regulation of the initial specification of retinal cells (*Ppb*; *En*), and development or differentiation (*Notch*). The Hedgehog protein is believed to play an important role in one of the fundamental signal transduction pathways; its homeodomain contains sequence-specific DNA-binding proteins that act as regulators of transcription (Wang et al. 2020). During embryogenesis, morphogenic pathways such as WNT and Hedgehog are constitutively active; however, the activity of these pathways decreases in adulthood. Interestingly we identified both morphogenes and the genes of proteins involved in their pathways (Frizzled was identified in a manual analysis (GenBank: MZ383818 and *En*) in the PNC. Notably, the Hedgehog and engrailed-1 sequences identified in the PNC were not identified in the eyestalk.

Set 3 of the genes, corresponding to the rhabdomeric phototransduction pathway associated with invertebrate eyes, had the highest number of PIA-identified genes, totaling 16 transcripts (Set 3, Table 3). Opsins are light receptors that activate G-protein pathways through cAMP, IP₃, and DAG. This pathway is important for inducing depolarization in invertebrate photoreceptors. We identified the codified region of the alpha subunit of several types of G-proteins (including Gq), as well as phospholipase C (PLC), which is important for processing diacylglycerol (DAG) from PIP₂. We also identified guanine nucleotide-binding protein subunit beta 5, which is involved in the termination of signaling initiated by the G protein-coupled receptors, as well as beta arrestin-1, an important regulatory element in the phototransduction pathway. This protein participates in receptor desensitization and resensitization processes. In this set, the PIA analysis also identified the gene *nonA*, which encodes a putative RNA-binding protein in *Drosophila*; its absence has been associated with an electroretinogram defect and reduced visual acuity in fly mutants (Jones and Rubins 1990; Rendahl et al. 1996). In this set, 15 sequences were common to both structures, with a high identity of 96–100%. The *P. clarkii* eyestalk transcriptome has 19 sequences identified as Arrestin; however, none was similar to the beta-arrestin-1 that we identified in the PNC.

In Set 4, the PIA pipeline identified two transcripts (Table 3); these sequences were two isoforms of the G protein-coupled receptor moody-like. We decided to keep these sequences in Table 3 because the conserved domains in these proteins are characteristic of the G protein-coupled receptors. This family contains several opsin family mem-

Table 3. Transcripts identified from PNC through PIA pipeline compared with crayfish eyestalk transcriptome data.

Gene	Pleonal nerve cord (current study)			Eyestalk (Manfrin et al. 2015)		
	Top BLAST hit-Protein	aa	Access number	Contig ID (Procl_ES)	aa	Homology (Percentage)
Set 3. Elements of the rhabdomeric phototransduction pathway						
<i>Rdgc</i>	Serine/threonine protein phosphatase 1	329	MN110024	983	329	100
<i>Ppp2cb</i>	Serine/threonine-protein phosphatase 2A catalytic subunit beta isoform	309	MN110029	1697	309	100
<i>G alpha</i>	Guanine nucleotide-binding protein G(q) subunit alpha	353	MF279133	1935_0	353	94
	Guanine nucleotide-binding protein G(s) subunit alpha	379	MN110031	1880_0	285	100
	Guanine nucleotide-binding protein G(i) subunit alpha	355	MN110025	6610_0	355	100
	Guanine nucleotide-binding protein G(o) subunit alpha	262	MN110018	2664_0	354	100
<i>G beta</i>	Guanine nucleotide-binding protein subunit beta-5-like	189	MN110034	5560_0	354	98
<i>Gnb1</i>	Guanine nucleotide-binding protein G(I)/G(S)/G(T) subunit beta-1	340	KY974308.1	1098_0	340	100
<i>Ggamma1</i>	Guanine nucleotide-binding protein subunit gamma-1	100	MT601685	3444_0	102	100
<i>nonA</i>	Protein no-on-transient A	467	MN110015	–	–	–
<i>Dagk</i>	Eye-specific diacylglycerol kinase isoform X3	902	MF279134	1599_0	467	100
<i>Plc</i>	1-Phosphatidylinositol 4,5-bisphosphate	733	MN110020	3323_0	1005	95
	Phosphodiesterase delta-4-like			2268_0	904	96
<i>Pkc</i>	cAMP-dependent protein kinase catalytic subunit 1	352	MN110019	2373	507	96
	Protein kinase C	602	MN110035	5727_0	747	100
<i>Arr</i>	Beta-arrestin 1	263	MN110013	WCS	–	–
<i>rdgB</i>	Phosphatidylinositol transfer protein beta isoform-like	270	MN110014	2227_0	270	100
Set 4. Opsins						
<i>moody</i>	Putative G-protein coupled receptor moody-like	504	MT601688	13547_0	739	100
<i>moody</i>	G-protein coupled receptor moody-like isoform X2	407	MT601689	6096_0	411	99
	Short wavelength-sensitive opsin	391	ALJ26468	11143_0	391	99
	Long wavelength-sensitive opsin	377	ALJ26467	23_0	377	100

Table 4. Transcripts identified from PNC through PIA pipeline compared with crayfish eyestalk transcriptome data

Gene	Pleonal nerve cord (current study)			Eyestalk (Manfrin et al. 2015)		
	Top BLAST hit-Protein	aa	Access number	Contig ID (Procl_ES)	aa	Homology percentage
Set 5. Components of ciliary phototransduction						
<i>Revrm</i>	Neurocalcin homolog isoform X2	192	MN110027	2966_0	192	99
<i>ncs-2</i>	Neuronal calcium sensor 2-like	188	MN110022	3948_0	188	100
<i>Rgs9</i>	Regulator of G-protein signaling 9-like	170	MN110033	5623_0	962	100
	Regulator of G-protein signaling 7-like	125	MN110036	3602_1	486	99
	Putative regulator of G protein signaling	255	MN110028	4872_0	1534	100

bers that are typical rhodopsin superfamily members. This set also contains two opsin sequences previously reported by other authors; although we did not identify them in the current analysis carried out with the PIA analysis, we consider it convenient to include them here because their expression in the PNC has already been reported (Kingston and Cronin 2015).

Set 5 includes genes identified by PIA analysis in the phylogenetic family of signaling cascades in ciliary photoreceptors (Table 4). The ciliary photoreceptors are traditionally associated with vertebrate eyes; however, several transcripts included in the phylogenetic tree from PIA for this type of photoreceptor were identified in the PNC transcriptome.

Table 5. Transcripts identified from PNC through PIA pipeline compared with crayfish eyestalk transcriptome data.

Gene	Pleonal Nerve Cord (Current study)			Eyestalk (Manfrin et al. 2015)		
	Top BLAST hit-Protein	aa	Access Number	Contig ID (Prcl_ES)	aa	Homology (Percentage)
Set 6. Elements of melanin synthesis pathway						
<i>Csad</i>	Cysteine sulfinic Acid Decarboxylase	417	MN110038	4782_0	603	100
<i>Ppo</i>	Prophenoloxidase	441	MH156427	2348_0	495	99
Set 7. Elements of pterin synthesis pathway						
<i>Xdh</i>	Aldehyde oxidase	435	MN110003	7559_0	1314	99
	Indole-3-acetaldehyde oxidase-like	536	MN110004	8366_0	1340	99
<i>Sepia</i>	Pyrimidodiazepine synthase	241	MN110006	5690_1	102	100
<i>Dhpr</i>	Dihydropteridine reductase-like	235	MN110005	1504_0	235	100
<i>Pcd</i>	Pterin-4-alpha-carbinolamine dehydratase-like	101	MN110007	2287_0	157	100
<i>Spr</i>	Sepiapterin reductase-like	185	MN110009	12527_0	274	100
Set 8. Elements of ommochrome synthesis pathway						
<i>Abcg1</i>	ATP-binding cassette sub-family G member 1-like	156	MN110008	6760_0	700	100
	ABC transporter, subfamily ABCB/MDR	270	MT942646	8046_0	1341	100
<i>Alad</i>	Delta-aminolevulinic acid dehydratase	280	MN110039	3984_0	338	100
<i>Alas2</i>	5-aminolevulinic acid synthase, Erythroid-specific, Mitochondrial-like isoform X5	215	MT942644	2230_0	534	99
<i>Uros</i>	Uroporphyrinogen-III synthase	252	MH156441	5238_0	345	99
<i>Urod</i>	Uroporphyrinogen decarboxylase	107	MN110037	4848_0	359	100

Potential’s regulators of G-protein signaling predominate in this group; the neurocalcin homolog has 96% identity with *Drosophila melanogaster*’s reported sequence and with neuronal calcium sensor 2-like protein (alignments not shown), which is another regulator of G protein-coupled receptors that act in a calcium-dependent manner. In this set, all sequences were also identified in the eyestalk, with 99–100% identity.

Sets 6–9 contain enzymes in several pigment biosynthesis pathways (Table 5). Prophenoloxidase activates the cascade to synthesize melanin, while cysteine sulfonic acid decarboxylase is part of the taurine biosynthesis pathway, which is related to various biological processes in response to cAMP. Sets 7 and 8 encompass enzymes that participate in the synthesis pathways of several pigments, such as brown ommochromes and red drosopterins. Both contribute to the typical eye color phenotype of *Drosophila* and serve as light-screening pigments; these are several types of pigments that have been reported in the integument underlying the exoskeleton and in the compound eyes of some arthropods (Ziegler 1961; Cerenius et al. 2008; Kim et al. 2013).

In the Ommochrome synthesis set, we recognized the scarlet-brown gene that encodes an ATP-binding domain of the ABC transporters family. This is a water-soluble domain of transmembrane ABC transporters; it uses the hydrolysis of ATP to translocate a variety of compounds across biological membranes and is also responsible for the transportation of guanine, tryptophan, and histamine precursors of eye pigments in planthopper (Jiang and Lin 2018), and *Drosophila melanogaster* (Borycz et al. 2008).

Set 9 in Table 5 contains 4 enzymes related to the Heme B biosynthesis pathway, one of the best-known complexes of the porphyrin family. The porphyrinoid pigments play crucial roles in protection against UV light (Martins et al. 2019), and in the processes of circadian rhythm maintenance and metabolism (Carter et al. 2017).

Table 6. Transcripts identified from PNC through PIA pipeline compared with crayfish eyestalk transcriptome data

Gene	Pleonal Nerve cord (current study)			Eyestalk (Manfrin et al. 2015)		
	Top BLAST hit-Protein	aa	Access Number	Contig ID (Procl_ES)	aa	Homolog Percentage
Set 10. Elements identified in the set of circadian clock						
<i>Slo</i>	Calcium-activated potassium channel variant 4	263	QIA97593	4724_0	1172	100
<i>Lark</i>	RNA-binding protein lark	308	QIA97594	2543_0	308	100

Table 7. Transcripts identified from PNC through PIA pipeline compared with crayfish eyestalk transcriptome data

Gene	Pleonal Nerve Cord (Current study)			Eyestalk (Manfrin et al. 2015)		
	Top BLAST hit-Protein	aa	Access Number	Contig ID (Procl_ES)	aa	Homology Percentage
Set 11. Elements associated with crystalline proteins						
<i>GstS1</i>	Glutathione S-transferase theta	221	MH156430.1	5690_1	241	100
<i>Aldb</i>	Aldehyde dehydrogenase (omega-crystallin)	523	MN110030	2528_0	523	100
<i>Cryaa</i>	Alpha-crystallin A chain	139	MT601686	721_0	163	24
<i>ibpB</i>	Small heat shock protein,	184	MG910470	554_0	184	100
<i>hif1a</i>	Hypoxia inducible factor 1 alpha	1054	MW981273	2830_0	523	96

Because light is the primary synchronizer in the regulation of circadian rhythms, the PIA pipeline facilitates identification of some transcripts related to the molecular pathway of the circadian clock. In Set 10 of Table 6, we identify a partial transcript of the Calcium-activated potassium channel transcript in crayfish. In *Drosophila*, this channel was sequenced by Atkinson et al. (1991). This potassium channel is activated by membrane depolarization and by increases in cytosolic Ca^{2+} ; it mediates the export of K^+ . We identified the partial sequence of a transcript that allowed us to deduce a 263-amino acid fragment. This fragment has 100% identity grade to the sequence from the eyestalk of crayfish (Procl_ES_4724_0) and has similarity of 92% to the 1184-amino acid sequence from *Drosophila melanogaster* (GenBank:AAA28902.1) (see <https://doi.org/10.5061/dryad.pg4f4qrqp>).

The identified gene *lark* in PNC has 100% identity to the corresponding sequence identified in the eyestalk (Procl_ES_2543_0) of the crayfish; it is 52% similar to that found in *Drosophila melanogaster* (GenBank: Q94901.1) (see <https://doi.org/10.5061/dryad.pg4f4qrqp>).

Set 11 contains transcripts related to soluble proteins called crystallins (Table 7). Crystallins are water-soluble proteins; in vertebrates, the refractive index of the lenses depends on the concentrations of these proteins. Previous research has proposed that, in vertebrates, crystallins have been recruited from stress-protective proteins as small heat-shock proteins (Tomarev and Piatyogorsky 1996). In the PNC transcriptome of crayfish, we have identified the transcript of the alpha-crystallin A chain, as well as 2 enzymes related to crystallins identified in cephalopods (S-crystallins and Ω -crystallins). In this phylogenetic family, the PIA pipeline also allows us to identify the transcript that encodes the small heat-shock protein that contains the alpha-crystallin domain (ACD) of alpha-crystallin-type small heat-shock proteins (sHsps). sHsps are small stress-induced proteins. In this set, we also identify hypoxia-inducible

factor 1 alpha, which contains the PAS domain. PAS domains have been found to bind ligands and act as sensors for light and oxygen in signal transduction (<https://www.ncbi.nlm.nih.gov/Structure/cdd/cddsrv.cgi>). These sequences were also identified in the eyestalk transcriptome, with 96–100% similarity; the alpha-crystallin A chain shows 24% similarity with the sequences in the eyestalk.

All genes identified here from the PNC were edited for annotation and submitted to the GenBank database of the National Center for Biotechnology Information (NCBI); the assigned accession number appears in the fourth column of each table. We have included Suppl. material 1 with all sequences available in the GenBank database (www.ncbi.nlm.nih.gov/genbank; see <https://doi.org/10.5061/dryad.pg4f4qrqp>).

Discussion

Invertebrates preserve various organs to sense light. In addition to retinal photoreceptors, crayfish possess extraretinal photoreceptors in the cerebroid ganglion and the abdominal nerve cord. These photoreceptor groups contribute differentially to phototactic motor behaviors and the synchronization of circadian rhythms (Wilkens and Larimer 1972; Edwards 1984; Simon and Edwards 1990; Fernández-de-Miguel and Aréchiga 1992; Rodríguez-Sosa et al. 2008; Sullivan et al. 2009; Rodríguez-Sosa et al. 2012).

We present in this study the putative molecular components of the extraocular phototransduction system identified from the transcriptome of the PNC of the crayfish *P. clarkii*. We identify 62 transcripts that encode proteins potentially involved in the development processes of photoreceptor structures, phototransduction cascades, pigment biosynthesis, crystalline structures, and circadian rhythms. This constitutes the first report on the comprehensive identification of genes with a putative functional identification in extraretinal phototransduction from the PNC of the crayfish *P. clarkii*.

The genetic information on the PNC in this study allows us to make comparisons to the eyestalk transcriptome of the same species, as reported by Manfrin et al. (2015). The comparison between the proteins deduced from transcriptomic sequences in the eyestalk and abdominal nerve cord shows a 100% identity grade in almost all sequences (Tables 1–7). We also note that, although some of the transcripts that we identified in the PNC transcriptome were partial sequences, in all cases it was nevertheless possible to identify characteristic conserved domains in the proteins translated. Our results confirm that most molecules of the transduction pathways are common to both retinal and extraretinal photoreceptors, as previously suggested by Gotow and Nishi (2008), and by Kingston and Cronin (2015).

However, we also found five transcripts in the PNC that we could not identify in the eyestalk transcriptome. These differences were in Sets 1, 2, and 3, suggesting some functional peculiarities between retinal and extraretinal photoreceptors. Set 1 (corresponding to the phylogenetic family of the retinoid pathway) contains the first 2 differences. One of these genes is *Rdh13*, which encodes retinol dehydrogenase 13; in humans, this enzyme participates in retinoid metabolism and oxidizes all-trans-retinol,

although it seems to reduce all-trans-retinal with much greater efficiency (Belyaeva et al. 2008). The other gene that we do not identify in the eyestalk is *Crabp1*, which encodes the cellular retinoic acid-binding protein 1-like protein, which may regulate the access of retinoic acid to the nuclear retinoic acid receptors.

The second group of genes listed in Table 2 contains several genes associated with development processes; among these are several transcriptional regulators. In this phylogenetic family, the *En* and *Hh* genes were not found in the eyestalk; these encode the proteins homeobox protein engrailed-1 and hedgehog protein, respectively. These transcription factors are involved in the development, survival, and differentiation of neuronal photoreceptors (Altieri et al. 2016; Li et al. 2016).

Interestingly, in the same set, we identified the expression of the *Pph* gene in the PNC. The protein encoded by this gene is the putative retinal homeobox protein Rx2, which plays a critical role in eye formation by regulating the initial specification of retinal cells. This transcription factor is necessary for mushroom body development in the *Drosophila* brain and is conserved between vertebrates and flies (Kraft et al. 2016).

Generally, the rhabdomeric photoreceptors are associated with invertebrate eyes; functional Set 3 corresponds to elements of rhabdomeric phototransduction. From the identified transcripts, we can identify the 1-phosphatidylinositol 4,5-bisphosphate phosphodiesterase delta-4-like protein (*plcd4*), which hydrolyzes phosphatidylinositol 4,5-bisphosphate (PIP2) to generate two second messenger molecules: DAG and inositol 1,4,5-trisphosphate (IP3). This confirms a previous study by Krusewzka and Larimer (1993).

In this set, we have also identified four different transcripts that encode the α subunits of the heterotrimeric G proteins. These proteins can be identified by their α subunits, and they are grouped into four families based on their sequences and functionality. The four G-protein families are $G\alpha_s$, $G\alpha_i$, $G\alpha_q$, and $G\alpha_{12}$ (Syrovatkina et al. 2016). In the PNC, we have identified members of three of these families: from the $G\alpha_i$ family, we identified two members ($G\alpha_i$ and $G\alpha_o$); the other two were $G\alpha_s$ and $G\alpha_q$. Previous research has established that the $G\alpha_s$ and $G\alpha_i$ families of G proteins may regulate adenylyl cyclases, leading to increased or reduced intracellular levels of cAMP, respectively; another research also shows that the $G\alpha_s$ subunit and cAMP participates in phototransduction in jellyfish (Koyanagi et al. 2008). In the simple photoreceptors (Ip-2 or Ip-1) of the abdominal ganglion of *Onchidium verruculatum*, phototransduction is triggered by a G_o -type protein coupled to guanylate cyclase. This cGMP cascade contrasts with the phototransduction cGMP cascade mediated by the G_t -type G protein coupled to phosphodiesterase in vertebrate photoreceptors (Gotow and Nishi 2008). The heterotrimeric G protein also contains $G\beta\gamma$ subunits, although we only identified a sequence of the $G\beta_5$ subunit that is generally expressed in the brain (Syrovatkina et al. 2016). It would be interesting to study whether the various G proteins identified are probably those that facilitate the various photoresponsive characteristics of CPRs. As we have previously noted, the extraretinal photoreceptor presents spontaneous activity, as well as a rhythmic and differential photoresponse to monochromatic stimulation of blue and green light. Importantly, these photorecep-

tors are also modulated by serotonin and dopamine and are coupled to G proteins (Welsh 1934; Rodríguez-Sosa et al. 2003, 2006, 2007, 2011; Pacheco-Ortiz et al. 2018; Sánchez-Hernández et al. 2018).

Notably, we did not identify any of the two opsins previously reported in both the eyestalk and the PNC of this species (Kingston and Cronin 2015), although it is possible that the PIA did not find a sufficient level of similarity to the sequences of the phylogenetic families that it uses for identification. However, in the eyestalk transcriptome reported by Manfrin et al. (2015), these two opsins are expressed. The sequence of the long-wavelength-sensitive opsin in the crayfish *P. clarkii* has been reported in three different studies (Hariyama et al. 1993; Kingston and Cronin 2015; Manfrin et al. 2015). A comparison between these sequences shows a similarity of 98–100% (Figure 1A). The short-wavelength-sensitive opsin recently reported in the eyestalk and PNC by Kingston and Cronin (2015) is also found in the list of transcriptomes identified in the eyestalk (Manfrin et al. 2015)^[20]. These two sequences are 100% identical (Figure 1B).

While the eyestalk transcriptome contains 19 sequences identified or related to the protein beta-arrestin, none were like the beta-arrestin-1 identified in the PNC. This protein participates in the deactivation of the ciliary and rhabdomeric cascades and is regenerated by retinal binding proteins (Peterson et al. 2017). This particularity merits further exploration in future studies, since beta-arrestin-1 may be a determining element in the characteristics of retinal and extraretinal photoresponsiveness in this crustacean.

Because ciliary photoreceptors are generally associated with vertebrate eyes, we did not expect to identify genes of both phototransduction cascades in this structure with simple photoreceptors. This finding suggests that these light-mediated biochemical processes are highly conserved and coexist in various invertebrate species, as previous studies have shown (Arendt et al. 2004; Gotow and Nishi 2008; Veraszto et al. 2018).

The physical appearance of the nervous tissue in the crayfish is of a whitish color; the presence of numerous enzymes that participate in the synthesis pathways of various pigments is remarkable. The pigment expression in this structure suggests that the pigments are associated with various functions. For example, one of the functional gene sets is related to the melanin synthesis pathway; melanin is a unique pigment with several functions and is found in all biological kingdoms (Eisenman and Casadevall 2012). It plays a major role in skin homeostasis by conferring photoprotection and is also involved in neutralizing free radicals and reactive oxygen species, promoting fitness and cell survival, and encapsulating harmful metabolites; it is synthesized in response to microbial infections in invertebrates (Casadevall et al. 2017; Maranduca et al. 2019; Zhang et al. 2019).

Similarly, pterin is a member of the group of compounds called pteridines. Some microorganisms utilize cyanide and heavy metals for the efficient production of pterin compounds, and the antimicrobial activity of pterin has been studied and substantiated by antagonistic activity against *Escherichia coli* and *Pseudomonas aeruginosa*. Furthermore, the pterin compound has been proven to inhibit the formation of biofilm. The extracted pterin compounds may function as antioxidants or antimicrobials (Mahendran et al. 2018) in various organisms such as *P. clarkii*.

A		
P35356.1	MSSWSNQPMDDYGLPSSNPFYGNFTVVDMAPKDILHMIHPHWYQYPPMNMMPYPLLLIFM	60
ALJ26467.1	MSSWSNQPMDDYGLPSSNPFYGNFTVVDMAPKDILHMIHPHWYQYPPMNMMPYPLLLIFM	60
Procl_ES_23_0	MSSWSNQPMDDYGLPSSNPFYGNFTVVDMAPKDILHMIHPHWYQYPPMNMMPYPLLLIFM *****	60
P35356.1	LFTGILCLAGNFVTIWFVMTKSLRTPANLLVVNLAMSDFLMMFTMFPMMVTCYHYHTWT	120
ALJ26467.1	LFTGILCLAGNFVTIWFVMTKSLRTPANLLVVNLAMSDFLMMFTMFPMMVTCYHYHTWT	120
Procl_ES_23_0	LFTGILCLAGNFVTIWFVMTKSLRTPANLLVVNLAMSDFLMMFTMFPMMVTCYHYHTWT *****	120
P35356.1	LGPTFCQVYAFGLNLCGCASIWTMVFITFDRYNVIVKGVAGEPLSTKKAASLWILTIIWVLS	180
ALJ26467.1	LGPTFCQVYAFGLNLCGCASIWTMVFITFDRYNVIVKGVAGEPLSTKKAASLWILTIIWVLS	180
Procl_ES_23_0	LGPTFCQVYAFGLNLCGCASIWTMVFITFDRYNVIVKGVAGEPLSTKKAASLWILTIIWVLS *****	180
P35356.1	ITWCIAPFFGWNRYVPEGNLTGCGTDYLSIEDILRSYLYDYSTWVYYLPL-LPIYCYVSI	239
ALJ26467.1	ITWCIAPFFGWNRYVPEGNLTGCGTDYLSIEDILRSYLYDYSTWVYYLPL-LPIYCYVSI	240
Procl_ES_23_0	ITWCIAPFFGWNRYVPEGNLTGCGTDYLSIEDILRSYLYDYSTWVYYLPL-LPIYCYVSI *****;*** : *****	240
P35356.1	IKAVAAHEKGMRDQAKKMGIKSLRNEEAQKTSACRLAKIAMTIVALWFIAWTPYLLINW	299
ALJ26467.1	IKAVAAHEKGMRDQAKKMGIKSLRNEEAQKTSACRLAKIAMTIVALWFIAWTPYLLINW	300
Procl_ES_23_0	IKAVAAHEKGMRDQAKKMGIKSLRNEEAQKTSACRLAKIAMTIVALWFIAWTPYLLINW *****	300
P35356.1	VGMFARSYLSFVYTIWGYVFAKANAVYNPVYAI SHPKYRAAMEKKLPCLSCKTE SDDVS	359
ALJ26467.1	VGMFARSYLSFVYTIWGYVFAKANAVYNPVYAI SHPKYRAAMEKKLPCLSCKTE SDDVS	360
Procl_ES_23_0	VGMFARSYLSFVYTIWGYVFAKANAVYNPVYAI SHPKYRAAMEKKLPCLSCKTE SDDVS *****	360
P35356.1	ESASTTTSSAEKKAESA- 376	
ALJ26467.1	ESASTTTSSAEKKAESA- 377	
Procl_ES_23_0	ESASTTTSSAEKKAESA* 377 *****	
B		
ALJ26468.1	MALLDGLTLPGAGMTNDTNLIRPALFRSGEGVAAGGRYEMRMLGWNTPSEYMDYVHPYWK	60
Procl_ES_11143_0	MALLDGLTLPGAGMTNDTNLIRPALFRSGEGVAAGGRYEMRMLGWNTPSEYMDYVHPYWK *****	60
ALJ26468.1	TFQAPNPFHLYMLAVLYIMFMFAALVGNVIVWFTSAKNLRTPSNMFIIINLAILDIFIMM	120
Procl_ES_11143_0	TFQAPNPFHLYMLAVLYIMFMFAALVGNVIVWFTSAKNLRTPSNMFIIINLAILDIFIMM *****	120
ALJ26468.1	LKTPVFIIVNSFNEGPIWGLKCDTFALMGSYSGVGGAVTNAATAYDRYKTIAPKPEAKIS	180
Procl_ES_11143_0	LKTPVFIIVNSFNEGPIWGLKCDTFALMGSYSGVGGAVTNAATAYDRYKTIAPKPEAKIS *****	180
ALJ26468.1	RGTALMMVVGIIWYASFWALLPLFNIWGRFVPEGFLTCTCFDYMSEDA STRAFVGSIFVF	240
Procl_ES_11143_0	RGTALMMVVGIIWYASFWALLPLFNIWGRFVPEGFLTCTCFDYMSEDA STRAFVGSIFVF *****	240
ALJ26468.1	AYIVPGSLVFFYFGQIFVHVRAHEQAMREQAKKMNVANLRVSGSHEDQEKSVEIRIAKVC	300
Procl_ES_11143_0	AYIVPGSLVFFYFGQIFVHVRAHEQAMREQAKKMNVANLRVSGSHEDQEKSVEIRIAKVC *****	300
ALJ26468.1	MGLFFLFLISWTPYAVVALIAAFGDRSKLTPLVSMIPALTCCKFVACVDPWVYAINHPRYR	360
Procl_ES_11143_0	MGLFFLFLISWTPYAVVALIAAFGDRSKLTPLVSMIPALTCCKFVACVDPWVYAINHPRYR *****	360
ALJ26468.1	LELQKRMFPWFCIHEEKPODTISQSTCETEK 391	
Procl_ES_11143_0	LELQKRMFPWFCIHEEKPODTISQSTCETEK 391 *****	

Figure. I. Comparative alignments of opsins reported in the crayfish *Procambarus clarkii* **A** long-wavelength-sensitive opsin (UniProtKB/Swiss-Prot: P35356.1; Hariyama et al. 1993); (GenBank: ALJ26467.1; Kingston and Cronin 2015); (Procl_ES_23_0; Manfrin et al. 2015) **B** short-wavelength-sensitive opsin (GenBank: ALJ26468.1; Kingston and Cronin 2015); (Procl_ES_11143_0; Manfrin et al. 2015)

We also identify four enzymes that participate in the biosynthesis of the heme group, a cofactor involved in multiple cellular processes. One of the best known of these is the binding of oxygen to hemoglobin and myoglobin, although it has also been established that heme can interact with transcription factors that regulate genes participating in the maintenance of circadian rhythms (Carter et al. 2017; Martins et al. 2019).

In the PNC transcriptome, we have identified two transcripts that encode proteins involved in diurnal rhythms (Table 6). The gene *lark* encodes an RNA-binding protein that may be required in *Drosophila* for circadian repression of eclosion (www.uniprot.org/uniprot/Q94901), as well as for the calcium-activated potassium channel *slowpoke* (GenBank: Q03720 and AAA28902.1). A study on *Drosophila* has recently reported that this potassium channel functions in central clock cells, in addition to multiple components of the circadian circuits; these authors suggest that it contributes to generating rhythms of daily neuronal activity and facilitates the propagation of circadian information through output circuits (Ruiz et al. 2021). While Sullivan et al. (2009) report that the CPRs do not originate the circadian rhythm from the locomotor activity in crayfish, the CPRs are essential for maintaining synchronization of this circadian rhythmicity in crayfish within the 24-h light-dark cycle (Rodríguez-Sosa et al. 2012). It would be interesting to study the participation of this calcium-activated potassium channel in the expression of the circadian spontaneous response of the CPRs in the PNC (Rodríguez-Sosa et al. 2008).

Finally, crystallins are proteins that contribute to the transparency and refractive index of the lens in vertebrates. However, their expression in the PNC is probably associated with other functions that have been described for crystallins outside of the lens; primarily, they have been linked to protective functions against some stressors and the maintenance of cytoplasmic order (Tomarev and Piatygorosky 1996; Slingsby and Wistow 2014).

Although retinal and extraretinal photoreceptors in crayfish show significant morphological differences regarding structure, the phototransduction pathways at the molecular level have common pathways, as we show in this study. Interestingly, these very different cell types share molecular components of photoreception and other associated metabolic pathways.

We believe that the knowledge of the molecular components involved in the phototransduction of the caudal photoreceptors and other associated metabolic pathways which we present in this study can serve as an essential primary resource for future research while also facilitating the comparative analysis of photoreception processes with other species of decapod crustaceans.

Conclusions

Unlike the image-forming function in the eyes, extraretinal photoreception has not been deeply studied, particularly at the molecular level. In this study, we have described 62 transcripts from the PNC of the crayfish *Procambarus clarkii*, using a bioinformatics tool that identifies phylogenetic families of light-interacting transcripts.

We compared these results to the crayfish eyestalk transcriptome described by other researchers (Kingston and Cronin 2015; Manfrin et al. 2015), finding that the high similarity in both transcriptomic sequences structures suggests that extraretinal and retinal photoreceptors share common mechanisms of phototransduction.

The molecular components described here potentially underlie photoreceptor development, pigment synthesis, phototransduction, and the regulation of circadian rhythm from the pleonal nerve cord of this species. We identify 5 transcripts that are expressed only in the transcriptome of the PNC. Furthermore, phototransduction in the extraretinal photoreceptors presents differences that merit further elucidation in future studies.

All these sequences are available in the GenBank database. We hope that the availability of these sequences will facilitate access for other researchers performing molecular-level studies and comparative analyses on these processes in future studies on decapod crustaceans.

Acknowledgments

This research was funded by Facultad de Medicina, UNAM, Grant FM/DI/128/2019 to LRS.

References

- Afgan E, Baker D, van den Beek M, Blankenberg D, Bouvier D, Čech M, Chilton J, Clements D, Coraor N, Eberhard C, Grüning B, Aysam Guerler A, Hillman-Jackson J, Von Kuster G, Rasche E, Soranzo N, Turaga N, Taylor J, Nekrutenko A, Goecks J (2016) The galaxy platform for accessible, reproducible and collaborative biomedical analyses: 2016 update. *Nucleic Acids Research* 44(W1): 3–10. <https://doi.org/10.1093/nar/gkw343>
- Altieri SC, Zhao T, Jalabi W, Romito-DiGiacomo RR, Maricich S M (2016) En1 is necessary for survival of neurons in the ventral nuclei of the lateral lemniscus. *Developmental Neurobiology* 76(11): 1266–1274. <https://doi.org/10.1002/dneu.22388>
- Arendt D, Tessmar-Raible K, Snyman H, Dorresteijn AW, Wittbrodt J (2004) Ciliary photoreceptors with a vertebrate-type opsin in an invertebrate brain. *Science* 306(5697): 869–871. <https://doi.org/10.1126/science.1099955>
- Atkinson N S, Robertson GA, Ganetzky B (1991) A component of calcium-activated potassium channels encoded by the *Drosophila* slo locus. *Science* 253(5019): 551–555. <https://doi.org/10.1126/science.1857984>
- Belyaeva OV, Korkina OV, Stetsenko AV, Kedishvili, NY (2008) Human retinol dehydrogenase 13 (RDH13) is a mitochondrial short-chain dehydrogenase/reductase with a retinaldehyde reductase activity. *Federation of European Biochemical Societies Journal* 275(1): 138–147. <https://doi.org/10.1111/j.1742-4658.2007.06184.x>
- Blankenberg D, Taylor J, Schenck I, He J, Zhang Y, Ghent M, Veeraraghavan N, Albert I, Miller W, Makova KD, Hardison RC, Nekrutenko A (2007) A framework for collabora-

- tive analysis of ENCODE data: making large-scale analyses biologist-friendly. *Genome Research* 17(6): 960–964. <https://doi.org/10.1101/gr.5578007>
- Borycz J, Borycz JA, Kubów A, Lloyd V, Meinertzhagen IA (2008) *Drosophila* ABC transporter mutants white, brown and scarlethave altered contents and distribution of biogenic amines in the brain. *Journal of Experimental Biology* 211: 3454–3466. <https://doi.org/10.1242/jeb.021162>
- Bruno MS, Kennedy D (1962) Spectral sensitivity of photoreceptor neurons in the sixth ganglion of the crayfish. *Comparative Biochemistry and Physiology* 6(1): 41–46. [https://doi.org/10.1016/0010-406X\(62\)90041-5](https://doi.org/10.1016/0010-406X(62)90041-5)
- Carter EL, Ramirez Y, Ragsdale SW (2017) The heme-regulatory motif of nuclear receptor Rev-erb β is a key mediator of heme and redox signaling in circadian rhythm maintenance and metabolism. *Journal of Biological Chemistry* 292(27): 11280–11299. <https://doi.org/10.1074/jbc.M117.783118>
- Casadevall A, Cordero RJB, Bryan R, Nosanchuk J, Dadachova E (2017) Melanin, Radiation, and Energy Transduction in Fungi. *Microbiology Spectrum* 5(2). <https://doi.org/10.1128/microbiolspec.FUNK-0037-2016>
- Cerenius L, Lee BL, Söderhäll K (2008) The proPO-system: Pros and cons for its role in invertebrate immunity. *Trends in Immunology*, 29(6): 263–271. <https://doi.org/10.1016/j.it.2008.02.009>
- Cronin TW, Goldsmith TH (1982) Photosensitivity spectrum of crayfish rhodopsin measured using fluorescence of metarhodopsin. *Journal of General Physiology* 79(2): 313–332. <https://doi.org/10.1085/jgp.79.2.313>
- Edwards Jr DH (1984) Crayfish extraretinal photoreception. I. Behavioral and motorneuronal responses to abdominal illumination. *Journal of Experimental Biology* 109(1): 291–306. <https://doi.org/10.1242/jeb.109.1.291>
- Eisenman HC, Casadevall A (2012) Synthesis and assembly of fungal melanin. *Applied Microbiology and Biotechnology*, 93(3): 931–40. <https://doi.org/10.1007/s00253-011-3777-2>
- Fernández-de-Miguel F, Aréchiga H (1992) Sensory inputs mediating two opposite behavioural responses to light in the crayfish *Procambarus clarkii*. *Journal of Experimental Biology* 164(1): 153–169. <https://doi.org/10.1242/jeb.164.1.153>
- Gotow T, Nishi T (2008) Simple photoreceptors in some invertebrates: Physiological properties of a new photosensory modality. *Brain Research* 1225: 3–16. <https://doi.org/10.1016/j.brainres.2008.04.059>
- Grabherr MG, Haas BJ, Yassour M, Levin JZ, Thompson DA, Amit I, Adiconis X, Fan L, Raychowdhury R, Zeng Q, Chen Z, Mauceli E, Hacohen N, Gnirke A, Rhind N, di Palma F, Birren BW, Nusbaum C, Lindblad-Toh K, Friedman N, Regev A (2011) Full-length transcriptome assembly from RNA-Seq data without a reference genome. *Nature Biotechnology* 29: 644–652. <https://doi.org/10.1038/nbt.1883>
- Haas B, Papanicolaou A, Yassour M, Grabherr M, Blood P, Bowden J et al. (2013) De novo transcript sequence reconstruction from RNA-seq using the trinity platform for reference generation and analysis. *Nature Protocols* 8: 1494–1512. <https://doi.org/10.1038/nprot.2013.084>
- Hariyama T, Ozaki K, Tokunaga F and Tsukahara Y (1993) Primary structure of crayfish visual pigment deduced from cDNA. *Federation of European Biochemical Societies Letters* 315(3): 287–292. [https://doi.org/10.1016/0014-5793\(93\)81180-8](https://doi.org/10.1016/0014-5793(93)81180-8)

- Jiang Y, Lin X (2018) Role of ABC transporters in White, Scarlet and Brown in brown planthopper eye pigmentation. *Comparative Biochemistry and Physiology. Part B, Biochemistry & Molecular Biology* 221(222): 1–10. <https://doi.org/10.1016/j.cbpb.2018.04.003>
- Jones KR, Rubin GM (1990) Molecular analysis of no-on-transient A, a gene required for normal vision in *Drosophila*. *Neuron* 4(5): 711–723. [https://doi.org/10.1016/0896-6273\(90\)90197-N](https://doi.org/10.1016/0896-6273(90)90197-N)
- Kiefer C, Sumser E, Wernet MF, Von Lintig J (2002) A class B scavenger receptor mediates the cellular uptake of carotenoids in *Drosophila*. *Proceedings of the National Academy of Sciences of the United States of America* 99(16): 10581–6. <https://doi.org/10.1073/pnas.162182899>
- Kim H, Kim K, Yim J (2013) Biosynthesis of drospterins, the red eye pigments of *Drosophila melanogaster*. Critical review. *International Union of Biochemistry and Molecular Biology Life* 65(4): 334–340. <https://doi.org/10.1002/iub.1145>
- Kingston A, Cronin T (2015) Short- and long-wavelength-sensitive opsins are involved in photoreception both in the retina and throughout the central nervous system of crayfish. *Journal of Comparative Physiology. A, Neuroethology, Sensory, Neural, and Behavioral Physiology* 201(12): 1137–1145. <https://doi.org/10.1007/s00359-015-1043-2>
- Koyanagi M, Tanako K, Tsukamoto H, Ohtsu K, Tokunaga F, Terakita A (2008) Jellyfish vision starts with cAMP signaling mediated by opsin-Gs cascade. *Proceedings of the National Academy of Sciences of the United States of America* 105(40): 15576–15580. <https://doi.org/10.1073/pnas.0806215105>
- Kraft KF, Massey EM, Kolb D, Walldorf U, Urbach R (2016) Retinal homeobox promotes cell growth, proliferation and survival of mushroom body neuroblasts in the *Drosophila* brain. *Mechanisms of Development* Vol. 142: 50–61. <https://doi.org/10.1016/j.mod.2016.07.003>
- Kruszewska B, Larimer JL (1993) Specific second messengers activate the caudal photoreceptor of crayfish. *Brain Research* 618(1): 32–40. [https://doi.org/10.1016/0006-8993\(93\)90425-M](https://doi.org/10.1016/0006-8993(93)90425-M)
- Larimer JL, Trevino DL, Ashby EA (1966) A comparison of spectral sensitivities of caudal photoreceptors of epigeal and cavernicolous crayfish. *Comparative Biochemistry and Physiology* 19(2): 409–415. [https://doi.org/10.1016/0010-406X\(66\)90150-2](https://doi.org/10.1016/0010-406X(66)90150-2)
- Li T, Fan J, Blanco-Sánchez B, Giagtzoglou N, Lin G, Yamamoto S, Jaiswal M, Chen K, Zhang J, Wei W, Lewis MT, Groves AK, Westerfield M, Jia J, Bellen HJ (2016) Ubr3, a Novel Modulator of Hh Signaling Affects the Degradation of Costal-2 and Kif7 through Poly-ubiquitination. *PLoS Genetics* 12(5): e1006054. <https://doi.org/10.1371/journal.pgen.1006054>
- Mahendran R, Thandeeswaran M, Kiran G, Arulkumar M, Ayub Nawaz KA, Jabastin J, Janani B, Anto Thomas T, Angayarkanni J (2018) Evaluation of Pterin, a Promising Drug Candidate from Cyanide Degrading Bacteria. *Current Microbiology* 75(6): 684–693. <https://doi.org/10.1007/s00284-018-1433-0>
- Manfrin C, Tom M, De Moro G, Gerdol M, Giulianini P, Pallavicini A (2015) The eyestalk transcriptome of red swamp crayfish *Procambarus clarkii*. *Gene* 557(1): 28–34. <https://doi.org/10.1016/j.gene.2014.12.001>

- Maranduca MA, Branisteanu D, Serban DN, Branisteanu DC, Stoleriu G, Manolache N, Serban IL (2019) Synthesis and physiological implications of melanic pigments. *Oncology Letters* 17(5): 4183–4187. <https://doi.org/10.3892/ol.2019.10071>
- Martins C, Rodrigo AP, Cabrita L, Henriques P, Parola AJ, Costa PM (2019) The complexity of porphyrin-like pigments in a marine annelid sheds new light on heme metabolism in aquatic invertebrates. *Scientific Reports* 9: e12930. <https://doi.org/10.1038/s41598-019-49433-1>
- Oakley T, Alexandrou M, Ngo R, Pankey M, Churchil, C, Chen W, Lopker K (2014) Osi-riis: accessible and reproducible phylogenetic and phylogenomic analyses within the galaxy workflow management system. *BioMed Central Bioinformatics* 15: e230. <https://doi.org/10.1186/1471-2105-15-230>
- Pacheco-Ortiz J, Sánchez-Hernández J, Rodríguez-Sosa L, Calderón-Rosete G, Villagran-Vargas E (2018) Left-right asymmetry in firing rate of extra-retinal photosensitive neurons in the crayfish. *General Physiology and Biophysics* 37(1): 13–21. https://doi.org/10.4149/gpb_2017040
- Peterson YK, Luttrell LM (2017) The diverse roles of arrestin scaffolds in G protein-coupled receptor signaling. *Pharmacological Review* 69(3): 256–97. <https://doi.org/10.1124/pr.116.013367>
- Porter ML, Steck M, Roncalli V, Lenz PH (2017) Molecular characterization of copepod photoreception. *Biological Bulletin* 233(1): 96–110. <https://doi.org/10.1086/694564>
- Rendahl KG, Gaukhshteyn N, Wheeler DA, Fry TA, Hall JC (1996) Defects in courtship and vision caused by amino acid substitutions in a putative RNA-binding protein encoded by the no-on-transient A (nonA) gene of *Drosophila*. *Journal of Neuroscience* 16(4): 1511–22. <https://doi.org/10.1523/JNEUROSCI.16-04-01511.1996>
- Rice P, Longden I, Bleasby A (2000) EMBOSS: the European Molecular Biology Open Software Suite. *Trends in Genetics* 16(6): 276–277. [https://doi.org/10.1016/S0168-9525\(00\)02024-2](https://doi.org/10.1016/S0168-9525(00)02024-2)
- Rodríguez-Sosa L, Calderón-Rosete G, Flores G (2008) Circadian and ultradian rhythms in the crayfish caudal photoreceptor. *Synapse* 62(9): 643–652. <https://doi.org/10.1002/syn.20540>
- Rodríguez-Sosa L, Calderón-Rosete G, Flores G, Porras MG (2007) Serotonin-caused phase shift of circadian rhythmicity in a photosensitive neuron. *Synapse* 61(10): 801–808. <https://doi.org/10.1002/syn.20425>
- Rodríguez-Sosa L, Calderón-Rosete G, Calvillo ME, Guevara J, Flores G (2011) Dopaminergic modulation of the caudal photoreceptor in crayfish. *Synapse* 65(6): 497–504. <https://doi.org/10.1002/syn.20866>
- Rodríguez-Sosa L, Calderón-Rosete G, Anaya V, Flores G (2012) The caudal photoreceptor in the crayfish: an overview. In: Akutawa E and Ozaki K (Eds) *Photoreceptors: Physiology, types and abnormalities*. Nova Science Publishers Inc, New York, 59-78.
- Rodríguez-Sosa L, Calderón-Rosete G, Porras-Villalobos MG, Mendoza-Zamora E, Anaya-González V (2006) Serotonin modulation of caudal photoreceptor in crayfish. *Comparative Biochemistry and Physiology. Toxicology & pharmacology* 142(3-4): 220–230. <https://doi.org/10.1016/j.cbpc.2005.10.006>

- Ruiz D, Bajwa ST, Vanani N, Bajwa TA, Cavanaugh DJ (2021) Slowpoke functions in circadian output cells to regulate rest:activity rhythms. *PLoS One* 16(5): e0251678. <https://doi.org/10.1371/journal.pone.0251678>
- Sánchez-Hernández J, Pacheco-Ortiz J, Rodríguez-Sosa L, Calderón-Rosete G, Villagran-Vargas E (2018) Asymmetric firing rate from crayfish left and right caudal photoreceptors Due to blue and green monochromatic light pulses. *Symmetry* 10(9): e389. <https://doi.org/10.3390/sym10090389>
- Simon TW, Edwards DH (1990) Light-evoked walking in crayfish: behavioral and neuronal responses triggered by the caudal photoreceptor. *Journal of Comparative Physiology A* 166: 745–755. <https://doi.org/10.1007/BF00187319>
- Slingsby C, Wistow GJ (2014) Functions of crystallins in and out of lens: Roles in elongated and post-mitotic cells. *Progress in Biophysics and Molecular Biology* 115(1): 52–67. <https://doi.org/10.1016/j.pbiomolbio.2014.02.006>
- Speiser D, Pankey M, Zaharoff A, Battelle B, Bracken-Grissom H, Breinholt J, Bybee SM, Cronin TW, Garm A, Lindgren AR, Patel NH, Porter ML, Protas ME, Rivera AS, Serb JM, Zigler KS, Crandall KA, Oakley TH (2014) Using phylogenetically-informed annotation (PIA) to search for light-interacting genes in transcriptomes from non-model organisms. *BioMed Central Bioinformatics* 15: e350. <https://doi.org/10.1186/s12859-014-0350-x>
- Sullivan JM, Genco MC, Marlow ED, Benton JL, Beltz BS, Sandeman DC (2009) Brain photoreceptor pathways contributing to circadian rhythmicity in crayfish. *Chronobiology International* 26(6): 1136–1168. <https://doi.org/10.3109/07420520903217960>
- Syrovatkina V, Alegre KO, Dey R, Huang XY (2016) Regulation, signaling and Physiological functions of G- proteins. *Journal of Molecular Biology* 428(19): 3850–3868. <https://doi.org/10.1016/j.jmb.2016.08.002>
- Tomarev SI, Piatyogorsky J (1996) Lens crystallins of invertebrates diversity and recruitment from detoxification enzymes and novel proteins. *European Journal of Biochemistry*. <https://doi.org/10.1111/j.1432-1033.1996.00449.x>
- Verasztó C, Gühmann M, Jia H, Rajan VB, Bezares-Calderón LA, Piñeiro-Lopez C, Randel N, Shahidi R, Michiels NK, Yokoyama S, Tessmar-Raible K, Jékely G (2018) Ciliary and rhabdomeric photoreceptor-cell circuits form a spectral depth gauge in marine zooplankton. *eLife* 7: e36440. <https://doi.org/10.7554/eLife.36440.001>
- Von Lintig J, Hessel S, Isken A, Kiefer C, Lampert JM, Voolstra O, Vogt K (2005) Towards a better understanding of carotenoid metabolism in animals. *Biochimica et Biophysica Acta* 1740(2): 122–31. <https://doi.org/10.1016/j.bbadis.2004.11.010>
- Wang Y, Wang B, Shao X, Liu M, Jiang K, Wang M, Wang L (2020) A comparative transcriptomic analysis in late embryogenesis of the red claw crayfish *Cherax quadricarinatus*. *Molecular Genetics and Genomics* 295(2): 299–311. <https://doi.org/10.1007/s00438-019-01621-4>
- Welsh JH (1934) The caudal photoreceptor and responses of the crayfish to light. *Journal of Cellular and Comparative Physiology* 4: 379–388. <https://doi.org/10.1002/jcp.1030040308>
- Wilkens LA, Larimer JL (1972) The CNS photoreceptor of crayfish morphology and synaptic activity. *Journal of Comparative Physiology* 80: 389–407. <https://doi.org/10.1007/BF00696436>

- Zhang P, Zhou S, Wang G, An Z, Liu X, Li K, Yin WB (2019) Two transcription factors cooperatively regulate DHN melanin biosynthesis and development in *Pestalotiopsis fici*. *Molecular Microbiology* 112(2): 649–666. <https://doi.org/10.1111/mmi.14281>
- Ziegler I (1961) Genetic aspects of ommochrome and pterin pigments. *Advances in Genetics* 10: 349–403. [https://doi.org/10.1016/S0065-2660\(08\)60121-2](https://doi.org/10.1016/S0065-2660(08)60121-2)

Supplementary material I

Appendix S1, S2

Authors: Gabina Calderón-Rosete, Juan Antonio González-Barrios, Celia Piña-Leyva, Hayde Nallely Moreno-Sandoval, Manuel Lara-Lozano, Leonardo Rodríguez-Sosa

Data type: Text

Explanation note: We have additional supporting information available online in the supporting tab for this article. **Appendix S1.** Some sequence alignments allow us to appreciate the degree of similarity among *Drosophila melanogaster*, the crayfish (*P. clarkii*) pleonal nerve cord, and the eyestalk. **Appendix S2.** Nucleotide sequence list referred from Tables 1–7. The supplementary materials are available also from Dryad (<https://doi.org/10.5061/dryad.pg4f4qrqp>).

Copyright notice: This dataset is made available under the Open Database License (<http://opendatacommons.org/licenses/odbl/1.0/>). The Open Database License (ODbL) is a license agreement intended to allow users to freely share, modify, and use this Dataset while maintaining this same freedom for others, provided that the original source and author(s) are credited.

Link: <https://doi.org/10.3897/zookeys.1072.73075.suppl1>

On two new species of deep-sea carrier crabs (Crustacea, Brachyura, Homolodromiidae, *Dicranodromia*) from Taiwan and the Philippines, with notes on other Indo-West Pacific species

Peter K. L. Ng¹, Chien-Hui Yang²

1 Lee Kong Chian Natural History Museum, National University of Singapore, 2 Conservatory Drive, Singapore 117377, Republic of Singapore **2** Institute of Marine Biology, National Taiwan Ocean University, 2 Pei-Ning Road, Keelung 20224, Taiwan

Corresponding author: Chien-Hui Yang (chyang@ntou.edu.tw)

Academic editor: I. S. Wehrtmann | Received 13 August 2021 | Accepted 1 November 2021 | Published 22 November 2021

<http://zoobank.org/3C4A5D71-A951-4B72-8055-EBDFF0785DED>

Citation: Ng PKL, Yang C-H (2021) On two new species of deep-sea carrier crabs (Crustacea, Brachyura, Homolodromiidae, *Dicranodromia*) from Taiwan and the Philippines, with notes on other Indo-West Pacific species. ZooKeys 1071: 129–165. <https://doi.org/10.3897/zookeys.1072.72978>

Abstract

The systematics of four species of the homolodromiid genus *Dicranodromia* A. Milne-Edwards, 1880, from East Asia and the Philippines is reappraised: *D. danielae* Ng & McLay, 2005, *D. doederleini* Ortman, 1892, *D. karubar* Guinot, 1993, and *D. martini* Guinot, 1995; and key characters such as the epistome, gonopods, and spermatheca are figured in detail. Two new species, *D. erinaceus* **sp. nov.** and *D. robusta* **sp. nov.**, are described from Taiwan and the Philippines, respectively. *Dicranodromia erinaceus* **sp. nov.** resembles *D. spinulata* Guinot, 1995, and *D. delli* Ah Yong, 2008 (from New Caledonia and New Zealand) but can be separated by its distinctly spinulated carapace surfaces and proportionately shorter fifth ambulatory legs. *Dicranodromia robusta* **sp. nov.** is superficially similar to *D. baffini* (Alcock & Anderson, 1899) and *D. karubar* Guinot, 1993, but can easily be separated by possessing a broad dorsoventrally flattened infraorbital tooth. A genetic study of the species using the mitochondrial cytochrome c oxidase I gene confirms that the taxa are distinct, with *D. erinaceus* **sp. nov.** coming out in a well-supported clade from congeners. The megalopa of *D. doederleini* is also reported for the first time.

Keywords

Comparative taxonomy, deep-sea crab, East Asia, Homolodromioidea, systematics.

Introduction

The deep-water carrier crabs of the homolodromiid genus *Dicranodromia* A. Milne-Edwards, 1880, are represented by 20 species from the Atlantic, Indian, and Pacific Oceans (Guinot 1995; Ng and McLay 2005; Ng and Naruse 2007; Ahyong 2008; Ng et al. 2008; Tavares and Lemaitre 2014). Of these, 11 species are known from the Indo-West Pacific: *D. baffini* (Alcock & Anderson, 1899), *D. chenae* Ng & Naruse, 2007, *D. crosnieri* Guinot, 1995, *D. danielae* Ng & McLay, 2005, *D. delli* Ahyong, 2008, *D. doederleini* Ortmann, 1892, *D. foersteri* Guinot, 1993, *D. karubar* Guinot, 1993, *D. martini* Guinot, 1995, *D. nagaii* Guinot, 1995, and *D. spinulata* Guinot, 1995.

We describe two additional species from Taiwan and the Philippines. The Taiwanese material had been misidentified as “*D. doederleini*” by earlier workers, while the Philippine specimens had been incorrectly identified by field collectors as “*D. delli*”. We also take this opportunity to update the character states of some poorly known species and refigure them so that they are better defined. In particular, we add male first and second gonopod characters for the species as they are useful to discriminate some of the taxa. Their taxonomy is also discussed. In addition, we also report on the larvae of an ovigerous female of *D. doederleini* which had been kept in the aquarium.

Materials and methods

Material examined is deposited in the National Taiwan Ocean University (NTOU), Keelung, Taiwan; and the Zoological Reference Collection (ZRC) of the Lee Kong Chian Natural History Museum, National University of Singapore. Measurements are provided in millimetres of the maximum carapace width and length. The ambulatory leg articles are measured along their maximum length while the width is determined at midlength where it is widest.

The terminology used follows Guinot (1995) and Davie et al. (1995). In *Dicranodromia*, the groove of G1 in which the G2 is inserted is on the dorsal surface of the structure (relative to the carapace), and in situ, the lobes present on the subdistal part are on the outer margin, i.e., directed laterally outwards. The following abbreviations are used: coll. = collected by; G1 = male first gonopod; G2 = male second gonopod; P2–P5 = pereopods 2–5 (ambulatory legs 1–4).

For the molecular analysis, a total of seven individuals were used (as indicated on the material examined of each species below). Two species, *D. danielae* and *D. robusta* sp. nov., could not be tested as they had originally been preserved in formalin. Crude genomic DNA was extracted from the muscles of the pleon using QIAamp DNA Micro Kit (Qiagen, Cat. No. 56304, Valencia, CA, USA) following the protocol of the manufacturer. The DNA barcoding gene (mitochondrial cytochrome c oxidase I, COI; cf. Hebert et al. 2005) was amplified using the universal primer set (LCO1490/HCO2198, 657 bp; Folmer et al. 1994). PCR reaction components, temperature cycling conditions and sequencing reaction followed those used in Ng

et al. (2018). For comparisons, the COI sequence of *Homolodromia kai* Guinot, 1993 (voucher number ZRC 2018.0109) was obtained and used as the outgroup for the analysis.

The resulting sequences were firstly translated into the corresponding amino acids by EditSeq (LASERGENE; DNASTAR) to check for pseudogenes (Song et al. 2008). BioEdit v.7.1.3.0 (Hall 1999) was then used to align and edit the COI dataset, with MEGA v. 7 (Kumar et al. 2016) used to calculate the uncorrected pairwise distances (*p*-distance). Maximum likelihood (ML) method was used to construct the phylogenetic tree by RAxML v.7.2.6 (Stamatakis 2006). ML analysis settings followed the model of general time reversible with a gamma distribution GTRGAMMA) for the COI dataset. Branch confidence of the tree topology was assessed using 1,000 bootstrap replicates (Felsenstein 1985).

Systematic account

Family Homolodromiidae Alcock, 1899

Genus *Dicranodromia* A. Milne-Edwards, 1880

Type species. *Dicranodromia ovata* A. Milne-Edwards, 1880, by monotypy; gender feminine).

Remarks. As the number of species has increased and more material has been examined since the revision by Guinot (1995), a revised key to *Dicranodromia* is provided below for the Indo-West Pacific species. To date, there are no shared species between the Atlantic and Indo-West Pacific.

Key to Indo-West Pacific species of *Dicranodromia*

- 1 Basal antennal article relatively short, stout; anteroexternal tooth long, subequal to or longer than rest of article2
- Basal antennal article more elongate; anteroexternal tooth short, distinctly shorter than rest of article7
- 2 Carapace and pereopods covered with short and very dense plumose setae, forming velvet-like tomentum, obscuring surfaces and margins of pereopods3
- Setae of various types and lengths on carapace and pereopods, can be relatively dense but never obscuring surfaces and margins of pereopods4
- 3 Carapace proportionately wider, anterolateral and posterolateral margins unarmed or only with small granules [southern Java and Moluccas]
..... *D. karubar* Guinot, 1993
- Carapace proportionately narrower, anterolateral and posterolateral margins lined with sharp spinules or granules [Indian Ocean].....
..... *D. baffini* (Alcock & Anderson, 1899)

- 4 Infraorbital tooth broad, dentiform to linguiform, subequal or larger than exorbital tooth [Philippines] *D. robusta* sp. nov.
 – Infraorbital tooth triangular, smaller than exorbital tooth..... 5
- 5 Anterior surface of epistome prominently spinose; P2 and P3 merus with distinct spines on flexor margin [Philippines] *D. danielae* Ng & McLay, 2005
 – Anterior surface of epistome at most granulate or with scattered spinules; flexor margin of P2 and P3 merus unarmed..... 6
- 6 P2 and P3 dactyli short, propodus more than twice length of dactylus [Philippines] *D. chenae* Ng & Naruse, 2007
 – P2 and P3 dactyli long, propodus 1.5–1.6× length of dactylus carapace [Philippines] *D. martini* Guinot, 1995
- 7 Dorsal surface of carapace covered with distinct spinules, especially along lateral parts, those on median parts may be present as granules; flexor margin of P2–P5 merus distinctly lined with spines 8
 – Dorsal surface of the carapace almost smooth, with granules or spinules present only on lateral parts; P2 and P3 merus unarmed except for flexor margin sometimes with spinules, P4 and P5 merus unarmed 11
- 8 Exorbital tooth triangular, dentiform; posterior margin of epistome prominently spinose [Madagascar] *D. crosnieri* Guinot, 1995
 – Exorbital tooth slender, spiniform; posterior margin of epistome entire, adjacent area smooth or with scattered spinules 9
- 9 Median part of dorsal surface of carapace covered with distinct spinules; submarginal area of posterior margin of epistome with several spinules; P2 and P3 relatively short (e.g., P3 propodus less than 7× longer than wide; propodus 1.7× length of dactylus) [New Caledonia; New Zealand] *D. spinulata* Guinot, 1995
 – Median part of dorsal surface of carapace covered with granules, not spinules; submarginal area of posterior margin of epistome unarmed; P2 and P3 relatively longer (e.g., P3 propodus more than 8× longer than wide; propodus 1.7× length of dactylus) ... 10
- 10 P2–P5 proportionately shorter (e.g., P3 merus 4.5× longer than wide; P5 merus just reaching branchiocardiac groove when folded dorsally) [Taiwan] *D. erinaceus* sp. nov.
 – P2–P5 proportionately longer (e.g., P3 merus 6.6× longer than wide; P5 merus longer and more slender, extending beyond branchiocardiac groove when folded dorsally) [New Zealand] *D. delli* Ahyong, 2008
- 11 Posterior margin of epistome entire; outer surface of palm in both sexes evenly covered with granules [Chesterfield Islands] *D. foersteri* Guinot, 1993
 – Posterior margin of epistome crenulate; median outer surface of palm in both sexes smooth, granules only present on subdorsal and subventral margins 12
- 12 Carapace and pereopods covered with numerous long stiff setae but not obscuring surfaces and margins [known for certain only from Japan] *D. doederleini* Ortmann, 1892
 – Carapace and pereopods densely covered with numerous setae of different types; partially obscuring carapace surface and margins, but almost completely obscuring surfaces and margins of pereopods [Japan] *D. nagaii* Guinot, 1995

***Dicranodromia doederleini* Ortmann, 1892**

Figures 1–3

Dicranodromia doederleini Ortmann, 1892: 549, pl. 26, fig. 4; Guinot 1995: 202, figs 2C, 11a, c, d, 12A–C; Ikeda 1998: 54–55, pl. 1 figs 1–6; Ng et al. 2008: 39 (for complete synonymy, see Guinot 1995: 202).

Material examined. JAPAN: 1 ♀ with 1 megalops (15.9 × 20.2 mm), Sagami Bay, from aquarium trade, 8 Apr. 2015 (ZRC 2017.1214, COI sequence: OK351331); 1 ovigerous ♀ (14.5 × 19.2 mm), 35°32.51'N, 139°54.74'E, Futtsu, Kanaya, Chiba Prefecture, 200–250 m, 19 Sep. 2007 (ZRC 2021.0469, COI sequence: OK351333); 1 ♂ (10.3 × 8.5 mm), station 29, 34°40.21'N, 139°18.62'E, SW of Izu-Oshima Island, Izu Islands, 289–307 m, TRV Shin'yo-maru, 2002 research cruise, coll. T. Komai, 24 Oct. 2002 (CBM-ZC 16572, COI sequence: OK351332).

Remarks. This species is well known (for synonymy and records, see Guinot 1995; Ikeda 1998) but may be a species complex, and specimens from outside the type locality in Japan all need to be rechecked (see Guinot 1995; Ng and McLay 2005).

One female specimen (ZRC 2017.1214) was imported to Singapore via the aquarium trade in early April 2015. On 8 April, the specimen was obtained by Paul YC Ng and observed to have between 10–20 large eggs under the pleon with the eyes just visible. It was kept in a cold-water aquarium (ca. 15–20°C) with other crustacean and fish species. On 18 April, he noted that several eggs had been released into the aquarium (Fig. 1D) which appeared ready to hatch, and that some of the egg membranes had ruptured revealing what appeared to be a dead first zoeal stage (Fig. 1E). One specimen, however, was apparently a freshly hatched and dead megalopa (Fig. 1F). He observed the first free-crawling megalopa on the female specimen on 24 April (Fig. 1B, G). Unfortunately, no larvae except one megalopa was preserved (PYC Ng, personal communication).

The observations above on the eggs and megalopa of *D. doederleini* provide some clarity on the larval development in the genus. While it is known the eggs are large and the development is abbreviated, it is not sure of the eggs hatch into an advanced zoeal stage or directly into megalopa. Caustier (1895) was the first to report on the first zoea of *Dicranodromia ovata* A. Milne-Edwards, 1880, from the Atlantic but he based this on unhatched embryos and unfortunately, the description was brief, and no figures were provided. Martin (1991) found a specimen of *D. felderi* Martin, 1990 from the western Atlantic, which had well-developed eggs and removed some embryos. On the basis of these, he described what he regarded was the first zoea. Guinot (1995: 105) reported that a specimen of *D. nagaii* from Japan had about 20 megalopae under the pleon and suggested the eggs hatched directly into this stage. The eggs of *D. doederleini* are full of yolk, and even the “first zoea” observed are of the lecithotrophic type, with yolk sacs and appendages, which are poorly or not setose (Fig. 1E). They are very similar to the condition observed or the dromiid *Cryptodromia pileifera* Alcock, 1900 which has only one lecithotrophic first zoeal stage before the megalopa (Tan et al. 1986). In *Cryptodromia pileifera*, however, the zoea is still able to swim and move around in

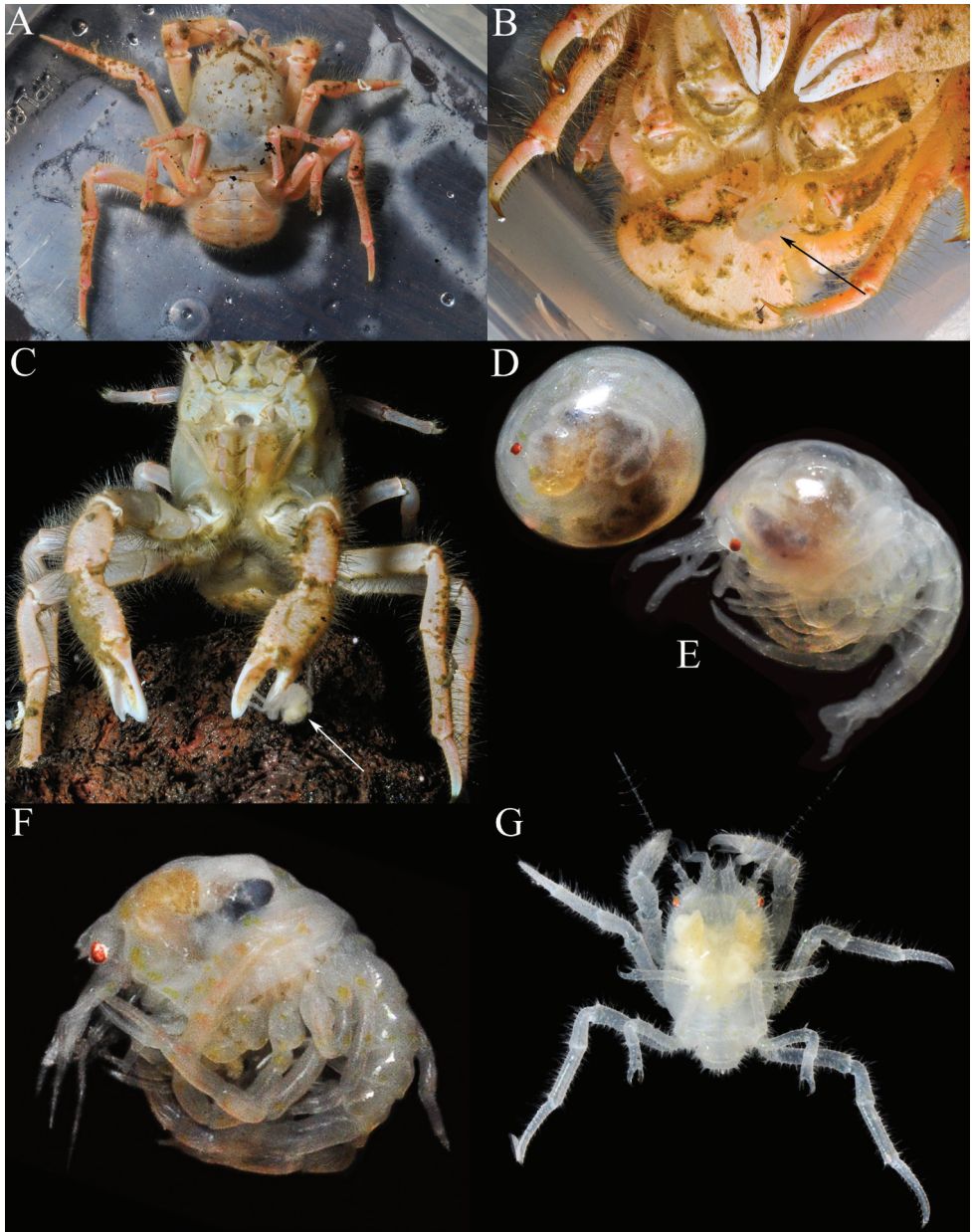


Figure 1. *Dicranodromia doederleini* Ortmann, 1892, ♀ (15.9 × 20.2 mm) (ZRC 2017.1214), Japan **A** colour in life (26 April 2015) **B** ventral surface showing megalopa (arrow) (26 April 2015) **C** frontal view showing megalopa crawling on chela (arrow) and larvae under pleon (24 April 2015) **D** fresh eyed egg (not preserved, 18 April 2015) **E** first zoea (not preserved, 18 April 2015) **F** freshly hatched megalopa (not preserved, 18 April 2015) **G** dorsal view of free moving megalops (26 April 2015). Photographs: PYC Ng.

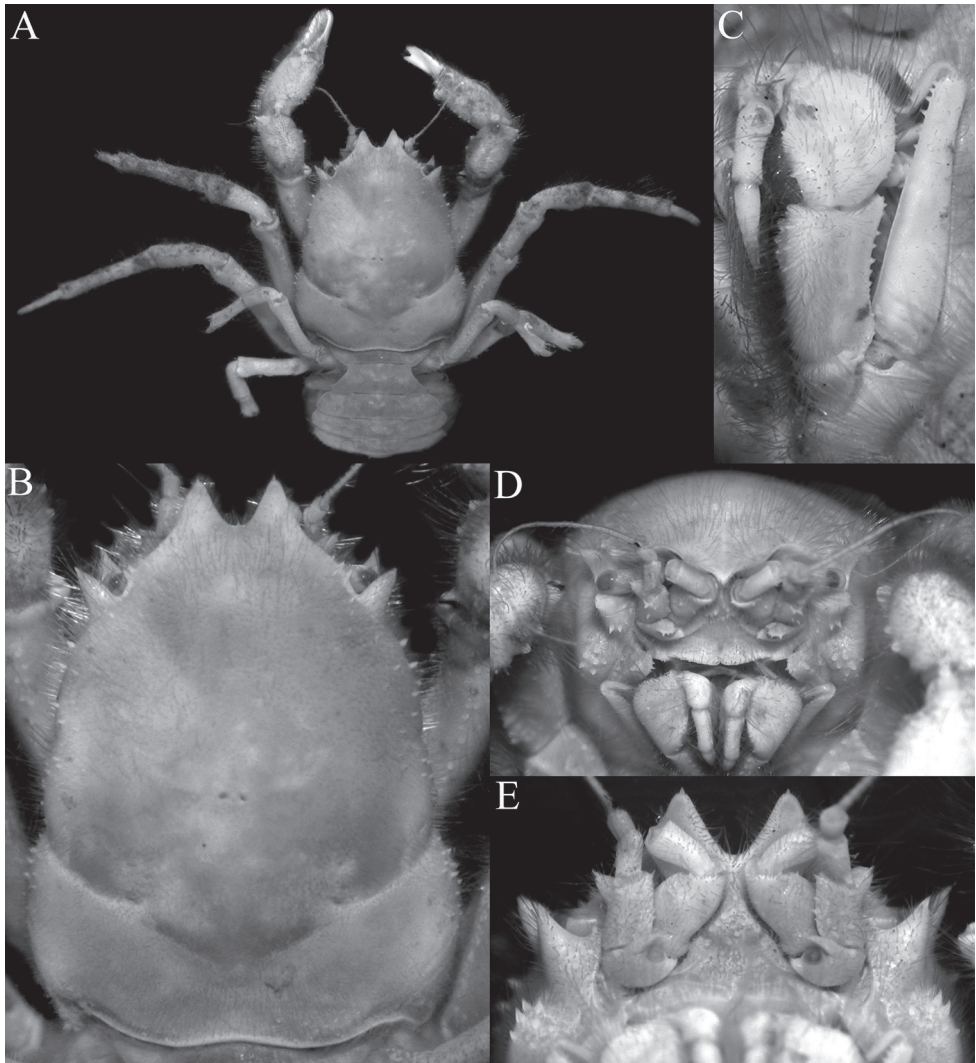


Figure 2. *Dicranodromia doederleini* Ortmann, 1892, ovigerous ♀ (14.5 × 19.2 mm) (ZRC 2021.0469), Japan **A** overall view **B** dorsal view of carapace **C** left third maxilliped **D** frontal view of cephalothorax **E** epistome, antennules, antennae and orbits.

the water column although it only lasts two days before metamorphosing. For the specimen of *D. doederleini* that was kept in the aquarium, it would appear that if it was natural, the young would develop into an advanced zoeal stage while still inside the egg membrane, and break free only after it metamorphoses into the megalopa. The transition between the “first zoea” and megalopa, however, is clearly very short, perhaps a day or less. The condition for *Dicranodromia* is thus probably similar to that

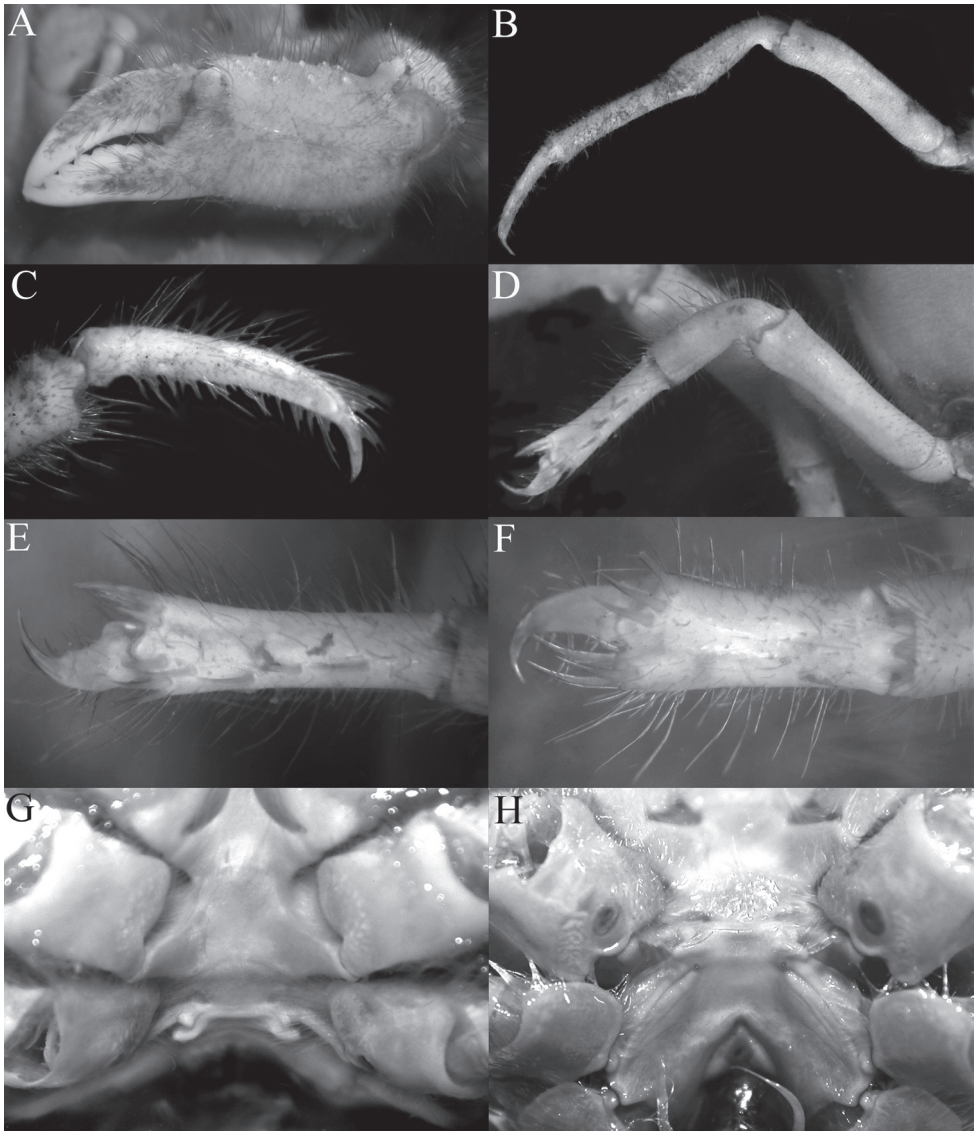


Figure 3. *Dicranodromia doederleini* Ortmann, 1892, ovigerous ♀ (14.5 × 19.2 mm) (ZRC 2021.0469), Japan **A** left chela **B** left P3 **C** right P3 dactylus **D** left P5 **E** left P5 propodus and dactylus **F** left P4 propodus and dactylus **G** anterior thoracic sternum and spermatheca **H** posterior thoracic sternum showing spermatheca and female gonopores.

of eubrachyuran marine crabs, some other podotreme crabs and various enbrachyurans like the epialtids *Paranaxia serpulifera* (Guérin, 1832) and *P. keesingi* Hosie & Hara, 2016 (Rathbun 1914, 1924; Morgan 1987; Hosie and Hara 2016), and the pilumnids *Pilumnus novaezealandiae* Filhol, 1885 and *P. lumpinus* Bennett, 1964 (cf. Wear 1967); taxa which undergo direct development.

***Dicranodromia martini* Guinot, 1995**

Figures 4–6, 11A–C

Dicranodromia martini Guinot, 1995: 221, figs 19a–e, 20A–C; Ng and Naruse 2007: 48, figs 1, 3a, b, 4; Ng et al. 2008: 39, fig. 11.

Material examined. PHILIPPINES: 1 ♂ (12.3 × 16.6 mm), station CP2396, 9°36.3'N, 123°42.0'E, Maribohoc Bay, Panglao, Bohol, Visayas, 609–673 m, PANGLAO 2005

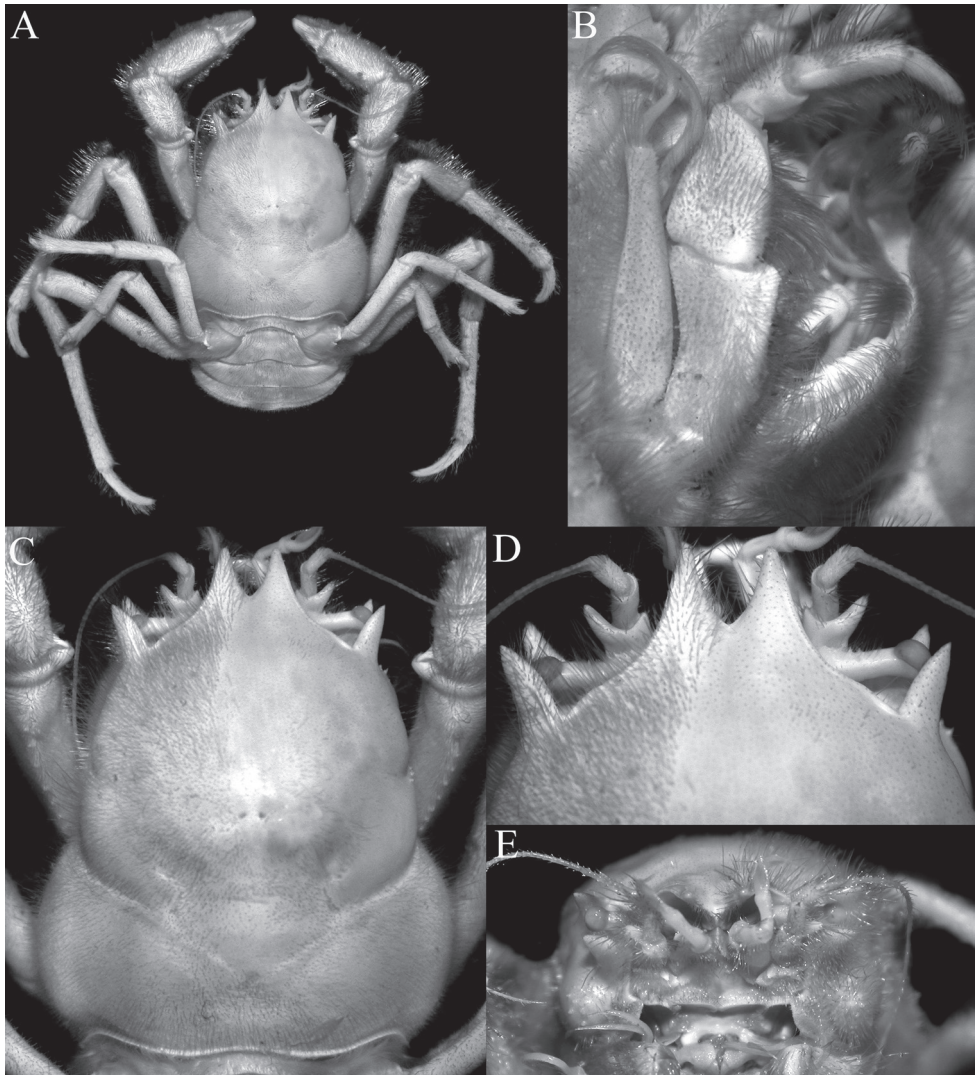


Figure 4. *Dicranodromia martini* Guinot, 1995, ♀ (28.1 v 34.2 mm) (ZRC 2007.0106), Philippines **A** overall view **B** right third maxilliped **C** dorsal view of carapace **D** anterior part of carapace (right side denuded) **E** frontal view of cephalothorax.

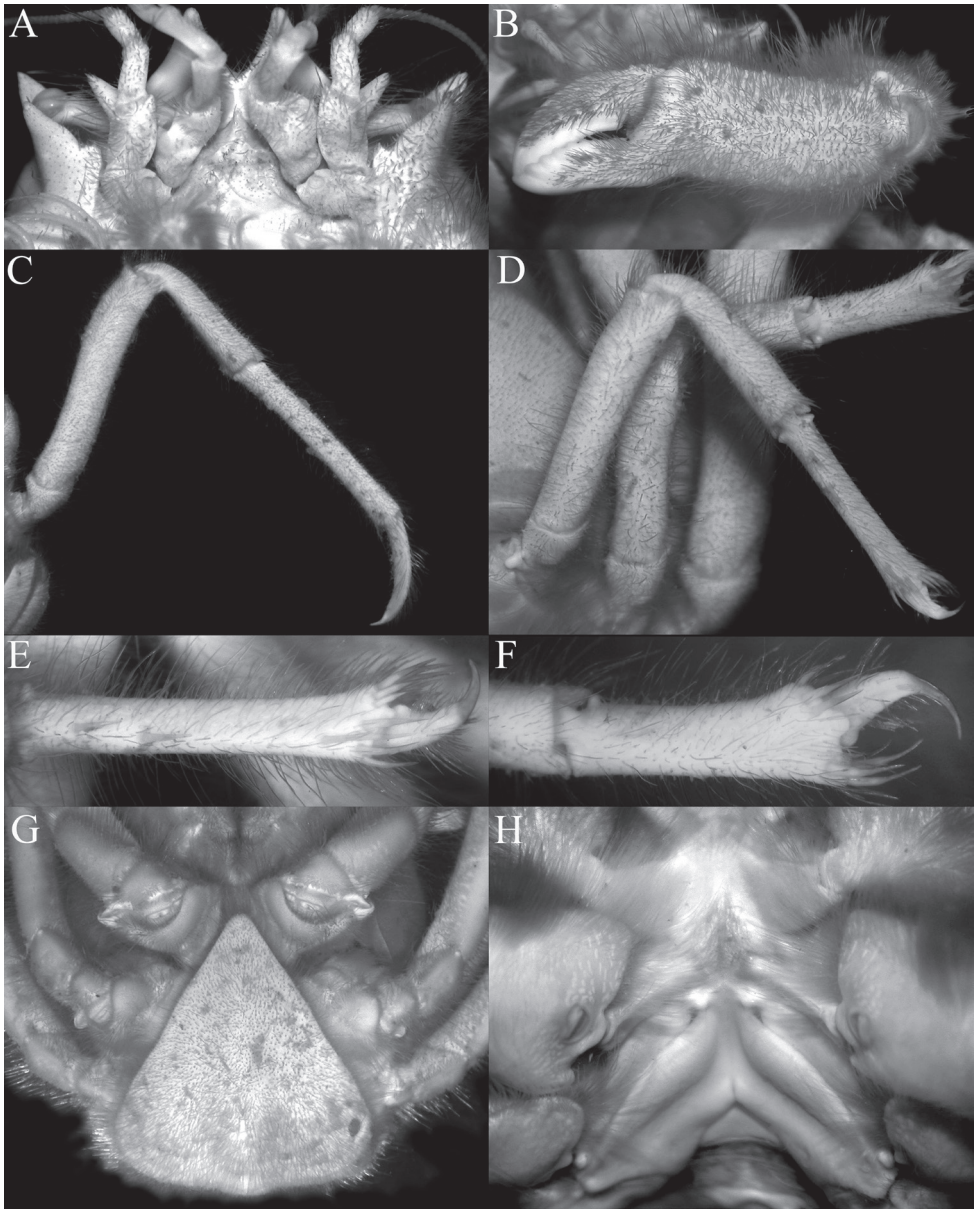


Figure 5. *Dicranodromia martini* Guinot, 1995, ♀ (28.1 × 34.2 mm) (ZRC 2007.0106), Philippines **A** epistome, antennules, antennae and orbits **B** left chela **C** right P3 **D** right P5 **E** right P5 dactylus **F** right P4 **G** telson **H** posterior thoracic sternum showing spermatheca and female gonopores.

Expedition, coll. MV DA-BFAR, 31 May 2005 (ZRC 2007.0105); 1 ♀ (28.1 × 34.2 mm), station CP2363, 9°06.0'N, 123°25.0'E, Bohol and Sulu Seas, 437–439 m, PANGLAO 2005 Expedition, coll. MV DA-BFAR, 26 May 2005 (ZRC 2007.0106, COI sequence: OK331337).



Figure 6. *Dicranodromia martini* Guinot, 1995, ♂ (12.3 × 16.6 mm) (ZRC 2007.0105), Philippines **A** overall view **B** dorsal view of carapace **C** anterior part of carapace (partially denuded) **D** male telson.

Remarks. Ng and Naruse (2007: 49) commented that the largest female they examined (28.1 × 34.2 mm, ZRC 2007.0106) has the carapace relatively more inflated with the posterolateral margin distinctly convex and the external orbital tooth more anteriorly directed when compared to smaller males. In addition, this female specimen is also relatively more hirsute (Fig. 4A, C, D versus Fig. 6A–C). We see a similar pattern of variation in *D. erinaceus* sp. nov., where the smaller males are less swollen and with less setae overall when compared to larger females (Fig. 16A, B versus Fig. 13A, B). In *D. karubar*, the exorbital tooth varies in the angle its directed outwards (Figs 8B, C, 10B). As such, the differences observed for the specimens of *D. martini* examined here are regarded as intraspecific and/or size related.

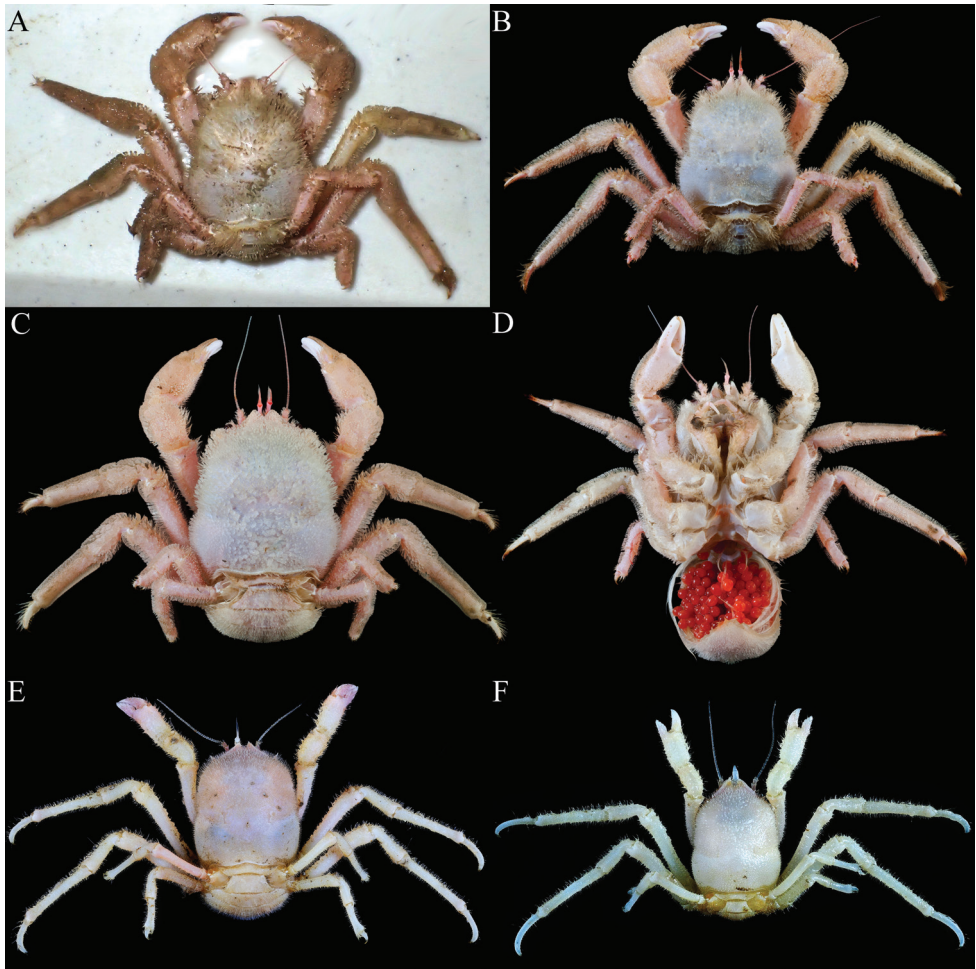


Figure 7. Colour in life. **A,B** *Dicranodromia karubar* Guinot, 1993, ♂ (28.7 × 34.7 mm) (ZRC 2020.0348), Java **C** *D. karubar* Guinot, 1993, ovigerous ♀ (30.1 × 35.5 mm) (ZRC 2020.0349), Java **D** *D. karubar* Guinot, 1993, ovigerous ♀ (24.8 × 31.5 mm) (ZRC 2020.0348), Java **E** *D. erinaceus* sp. nov., holotype ♀ (14.0 × 18.0 mm) (NTOU B00126), Taiwan **F** *D. erinaceus* sp. nov., paratype ♂ (6.9 × 9.5 mm) (ZRC 2021.0084), Taiwan. Photographs: T.-Y. Chan.

Dicranodromia karubar Guinot, 1993

Figures 8–10, 11D–F

Dicranodromia karubar Guinot, 1993: 213, figs 15A–C, 16A–D, 25A, B; Ng et al. 2008: 39; Mendoza et al. 2021: 284, fig. 1A, B.

Material examined. INDONESIA: 1 ♂ (28.7 × 34.7 mm), 3 ovigerous ♀♀ (24.8 × 31.5 mm, 27.1 × 33.4 mm, 27.6 × 33.8 mm), station CP39, 8°15.885'S, 109°10.163'E – 8°16.060'S, 109°10.944'E, 528–637 m, substrate partially muddy, plenty of glass sponges,

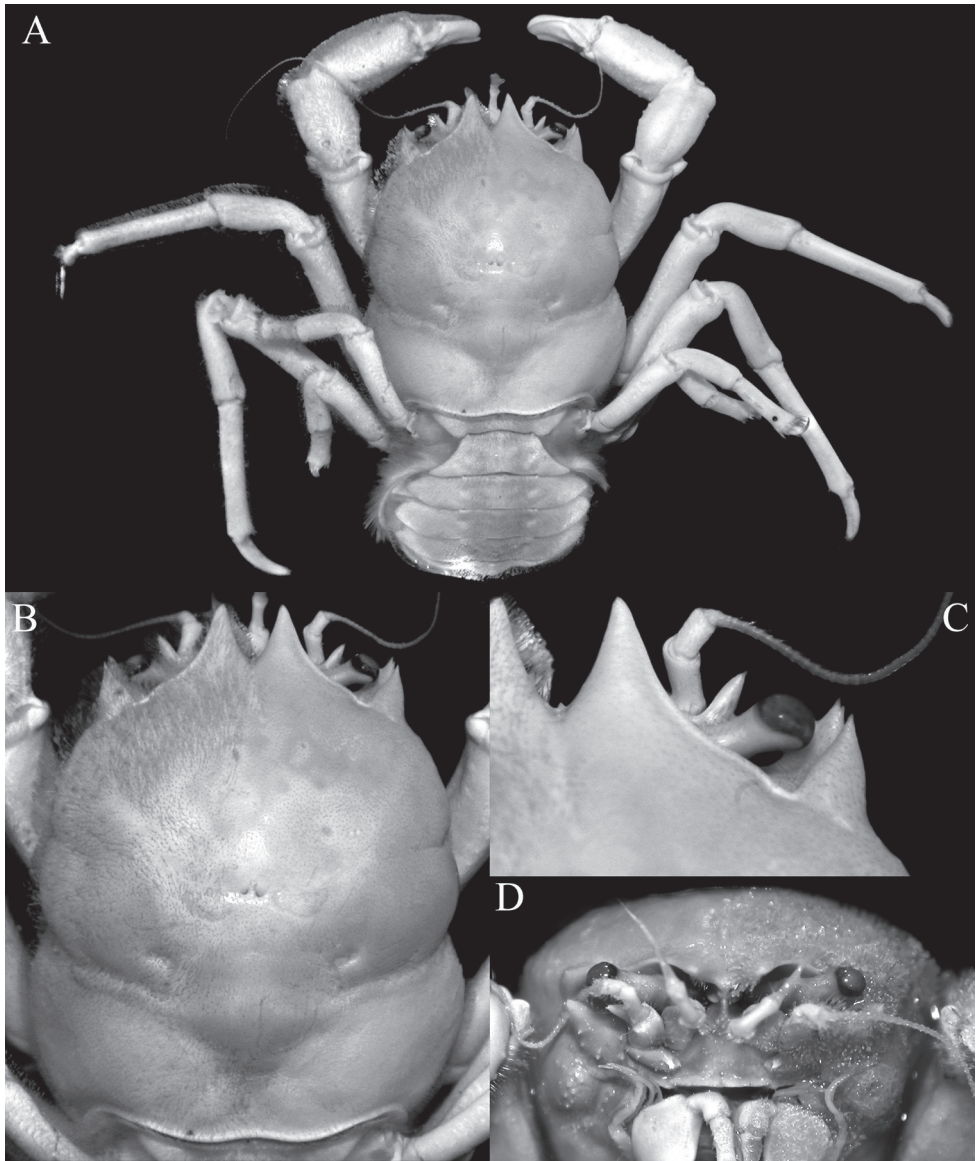


Figure 8. *Dicranodromia karubar* Guinot, 1993, ♀ (27.1 × 33.4 mm) (ZRC 2020.0348), Java **A** overall view **B** dorsal view of carapace **C** anterior right part of carapace (denuded) **D** frontal view of cephalothorax.

echinoderms, polychaeta, galatheids, fishes, sea anemone, gastropods and bivalves, south of Cilacap, south Java, Indian Ocean, South Java Deep Sea cruise, coll. beam trawl, 30 Mar. 2020 (ZRC 2020.0348); 1 ovigerous ♀ (30.1 × 35.5 mm), station CP51, 7°04.874'S, 106°25.396'E – 7°05.348'S, 106°25.044'E, 569–657 m, substrate coarse sand, mud and some plastic trash, small crabs, ophiuroids, stalk crinoids, chitons, limpets and sea daisies on fallen bamboo, Pelabuhanratu Bay, south Java, Indian Ocean, South Java Deep Sea cruise, coll. beam trawl, 2 Apr. 2020 (ZRC 2020.0349, COI sequence: OK331336).

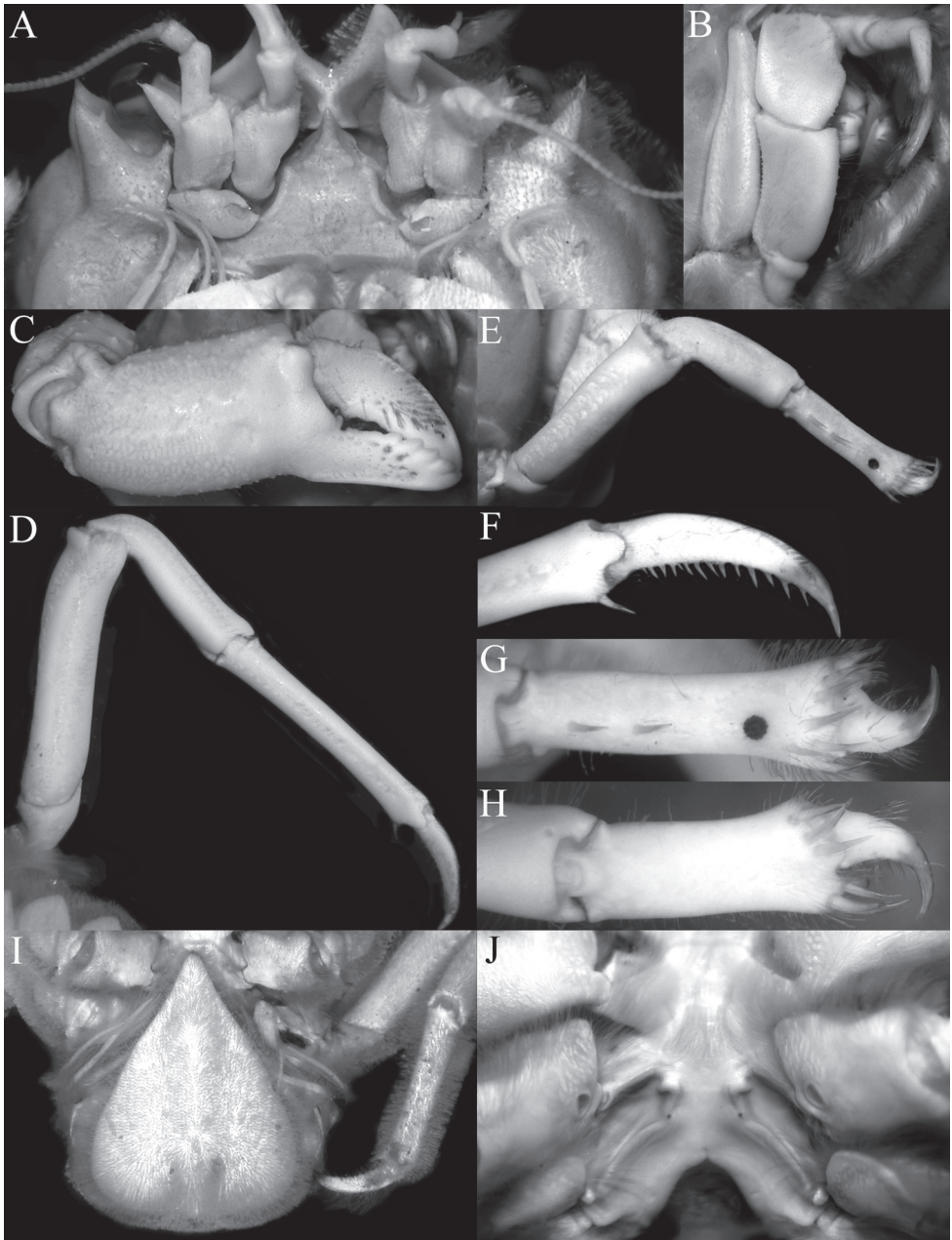


Figure 9. *Dicranodromia karubar* Guinot, 1993. **A–H, J** ♀ (27.1 × 33.4 mm) (ZRC 2020.0348), Java **I** ♀ (27.6 × 33.8 mm) (ZRC 2020.0348), Java **A** epistome, antennules, antennae and orbits **B** left third maxilliped **C** right chela (denuded) **D** right P3 (denuded) **E** right P3 dactylus (denuded) **F** right P5 (denuded) **G** right P5 propodus and dactylus (partially denuded) **H** right P4 propodus and dactylus (partially denuded) **I** telson **J** posterior thoracic sternum showing spermatheca and female gonopores.



Figure 10. *Dicranodromia karubar* Guinot, 1993. **A–C** ♂ (28.7 × 34.7 mm) (ZRC 2020.0348), Java **D** ♀ (27.6 × 33.8 mm) (ZRC 2020.0348), Java **A** overall view **B** dorsal view of carapace **C** telson **D** left P5 propodus and dactylus.

Remarks. Mendoza et al. (2021) recently recorded *D. karubar* from southern Java, over 1000 km from its type locality in the Moluccas. The specimens, however, agree very well with the descriptions and figures of Guinot (1995) and they are clearly conspecific.

Guinot (1995: 215) noted that the rostrum of this species is at most a tubercle, which is in conformity with the present material. The merus, carpus and dactylus were

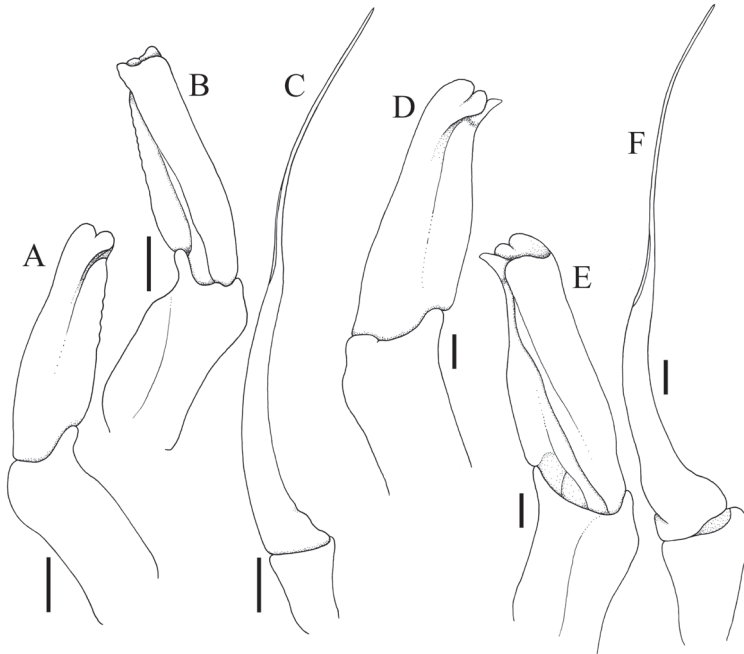


Figure 11. **A–C** *Dicranodromia martini* Guinot, 1995, ♂ (12.3 × 16.6 mm) (ZRC 2007.0105), Philippines **D–F** *D. karubar* Guinot, 1993, ♂ (28.7 × 34.7 mm) (ZRC 2020.0348), Java **A, D** left G1 (ventral view) **B, E** left G1 (dorsal view) **C, F** left G2. Setae for all structures not figured. Scale bars: 1.0 mm.

described as unarmed by Guinot (1995), but the P5 propodus actually has one or two spines on the outer surface, which are hard to see as the dense plumose setae obscure them. In some specimens, the P5 dactylus has a prominent spine on the extensor margin (Fig. 10D), but as reported by Ng and Naruse (2007), it is absent in others (Fig. 9G, H). The form of the exorbital tooth varies to some degree. In the female specimens, the tooth is clearly directed anteriorly (Fig. 8B, C) but in the male, it is pointed obliquely laterally (Fig. 10B).

The setae on *D. karubar* are unusual in that they are plumose at the distal part (Guinot 1995: fig. 16D). When the animals are freshly collected, the setae lock together to form a dense coat, which traps fine mud and completely obscures the carapace and pereopod surfaces and margins (Fig. 7A). After the specimen is cleaned gently with a brush and the sediment removed, the surfaces and margins become more visible with the distal plumose parts no longer meshed together. The margins of the pereopods, however, are still partially obscured as the setae there are denser (Fig. 7B, C). In the form of the setae, *D. karubar* is most similar to *D. baffini* from the Indian Ocean, although the tomentum of the latter species is relatively less dense (cf. Padate et al. 2020: fig. 2a).

Dicranodromia karubar can easily be separated from *D. baffini* by its proportionately broader carapace (Figs 8B, 10B) (versus relatively narrower and longer in *D. baffini*; cf. Guinot 1995: fig. 13, Padate et al. 2020: fig. 2a); the antero- and posterolateral

margins almost smooth, except sometimes for a few scattered granules (Figs 8B, 10B) (versus lined with granules and spinules in *D. baffini*; cf. Guinot 1995: fig. 13, Padate et al. 2020: fig. 2a); and the subdistal lobe on the outer margin of the endopod curved and beak-like (Fig. 11D, E) (versus lobe rounded in *D. baffini*; cf. Padate et al. 2020: fig. 2g, i). Based on the figures of Gordon (1950), Guinot (1995: fig. 16C) commented that the structure of the spermatheca was different in the two species, but we do not discern any major differences since both species possess an unusual and prominent comma-shaped tubercle on each side of sternite 7, with the spermatheca at the base of this tubercle (Fig. 9J). The spermathecal structure in the *D. baffini* from the Andamans (cf. Padate et al. 2020: fig. 2j) is almost identical to the condition observed in *D. karubar* (Fig. 9J). Alcock and Anderson (1899: 8) described the structure as “sternal grooves of the female end, without tubercles, at the level of the openings of the oviducts”, which does not match the description and figures of Gordon (1950: 205, text-fig. 1) and Padate et al. (2020: fig. 2j). As noted by Padate et al. (2020: 3), the condition observed by Alcock and Anderson (1899) may be because their specimen was a juvenile.

Dicranodromia karubar is known thus far only from the Moluccas and eastern part of the Indian Ocean while *D. baffini* has been recorded from western India, Maldives and Andamans (Alcock 1899, 1901; Gordon 1950; Padate et al. 2020).

All the females of *D. karubar* collected from the south Javan cruise were ovigerous, the eggs being bright red in life, in a prominent brood pouch (Fig. 7D). One female specimen (27.6 × 33.8 mm, ZRC 2020.0348) had 362 eggs, each about 2.5 mm in diameter.

Dicranodromia danielae Ng & McLay, 2005

Figure 12

Dicranodromia danielae Ng & McLay, 2005: 40, figs 1–4; Ng and Naruse 2007: 47, fig. 3c; Ng et al. 2008: 39.

Material examined. PHILIPPINES: holotype ovigerous ♀ (broken, 10.8 × 14.2 mm), Balicasag Island, Panglao, Bohol, Visayas, in tangle nets, ca. 200–300 m, coll. local shell fishermen, 2 Mar. 2004 (ZRC 2005.0094).

Remarks. The broken holotype female was re-examined and some characters need to be added or amended from Ng and McLay (2005). Ng and Naruse (2007: fig. 3c) had already noted that the P5 dactylus has a distinct spine on the extensor margin (Fig. 12F, G); but in addition, the P5 propodus has three spines on the outer surface (Fig. 12G). The P2 and P3 meri were described being unarmed but this is not correct. The extensor margin has low spines while the flexor margin has a row of slender spines partially covered by the dense stiff setae (Fig. 12D). In addition, the basal antennal article is relatively short with the anteroexternal tooth long and subequal in length to the article (Fig. 12C). In addition, the epistome of this species is unusual in that the distal part is strongly spinose, with the median lateral part possessing a sharp anteriorly directed tooth; and the rostrum consists of two lateral

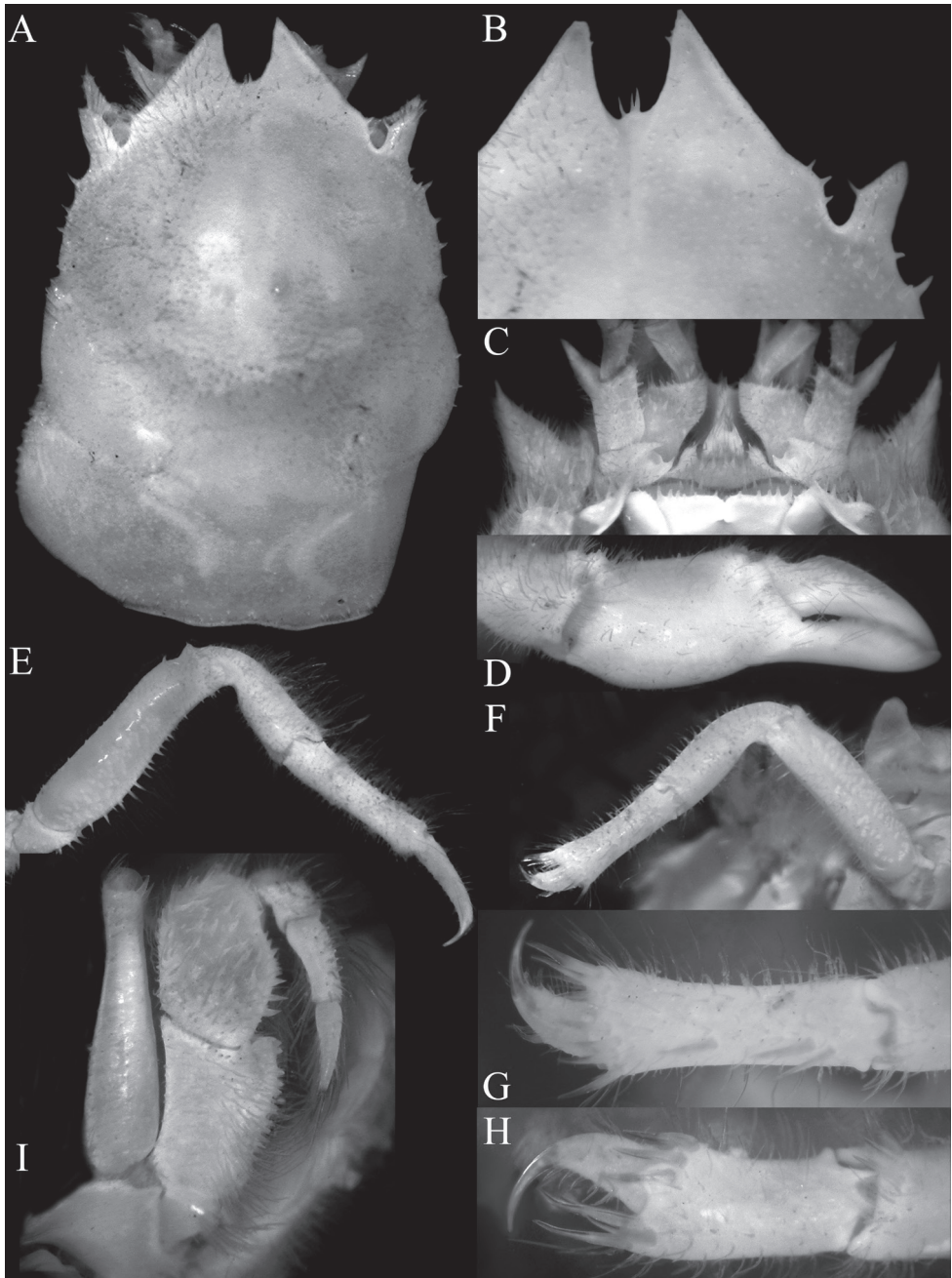


Figure 12. *Dicranodromia danielae* Ng & McLay, 2005, holotype ovigerous ♀ (broken, 10.8 × 14.2 mm) (ZRC 2005.0094), Philippines **A** dorsal view of carapace **B** frontal region showing rostrum **C** epistome, antennules, antennae and orbits **D** right chela **E** right P3 **F** left P5 **G** left P5 propodus and dactylus **H** left P4 propodus and dactylus **I** right third maxilliped.

and one median slender spinules (Fig. 12B, C). The merus of the third maxilliped is distinctive, being strongly spinose, with the inner margin lined with strong spines; the exopod is essentially unarmed (Fig. 12I).

Some of the characters of *D. danielae* resemble the male specimen 9.7×14.0 mm from Uraga Strait in Japan ($35^{\circ}4.833'N$, $139^{\circ}38.3'E$) which Guinot (1995: 207, fig. 11b) referred to "*Dicranodromia* aff. *doederleini*". She described the carapace, proepistome, antennae, antennules, buccal frame, ventral surfaces and merus of the third maxilliped are being more spiny than typical *D. doederleini* even though the outer surface of the chela was smooth. The more spinous features of the specimen (notably the ventral surfaces, antennae, epistome and third maxillipeds), resemble the condition in *D. danielae*, but whether the flexor margin of the pereopods of the specimen was also spinous was not stated. In addition, the carapace of *D. danielae* is less spinous compared to that figured by Guinot (1995: fig. 11b) for her "*Dicranodromia* aff. *doederleini*". It would appear that this Japanese specimen is a species close to, but probably different from, *D. danielae*.

***Dicranodromia erinaceus* sp. nov.**

<http://zoobank.org/C1BEA5CC-F350-47D1-8A66-ECBFC3606197>

Figures 7E, F, 13–16, 21A, B, D–F, K–M

Dicranodromia doederleini – Ho et al. 2004: 643, fig. 1B; Ah Yong et al. 2009: 129, fig. 93 (not fig. 94); Ng et al. 2017: 27 (list). (non *Dicranodromia doederleini* Ortman, 1892)

Material examined. TAIWAN: holotype ♀ (14.0×18.0 mm), station CP4091, $22^{\circ}14'N$, $119^{\circ}59'E$, among numerous mud tubes, off small Liu-Qiu Island, south-east Taiwan, 974–994 m, coll. N.O. Ocean Researcher 1, 27 May 2013 (NTOU B00126); paratypes 2 ♀♀ (13.2×17.6 mm, 13.8×18.5 mm), same data as holotype (ZRC 2020.0467, COI sequence: OK351335); 1 ♂ (6.9×9.5 mm), station CP4212, $22^{\circ}18.34'N$, $119^{\circ}59.51'E$, southwestern Taiwan, 961–1008 m, coll. T.-Y. Chan, 15 Nov. 2020 (ZRC 2021.0084, COI sequence: OK331334); 1 ♂ (8.2×12.5 mm), station CP4212, $22^{\circ}18.34'N$, $119^{\circ}59.51'E$, southwestern Taiwan, 961–1008 m, coll. T.-Y. Chan, 15 Nov. 2020 (ZRC 2021.0085). Others: 1 ♀ (7.5×11.1 mm, carapace badly damaged), $24^{\circ}26.9'N$, $122^{\circ}18.1'E$, Taiwan, 638–824 m, coll. R/V "Fishery Researcher 1", 4 August 2000 (NTOU B00127).

Diagnosis. Carapace longitudinally subovate, widest across intestinal-mesobranchial regions; dorsal surface prominently convex, lateral surfaces covered with numerous spinules, those on median part relatively lower, sometimes granular, with short stiff setae, denser on lateral parts but not obscuring margins; short stiff setae present on pereopods, thoracic sternum and pleon but not obscuring surface or margins.

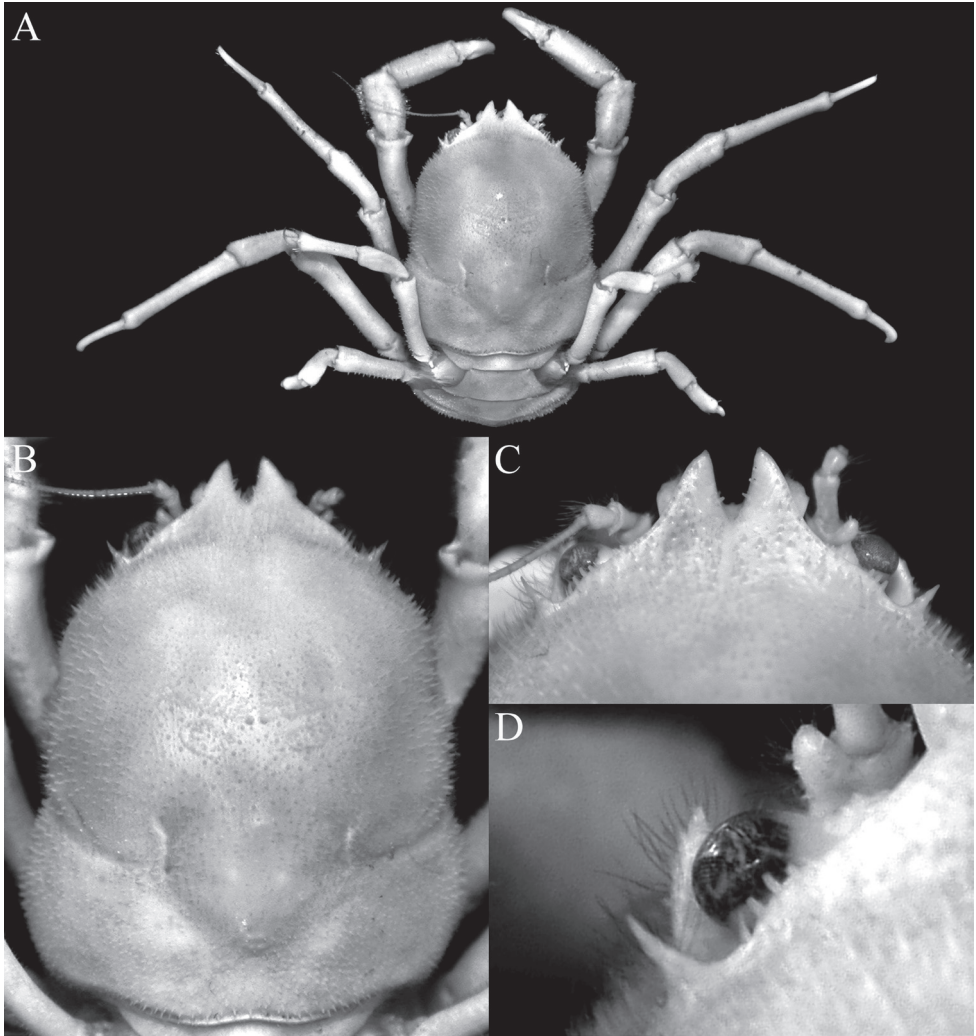


Figure 13. *Dicranodromia erinaceus* sp. nov., holotype ♀ (14.0 × 18.0 mm) (NTOU B00126), Taiwan **A** overall view **B** dorsal view of carapace **C** front and anterior part of carapace **D** left orbit and first anterolateral spine.

Branchiocardiac groove distinct, curving medially anteriorly. Each pseudorostral lobe triangular, inner margin straight, outer margin gently convex, directed anteriorly, inner margin with two or three spinules; exorbital tooth spiniform, directed obliquely laterally, anterior margin with two or three spinules; supraorbital margin separated from external orbital tooth by shallow concave cleft, posterior part with three spines; infraorbital margin with prominent triangular lobe, posterior margin with spinules, just visible in dorsal view. Rostrum present as one or two longer spinules in small specimens, barely discernible or just visible as a sharp granule in larger specimens. Epistome covered with spinules on anterior half; posterior half gently upturned, with

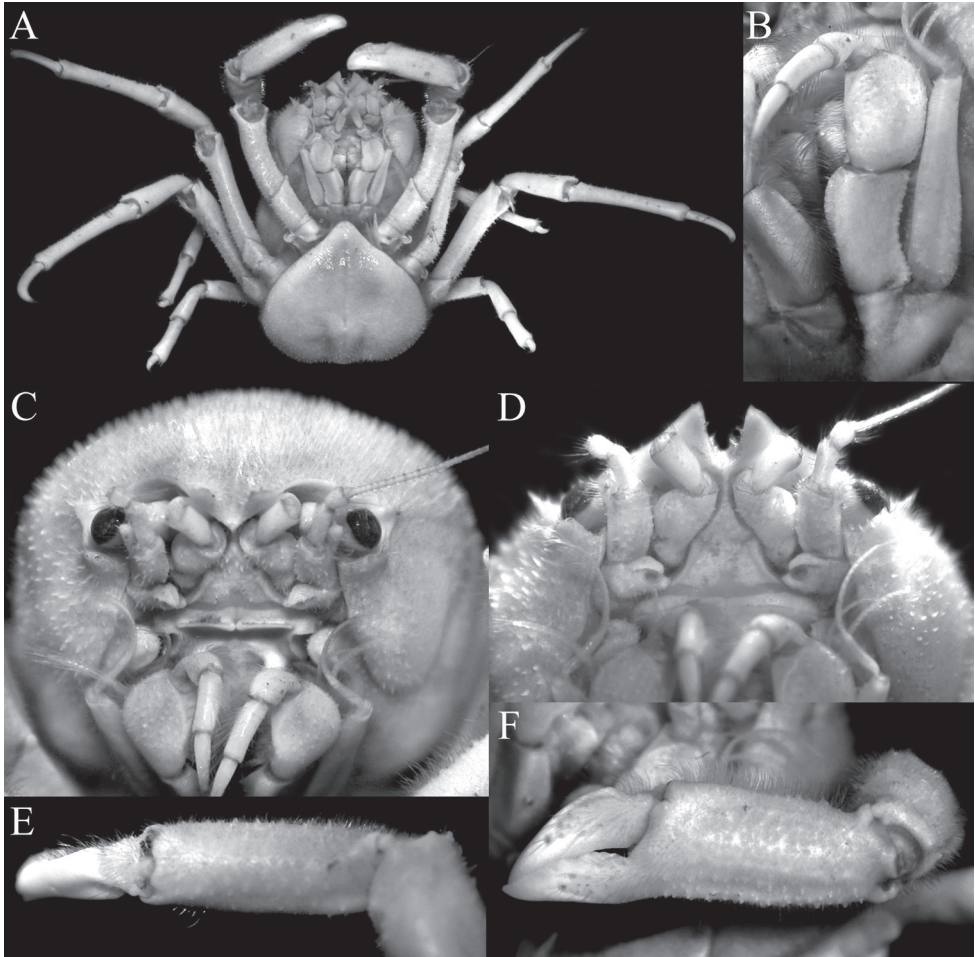


Figure 14. *Dicranodromia erinaceus* sp. nov., holotype ♀ (14.0 × 18.0 mm) (NTOU B00126), Taiwan **A** ventral view of cephalothorax **B** left third maxilliped **C** frontal view of cephalothorax **D** epistome, antennules, antennae and orbits **E** dorsal view of right chela **F** left chela.

median fissure, surface not covered with spinules, posterior margin entire. Basal antennal article subquadrate; surfaces covered by spinules and granules; anteroexternal tooth short. Eyes with short peduncle. Third maxilliped relatively narrow; merus subovate with low anterointernal lobe, slightly shorter than ischium; ischium subtrapezoidal, distal half wider than proximal part with inner margin convex; palp (carpus, propodus, dactylus) long, reaching to median part of ischium when folded; exopod with proximal third widest, outer margin with low sharp granules on proximal third. Chelipeds densely covered with stiff setae on most parts; merus and carpus with outer surface and margins lined with spinules and granules; palm relatively short, outer surface and margins covered with numerous sharp granules; fingers thick, wide, occluding surface hollowed; pollex with deep U-shaped depression distally. P2 and P3

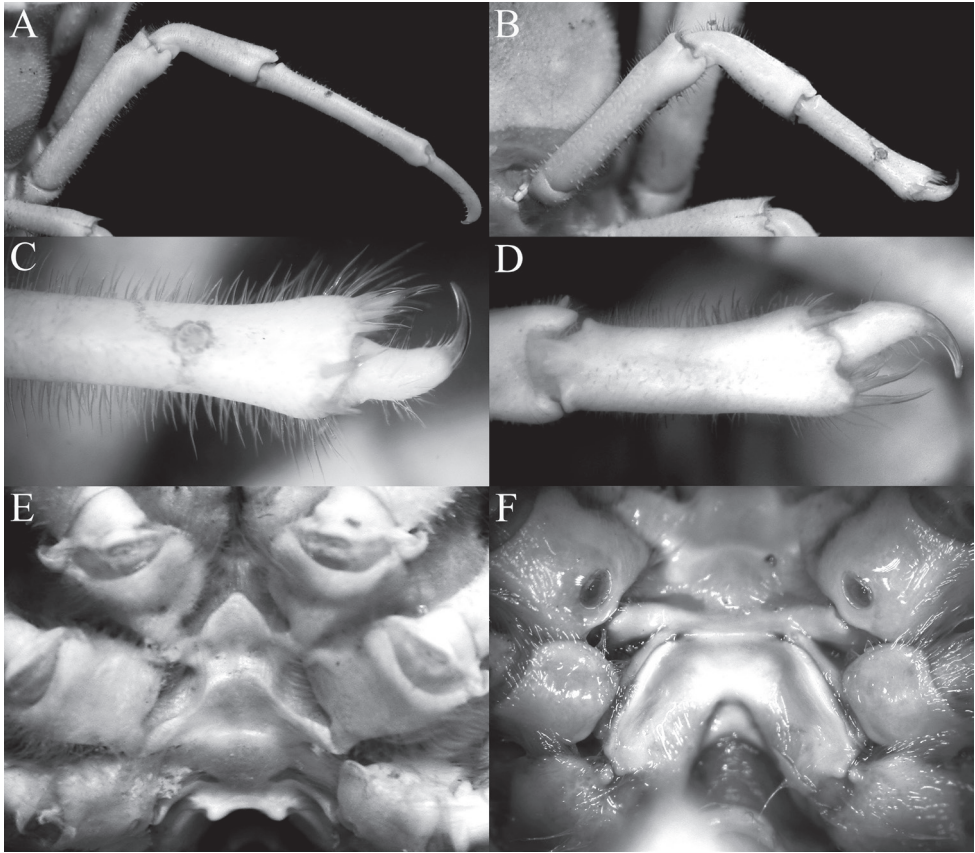


Figure 15. *Dicranodromia erinaceus* sp. nov. **A–E** holotype ♀ (14.0 × 18.0 mm) (NTOU B00126), Taiwan **F** paratype ♀ (13.8 × 18.5 mm) (ZRC 2020.0467), Taiwan **A** right P3 **B** right P5 **C** right P5 propodus and dactylus **D** right P4 propodus and dactylus **E** anterior thoracic sternum and spermatheca **F** posterior thoracic sternum showing spermatheca and female gonopores.

relatively long, P3 longer than P2; merus with low tooth on distal extensor margin, length to width ratio of P2 and P3 merus 5.2 and 4.5, respectively; proximal part of extensor margin with low spinules, flexor margin with numerous spinules; propodus almost straight, unarmed, length to width ratio of P2 and P3 propodus 6.7 and 8.0, respectively; dactylus sickle-shaped, flexor margin lined with 15 or 16 spines, terminating in strongly incurved claw, propodus about twice length of dactylus. P4 stouter, shorter than P5; length to width ratio of P4 and P5 merus 3.5 and 5.0, respectively; proximal part of extensor margin of merus with low spinules, flexor margin with numerous spinules; P4 and P5 propodus without median spinules on outer surface, length to width ratio of P4 and P5 propodus 3.5 and 4.7, respectively, distal margin fringed by sharp spines bracketing dactylus; dactylus claw-like, strongly incurved, extensor margin unarmed, flexor margin unarmed or with two weak spines. Thoracic sternite 7 with strong transverse ridge from posterior inner part of female gonopore,

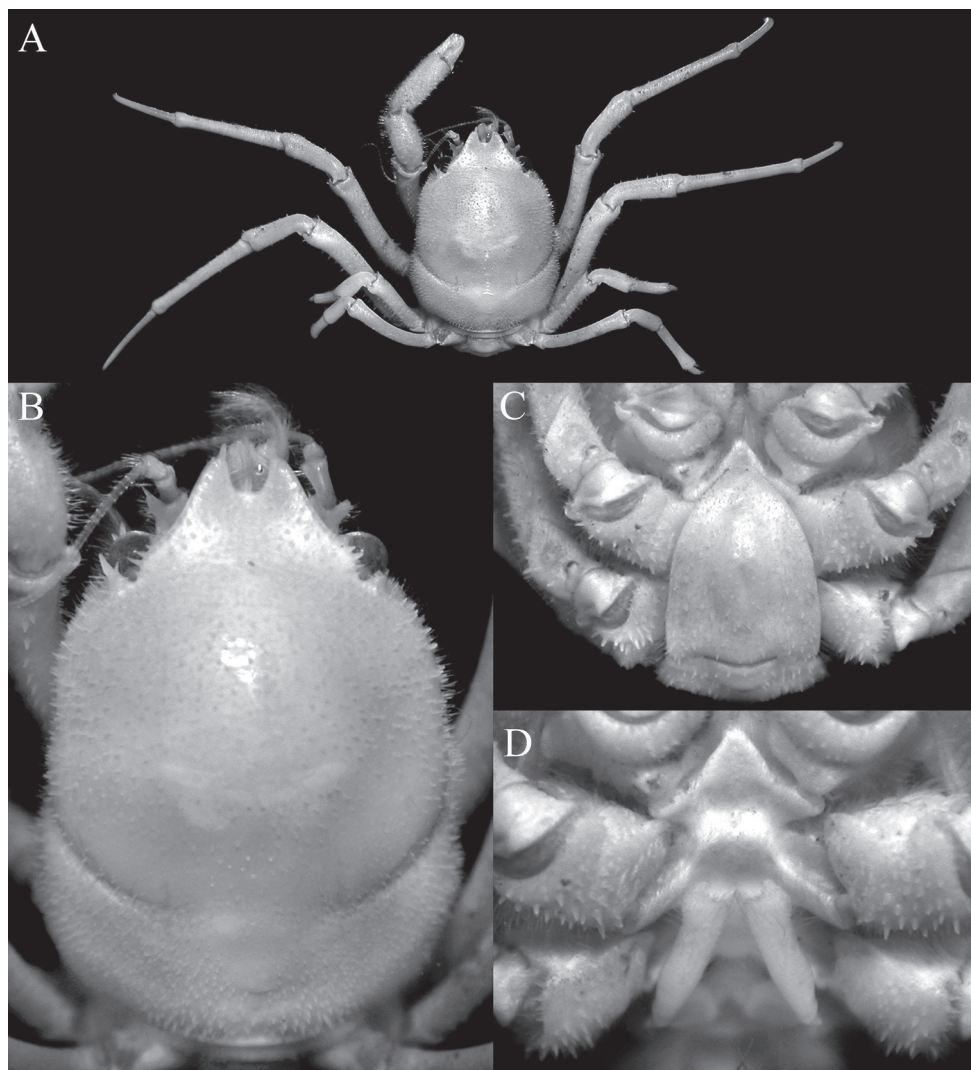


Figure 16. *Dicranodromia erinaceus* sp. nov., paratype ♂ (8.2 × 12.5 mm) (ZRC 2021.0085), Taiwan **A** overall view **B** dorsal view of carapace **C** pleon **D** anterior thoracic sternum and G1s in situ.

lateral part raised, forming triangular tubercle, curving posteriorly to join oblique ridge formed by sternites 7 and 8 with distinct groove between them that leads to spermathecal aperture at centre of triangular tubercle. Male and female pleons with six free somites and telson; male telson distinctly subovate; female telson wide, triangular, with gently sinuous margins. G1 stout, endopod distally covered by dense long setae, subdistal part of outer margin with two lobes, proximal lobe larger, prominent; G2 endopod gradually tapering to sharp tip.

Variation. None of the specimens examined had a spine or spinule on the extensor margin of the P5 dactylus; and outer surface of the P5 propodus was also unarmed

(Fig. 21E). Most of the flexor margins of the dactylus were not armed with obvious spines or spinules, although two or three stout setae may be present.

Etymology. The species is named after the hedgehog, *Erinaceus*, alluding to the spiny appearance of the carapace and legs. The name is used as a noun in apposition.

Remarks. *Dicranodromia erinaceus* sp. nov. belongs to the same group of species as *D. spinulosa* and *D. delli* in its spinose carapace surface and pereopods, slender and spiniform exorbital tooth, and an acutely triangular suborbital tooth. *Dicranodromia erinaceus* is most similar to *D. delli* from New Zealand but can be distinguished by the ischium of the third maxilliped being relatively shorter and wider especially at the distal half (Fig. 14B) (versus more slender and rectangular in *D. delli*, cf. Ah Yong 2008: fig. 4C); proportionately shorter P2 and P3 (e.g., P3 merus 4.5× longer than wide, propodus 8.0× longer than wide, Figs 13A, 15A) (versus P3 merus 6.6× longer than wide, propodus 11.1× longer than wide in *D. delli*, cf. Ah Yong 2008: fig. 2A, 3D); the proportionately shorter and stouter P4 and P5 (e.g., P5 merus just reaches the branchiocardiac groove in dorsal position, Figs 13A, 15B) (versus longer and more slender, extending beyond branchiocardiac groove in dorsal position in *D. delli*, cf. Ah Yong 2008: fig. 2A, B); the relatively stouter palm (Fig. 14F) (versus more slender in *D. delli*, cf. Ah Yong 2008: fig. 3B); and the proportionately wider female telson (Fig. 14A) (versus less wide in *D. delli*, cf. Ah Yong 2008: fig. 3C). The holotype and only known specimen of *D. delli*, an ovigerous female 15.5 × 19.0 mm from Nukuliau Seamount in New Zealand, is comparable in size to the ovigerous female holotype of *D. erinaceus* (14.0 × 18.0 mm) so the differences are not size-related. The characters of P2–P5 and third maxilliped are also obvious in the smaller female paratype of *D. erinaceus* as well as in the smaller male paratypes.

Compared to *D. spinulosa*, *D. erinaceus* can be separated by the carapace being proportionately wider (Figs 13B, 16B) (versus carapace transversely narrower in *D. spinulosa*, cf. Guinot 1995: fig. 21a; Ah Yong 2008: fig. 1C); the median dorsal surface of the carapace covered with low sharp granules (Figs 13B, 16B) (versus covered with spinules in *D. spinulosa*, cf. Guinot 1995: fig. 21a; Ah Yong 2008: fig. 1C); the submarginal surface of the posterior margin of the epistome is unarmed (Fig. 14C, D) (versus area armed with short spines in *D. spinulosa*, cf. Guinot 1995: fig. 22B); the ischium of the third maxilliped relatively shorter and wider especially at the distal half (Fig. 14B) (versus more slender and rectangular in *D. spinulata*, cf. Guinot 1995: fig. 21c); the relatively longer P2 and P3 (e.g., P3 propodus 8.0× longer than wide, Figs 13A, 15A) (versus P3 propodus less than 7× longer than wide), the P2 and P3 propodus twice the length of the dactylus (Fig. 15A) (versus 1.7× in *D. spinulosa*; Guinot 1995: fig. 21a; Ah Yong 2008: fig. 1C); and the male telson subovate in shape (Fig. 16C) (versus triangular in *D. spinulosa*, cf. Guinot 1995: figs 21c, 25D). *Dicranodromia spinulosa* was described from three males and one female from New Caledonia, the holotype female being 7.5 × 11.0 mm; a size comparable to that of the male specimens of *D. erinaceus* we examined.

Ho et al. (2004) recorded *D. doederleini* from Taiwan from one badly damaged female specimen from northeastern Taiwan (see also Ah Yong et al. 2009). The specimen is now referred to *D. erinaceus*.

***Dicranodromia robusta* sp. nov.**

<http://zoobank.org/ADCE5085-D836-4A3E-8CF9-5BEB79ED3FE1>

Figures 17–20, 21C, G–J, N–P

Material examined. PHILIPPINES: **Holotype** ♀ (19.6 × 26.4 mm), ca. 5°24'N, 125°22.5'E, Balut Island, Sarangani Islands, Davao Occidental Province, south of Mindanao Island, coll. tangle nets, local fishermen, 26 Nov. 2017 (ZRC 2018.0161); **Paratype** ♂ (15.2 × 21.0 mm), same location as holotype, coll. tangle nets, local fishermen, 2017 (ZRC 2018.0095).

Diagnosis. Carapace longitudinally subquadrate, widest across intestinal-meso-branchial regions; dorsal surface gently convex, lateral surfaces covered with low spinules, median part smooth, margins with scattered short stiff setae, not obscuring margins; short stiff setae present on pereopods, thoracic sternum and pleon but not obscuring surface or margins. Branchiocardiac groove distinct, curving medially anteriorly. Each pseudorostral lobe triangular, inner margin straight, outer margin gently convex, directed anteriorly, inner margin entire; exorbital tooth dentiform, directed obliquely laterally, anterior margin with two or three spinules; supraorbital margin separated from external orbital tooth by shallow concave cleft, posterior part with five or six spinules; infraorbital margin with large dorsoventrally flattened lobe which is dentiform to linguiform, larger than exorbital tooth, distal part with spine, anterior margin with two spinules, prominently visible in dorsal view. Rostrum present as one sharp granule. Epistome covered with scattered granules on anterior half; posterior half gently upturned, with median fissure, surface not covered with spinules, posterior margin gently convex, median part entire, lateral part gently serrate. Basal antennal article subquadrate; surfaces covered by spinules and granules; anteroexternal tooth short. Eyes with long peduncle. Third maxilliped relatively narrow; merus subovate with low anterointernal lobe, shorter than ischium; ischium subtrapezoidal, distal half slightly wider than proximal part; palp (carpus, propodus, dactylus) long, reaching to median part of ischium when folded; exopod with proximal third widest. Chelipeds covered with stiff setae on most parts; merus and carpus with margins uneven or lined with granules; palm relatively short, subdorsal and subventral margins with low sharp granules, median part smooth; fingers thick, wide, occluding surface hollowed; pollex with deep U-shaped depression distally. P2 and P3 relatively short, P3 longer than P2; merus with low tooth on distal extensor margin, length to width ratio of P2 and P3 merus 4.2 and 3.9, respectively; margins unarmed; propodus almost straight, unarmed, length to width ratio of P2 and P3 propodus 5.2 and 6.4, respectively; dactylus curved, flexor margin lined with 8 or 9 spines, terminating in strongly gently curved claw, propodus about 2.4× length of dactylus. P4 stouter, shorter than P5; length to width ratio of P4 and P5 merus 2.4 and 3.4, respectively; margins of merus unarmed; P4 and P5 propodus with submedian spinule on distal third of outer surface, length to width ratio of P4 and P5 propodus 2.3 and 3.6, respectively, distal margin fringed by sharp spines bracketing dactylus; dactylus claw-like, strongly incurved, extensor margin with median spine or absent, flexor margin with 2–4 spines. Thoracic sternite 7 with low transverse ridge from posterior

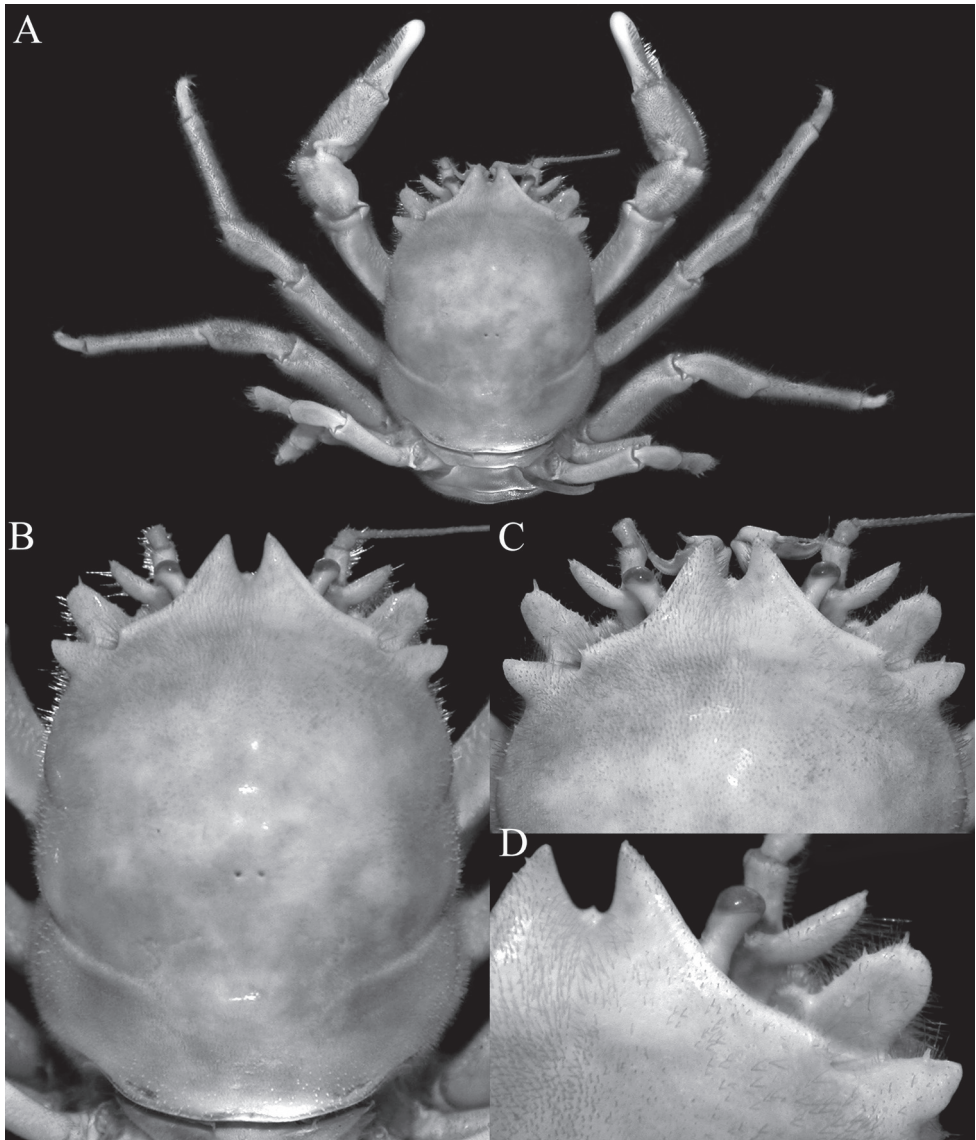


Figure 17. *Dicranodromia robusta* sp. nov., holotype ♀ (19.6 × 26.4 mm) (ZRC 2018.0161), Philippines
A overall view **B** dorsal view of carapace **C** front and anterior part of carapace **D** right front, orbit and first anterolateral spine

inner part of female gonopore, lateral part high, forming triangular tubercle, curving posteriorly to join oblique ridge formed by posterior part of sternite 7, just before suture with sternite 8, groove between sternites 7 and 8 curve to join spermathecal aperture at base of triangular tubercle. Male and female pleons with 6 free somites and telson; male telson distinctly elongate, triangular with gently convex lateral margins; female telson triangular, with gently convex margins. G1 stout, endopod distally covered by dense

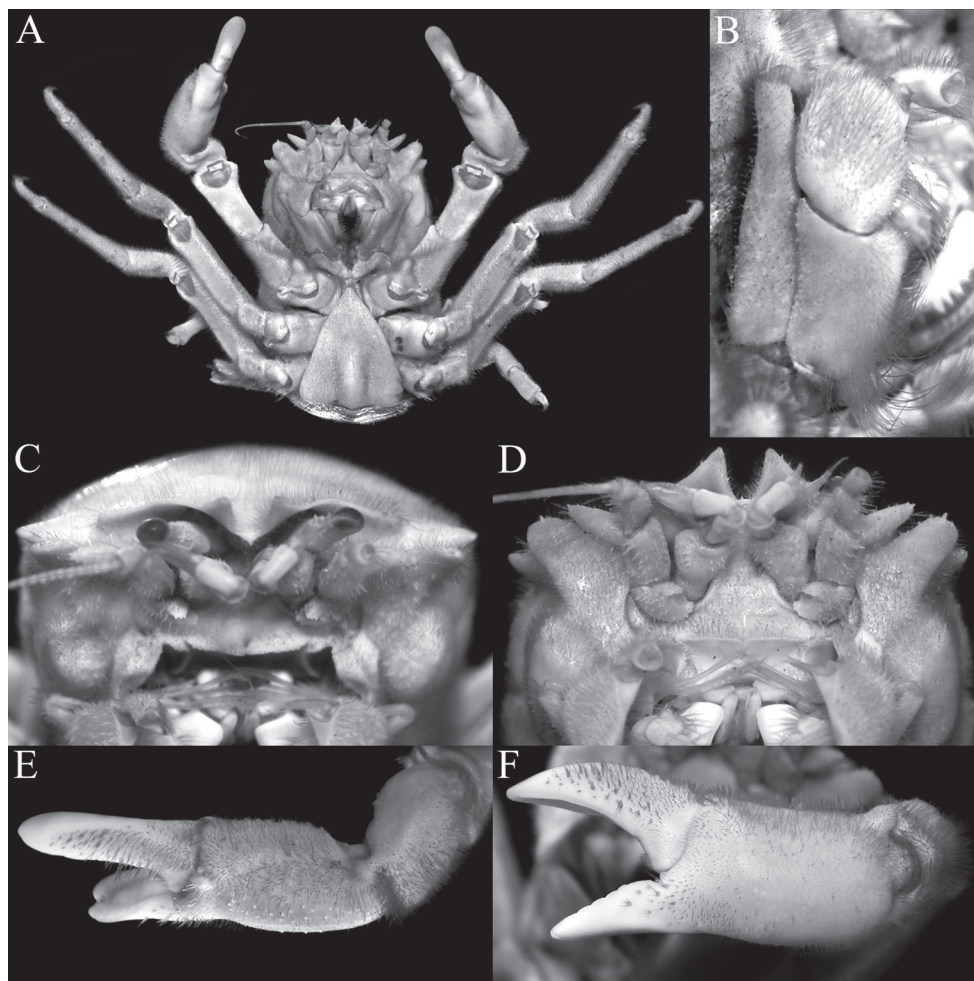


Figure 18. *Dicranodromia robusta* sp. nov., holotype ♀ (19.6 × 26.4 mm) (ZRC 2018.0161), Philippines **A** ventral view of cephalothorax **B** left third maxilliped **C** frontal view of cephalothorax **D** epistome, antennules, antennae and orbits **E** dorsal view of left chela **F** left chela.

long setae, subdistal part of outer margin with two lobes, the distal one being more prominent; G2 endopod gradually tapering to sharp tip.

Variation. In the holotype female, the left P5 dactylus has a prominent spine on the extensor margin (Fig. 21I), but there is none on the right side (Fig. 21H). The P5 dactyli of the paratype male are armed a spinule on the extensor margin. Both specimens possess the spine on the outer surface of the P5 propodus (Fig. 21H, I).

Etymology. The species is named after the Latin *robusta* for stout, alluding to the stocky appearance of the species.

Remarks. The most diagnostic character of *D. robusta* sp. nov. is the large dors-oventrally flattened infraorbital tooth, which is dentiform to linguiform, clearly visible

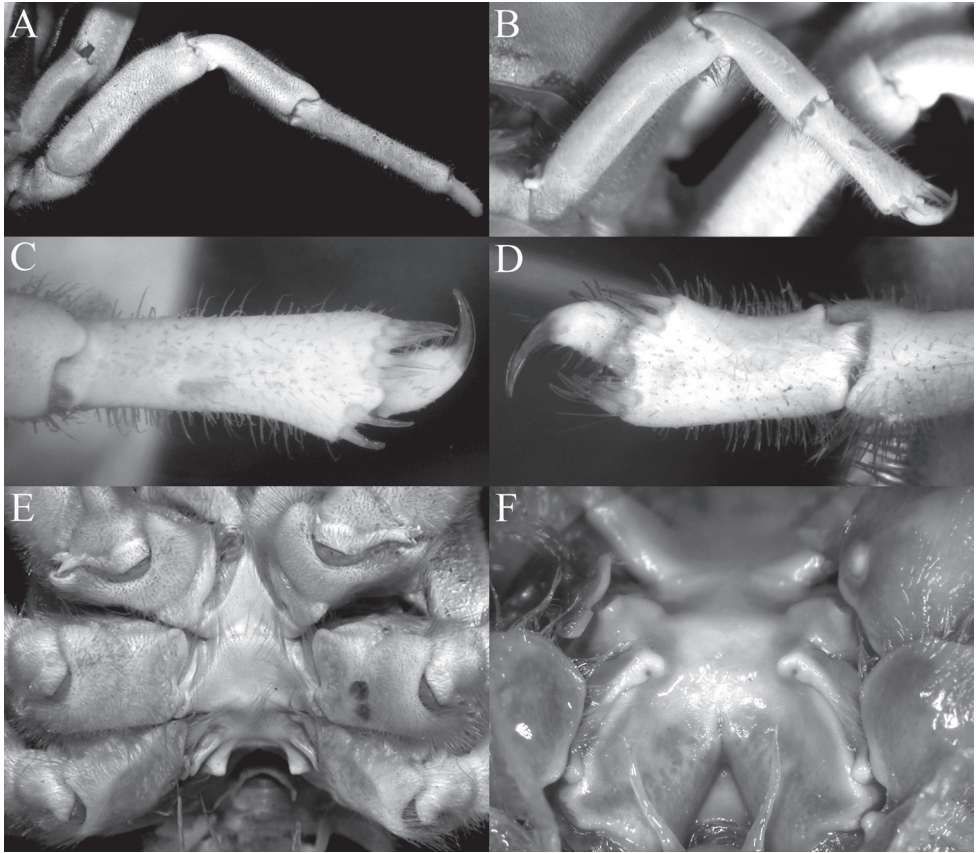


Figure 19. *Dicranodromia robusta* sp. nov., holotype ♀ (19.6 × 26.4 mm) (ZRC 2018.0161), Philippines **A** right P3 **B** right P5 **C** right P5 propodus and dactylus **D** left P4 propodus and dactylus **E** anterior thoracic sternum and spermatheca **F** posterior thoracic sternum showing spermatheca.

in dorsal view, and distinctly larger than the exorbital tooth (Figs 17B–D, 20B). No other Indo-West Pacific species of *Dicranodromia* has such a large and wide infraorbital tooth. The long anteroexternal tooth on the basal antennal article allies *D. robusta* with *D. martini* (cf. Guinot 1995: fig. 20B), *D. baffini* (cf. Alcock 1899: pl. 2 fig. 1a; Alcock 1901: pl. 1 fig. 1a), *D. danielae* (cf. Ng and McLay 2005: fig. 3A, B) and *D. cheneae* (cf. Ng and Naruse 2007: fig. 5b) but the structure of the infraorbital tooth easily distinguishes it from them.

The carapace shape of *D. robusta* is distinctly more quadrate (Figs 17A, B, 20A, B) than the more pyriform *D. martini* described from the Philippines (cf. Figs 4A, C, 6A, B; Guinot 1995: fig. 19b; Ng and Naruse 2007: fig. 1a–c); the posterior margin of the epistome is entire (Fig. 18C) (versus margin gently crenulate in subventral view in *D. martini*, cf. Guinot 1995: fig. 20B); P2 and P3 are prominently shorter with the dactylus especially short (e.g., P3 merus 3.9× longer than broad, propodus 6.4× longer than broad, Fig. 19A) (versus P3 merus 7.0× longer than broad, propodus 7.2× longer

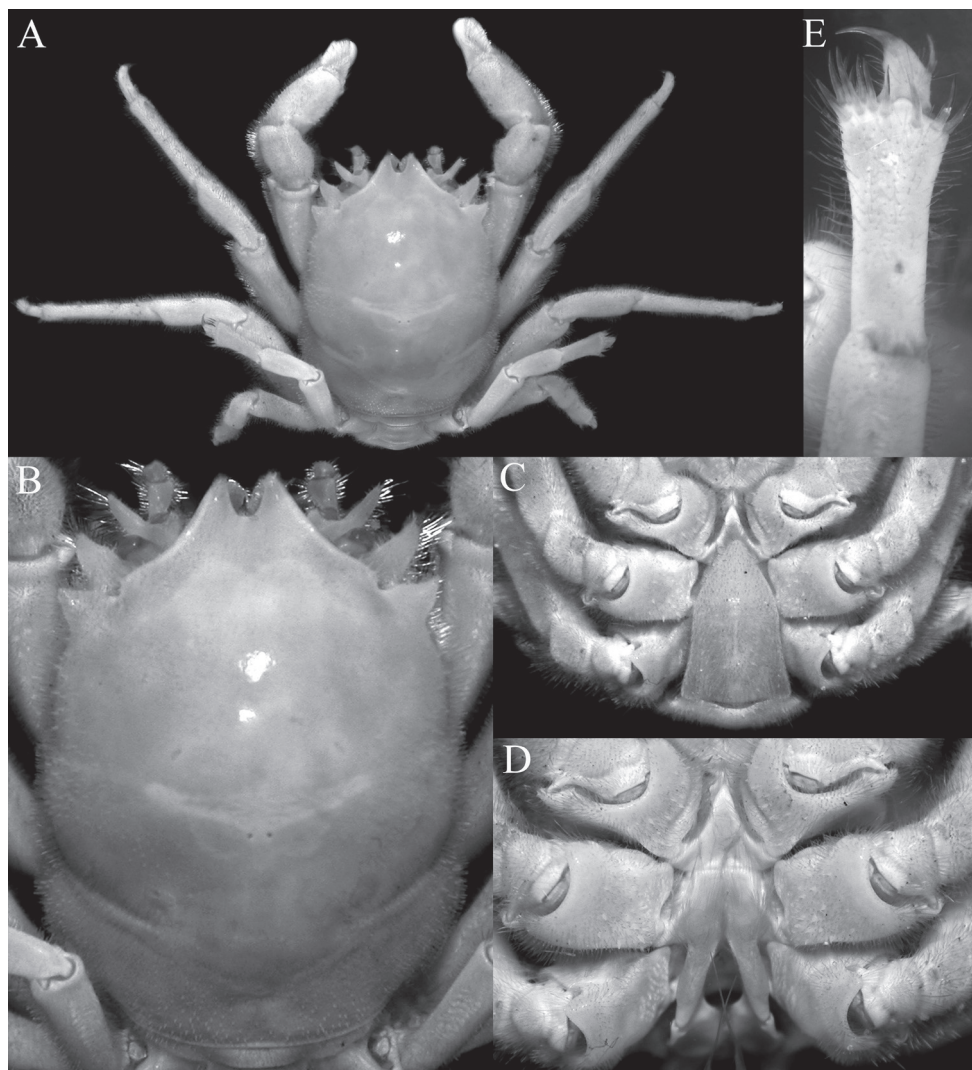


Figure 20. *Dicranodromia robusta* sp. nov., paratype ♂ (15.2 × 21.0 mm) (ZRC 2018.0095), Philippines **A** overall view **B** dorsal view of carapace **C** pleon **D** anterior thoracic sternum and G1s in situ.

than broad in *D. martini*, cf. Figs 4A, 5C, 6A; Guinot 1995: figs 19a, e, 20C); P4 and P5 are much shorter (e.g., P4 merus just reaching branchiocardiac groove when folded dorsally, Figs 17A, 19B, 20A) (versus P4 merus long, reaching beyond branchiocardiac groove when folded dorsally in *D. martini*, cf. Figs 4A, 5D, 6A; Guinot 1995: fig. 19a); and the male telson is lingulate (Fig. 20C) (versus more elongate in *D. martini*, cf. Fig. 6D; Guinot 1995: fig. 19c).

Compared to *D. baffini* from the Indian Ocean, *D. robusta* has a more quadrate carapace (Figs 17A, B, 20A, B) (versus more pyriform in *D. baffini*, cf. Alcock 1899: pl. 2 fig. 1a; Guinot 1995: fig. 13; Padate et al. 2020: fig. 2a); and the P2 and P3 dactylus

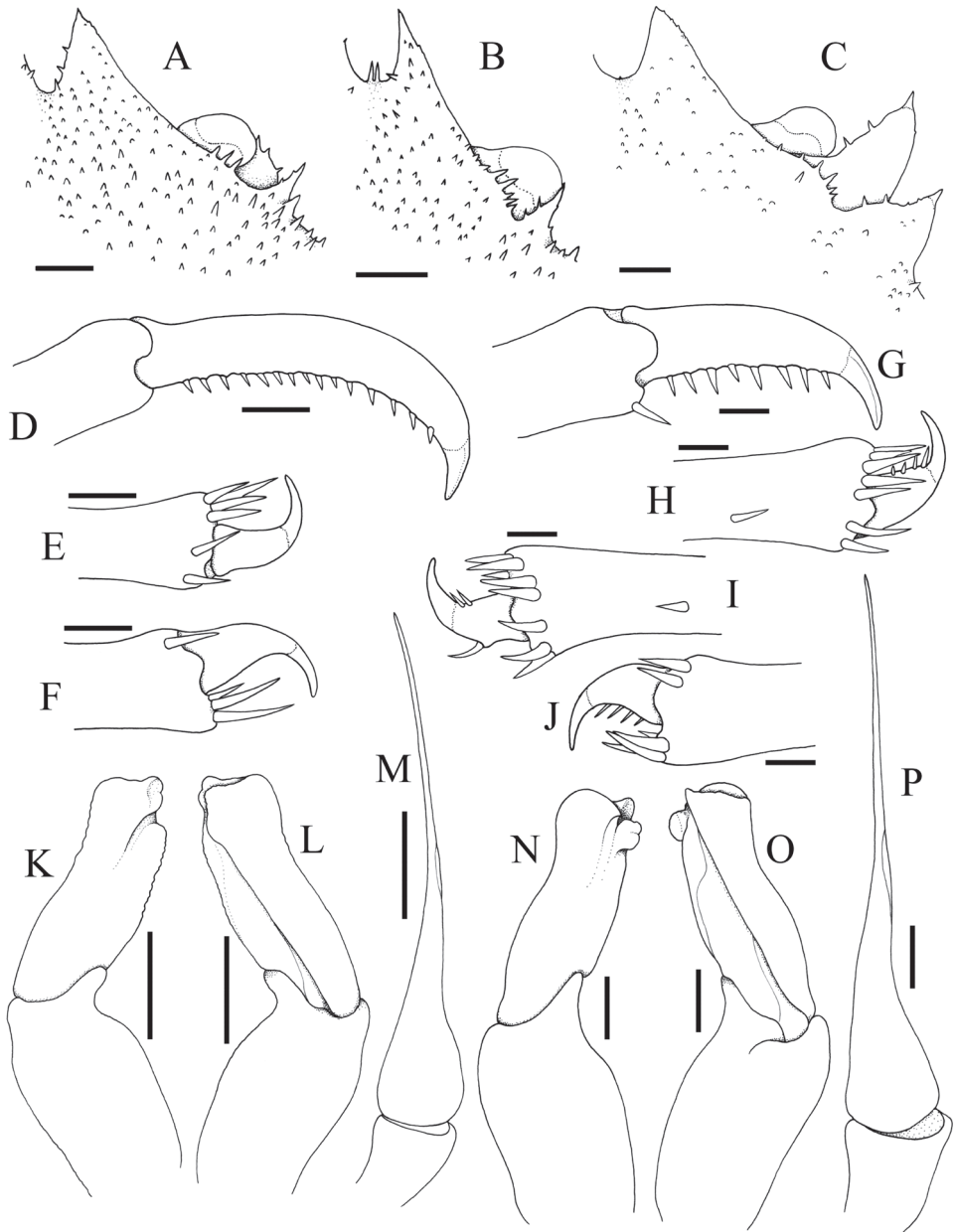


Figure 21. **A** *Dicranodromia erinaceus* sp. nov., holotype ♀ (14.0 × 18.0 mm) (NTOU B00126), Taiwan **B, D–F, K–M** *D. erinaceus* sp. nov., paratype ♂ (8.2 × 12.5 mm) (ZRC 2021.0085), Taiwan **C, G–J, N–P** *D. robusta* sp. nov., paratype ♂ (15.2 × 21.0 mm) (ZRC 2018.0095), Philippines **A–C** right anterior part of carapace (setae removed or not drawn) **D** right P3 propodus and dactylus **E** right P5 propodus and dactylus **F** right P4 propodus and dactylus **G** right P3 propodus and dactylus **H** right P5 propodus and dactylus **I** left P5 propodus and dactylus **J** left P4 propodus and dactylus **K, N** left G1 (ventral view) **L, O** left G1 (dorsal view) **M, P** left G2. Setae for all structures not figured. Scale bars: 1.0 mm.

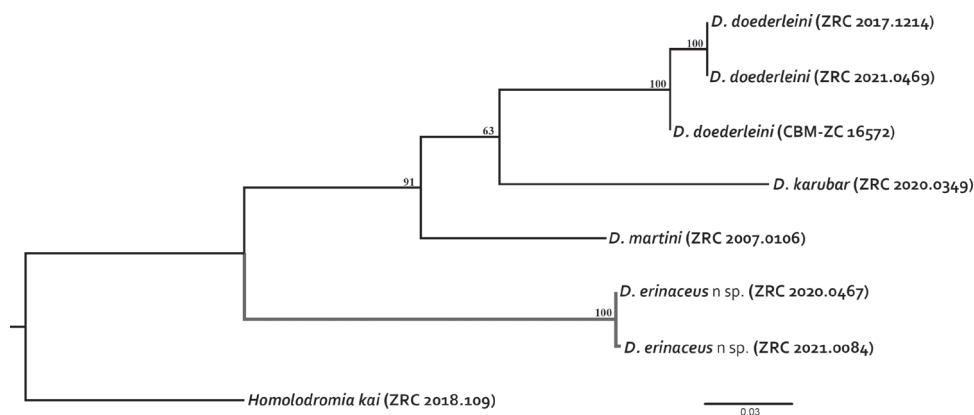


Figure 22. Maximum likelihood phylogenetic tree for *Dicranodromia erinaceus* sp. nov. based on the COI gene dataset. *Homolodromia kai* Guinot, 1993 was chosen as outgroup. Maximum likelihood bootstrap value is represented as above the branches. Values less than 50 are not shown.

is distinctly shorter (Figs 19A, 21G) (versus longer in *D. baffini*, cf. Alcock 1899: pl. 2 fig. 1a; Guinot 1995: fig. 13). With regards to the relatively shorter P2 and P3 dactyli, *D. robusta* resembles *D. chenae*, described from a single large ovigerous female from the central Philippines. *Dicranodromia robusta*, however, can easily be distinguished in having the outer margin of the pseudorostral lobe is almost straight and the structure is directed anteriorly (Figs 17B–D, 20B) (versus outer margin of the pseudorostral lobe is distinctly convex with the structure gradually curved inwards towards the median in *D. chenae*, cf. Ng and Naruse 2007: fig. 5A); the ischium of the third maxilliped is short and rectangular (Fig. 18B) (versus distinctly longer and more slender in *D. chenae*, cf. Ng and Naruse 2007: fig. 5b); the female telson is relatively more elongate (Fig. 18A) (versus proportionately wider and shorter in *D. chenae*, cf. Ng and Naruse 2007: fig. 2b); and the spermatheca is on the prominently raised part around the suture between sternites 7 and 8 and ends at the centre of the triangular tubercle on sternite 6 (Fig. 19F) (versus spermatheca is not prominently raised and ends at the base of the triangular tubercle in *D. chenae*, cf. Ng and Naruse 2007: fig. 8).

Dicranodromia robusta can be separated from *D. danielae* in having the exorbital tooth distinctly triangular to linguiform (Figs 17B–D, 21C) (versus subtrapezoidal in *D. danielae*, cf. Fig. 12A, B; Ng and McLay 2005: figs 1B, 4A); the posterior margin of the epistome is entire (Fig. 18C) (versus clearly serrate in *D. danielae*, cf. Fig. 12C; Ng and McLay 2005: fig. 4C); the median part of the outer surface of the chela is granular (Fig. 18E, F) (versus smooth in *D. danielae*, cf. Fig. 12D; Ng and McLay 2005: fig. 3A, B); and P2–P5 are all proportionately longer with the flexor margins of the meri not spinate (Figs 17A, 19A, 20A) (versus relatively shorter in *D. danielae* with the meri of P2 and P3 distinctly spinate, cf. Fig. 12E, F; Ng and McLay 2005: fig. 1A).

Discussion

Ng and Naruse (2007) discussed the value of the spine present on the extensor margin of P5 dactylus as a taxonomic character. They noted that it was sometimes present in *D. martini* (cf. comparative material examined above; Ng and Naruse 2007: fig. 3a, b) and was present on the holotype of *D. danielae* (cf. Ng and Naruse 2007: fig. 3c; Fig. 12F, G). In the specimens of *D. doederleini* examined, none of the P5 dactyli possess this spine (Fig. 3D, E). The presence and absence of this spine must therefore be used with caution. The setae on the P5 propodus are a mixture of setae and spines, but there are some setae which are intermediate in proportions, suggesting that the setae and spines are homologous structures, the “spines” on the distal edge and the outer surface of the P5 propodus, and “spines” on the flexor margin of the dactylus are almost certainly derived from the setae. They all have a clearly defined base and articulate with the cuticle. Normal spines and granules are part of the cuticle and there is no defined base. That being said, the extensor margin of the P5 dactylus in all the specimens of *D. doederleini* and *D. erinaceus* sp. nov. we examined are unarmed (Figs 3D, E, 15B, C). In the case of *D. karubar*, some of the P5 dactyli have spines while others do not (Figs 9G, 10D). For *D. robusta* sp. nov., the dactylar spine on the extensor margin is present in both specimens (but missing on the right leg in the holotype), and in addition, there is a prominent spine on the median outer surface of the P5 propodus which is always present (Fig. 21H, I). In *D. doederleini*, the P5 propodus has two or three spines on the outer surface (Fig. 3D, E); there are two spines in *D. martini*, with one or two spines in *D. karubar* (Fig. 9G), while in *D. erinaceus* sp. nov., the P5 propodus is unarmed (Fig. 15B, C).

The armature of the posterior margin of the epistome is a useful character but must be used carefully as well. In species like *D. danielae*, the margin is prominently spinose even when viewed frontally, with spines appearing more prominent when the margin is viewed subventrally (Fig. 12C). In *D. doederleini* and *D. karubar*, the posterior margin is almost entire or only weakly crenulate when viewed frontally or subventrally (Figs 2D, 8D, 9A). In *D. martini*, the margin appears almost entire in frontal view (Fig. 4E) but when viewed subventrally, it is weakly crenulated and uneven, as figured by Guinot (1995: fig. 20B). The structure of the proepistome, present in all the species examined, is relatively conservative, being separated from the epistome only by the lateral clefts, and for all the species, it is triangular in shape and slightly “sunken” into the distal margin of the epistome. In most species, the surface of the proepistome is covered with low granules and setae (Figs. 2E, 5A, 9A, 14D, 18D); but in *D. danielae*, the lateral parts have long spinules and the surface also has short spinules (Fig. 12C).

Guinot (1995: fig. 2C) noted that the actual rostrum of *Dicranodromia*, when visible, is present only as a small median tooth or spinule between the two pseudorostral teeth. It must be noted that this character is probably variable to some degree. In *D. martini*, there is no trace of a rostrum (Figs 4D, 6C). In *D. doederleini*, the rostrum is a distinct sharp granule (Fig. 2B; Guinot 1995: fig. 12B). When it is present as a spinule, the structure may be small, brittle and can easily be broken off. In one of the

paratype males of *D. erinaceus* sp. nov. (ZRC 2021.0085), the rostrum is composed of three small, slender spinules, which are very minute and delicate (Fig. 21B). The rostral spinules are not clearly visible on the large female specimens of *D. erinaceus* sp. nov. but it may simply have been lost. In *D. danielae*, there are three spinules (Fig. 12B). In *D. robusta* sp. nov., the rostrum is just a sharp but relatively low granule that is barely discernible (Figs 17C, D, 21C), as in the case of *D. karubar* (Fig. 8D). As such, this character should not be relied on to separate taxa.

In general, all species have spinules on some part of the carapace and these are often surrounded by stiff setae which partially obscure the spinules. Cleaning must be done with great care as the spinules (and even some of the spines) are brittle and break easily.

The structures of the G1 and G2 have not been used to separate species and Guinot (1995) only figured them for one American species (*D. maheuxii*). The G1 endopod is the main character and, while they all have a similar shape, the relative proportions differ and the subdistal part of the outer margin has two lobes of differing shapes and sizes. The G1 of the four species examined here show that there are differences between some taxa and can be used as a taxonomic character. The most distinctive is the G1 of *D. karubar*, in which the subdistal lobe on the outer margin of the endopod is curved and beak-like (Fig. 11D, E), distinct from the more rounded structure of its most similar species, *D. baffini*. The G1 endopods of *D. martini* and *D. karubar* (Fig. 11A, B, D, E) are also proportionately longer than those of *D. erinaceus* sp. nov. and *D. robusta* sp. nov. (Fig. 21K, L, N, O). In addition, the subdistal lobe on the outer margin of the G1 endopod in *D. robusta* (Fig. 21N, O) is distinctly more pronounced than either *D. martini* or *D. erinaceus* sp. nov. (Figs 11A, B, 21K, L). As such, G1 structures for *Dicranodromia* species should be described and figured as part of species descriptions.

Guinot (1995: 182) placed more emphasis on the structure of the spermathecal apertures and associated structures on thoracic sternites 7 and 8, pointing that there are clear differences between species. One of the characteristic features is that all the species have a pair of enlarged tubercles on each side of thoracic sternite 7 which are anterior or adjacent to the spermatheca. When viewed frontally, they appear as a pair of rounded or triangular tubercles (Figs 3G, 5H, 9J, 15E, 19F). In some species like *D. doederleini*, *D. martini*, *D. karubar* and *D. robusta* sp. nov., the two tubercles are separate (Figs 3G, 5H, 9J) but in *D. erinaceus* sp. nov., the two tubercles are connected by a clear ridge that bridges them (Fig. 15E). In *D. doederleini*, the tubercle is distinctively curved laterally outwards (Fig. 3G). In two species, *D. baffini* and *D. karubar*, the tubercle is distinctively comma-shaped, with the spermatheca positioned posteriorly to it (Fig. 9J). The suture between sternites 7 and 8, which joins the spermatheca is also differently structured. In most species, the suture is level with the rest of the sternal surface (Figs 3H, 5H, 9J, 19F). In most species, the spermatheca is posterior to the sternal tubercle (Figs 3H, 5H, 19F). In one species, *D. erinaceus* sp. nov., however, the suture is distinctly raised, on a prominent ridge and joins the spermatheca laterally (Fig. 15F).

The molecular analyses using COI sequences closely supported the morphological observations. There was some intraspecific divergence in the three individuals of *D. doederleini* tested (GenBank accession nos. OK351331-OK351333), ranging

from 0–1.2%, while that in two specimens of *D. erinaceus* sp. nov. (accession nos. OK351334–OK351335) was 0.2%. In *Dicranodromia*, the divergence at the species level was 9.6–14.0%, with *D. erinaceus* sp. nov. distinct from the tested species by 12.8–14.0%. The outgroup *H. kai* (accession no. OK351338) has a minimal divergence of 12.6–12.8% with *D. erinaceus* sp. nov., and a maximal value of 14.2% with *D. karubar*. The maximum likelihood tree also showed *D. erinaceus* sp. nov. to form an independent clade from other *Dicranodromia* species with an extremely high support (MLb = 100) (Fig. 22). The significance of this divergence will need to be re-appraised when more species of *Dicranodromia* (especially the American taxa) can be tested to see if the genus is monophyletic.

Noteworthy is that the Philippines has four species: *D. danielae*, *D. chenaе*, *D. martini* and *D. robusta* sp. nov. Two of the species (*D. chenaе* and *D. martini*) were collected by trawls, the substrate being more level and less rocky. Like *D. danielae*, *D. robusta* sp. nov. was collected by tangle nets set in deep-water, which may explain why it has not been collected until now. Deep-water habitats with steep rocky substrates are difficult to sample, and the fauna is often different from those occurring in flatter substrates (see Ng et al. 2009; Mendoza et al. 2010). Several other brachyuran taxa show the same pattern, notably in Majoidea (e.g., see Ng and Richer de Forges 2015; Richer de Forges and Ng 2008; Richer de Forges et al. 2021).

Acknowledgements

We thank T. Komai for his kind help with specimens. Paul Ng kindly passed us the specimen and shared the photographs of live *D. doederleini*. Thanks are due to Evelyn Antig (Palaone Trading) in the Philippines for help with and information on the two specimens from Mindanao. The SJADES cruise which obtained *D. karubar* was a joint Indonesian-Singapore expedition to southern Java funded by the National University of Singapore and the Research Center for Oceanography, Indonesian Institute of Sciences (LIPI), and supported by their respective Ministries of Foreign Affairs under the RISING 50 program to promote bilateral co-operation. We thank Bertrand Richer de Forges for his invaluable help with the cruise and trawling efforts, as well as Tin-Yam Chan and his team for their invaluable help in the trawling work and other support. We are also most grateful to Danièle Guinot, Tohru Naruse, and Shane Ah Yong for their many suggestions which have improved the manuscript.

References

- Ahyong ST (2008) Deepwater crabs from seamounts and chemosynthetic habitats off eastern New Zealand (Crustacea: Decapoda: Brachyura). *Zootaxa* 1708: 1–72. <https://doi.org/10.11646/zootaxa.1708.1.1>

- Ahyong ST, Naruse T, Tan SH, Ng PKL (2009) Part II. Infraorder Brachyura: Sections Dromiacea, Raninoida, Cyclodorippoida. In: Chan T-Y, Ng PKL, Ahyong ST, Tan SH (Eds) Crustacean Fauna of Taiwan: Brachyuran Crabs, Volume I. Keelung, Taiwan, 27–180.
- Alcock A (1899) An account of the Deep-Sea Brachyura collected by the Royal Indian marine survey ship INVESTIGATOR. Printed by order of the Trustees of the Indian Museum, Calcutta, 87 pp, pls 1-4. <https://doi.org/10.5962/bhl.title.10330>
- Alcock A (1901) Catalogue of the Indian Decapod Crustacea in the collection of the Indian Museum. Part 1. Brachyura. Fasciculus 1. Introduction and Dromides or Dromiacea (Brachyura Primigenia). Trustees of the Indian Museum, Calcutta. 1–80.
- Alcock A, Anderson ARS (1899) Natural history notes from H. M. Royal Indian Marine Survey Ship ‘Investigator,’ Commander T. H. Heming, R. N., commanding. Series III, no. 2. An account of the deep-sea Crustacea dredged during the surveying-season of 1897-98. *Annals and Magazine of Natural History* (7) 3: 1–27. <https://doi.org/10.1080/00222939908678071>
- Caustier E (1895) Sur le développement embryonnaire d’un Dromiacé du genre *Dicranodromia*. *Comptes rendus Hebdomadaires des Séances de l’Académie des Sciences, Paris* 120: 573–575.
- Davie PJF, Guinot D, Ng PKL (2015) Anatomy and functional morphology of Brachyura. In: Castro P, Davie PJF, Guinot D, Schram FR, von Vaupel Klein JC (Eds) *Treatise on Zoology – Anatomy, Taxonomy, Biology. The Crustacea* (Vol. 9C–I): Decapoda: Brachyura (Part 1). Brill, Leiden, 11–163. https://doi.org/10.1163/9789004190832_004
- Felsenstein J (1985) Confidence limits in phylogenies: an approach using the bootstrap. *Evolution* 39: 783–791. <https://doi.org/10.1111/j.1558-5646.1985.tb00420.x>
- Folmer O, Black M, Hoeh W, Lutz R, Vrijenhoek R (1994) DNA primers for amplification of mitochondrial cytochrome c oxidase subunit I from diverse metazoan invertebrates. *Molecular Marine Biology and Biotechnology* 3: 294–299.
- Gordon I (1950) Crustacea Dromiacea. Part I: Systematic account of the Dromiacea collected by the “John Murray” Expedition. Part II. The morphology of the spermatheca in certain Dromiacea. *Scientific Reports of the John Murray Expedition 1933–34* 9(3): 201–253, figs 1–26, pl. 1.
- Guinot D (1993) Données nouvelles sur les crabes primitifs (Crustacea Decapoda Brachyura Podotremata). *Comptes Rendus Hebdomadaires de Séances de l’Académie des Sciences, Paris* 316 (10): 1225–1232.
- Guinot D (1995) Crustacea Decapoda Brachyura: Révision de la famille des Homolodromiidae Alcock, 1900. In: Crosnier A (Ed) *Résultats des Campagnes MUSORSTOM. Volume 13, Mémoires du Muséum national d’Histoire naturelle* 163: 155–282.
- Hall TA (1999) BioEdit: A user-friendly biological sequence alignment editor and analysis program for Windows 95/98/ NT. *Nucleic Acids Symposium Series* 41: 95–98.
- Hebert PDN, Cywinska A, Ball SL, deWaard JR (2005) Biological identifications through DNA barcodes. *Proceedings of the Royal Society of London B* 270: 313–321. <https://doi.org/10.1098/rspb.2002.2218>
- Ho P-H, Ng PKL, Chan T-Y, Lee D-A (2004) New records of 31 species of brachyuran crabs from the joint Taiwan-France Expeditions, “TAIWAN 2000” and “TAIWAN 2001”, off deep waters in Taiwan. *Crustaceana* 77(6): 641–668. <https://doi.org/10.1163/1568540041958617>

- Hosie AM, Hara A (2016) Description of a new species of brooding spider crab in the genus *Paranaxia* Rathbun, 1924 (Brachyura: Majoidea), from northern Australia and Indonesia. *Zootaxa* 4127(1): 121–134. <https://doi.org/10.11646/zootaxa.4127.1.6>
- Ikeda H (1998) The deep-sea crabs of Sagami Bay. Hayama Shiosai Museum, Japan, 180 pp.
- Kumar S, Stecher G, Tamura K (2016) MEGA7: Molecular evolutionary genetics analysis version 7.0 for bigger datasets. *Molecular Biology and Evolution* 33: 1870–1874. <https://doi.org/10.1093/molbev/msw054>
- Martin JW (1991) Crabs of the family Homolodromiidae. III. First record of the larvae. *Journal of Crustacean Biology* 11(1): 156–161. <https://doi.org/10.2307/1548553>
- Mendoza JCE, Naruse T, Tan SH, Chan T-Y, Richer De Forges B, Ng PKL (2010) Case studies on decapod crustaceans from the Philippines reveal deep, steep underwater slopes as prime habitats for ‘rare’ species. *Biological Conservation* 19: 575–586. <https://doi.org/10.1007/s10531-009-9744-x>
- Mendoza JCE, Richer de Forges B, Safaruan MD, Ng PKL (2021) Checklist of the Brachyura (Crustacea: Decapoda) collected by the SJADES 2018 biodiversity cruise in the Sunda Strait and southwestern Java, Indonesia. *Raffles Bulletin of Zoology, Supplement* 36: 277–304.
- Milne-Edwards A (1880) Etudes préliminaires sur les Crustacés, 1ère Partie. Reports on the Results of Dredging under the Supervision of Alexander Agassiz, in the Gulf of Mexico, and in the Caribbean Sea, 1877, ‘78, ‘79, by the U.S. Coast Survey Steamer “Blake”, Lieut. Commander C. D. Sigsbee, U.S.N., and Commander J. R. Bartlett, U.S.N., Commanding, VIII. *Bulletin of the Museum of Comparative Zoology, Harvard University* 8(1): 1–68, pls 1, 2.
- Morgan GJ (1987) Brooding of juveniles and observations on dispersal of young in the spider crab *Paranaxia serpulifera* (Guérin) (Decapoda, Brachyura, Majidae) from Western Australia. *Records of the Western Australian Museum* 13: 337–343.
- Ng PKL, Guinot D, Davie PJF (2008) *Systema Brachyurorum: Part I. An annotated checklist of extant brachyuran crabs of the world.* *Raffles Bulletin of Zoology, Supplement* 17: 1–286.
- Ng PKL, Ho P-H, Lin C-W, Yang C-H (2018) The first record of an eastern Pacific invasive crab in East Asian waters: *Amphithrax armatus* (Saussure, 1853) (Crustacea: Brachyura: Majoidea: Mithracidae) in Taiwan. *Journal of Crustacean Biology* 38(2): 198–205. <https://doi.org/10.1093/jcobiol/rux109>
- Ng PKL, McLay CL (2005) *Dicranodromia danielae*, a new species of homolodromiid crab from the Philippines (Crustacea: Decapoda: Brachyura). *Zootaxa* 1029: 39–46. <https://doi.org/10.11646/zootaxa.1029.1.3>
- Ng PKL, Mendoza JCE, Manuel-Santos M (2009) Tangle net fishing, an indigenous method used in Balicasag Island, central Philippines. *Raffles Bulletin of Zoology, Supplement* 20: 39–46.
- Ng PKL, Naruse T (2007) On two species of deep sea homoloid crabs of the genus *Dicranodromia* (Crustacea: Decapoda: Brachyura: Homolodromiidae) from the Philippines, with description of a new species. *Raffles Bulletin of Zoology, Supplement* 16: 47–53.
- Ng PKL, Richer de Forges B (2015) Revision of the spider crab genus *Maja* Lamarck, 1801 (Crustacea: Brachyura: Majoidea: Majidae), with descriptions of seven new genera and 17 new species from the Atlantic and Indo-West Pacific. *Raffles Bulletin of Zoology* 63: 110–225.

- Ng PKL, Shih H-T, Ho P-H, Wang C-H (2017) An updated annotated checklist of brachyuran crabs from Taiwan (Crustacea: Decapoda). *Journal of the National Taiwan Museum* 70(3 & 4): 1–185.
- Ortmann AE (1892) Die Abtheilungen Hippidea, Dromiidea und Oxystomata. Die Decapoden-Krebse des Strassburger Museums, mit besonderer Berücksichtigung der von Herrn Dr. Döderlein bei Japan und bei den Liu-Kiu-Inseln gesammelten und zur Zeit im Strassburger Museum aufbewahrten Formen. Theil V [= Part V]. *Zoologische Jahrbücher, Abtheilung für Systematik Geographie und Biologie der Thiere* 6(4): 532–588, pl. 26. <https://doi.org/10.5962/bhl.part.26456>
- Padate VP, Amritha KM, Cubelio SS, Saravanane N, Sudhakar M, Ng PKL (2020) Deep-water Brachyura from the surveys of the FORV Sagar Sampada off the Andaman and Nicobar archipelagos, India. *Regional Studies in Marine Science* 35: e101117. <https://doi.org/10.1016/j.rsma.2020.101117>
- Rathbun MJ (1914) Stalk-eyed crustaceans collected at the Monte Bello Islands. *Proceedings of the Zoological Society of London* 84(3): 653–664. <https://doi.org/10.1111/j.1469-7998.1914.tb07055.x>
- Rathbun MJ (1924) Results of Dr. E. Mjöberg's Swedish scientific expeditions to Australia 1910–1913 37. Brachyura, Albuneidae and Porcellanidae. *Arkiv för Zoologi* 16: 1–33.
- Richer de Forges B, Lee BY, Ng PKL (2021) Spider crabs from the SJADES 2018 biodiversity cruise in Indonesia, with descriptions of one new genus and five new species, including one from Western Australia (Crustacea: Brachyura: Majoidea). *Raffles Bulletin of Zoology, Supplement* 36: 211–257.
- Richer de Forges B, Ng PKL (2008) New records of deep-sea spider crabs of the genus *Cyrtomaia* Miers, 1886, from the Pacific Ocean, with description of a new species (Crustacea: Decapoda: Brachyura: Majidae). *Zootaxa* 1861: 17–28. <https://doi.org/10.11646/zootaxa.1861.1.2>
- Song H, Buhay JE, Whiting MF, Crandall KA (2008) Many species in one: DNA barcoding overestimates the number of species when nuclear mitochondrial pseudogenes are coamplified. *Proceedings of the National Academy of Sciences of the United States of America* 105: 13486–13491. <https://doi.org/10.1073/pnas.0803076105>
- Stamatakis A (2006) RAxML-VI-HPC: maximum likelihood based phylogenetic analyses with thousands of taxa and mixed models. *Bioinformatics* 22: 2688–2690. <https://doi.org/10.1093/bioinformatics/btl446>
- Tan LWH, Lim SSL, Ng PKL (1986) The complete larval development of the dromiid crab, *Cryptodromia pileifera* Alcock, 1899 (Decapoda: Dromiidae) in the laboratory. *Journal of Crustacean Biology* 6(1): 111–118. <https://doi.org/10.2307/1547934>
- Tavares M, Lemaitre R (2014) New morphological and distributional information on Homolodromiidae and Homolidae (Decapoda: Brachyura) from the Americas, with description of a new species and comments on western Pacific species. *Journal of Crustacean Biology* 34(4): 504–524. <https://doi.org/10.1163/1937240X-00002243>
- Wear RG (1967). Life history studies on New Zealand Brachyura 1. Embryonic and post embryonic development of *Pilumnus novaezealandiae* Filhol, 1886, and of *P. lumpinus* Bennett, 1964 (Xanthidae, Pilumninae). *New Zealand Journal of Marine and Freshwater Research* 1: 482–535. <https://doi.org/10.1080/00288330.1967.9515221>

Taxonomy of the *Proisotoma* complex. VI. Rediscovery of the genus *Bagnallella* Salmon, 1951 and epitoky in *Bagnallella davidi* (Barra, 2001), comb. nov. from South Africa

Mikhail Potapov¹, Louis Deharveng², Charlene Janion-Scheepers^{3,4}

1 Moscow State Pedagogical University, Kibalchicha str., 6, korp. 3, Moscow, 129278, Russia **2** Institut de Systématique, Evolution, Biodiversité, ISYEB-UMR 7205-CNRS, MNHN, UPMC, EPHE, Museum national d'Histoire naturelle, Sorbonne Universités, 45 rue Buffon, CP50, F-75005 Paris, France **3** University of Cape Town, Department of Biological Sciences, Rondebosch, 7701, Private Bag x3, South Africa **4** Iziko Museums of South Africa, Cape Town, 8000, South Africa

Corresponding author: Charlene Janion-Scheepers (charlene.janion-scheepers@uct.ac.za)

Academic editor: Wanda M. Weiner | Received 8 July 2021 | Accepted 20 October 2021 | Published 23 November 2021

<http://zoobank.org/99A66CB2-FE4B-466C-B679-1B0589A50DFC>

Citation: Potapov M, Deharveng L, Janion-Scheepers C (2021) Taxonomy of the *Proisotoma* complex. VI. Rediscovery of the genus *Bagnallella* Salmon, 1951 and epitoky in *Bagnallella davidi* (Barra, 2001), comb. nov. from South Africa. ZooKeys 1072: 167–186. <https://doi.org/10.3897/zookeys.1072.71307>

Abstract

The genus *Bagnallella* Salmon is restored and given a diagnosis. It takes an intermediate position between *Proisotoma* Börner and *Cryptopygus* Willem complexes and is characterized by the separation of the two last abdominal segments (like in *Proisotoma*) and 3 and 5 s-chaetae on the fourth and fifth abdominal segments (like in *Cryptopygus* and its allies). A list of and key to species belonging to *Bagnallella* is given. *Bagnallella biseta* **comb. nov.**, *B. dubia* **comb. nov.**, *B. sedecimoculata* **comb. nov.**, and *B. tenella* **comb. nov.** are commented and redescribed. Morphology of *Bagnallella davidi* (Barra), **comb. nov.** is described from the specimens from South Africa. So far *B. davidi* appears to be a complex of forms differing in size of the furca and macrochaetae. Two types of strongly modified males were found and described. Antennae, ventral side of abdomen, posterior edge of abdominal tergites, and mandibles are affected with epitoky. The nature of the discovered strong polymorphism is unclear.

Keywords

Collembola, polymorphism, supermale

Introduction

Knowledge on the Collembola of South Africa has increased significantly over the last decade, with most new species described from the Western Cape Province where the majority sampling has been made (Janion-Scheepers et al. 2015). From these collections, a rich diversity of Isotomidae has been discovered, including *Parisotoma* (Potapov et al. 2011) and *Cryptopygus* (Potapov et al. 2020). From these collections, we also recorded three known species (*P. davidi*, *P. tenella*, *P. sedecimoculata*), which resemble the genus *Cryptopygus* but have Abd. V and VI separated. Thus, these species cannot be attributed to any genus of the *Cryptopygus* complex but rather belong to the *Proisotoma* complex. This paper determines the position of these three species by recovering a genus erected in the past by Salmon (1951). Also, several other species mostly distributed in the Southern Hemisphere belong to this taxon. In addition, we describe an unusual polymorphism in *Proisotoma davidi* (Barra, 2001) which remains unsolved.

Materials and methods

Abbreviations

A.B.	A. Bedos
Abd. I–VI	abdominal segments I–VI
Ant. I–IV	antennal segments I–IV
bms	basal micro s-chaeta on antennal segments
C.J.	C. Janion-Scheepers
L.D.	L. Deharveng
M	macrochaeta
MNHN	Museum national d’Histoire naturelle
ms	micro s-chaeta(e) (= microsensillum(a) auct.)
PAO	postantennal organ
s-chaetae	macro s-chaeta or s-chaetae (= macrosensillum(a) or sensillum(a) auct.)
SAMC	South African Museum, Cape Town
Th. II–III	thoracic segments II and III
Ti	tibiotarsus

Redescription of the genus *Bagnallella* Salmon, 1951

Bagnallella Salmon, 1951

Type species. *Folsomia sedecemoculata* Salmon, 1943

Diagnosis. Anurophorinae with all abdominal segments clearly separated and a *Proisotoma*-like furca: manubrium with few anterior chaetae (1+1-3+3), dens slender,

crenulated, with rather numerous anterior and posterior chaetae, mucro clearly set off from dens, with two or three teeth. 7+7-8+8 ocelli in known species. With simple or bifurcate maxillary palp and four sublobal hairs, two or four prelabral chaetae. Macro s-chaetae 22235 on Abd.I-V. Tergal macro s-chaetae on abdomen situated in front of p-row of chaetae. B-row of chaetae on Ti.1–2 complete (both B4 and B5 present). Ventral chaetae on Th.III present or absent. Sexual dimorphism present or absent.

Position of the genus in the subfamily Anurophorinae. To date an appropriate generic name did not exist for the small group species related to *Proisotoma* Börner, 1901 sensu lato which were discussed in the monograph of Potapov et al. (2006). This group, so-called “*Proisotoma tenella, ripicola, biseta*”, consists of forms sharing characters such as: the three last abdominal segments separated, manubrium with anterior chaetae, four prelabral chaetae, and presence of three and five s-chaetae on Abd.IV and V, respectively.

Recently, one more species, *Proisotoma sedecimoculata* (Salmon, 1943), became a probable candidate to belong to this group (Potapov and Janion 2017). This species was described by Salmon (1943) as *Folsomia sedecimoculata* and was afterwards proposed as a generotype for the new genus *Bagnallella* Salmon, 1951. *Bagnallella* was erected based on three last abdominal segments fused, bidentate mucro and eight ocelli. Later, *Bagnallella* was lost in the taxonomy of the subfamily and was mostly treated as a junior synonym of either *Folsomia* or *Proisotoma*. After the examination of the type specimen, it was discovered that the three last abdominal segments were actually separated (Potapov and Janion-Scheepers 2017). Here, we suggest restoring *Bagnallella* for the group of species mentioned above, rather than erecting a new generic name. Several other forms described under different generic names also fit to *Bagnallella* at lesser or larger degree of accuracy. For these species, the two *Bagnallella* key characters were mentioned in the associated descriptions or were seen by us, apart from three forms with unknown sensillar chaetotaxy. Nevertheless, we suppose the last ones (notated with question marks in the list of species of *Bagnallella* below) belong to the genus. Among these species, *Bagnallella sedecimoculata* is poorly described and so is not the best to be a generotype, but we prefer to keep a generic name already created by John Salmon.

The incertae sedis genus *Bagnallella* combines the characters of two large generic groups by the separation of its two last abdominal segments and the presence of three and five s-chaetae on Abd.IV and V respectively in characteristic position. The former character is a diagnostic feature of the *Proisotoma* Börner, 1901 complex, the latter indicates basic set of s-chaetae in *Cryptopygus* Willem, 1902 and related genera belonging to *Cryptopygus* complex (Potapov et al. 2006, 2013, 2020). The latter complex is characterized by the fusion of the two last abdominal segments. The genus *Bagnallella* takes a neatly intermediate position between *Cryptopygus* (*Cryptopygus* complex, Southern Hemisphere) and *Scutisotoma* (*Proisotoma* complex, Northern Hemisphere). The three genera share, apart from the characters of the subfamily, the presence of a furca, a mid-tergal position of macro s-chaetae on body tergites, and the absence of any specific apomorphy. The combinations of the two key characters mentioned above are shown in Figure 1. After the separation of the two last abdominal segments, we suggest treating *Bagnallella* in the *Proisotoma* complex.

Distribution and ecology of *Bagnallella*. The genus is distributed worldwide. More local species (*B. davidi*, *B. douglasi*, *B. mishai*, *B. biseta*, *B. koepckeii*) are distributed in the Southern Hemisphere that indicates further relation to the “austral” genus *Cryptopygus*. Due to apparent ruderal *B. tenella* and pioneer *B. ripicola*, the genus also occurs in the Northern Hemisphere. The ecology of the former species is especially remarkable, as *B. tenella* is often recorded in mass abundances (Agrell 1939; Arle 1970; Neves and Mendonça 2016). We speculate that *B. davidi* has an unusual biology and ecology due to its morphological modifications (described below).

World list of the genus *Bagnallella*

- Bagnallella biseta* (Rapoport, 1963), comb. nov.
Bagnallella davidi (Barra, 2001), comb. nov.
Bagnallella dubia (Deharveng, 1981), comb. nov.
Bagnallella douglasi (Mendonça, Queiroz & Silveira, 2015), comb. nov.
 ? *Bagnallella koepckeii* (Winter, 1967), comb. nov.
Bagnallella mishai (Mendonça et Silveira, 2019), comb. nov.
 ? *Bagnallella nigromaculosa* (Folsom, 1932), comb. nov.
 ? *Bagnallella paronai* (Börner, 1907), comb. nov.
Bagnallella ripicola (Linnaniemi, 1912), comb. nov.
Bagnallella sedecimoculata (Salmon, 1943), comb. nov.
Bagnallella tenella (Reuter, 1895), comb. nov.

Key to known species of *Bagnallella**

- | | | |
|---|---|---|
| 1 | Mucro tridentate (Fig. 10) | 2 |
| – | Mucro bidentate (Fig. 3) | 3 |
| 2 | Dens with 4 anterior and 4 posterior chaetae (Fig. 10) | |
| | <i>B. davidi</i> (Barra), South Africa | |
| – | Dens with 15–16 anterior and 12–13 posterior chaetae | |
| | <i>B. mishai</i> (Mendonça & Silveira), Brazil | |
| 3 | Manubrium with 1+1 anterior chaetae (Fig. 3) | 4 |
| – | Manubrium with 2–3+2–3 anterior chaetae (Fig. 7) | 6 |
| 4 | Dens with more than 20 anterior and 15 posterior chaetae. 4 prelabral chaetae | |
| | <i>B. ripicola</i> (Linnaniemi), Europe | |
| – | Dens with fewer than 17 anterior and 8 posterior chaetae (Figs 2, 3). 2 prelabral chaetae | 5 |
| 5 | Ventrum of Th.III with chaetae | <i>B. dubia</i> (Deharveng), sub-Antarctic |
| – | Ventrum of Th.III without chaetae | |
| | <i>B. sedecimoculata</i> (Salmon), New Zealand | |

* Some known species of the Proisotoma complex with insufficient description may belong to the genus *Bagnallella*.

- 6 Manubrium with 2+2 anterior chaetae, 7 ocelli
 *B. douglasi* (Mendonça, Queiroz & Silveira), Brazil
 – Manubrium with 3+3 anterior chaetae, 8 ocelli7
 7 Dens with more than 40 anterior chaetae.....
 *B. biseta* (Rapoport), Argentina, *B. koepcke* (Winter), Peru**
 – Dens with fewer than 30 anterior chaetae (Fig. 7)
 *B. tenella* (Reuter), cosmopolitan, *B. nigromaculosa* (Folsom), Hawaii Is**

Descriptions and remarks to species of the genus. Below we give the diagnosis, description, remarks, and distribution, with, if possible, ecological remarks of all species of *Bagnallella*. Some sections may be omitted if the associated species have good morphological descriptions in the literature.

***Bagnallella biseta* (Rapoport, 1963), comb. nov.**

Proisotoma biseta Rapoport, 1963

Material examined. Adult male from Argentina under label “Tucuman, 19/4/59, entre maderas ...”, deposited in the Museum national d’Histoire naturelle (MNHN), Paris, France. This individual was obviously among the material the original description was based on by E.H. Rapoport.

Diagnosis. Maxillary palp bifurcate, four prelabral chaetae. Dens with ~50 anterior chaetae. Mucro bidentate. Anterior side of manubrium with 3+3 chaetae. 33/22235 s and 11/111 ms on body. Ventral chaetae absent on Th.III.

Description. Maxillary outer lobe with four sublobal hairs, maxillary palp bifurcate. Labral formula as 4/5,5,4. Guard chaeta e7 present on labium. Ant. III without bms and with five distal s (including one lateral), without additional s-chaetae. Th. I, II, and III without ventral chaetae. S-formula as 33/22235 (s), 11/111 (ms). Tibiotarsal tenent chaetae (1,1,1) clearly clavate. Tibiotarsi 1–2 with more than 24 chaetae. Ventral tube with 6+5 chaetae (in the adult male studied). Retinaculum with 4+4 teeth and two chaetae. Dens long and slender, with numerous crenulations, many (~50) anterior and 17 (in the adult male studied) posterior chaetae. Anterior side of manubrium with 3+3 chaetae. Mucro bidentate.

Discussion. Our redescription is based on one individual of E. Rapoport, and more material is needed to complete the understanding of *B. biseta*. The species obviously belongs to the genus *Bagnallella* by separation of two last abdominal segments and s-chaetotaxy of Abd.IV and V. After chaetotaxy of tibiotarsi, ventral tube, and dens, *B. biseta* appears to be a more polychaetotic species than its congeners. The close relation of *B. biseta* and *B. tenella* (sharing 3+3 manubrial chaetae) is doubtful due to

** At present *Bagnallella biseta* cannot be reliably discriminated from *Proisotoma koepcke* based on the existing descriptions. A similar problem exists with *B. tenella* and *P. nigromaculosa*.

difference in maxillary palp (bifurcate vs simple). The independence of *B. koepckei* and *B. paronai* from *B. biseta* call for further verification. *Bagnallella paronai* is not included in the key due to the incomplete diagnosis.

Distribution. Argentina and Chile (see Mari Mutt and Bellinger 1990 for details).

***Bagnallella dubia* (Deharveng, 1981), comb. nov.**

Figures 3, 4

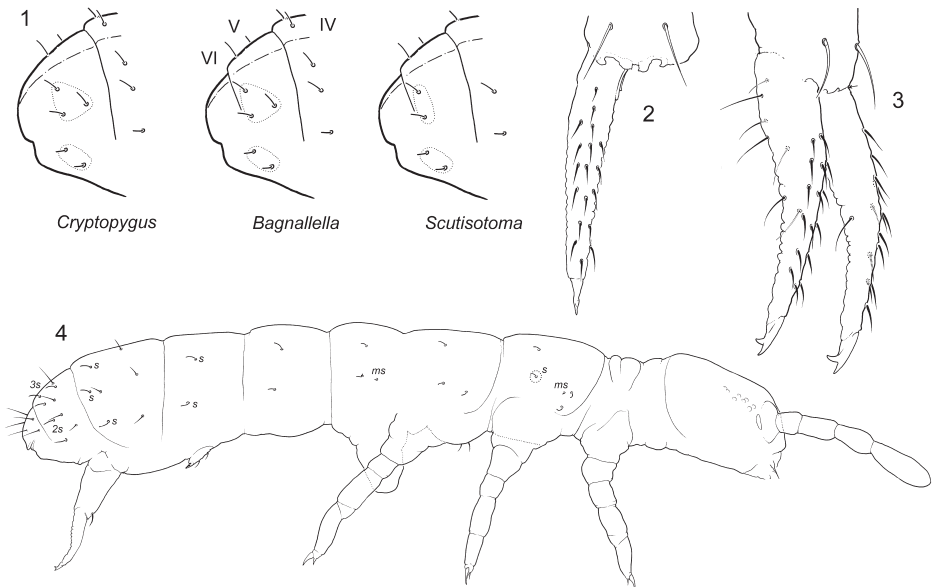
Cryptopygus dubius Deharveng, 1981

Material examined. New Zealand, South Island, Central Otago, Pisa Range and Old Man's Range, high alpine zone, different sites, 17.02.2014, M. Minor leg.

Diagnosis. Maxillary palp bifurcate, two prelabral chaetae. Dens with 12–16 anterior chaetae. Mucro bidentate. Anterior side of manubrium with 1+1 chaetae. 33/22235 s and 10/100 ms on body. 2+2 ventral chaetae on Th.III.

Description. Colour grey. Cuticle, ocelli, outer mouth parts, and antennae as in *B. sedecimoculata*. PAO as long as 0.8–0.9 Ant. I and as 1.4–1.5 as long as Claw III. Ventral side of head with 4+4 postlabial chaetae. Th.III with 2+2 ventral axial chaetae.

Macrochaetae weakly differentiated, medial ones on Abd.V about as long as 0.4–0.5 of tergal midline. S-chaetae weakly differentiated. S-formula as 43/22235 (s), 10/100 (ms) (Fig. 4). S-chaetae on Abd.I–III in mid-tergal position. Tibiotarsi 1–2



Figures 1–4. S-patterns of Abd. IV–VI in the genera *Cryptopygus* *Bagnallella* and *Scutisotoma* (1) *B. sedecimoculata* (2) and *B. dubia* (3, 4) 2, 3 furca, anterior view 4 macrochaetae and s and ms-chaetae on body. s = s-chaetae, ms = ms-chaetae.

with 21 chaetae, Tibiotarsi 3 with few additional chaetae. Tibiotarsal tenent chaetae not developed. Ventral tube with 4+4 laterodistal and usually with five posterior chaetae. Retinaculum with 4+4 teeth and two chaetae. Anterior furcal subcoxae with 13–15 chaetae, posterior ones with 7–9. Anterior side of manubrium with 1+1 distal chaetae. Dens with 12–16 anterior chaetae, posterior side of dens with crenulation and seven chaetae (Fig. 3). Mucro bidentate. Ratio of manubrium : dens : mucro = 6.0–6.7 : 5.0–6.0 : 1. Males present, with two thin spurs on Tibiotarsi I.

Discussion. This species was named after its dubious position in generic system of *Proisotomal Cryptopygus* (Deharveng 1981). It resembles *B. sedecimoculata* (see the Discussion below) and apparently belongs to the genus *Bagnallella* by separation of two last abdominal segments and s-chaetotaxy of Abd.IV and V. Our specimens from New Zealand match the first description.

Distribution. *Bagnallella dubia* was described from Marion Island and recorded in Macquarie Island (Greenslade and Wise 1986) and alpine sites of New Zealand (Babenko and Minor 2015). The species is possibly widely distributed in cold sites of high altitudes of the Southern Hemisphere. Its occurrence in Australia (Greenslade 2006) needs to be verified.

***Bagnallella douglasi* (Mendonca, Queiroz & Silveira, 2015), comb. nov.**

Proisotoma douglasi Mendonca, Queiroz & Silveira, 2015.

Discussion. The species can be attributed to *Bagnallella* by the two key characters of the genus. It is characterized by 33/22235 s, 11/111 ms, bifurcate maxillary palp, long polychaetotic dens (34-35/14), and bidentate mucro. The presence of seven ocelli and 2+2 chaetae on anterior side of manubrium are two unique characters among members of the genus.

Distribution. This species is currently only known from SE Brazil.

***Bagnallella mishai* (Mendonca & Silveira, 2019), comb. nov.**

Scutisotoma mishai Mendonca & Silveira, 2019

Discussion. It is an easily recognizable species by 43/22235 s, 11/111 ms, simple maxillary palp, dens (15-16/12-13), and tridentate mucro.

Distribution. One locality in southeastern Brazil.

***Bagnallella ripicola* (Linnaniemi, 1912), comb. nov.**

Proisotoma ripicola Linnaniemi, 1912

Diagnosis. Maxillary palp bifurcate, four prelabral chaetae. Ant. I with many additional chaetae. Dens long and slender, with 20–30 anterior chaetae or more. Mucro bidentate. Anterior side of manubrium with 1+1 chaetae. 33/22235 s and 11/111 ms on body. Lateral s-chaetae on Abd.IV shifted to ventral side. Without ventral chaetae on Th.III.

Discussion. The full redescription is given by Fjellberg (2007).

Distribution and ecology. Europe. It prefers sandy places along the edge of water.

Bagnallella sedecimoculata (Salmon, 1943)

Figure 2

Folsomia sedecimoculata Salmon, 1943

Holotoma sedecimoculata (Salmon, 1943)

Proisotoma sedecimoculata (Salmon, 1943)

Material examined. South Africa, Western Cape, Stellenbosch, Jonkershoek Nature Reserve, canyon to waterfall, SAF-086, 34.005570°S, 18.992067°E, 15/03/2008, forest litter, Berlese, L.D. and A.B. leg.; Somerset, Helderberg, SAF-107, SAF-109, SAF-116, 34.040883°S, 18.873649°E, alt. 600 m, 04/03/2009, native forest litter, L.D. and A.B. leg.; Cape Town, Wynberg, Table Mountain, second collapse, SAF-141, 33.987637°S, 18.405750°N, alt. 725 m, 10/03/2009, native forest litter, L.D. and A.B. leg.; Constantia, Silvermine, in a small forest patch above Tokai, SAF-235, 34.038273°S, 18.395478°E, alt. 390 m, 06/11/2010, dead wood, D. Porco leg.; Kalk Bay, Echo Valley, Spes Bona forest, SAF-555, 01/03/2019, Afromontane forest, moss on rock, L.D. and A.B. leg.

New Zealand. NZL-049, Rotoiti: Lakes Rototonga and Rotoatua, 08/01/1996, primary forest, litter, L.D. and A.B. leg.

Australia. Victoria, July 2010, University Ballarat, St. Helens, 37.629979°S, 143.890801°E, *Eucalyptus* plantation, moss, P. Greenslade leg.

Macquarie Island, Bauer Bay, 54.5549°S, 158.8760°E, April 2016, Turf sample, Berlese extraction, L. Phillips leg.

Diagnosis. Maxillary palp bifurcate, two prelabral chaetae. Dens slender, with 16–20 anterior chaetae. Mucro bidentate. Anterior side of manubrium with 1+1 chaetae. 33/22235 s and 10/100 ms on body. Without ventral chaetae on Th.III.

Description. Colour grey. Cuticle outwardly smooth. 8+8 ocelli, G and H smaller. PAO about as long as 0.8 Ant. I and as 1.1–1.3 Claw III. Maxillary outer lobe with four sublobal hairs and bifurcate maxillary palp. Labral formula as 2/554. Labium full set of guards (e7 present), three proximal and four basomedian chaetae. Ventral side of head with 4–5+4–5 postlabial chaetae. 11 chaetae on Ant.I, with three basal micro s-chaetae (*bms*), of which one *bms* large, and two ventral s-chaetae (*s*), Ant.II with three *bms* and one laterodistal *s*, Ant.III with one *bms* and six distal *s* (including two lateral). Thorax without ventral axial chaetae.

Macrochaetae weakly differentiated, medial ones on Abd.V as long as 0.4–0.5 of tergal midline. S-chaetae weakly differentiated. S-formula as 43/22235 (s), 10/100 (ms). S-chaetae on Abd.I–III in mid-tergal position. General pattern of chaetotaxy as in *B. dubia* (Fig.4). Ti.1–2 with 21 chaetae, Ti.3 with few additional chaetae. Tibio-tarsal tenent chaetae not developed. Ventral tube with 4+4 laterodistal and usually with six posterior chaetae (four in a transversal row). Retinaculum with 4+4 teeth and two chaetae. Anterior furcal subcoxae with 11–15, posterior ones with 7–9 chaetae. Anterior side of manubrium with 1+1 distal chaetae (Fig. 2). Dens with 17–19(16–20) anterior chaetae, posterior side of dens with crenulation and seven chaetae (Fig. 2). Mucro bidentate. Ratio of manubrium : dens : mucro = 5.3–6.3 : 5.9–6.7 : 1.

Discussion. *Bagnallella sedecimocolata* was described from New Zealand and was designated as type species for the genus *Bagnallella* (see the discussion to the genus above). The type specimen from New Zealand was studied (Potapov and Janion 2017), although only one generic character (separation of two abdominal segments) was proven. The redescription given above is based mostly on the South African material which looks conspecific to one individual in hand from New Zealand (L.D. and A.B. leg.). *Bagnallella sedecimocolata* resembles *B. dubia* and differs by ventral chaetae on Th.III (absent vs present) and a few more anterior chaetae on dens (16–20 vs 12–16). The latter character is not stable enough to separate the two species.

Distribution. Probably widely distributed. So far with scattered records in the South Hemisphere (New Zealand, Australia, South Africa, Macquarie Island).

Bagnallella tenella (Reuter, 1895), comb. nov.

Figures 5–8

Isotoma tenella Reuter, 1895

Proisotoma tenella (Reuter, 1895)

Proisotoma simplex Folsom, 1937

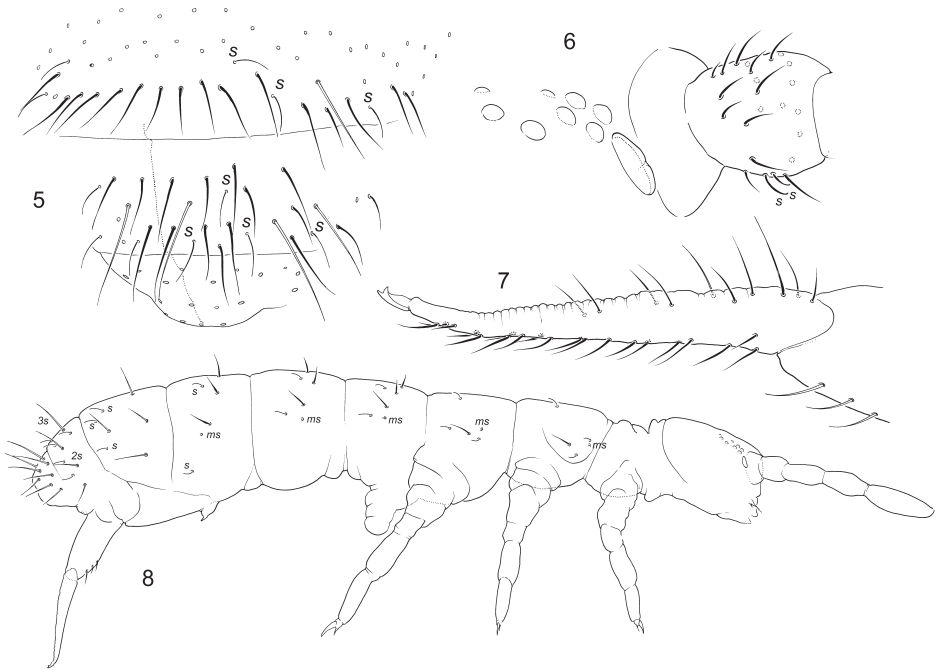
Proisotoma alba Yosii, 1939

Material examined. South Africa, Western Cape, Haarwegskloof, Swellendam, 34.3425°S, 20.3167°E, 18.vii.2017, litter trap (R17) with *Dicerotheramnus rhinocerotis* litter, O. Cowan leg.; Haarwegskloof, Swellendam, 34.3444°S, 20.3225°E, 18.vii.2017, litter trap (A17) with *Medicago sativa* litter, O. Cowan leg.; Eastern Cape, Baviaanskloof, 33.7311°S, 23.9655°E, 24.iv.2013, BAV_F_49, A. Liu leg.; Free State Province, Bankfontein Farm, 30.0567°S, 24.8942°E, 24.iv.2019, Berlese-Tullgren, tree leaf litter, H. Badenhorst leg.

Cuba, Cienfuegos Province, 1984, J. Banasco-Almenteros leg.

Indonesia, Lombok Island, vic. Toko Nusa Sari, marine beech, 8.7411° S, 116.0011° E, 4.IV.2017, V. Makarov leg.

Brazil, Espirito Santo, Domingos Martins, Arace, 4.VII.2000, M. Culik leg.



Figures 5–8. *Bagnallella tenella* **5** chaetotaxy of posterior part of Abd. IV, Abd.V and VI **6** ocelli, PAO, and Ant. I **7** furca, lateral view **8** macrochaetae and s and ms-chaetae on body. s = s-chaetae, ms = ms-chaetae.

Diagnosis. Maxillary palp simple. Four prelabral chaetae. Dens slender, with ca 20–30 anterior chaetae. Mucro bidentate. Anterior side of manubrium with 3+3 chaetae. 33/22235 s and 11/111 ms on body. No ventral chaetae on Th.III.

Description. Colour grey of different intensity. Cuticle outwardly smooth. 8+8 ocelli, G and H smaller. PAO (Fig. 6) about half as long as width of Ant.I and 0.8–0.9 as long as Claw 3. Maxillary outer lobe with four sublobal hairs and simple maxillary palp. Labral formula as 4/554. Labium without guards e7, with three proximal and four basomedian chaetae. Ventral side of head with 4-5+4-5 postlabial chaetae. With several additional chaetae on Ant.I. Ant.I with three basal micro s-chaetae (*bms*), one dorsal large, Ant.II with three *bms*, Ant. III without *bms*. Thorax without ventral axial chaetae. Macrochaetae rather long, differentiated (11/3334), medial ones on Abd.V about as long as tergal midline. S-chaetae on tergites slightly shorter than ordinary chaetae. S-formula as 33/22235 (s), 11/111 (*ms*) (Figs 5, 8). S-chaetae subequal, on Abd.I–III in mid-tergal position. Micro s-chaetae on Abd.I–II in front of lateral s-chaetae, on Abd.III between medial and lateral s-chaetae (Fig. 8). Tibiotarsal tenent chaetae (1,1,1) often present, weakly clavate (see Discussion). Retinaculum with 4+4 teeth and 1–2 chaetae. Furca long. Anterior side of manubrium with 3+3 chaetae arranged in two lines (Fig. 7). Dens with more than 20 anterior chaetae, posterior side of dens with crenulation and 7–10 chaetae (Fig. 7). Mucro bidentate. Ratio of manubrium : dens : mucro = 7–8 : 9 : 1.

Discussion. The species belongs to the genus *Bagnallella* by having two last abdominal segments separated and three and five s-chaetae on Abd. IV and V. It shares 3+3 anterior chaetae on manubrium with *B. biseta*, *B. koepcke*, and *B. paronai* from South America from which it differs by fewer chaetae on dens.

Number of posterior chaetae on dens, clavate tibiotarsal chaetae, and chaetae on retinaculum vary. We treat all this variation within one species, but further study is needed. The independence of *Proisotoma nigromaculosa* (Hawaiian Islands) is doubtful.

Although we have no material from Europe, Stach's (1947) concept of *P. tenella* based on the specimens from Poland is accepted by us (for details see Potapov 2001; Fjellberg 2007). Our tropical material fits Stach's (1947) descriptions.

Distribution and ecology. Widely distributed cosmopolitan species. Common in tropics. In higher latitudes only in protected soils.

Description of *Bagnallella davidi* and its forms in South Africa

Bagnallella davidi (Barra, 2001), **comb. nov.**

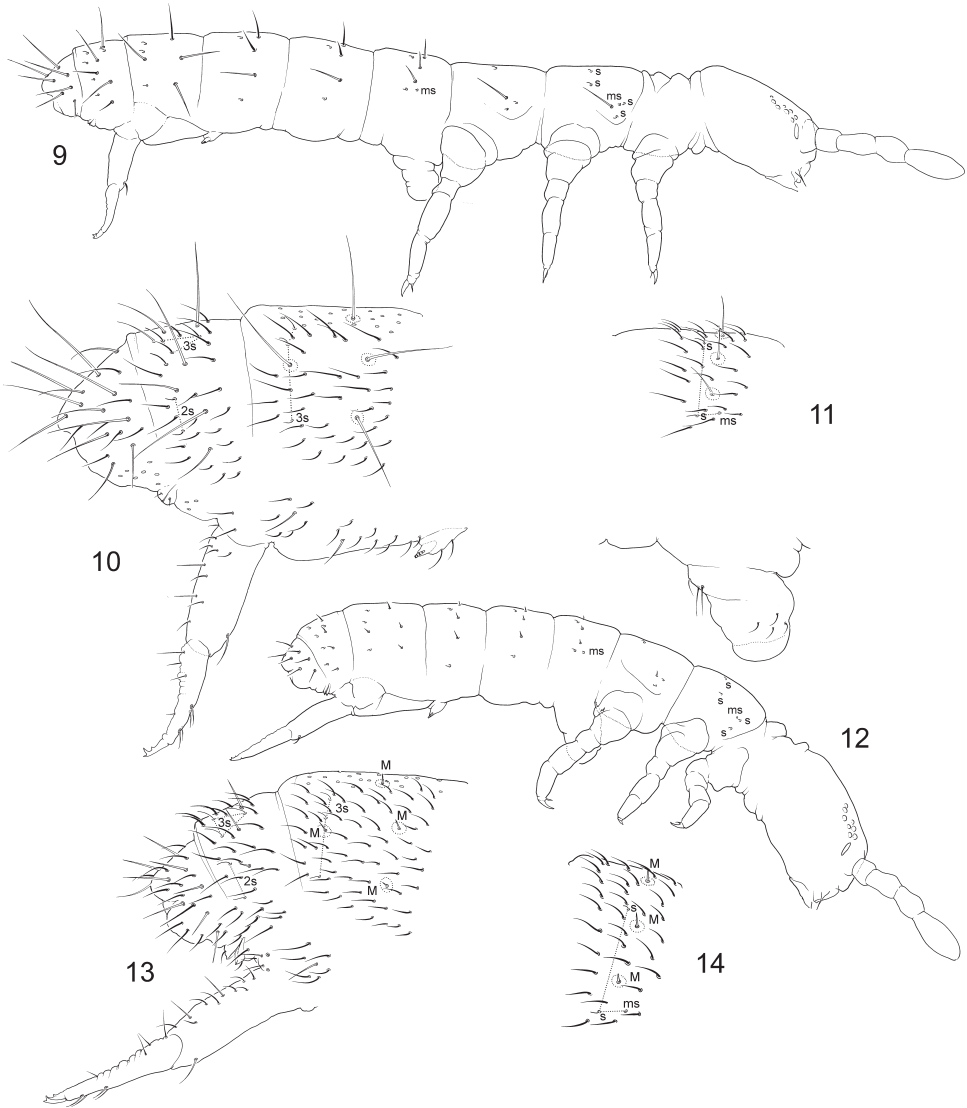
Figures 9–24

Proisotoma davidi Barra, 2001

Material examined. Typical form: South Africa, Free State Province, Bankfontein Farm, 30.0567°S, 24.8942°E, 24.iv.2019, Berlese-Tullgren: tree leaf litter, H. Badenhorst leg.; South Africa, Western Cape, Haarwegskloof, Swellendam, 34.3422°S, 20.3169°E, 18.vii.2017, litter trap (G18) with *Pentameris eriostoma* litter, O. Cowan leg., South Africa, SAF 583 (11.m CJ SWB); Prince Albert: Swartberg North: road to Swartberg Pass, 11/03/2019, meadow, moss, C.J. leg.

Short-haired form: South Africa, Western Cape, Haarwegskloof, Swellendam, 34.3534°S, 20.3042°E, 18.vii.2017, litter trap (A4) with *Medicago sativa* litter, O. Cowan leg.; Cederberg Wilderness area, Litter trap CED588; South Africa, Western Cape, Cederberg Wilderness area, Litter trap CED394; Jonkershoek Nature Reserve, 33.9891°S, 18.9575°E, 05.ix.2011, Litter trap (J4, 124); Jonkershoek Nature Reserve, 33.9891°S, 18.9575°E, 30.vii.2009, Litter trap, C.J. leg.; J2, 32.1; Landdroskop, Jan. 2012, H. Basson leg.; Prince Albert, Swartberg North, Swartberg crest, 12/03/2019, SAF-612, SAF-618, meadow, litter and soil, L.D., C.J. and A.B. leg.

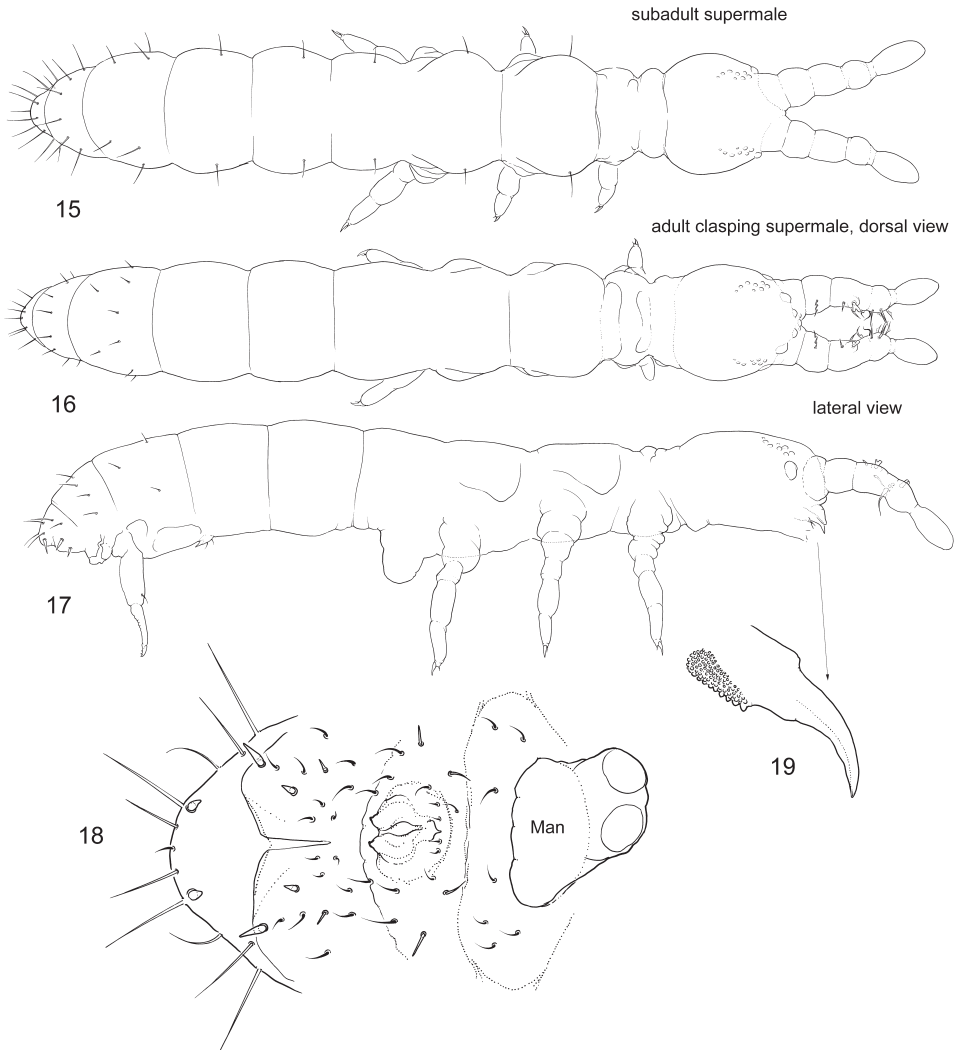
Intermediate form: South Africa, Western Cape, Haarwegskloof, Swellendam, 34.3345°S, 20.3187°E, 18.vii.2017, litter trap (R24) with *Dicerotheramnus rhinocerotis* litter, O. Cowan leg.; Prince Albert, Swartberg North, Swartberg crest, SAF-612, 12/03/2019, meadow, litter, L.D., C.J. and A.B. leg.; Prince Albert, Swartberg North, Swartberg crest, SAF-618, 12/03/2019, meadow, soil, L.D., C.J. and A.B. leg.; Prince Albert, Swartberg North, road to Swartberg Pass, SAF-601, 12/03/2019, meadow, litter and soil, L.D., C.J. and A.B. leg.; Prince Albert, Swartberg North, Swartberg crest, SAF-614, 12/03/2019, moss on rock, Berlese, L.D., C.J. and A.B. leg.



Figures 9-14. *Bagnallella davidi*, normal long-haired (9-11) and short-haired form (12-14) 9, 12 macrochaetae and s and ms-chaetae on body 10, 13 posterior part of abdomen 11, 14 Abd.I. s = s-chaetae, ms = ms-chaetae.

“Clasping supermales”: SAF-601, South Africa: Western Cape: Prince Albert: Swartberg North: road to Swartberg Pass, 12/03/2019, meadow, litter and soil, L.D., C.J. and A.B. leg.

“Spiny supermales”: SAF-554; South Africa: Western Cape: Kalk Bay: Echo Valley: Spes Bona forest, 01/03/2019, Afromontane forest, moss and lichen on rock, L.D. and A.B. leg.



Figures 15–19. *Bagnallella davidi*, the “clasping supermale” **15** subadult individual, dorsal view **16, 17** adult, dorsal **16** and lateral **17** views **18** posterior part of abdomen in adult male, ventral view **19** mandible. Man = Manubrium.

Diagnosis. 3+3 postlabial chaetae. Maxillary palp simple. Dens with four anterior and four posterior chaetae. Mucro tridentate, teeth arranged in a line. Anterior side of manubrium with 1+1 chaetae. 43/22235 s and 10/100 ms on body (Figs 9–11). No ventral chaetae on Th.III. Typical form of species with long macrochaetae (Fig. 10).

Description. Maxillary outer lobe with four sublobal hairs, maxillary palp simple. Labral formula as 4/5,5,4. Labium with five usual papillae (–E) and labial formula A1B4C0D4E6, guard chaeta e7 absent, three proximal and four basomedian chae-

tae. Ventral side of head with 3+3 chaetae. PAO shorter than Ant.I width (0.6–0.8). Ant. I with 11 common chaetae, two ventral s-chaetae (s) and three bms, of which one dorsal long, chaeta-like (this ms was calculated together with common chaetae in first description, 12 at whole); Ant. II with three bms and one latero-distal s; Ant. III with one bms and with six distal s (including two lateral), without additional s-chaetae. Organite pin-like, not very small. Empodial appendage about half as long as Claw. Anterior and posterior furcal subcoxae with 9–14 and 7–8 chaetae, respectively. Male spurs on tibiotarsi 3 thin, stick-like. Th. I–III without ventral chaetae. Ratio manubrium : dens : mucro as 4.4–5.0 : 3.3–3.8 : 1; dens : Claw as 3.3–3.6 (for the typical form).

Discussion. *Bagnallella davidi* is a rather peculiar species of the genus due to few chaetae on dens (vs many more chaetae both on anterior and posterior sides), tridentate mucro (shared with *B. mishai* only), and 3+3 postlabial chaetae (vs 4+4 or more in other species). The first description is almost complete and, therefore, we made very few additions concerning mouth parts. The species exhibits high variation in length of macrochaetae and show different modifications of males. All the forms (described below) can indicate either high plasticity of a single species or the complex of separate although closely related species, calling for further morphological, biological, ecological, and molecular investigations.

Distribution. Eastern Cape, Amatola Mountains (type location) and widely in the Western Cape and Free State (our material) provinces of South Africa.

Polymorphism of *Bagnallella davidi*

1. “Typical” form (Figs 9–11). *B. davidi* was described in this form (Barra 2001). Macrochaetae on body segments are long. Ratios: Mac on Abd.V as long as 0.7–1.0 of tergal midline. Mac : Abd.V width = 0.7–1.0; Mac : mucro = 3.3–4.1; Mac : dens = 0.8–1.1 (Fig. 9). In *Proisotoma* complex, so long macrochaetae is a unique character among species of *Bagnallella* and sometimes occur in the genera *Weberacantha* Christiansen, *Narynia* Martynova and *Folsomides* Stach. This form was found in juvenile and fully adult specimens, both in females and males.

2. “Short-haired” form (Figs 12–14). Macrochaetae are short, shorter than common chaetae on most abdominal segments. Ratios: Mac : Abd.V Mac on Abd.V as long 0.2–0.3 of tergal midline; Mac : mucro = 0.9–1.4; Mac : dens 0.2–0.3. In spite of their small size, macrochaetae are erect and stiff and so well recognized indicating their possible ecomorphic nature although the integument and mouthparts are not modified. Head and furca appear to be relatively larger than in typical form. Ratio manubrium : dens : mucro as 5.1–6.6 : 4.1–5.8 : 1; dens : Claw as 3.3–4.5. All other significant characters (s-chaetotaxy, mouth parts, chaetotaxy of extremities) are as in typical form. All instars and both sexes can belong to this form.

We also found individuals with middle-sized macrochaetae (as in Fig. 15), which is on Abd.V twice as long as mucro (vs 3.3–4.1 in typical form and 0.9–1.4 in short-



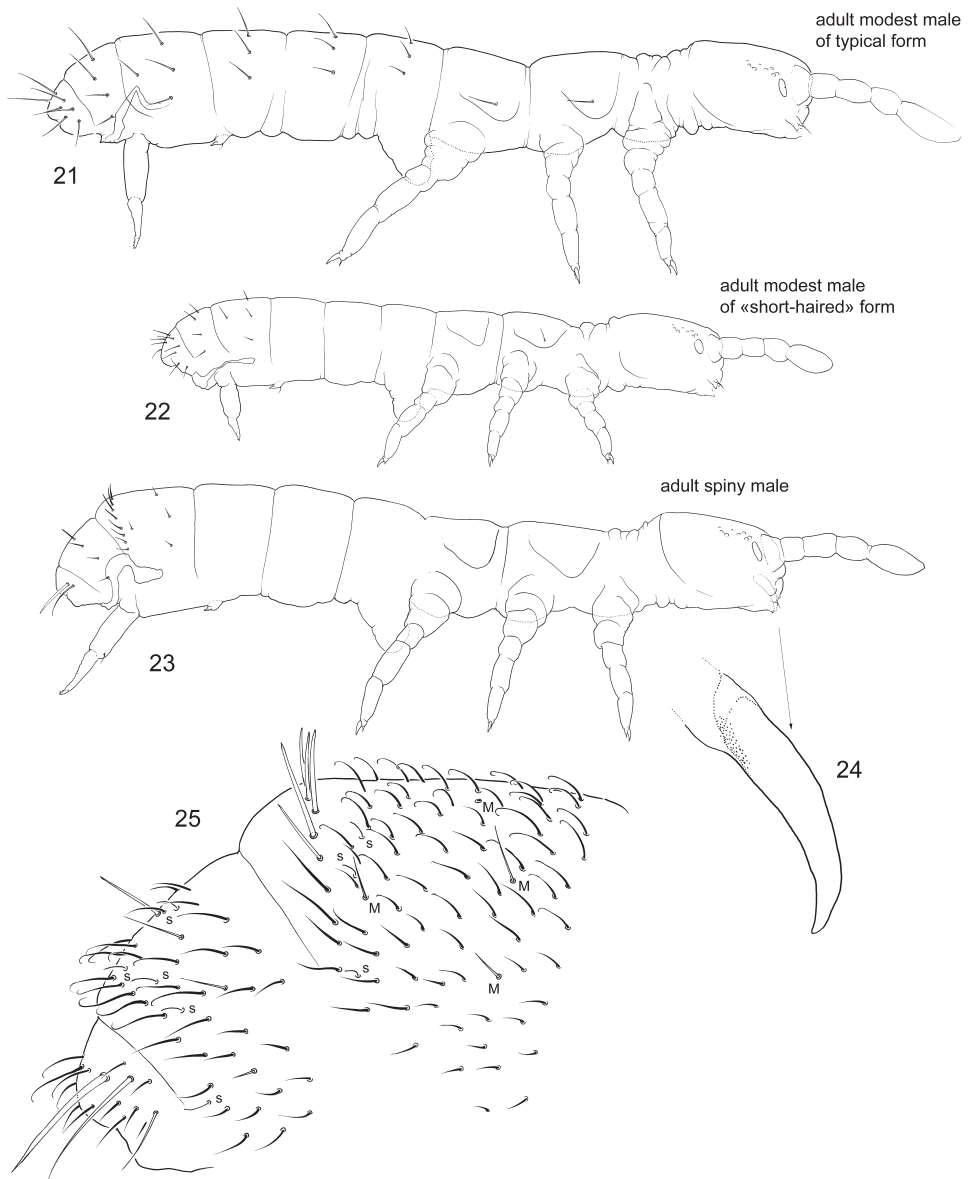
Figures 20. *Bagnallella davidi*, anterior part of head and antennae in adult “clasp supermale”.

haired form) and half as long as dens (vs subequal to dens in typical form and 0.2–0.3 as dens in short-haired form).

Each studied population consists of only one of the forms, and we have not found a continuous range of macrochaetae variability, apart from short-haired clasp supermales occurring in “normal” populations.

3. “Clasp supermales” (Figs 15–20). Ant.I–III expanded and partly fused. Antennae joints probably lost mobility. Inner side of Ant.II and III is armed with thickened, flame-shaped, and bifurcate chaetae which probably form a clasp organ. Front of head have chitinized tubercles. Anal valves are armed with spines. Mandibles without apical teeth. Macrochaetae short. Subadult clasp supermales, i.e., males without fully developed genital plate and without developed ejaculatory duct, have also expanded antennae although without modified chaetae on inner their side. They show normal (longer than on adult supermales) macrochaetae and normal mandibles and have no spines on anal valves (Fig 15–20). The females of the same population belong to the form with middle-sized macrochaetae.

4. “Spiny supermales” (Figs 23–25). One of the males has a row of spiny p-chaetae on Abd.IV and strong thickened macrochaetae on lateral parts of Abd.VI. Other macrochaetae on the body are weakly developed. Common chaetae on dorsum of Abd.IV–VI curved at apex (Fig. 25). Mandibles without apical teeth and molar plate (Fig. 24). Outer mouth parts (labrum, maxillary outer lobe, and labium) not fully developed.



Figures 21–25. *Bagnallella davidi* unmodified (21, 22) and “spiny supermale” (23–25) 21–23 lateral view 24 mandible 25 posterior part of abdomen, lateral view. s = s-chetae, M = macrochaetae.

Unmodified males are much more frequent than the two male forms described above. In most populations, only unmodified males are known. They can show all possible length of macrochaetae and belong to associated forms (Figs 21, 22).

Discussion

If present, the clasping organ of Collembola is formed by two symmetrical complexes associated with, respectively, left and right antennae, or, more rarely, other limbs. Paired “clasps” are evolutionary formed in different taxa, for example, in the family Sminthuridae, *Vertagopus reuteri* (Schött, 1893), *Rhodanella minus* Denis, 1928, *Seira raptora* (Zepelini & Bellini, 2006) (Delamare Deboutteville et al. 1969; Betsch 1980; Fjellberg 1982; Bellini et al. 2009). In “clasping supermales” of *Bagnallella davidi*, all modified chaetae (curved spines, flame-shaped, flattened, and bifurcate) are found on the inner side of the antennae, forming a unique type of clasping organ. This allows males to grasp females between the two antennae at the axial region. The only possible similar case was described in *Vertagopus pseudocinereus* Fjellberg, 1975, which clasps the female with right and left antennae. This species has curved and serrated chaetae on antennae, without any strong modifications (Goloschapova et al. 2006: fig. 2). We can assume that males of *B. davidi* uses this unpaired “clasp” (Fig. 20) in a similar manner, for clasping onto the female.

The function of the spiny row in “spiny supermales” of *B. davidi* is more difficult to explain. The armature of the posterior row on Abd. IV somewhat resembles backward-shifting macrochaetae in males of *Scutisotoma acorrelata* Potapov, Babenko & Fjellberg, 2006, while strong lateral macrochaetae on Abd. VI indicate some similarity to *Ephemerotoma huadongensis* (Chen, 1985), which shows similar armature on both Abd. V and VI (described by Potapov et al. 2015, 2020, respectively).

Acknowledgements

This work was partly funded by the SA (NRF) / Russia (RFBR) Joint Science and Technology Research Collaboration project no. 19-516-60002 (FRBR) and no. 118904 (NRF) awarded to M. Potapov and C. Janion-Scheepers, respectively, and SA-France (Protea I and II) awarded to L. Deharveng. We thank D. Porco, P. Greenslade, O. Cowan, H. Badenhorst, H. Basson, V. Makarov, and M. Culik for providing their material for study, and SANParks and Cape Nature for collecting permits.

References

- Agrell I (1939) Zur Kenntnis der schwedischen Collembolen mit Beschreibung von vier neuen Arten und einigen Varietäten. *Opuscula Entomologica* 1939: 159–168.
- Arlé R (1970) Una nova especie de *Onychiurus* (Collembola – Onychiuridae) de ocorencia periodica em Belem (Para). *Boletim do Museu Paraense Emílio Goeldi. Serie zoologia* 72: 1–11.
- Babenko A, Minor M (2015) *Austrodontella monticola* sp. nov., a new species of Collembola from montane New Zealand. *Zootaxa* 3974: 122–128. <https://doi.org/10.11646/zootaxa.3974.1.9>

- Barra JA (2001) *Proisotoma davidi* sp. nov. from Cape Province (South Africa) (Collembola). Deutsche Entomologische Zeitschrift 48: 23–26. <https://doi.org/10.1002/mmnd.4800480103>
- Bellini BC, Pais AP, Zeppelini D (2009) A new species of *Seira* Lubbock (Collembola: Entomobryidae) from Brazil with sexually dimorphic legs. Zootaxa 2080: 38–46. <https://doi.org/10.11646/zootaxa.2080.1.3>
- Betsch J-M (1980) Éléments pour une monographie des collemboles symphypléones (Hexapodes, Aptérygotes). Mémoires du Museum National d'Histoire Naturelle, Série A, Zoologie 116: 1–227.
- Börner C (1901) Zur Kenntnis der Apterygoten-Fauna von Bremen und der Nachbardistrikte. Beitrag zu einer Apterygoten-Fauna Mitteleuropas. Abhandlungen des Naturwissenschaftlichen Vereins zu Bremen 17: 1–140. <https://doi.org/10.5962/bhl.part.18332>
- Börner C (1907) Collembolen aus Ostafrika, Madagaskar und Südamerika. In: A. Voeltzkow (Ed) Reise in Ostafrika in den Jahren 1903–1905, mit Mitteln der Hermann und Elise geb. Heckmann Wentzel-Stiftung ausgeführt. Wissenschaftliche Ergebnisse., E. Schweizerbart'sche Verlagbuchhandlung, Stuttgart, 47–178.
- Chen BR (1985) Six new species of the family Isotomidae (Collembola). Contributions of Shanghai Institute of Entomology 5: 183–193.
- Deharveng L (1981) Collemboles des Îles subantarctiques de l'Océan Indien, Mission J. Travé 1972–1973. Comité National Française des Recherches Antarctiques 48: 33–109.
- Delamare Deboutteville C, Jacquemart S, Poivre G (1969) Rescription de *Rhodanella minos* (Denis) Bulletin de l'Institut Royal des Sciences Naturelles de Belgique 45: 1–11.
- Denis J (1928) Sur deux collemboles de la Somalie italienne. Le dimorphisme sexuel de *Vertagopus minos* sp. nov. Bollettino della Società Entomologica Italiana 60: 1–6.
- Fjellberg A (1982) Redescriptions of *Vertagopus brevicaudus* (Carpenter, 1900) and *V. reuteri* (Schött, 1893), two arctic species of Collembola (Isotomidae). Entomologia Scandinavica 13: 141–147. <https://doi.org/10.1163/187631282X00048>
- Fjellberg A (1975) *Vertagopus pseudocinereus* n. sp. A new species of Collembola (Isotomidae) from North Norway. Insect Systematics & Evolution 6:212–214. <https://doi.org/10.1163/187631275X00037>
- Fjellberg A (2007) The Collembola of Fennoscandia and Denmark. Part II: Entomobryomorpha and Symphypleona. Fauna Entomologica Scandinavica 42: 1–264. <https://doi.org/10.1163/ej.9789004157705.i-265>
- Folsom JW (1932) Hawaiian Collembola. Proceedings of the Hawaiian Entomological Society 8: 51–80.
- Folsom JW (1937) Nearctic Collembola or springtails of the family Isotomidae. Bulletin of the United States National Museum 68: 1–144. <https://doi.org/10.5479/si.03629236.168.1>
- Greenslade P (2006) The Invertebrates of Macquarie Island. Australian Antarctic Division, Kingston, 326 pp.
- Greenslade P, Wise KAJ (1986) Collembola of Macquarie Island. Records of the Auckland Institute of Science 23: 67–97.
- Goloschapova NP, Potapov MB, Chernova NM (2006) Sexual behaviour in Isotomidae (Collembola). Pedobiologia 50: 111–116. <https://doi.org/10.1016/j.pedobi.2005.12.006>

- Janion-Scheepers C, Deharveng L, Bedos A, Chown SL (2015) Updated list of Collembola species currently recorded from South Africa. *ZooKeys* 503: 55–88. <https://doi.org/10.3897/zookeys.503.8966>
- Linnaniemi WM (1912) Die Apterygotenfauna Finlands. II, Spezieller Teil. Druckerei der Finnischen Literaturgesellschaft, Helsingfors, 396 pp.
- Mari Mutt JA, Bellinger PF (1990) A Catalog of the Neotropical Collembola, Including Nearctic Areas of Mexico. Sandhill Crane Press, Gainesville, 237 pp.
- Mendonça MC, Queiroz G, Silveira TC (2015) Two new species of *Proisotoma* Börner, 1901 from Southeastern Brazil (Collembola: Isotomidae). *Soil Organisms* 87: 61–60.
- Mendonça MC, Silveira TC (2019) A peculiar new species of *Scutisotoma* Bagnall, 1949 (Collembola: Isotomidae) from Brazil. *Soil Organisms* 91: 1–6.
- Neves ACR, Mendonça MC (2016) Recaracterização da espécie *Proisotoma tenella* (Reuter, 1895) (Collembola: Isotomidae) In: Da-Silva ER, Passos MIS, Aguiar VM, Lessa CSS and Coelho LBN (Eds), Anais do III Simpósio de Entomologia do Rio de Janeiro. Universidade Federal do Estado do Rio de Janeiro, Rio de Janeiro, 52 pp.
- Potapov M, Babenko A, Fjellberg A (2006) Taxonomy of the *Proisotoma* complex. Redefinition of genera and description of new species of *Scutisotoma* and *Weberacantha* (Collembola, Isotomidae). *Zootaxa* 1382: 1–74. <https://doi.org/10.11646/zootaxa.1382.1.1>
- Potapov M, Gao Y, Deharveng L (2013) Taxonomy of the *Cryptopygus* complex. I. *Pauropygus*—a new worldwide littoral genus (Collembola, Isotomidae). *ZooKeys* 304: 1–16. <https://doi.org/10.3897/zookeys.304.4083>
- Potapov M, Janion C, Deharveng L (2011) Two new species of *Parisotoma* (Collembola: Isotomidae) from the Western Cape, South Africa. *Zootaxa* 2771: 17–24. <https://doi.org/10.11646/zootaxa.2771.1.2>
- Potapov M, Janion-Scheepers C (2017) A review of Salmon's *Folsomia* types from New Zealand (Collembola). *New Zealand Entomologist*: Vol. 40:1–7.
- Potapov MB, Janion-Scheepers C, Deharveng L (2020) Taxonomy of the *Cryptopygus* complex. III. The revision of South African species of *Cryptopygus* and *Isotominella* (Collembola, Isotomidae). *ZooKeys* 945: 99–127. <https://doi.org/10.3897/zookeys.945.51860>
- Potapov M, Kahrarian M, Deharveng L, Shayanmehr M (2015) Taxonomy of the *Proisotoma* complex. V. Sexually dimorphic *Ephemerotoma* gen. nov. (Collembola: Isotomidae). *Zootaxa* 4052(3): 345–358. <https://doi.org/10.11646/zootaxa.4052.3.4>
- Potapov M, Huang C-W, Gulgenova A, Luan Y-X (2020) New and little known Isotomidae (Collembola) from the shore of Lake Baikal and saline lakes of continental Asia. *ZooKeys* 935: 1–24. <https://doi.org/10.3897/zookeys.935.49363>
- Reuter OM (1895) Finlands Collembola och Thysanura. Apterygogenea Fennica. Helsingfors, 203 pp.
- Rapoport EH (1963) Collembolos de Bahia Blanca (Argentina). VI. *Revista de la Sociedad Entomológica Argentina* 26: 35–39.
- Salmon JT (1943) The genus *Folsomia* (Collembola) in New Zealand. *Transactions and Proceedings of the Royal Society of New Zealand* 73: 73–75.
- Salmon JT (1951) Keys and bibliography to the Collembola. *Zoology Publications from Victoria University College* 8: 1–82.

- Schött H (1893) Systematik und Verbreitung Palaearktischer Collembola. Kongliga Vetenskaps-Akademiens Handlingar 25: 1–100. <https://doi.org/10.5962/bhl.title.8645>
- Stach J 1947. The apterygotan fauna of Poland in relation to the world-fauna of this group of insects. Family: Isotomidae. Polska Akademia Umiejętności, Acta Monographica Musei Historiae Naturalis, Kraków, 488 pp.
- Willem V (1902) Les collemboles recueillis par l'expédition antarctique belge. Annals of the Society for Entomology of Belgium 45: 260–262.
- Winter C (1967) Beiträge zur Kenntnis der neotropischen Collembolenfauna. Senckenbergiana Biologica 4: 37–69.
- Yosii R (1939) Isotomid Collembola of Japan. Acta Entomologica 2: 344–392.
- Zeppelini D, Bellini BC (2006) Two *Seira* Lubbock 1869 (Collembola, Arthropleona, Entomobryidae) new to science, with remarkable secondary sexual characters. Zootaxa 1185: 21–35. <https://doi.org/10.11646/zootaxa.1185.1.2>